CHEMICAL REVIEWS

pubs.acs.org/CR

Review

Microstructural and Dynamical Heterogeneities in Ionic Liquids

Yong-Lei Wang,* Bin Li, Sten Sarman, Francesca Mocci, Zhong-Yuan Lu, Jiayin Yuan, Aatto Laaksonen, and Michael D. Fayer

Cite This: *Chem. Rev.* 2020, 120, 5798−5877

Read Online

ACCESS | Metrics & More | Article Recommendations

ABSTRACT: Ionic liquids (ILs) are a special category of molten salts solely composed of ions with varied molecular symmetry and charge delocalization. The versatility in combining varied cation−anion moieties and in functionalizing ions with different atoms and molecular groups contributes to their peculiar interactions ranging from weak isotropic associations to strong, specific, and anisotropic forces. A delicate interplay among intra- and intermolecular interactions facilitates the formation of heterogeneous microstructures and liquid morphologies, which further contributes to their striking dynamical properties. Microstructural and dynamical heterogeneities of ILs lead to their multifaceted properties described by an inherent designer feature, which makes ILs important candidates for novel solvents, electrolytes, and functional materials in academia and industrial applications. Due to a massive number of combinations of ion pairs with ion species having distinct molecular structures and IL mixtures containing varied molecular solvents, a comprehensive understanding of their hierarchical structural and dynamical quantities is of great significance for a rational selection of ILs with appropriate properties and thereafter advancing their macroscopic functionalities in applications. In this review, we comprehensively trace recent advances in understanding delicate interplay of strong and weak interactions that underpin their complex phase behaviors with a particular emphasis on understanding heterogeneous microstructures and dynamics of ILs in bulk liquids, in mixtures with cosolvents, and in interfacial regions.

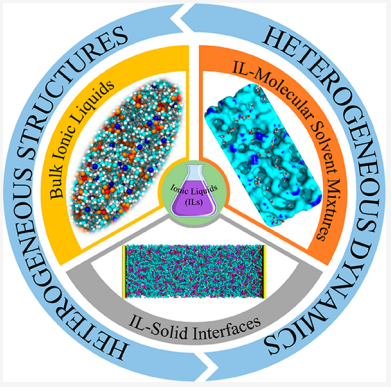

CONTENTS

Received: October 29, 2019
Published: April 15, 2020

https://dx.doi.org/10.1021/acs.chemrev.9b00693
Chem. Rev. 2020, 120, 5798−5877

1. INTRODUCTION

Ionic liquids (ILs) are liquid molten salts, typically composed of bulky and asymmetrical organic cations and organic or inorganic anions with their melting points below 100 °C. The history of ILs generally credits the German chemist Paul Walden with the first documented salt material at ambient temperature in 1914.[1] He synthesized an ionic salt, ethylammonium nitrate (EAN), which displays a melting point of 12 °C and a rather low viscosity. Unfortunately, apart from a brief mention of this work in a study of parachor and chemical constitutions of some fused metals and salts in 1929,[2] this early report did not receive much consideration from various scientific communities, and it was not anticipated that such salt materials would become of widespread interest in the future.

Nearly 40 years later, Hurley and Wier recognized the potential benefit of decreasing melting points of molten salt materials via synthesis of organic chloroaluminates by mixing aluminum compounds with alkylpyridinium chloride salts. The obtained organic chloroaluminates are now considered as the first generation of ILs.[3] However, these haloaluminate ILs suffer from their high sensitivity to atmospheric moisture and thus require handling under strict anhydrous conditions to avoid their hydrolysis. In addition, it is not feasible to regulate their acidity and basicity.[3] More specific investigations of these haloaluminate compounds started in the 1970s.[4,5] In the 1980s, ILs were proposed as solvents for organic synthesis, and scientific interest in ILs began to spread and the range of investigations began to broaden. A significant contribution from Wilkes and Zaworotko on "*Air and water stable 1-ethyl-3-methylimidazolium based ionic liquids*" in 1992 is seen by most researchers as ushering a new stage for the development of ILs,[5,6] even though some ILs had been predicted previously[7] and other air- and moisture-stable ILs have been used in laboratory settings.[8] Unlike haloaluminate salts, this new generation of ILs can be obtained, handled, and stored outside a glovebox. By a careful selection of cation−anion combinations, it is possible to prepare a large variety of ILs. These pioneering works and significant breakthroughs in IL communities opened up avenues for a surge of research on ILs and initiated paramount research activities across areas of physics, chemistry, biology, materials science and engineering, and environmental science, which are subjects of numerous reviews,[9−34] special themed issues in prestigious journals,[35−42] and book chapters.[43−49]

ILs have multifaceted and remarkable physicochemical characteristics, such as negligible volatilities, reasonable conductivity−viscosity properties, extended liquid-state temperature ranges, wide electrochemical windows, high thermal- and chemical-oxidative stabilities, as well as excellent capabilities to dissolve liquid and solid solute molecules having distinct polarities.[25,50] An additional fascinating character of ILs is that these physicochemical quantities related to hydrophobicity, polarity, and solvent power as well as their microstructural organization can be widely tuned by combinations of different cations and anions, by introducing a controllable amount of solutes in IL matrixes, and by mutating specific atoms in constituent ions.[25,50] Therefore, ILs are always referred to tunable, tailorable, task-specific, and designer solvents. These striking features render ILs as dependable candidates and benign alternatives to conventional molecular solvents in material synthesis to control precise structures and patterns of nanomaterials;[23,24] valuable reaction media in catalytic chemistry to provide optimized chemical enantioselectivity;[24,51] promising working fluids in separation technology via absorption of specific gas molecules;[29,52] unique tunable platforms to design task-specific advanced materials to dissolve celluloses and proteins;[23,29] reliable solvent electrolytes in electrochemical devices with tunable electrochemical windows and ion conductivities;[14,19,53−57] and useful lubricants and lubricant additives in tribology to reduce frictions between solid sliding contacts under harsh conditions.[22,30,58] As a result of enormous number of promising applications, the playing field for additional applications and related investigations for physicists, chemists, biologists, materials scientists, and engineers is vast and has yet to see its limitation.

The rapid upswing and wide applications of ILs in academia and industrial communities stem from a direct consequence of peculiar intra- and intermolecular interactions among constituent ions. These molecular interactions range from weak, isotropic, and nonspecific forces (e.g., solvophobic, van der Waals (vdW), dispersion forces, *etc.*) to strong (Coulombic), anisotropic, and specific forces (e.g., charge, dipole, and multiple interactions as well as hydrogen bonding (HB) interactions, *etc.*). Favorable vdW and dispersion associations among apolar moieties and decisive Coulombic interactions among polar moieties in constituent ions are key driving forces to construct remarkable liquid structures in IL matrixes.[18,30] In addition, Coulombic interactions among ion species are isotropic, which enables a substantial assortment of secondary directional interactions, such as dipole−dipole, dipole−induced dipole, multipoles, and possible $\pi-\pi$ stacking interactions as well as HB coordinations between ion species having heteroaromatic rings with delocalized charges.[17,59−61] These delicate interactions have considerable entropic contribution, facilitate additional stabilization, and direct the formation of remarkable ion clusters, paving the road for complex, higher order self-assembled liquid structures of ILs in bulk liquids and in confined environments.[15,18,30,62,63]

Moreover, not all but a vast number of ILs can be categorized as having polar and apolar components, and therefore can be regarded as nanosegregated fluids with polar (apolar) networks permeated by apolar (polar) domains. A subtle balance of intermolecular interactions between constituent ions and associations between polar and apolar components defines their peculiar transport properties including thermal conductivities (for heat transfer), liquid viscosities (for momentum transfer), and diffusion coefficients (for mass transfer). In addition, ion (electrical) conductivities of ILs are significant[64,65] as ILs are solely composed of ions.

https://dx.doi.org/10.1021/acs.chemrev.9b00693
Chem. Rev. 2020, 120, 5798−5877

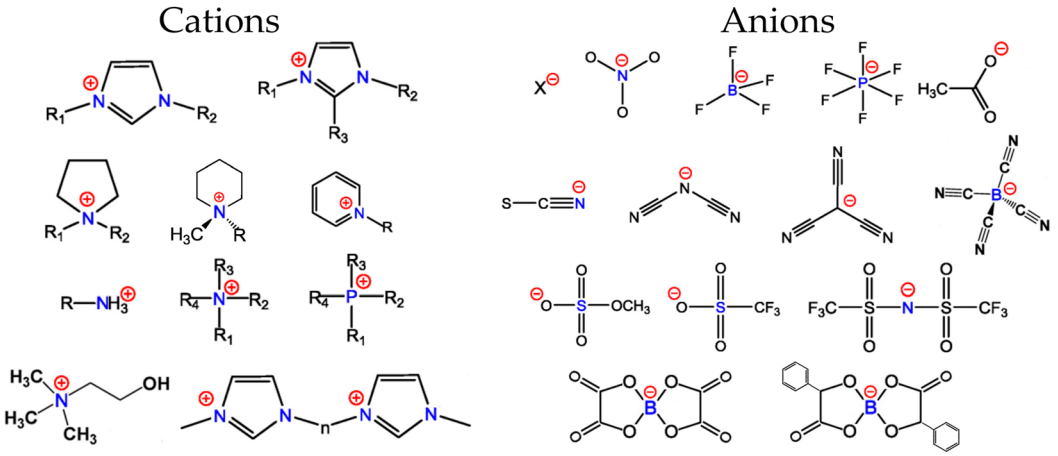

Figure 1. Chemical structures of typical cations and anions. Cations: dialkylimidazolium ($[C_nC_mIM]$), trialkylimidazolium, dialkylpyrrolidinium ($[C_nC_mPYRR]$), 1-alkyl-methylpiperidinium ($[C_nMPIP]$), *N*-alkylpyridinium ($[C_nPYRI]$), alkylammonium, tetraalkylammonium ($[N_{i,j,k,l}]$), tetraalkylphosphonium ($[P_{i,j,k,l}]$), 2-hydroxyethyl-trimethylammonium (cholinium, [CH]), and di-imidazolium ($[C_n(MIM)_2]$). Anions: halides, nitrate, tetrafluoroborate, hexafluorophosphate, acetate, thiocyanate, dicyanamide, tricyanomethanide, tetracyanoborate, methylsulfate, trifluoromethanesulfonates, bis(trifluoromethylsulfonyl)imide, bis(oxalato)borate, and bis(mandelato)borate. Adapted with permission from ref 13. Copyright 2017 American Chemical Society.

These properties play central roles in electrochemical applications.

ILs are generally much more viscous than their neutral binary mixture counterparts,[66−68] and some ILs become less viscous when ion charges are more homogeneously distributed over molecular frameworks or with addition of molecular solutes to IL matrixes. These aspects are expected to weaken Coulombic interactions among constituent ions and thereafter influence their dynamic properties. ILs exhibit slow dynamics that are typically characterized by subdiffusivities and nonexponential relaxations. The overall nonexponential dynamics of ILs are ascribed to a superposition of exponential relaxations of constituent ions with different relaxation times,[66,69] which is in accordance with relaxations of glass forming liquids,[70] colloids, and polymer melts[71] that exhibit distinct structural and dynamical heterogeneities at extended spatiotemporal scales.

Microstructural and dynamical heterogeneities are hallmark features of striking properties that ILs can possess. To date, almost all known physical chemistry techniques have been adopted to study these heterogeneities of ILs. Spectroscopic experiments (two-dimensional infrared (2D IR) spectroscopy,[72−75] dielectric spectroscopy,[76,77] direct recoil spectroscopy (DRS),[78,79] Fourier transform-infrared (FT-IR) spectroscopy,[80−82] light scattering spectroscopy,[83,84] nuclear magnetic resonance (NMR) spectroscopy,[85−88] optical-heterodyne-detected optical Kerr effect (OHD-OKE) spectroscopy,[89−95] sum frequency generation (SFG) vibrational spectroscopy,[96−101] ultrafast infrared spectroscopy,[91−93,102] neutron diffraction,[103,104] reflectivity[105−107] and scattering spectroscopies,[108−113] X-ray photoelectron spectroscopy (XPS),[114−116] X-ray diffraction (XRD),[117,118] X-ray reflectivity (XRR),[119−122] and X-ray scattering spectroscopies,[123−126] *etc.*), atomic force microscopy (AFM),[127−130] scanning tunneling microscopy (STM),[131−134] surface force techniques (surface force apparatus (SFA),[135,136] and surface force balance (SFB)[137−140]), polarization sensitive pump−probe (PSPP) measurements,[75,141] and computer simulations (density functional theory (DFT) calculations,[142−151] *ab initio*,[152−154] atomistic,[75,150,155−181] and coarse-grained (CG) molecular dynamics (MD) simulations[55,66−68,133,182−185]) have provided tremendous insights into heterogeneous microstructures and dynamics of ILs in bulk liquids, in mixtures with cosolvents, and in interfacial regions.

The purpose of this review is to trace recent advances in understanding striking and complex phase behaviors of ILs and to describe how delicate interplay of strong interactions and weak associations underpins their complex physicochemical properties with a particular emphasis on microstructural and dynamical heterogeneities of ILs at varied conditions. The versatility in combining different cations and anions with varied charge delocalization, and the flexibility in mutating specific atoms in constituent ions indicate that a huge number of ILs with distinct physicochemical and structural properties is accessible for applications. It is predicted that there are $\sim 10^6$ pure ILs that can be easily prepared in laboratory, leading to a possibility of 10^{12} binary combinations and 10^{18} ternary IL mixtures potentially available.[9] These numbers are still growing exponentially due to advanced synthetic procedures and technologies. It is difficult to coordinate microstructural and dynamical heterogeneities of all possible ILs. Therefore, in this contribution, we mainly focus on four IL families consisting of imidazolium, pyrrolidinium, (tetra)alkylammonium, and tetraalkylphosphonium cations due to their extensive usage in industrial applications. The anions of interest are the most popular ones, which can be either inorganic or organic entities including halides, nitrate ($[NO_3]$), tetrafluoroborate ($[BF_4]$), hexafluorophosphate ($[PF_6]$), acetate ([OAc]), alkylphosphate, alkylsulfonate, alkylsulfate ($[C_nSO_4]$), trifluoromethylsulfonate ([TFO]), bis(trifluoromethanesulfonyl)imide ($[NTF_2]$), and orthoborates. A nonexhaustive list of ion species discussed in this review is provided in Figure 1.

2. PURE IONIC LIQUIDS

In IL community, ILs were originally assumed to fall within a conventional scheme of molecular liquids as coherent, irregular, and essentially homogeneous systems.[4,17,18] Bulk ILs were widely treated as similar to high-temperature molten salts (like NaCl) or highly concentrated salt solutions. However, more recently it has been determined that ILs

https://dx.doi.org/10.1021/acs.chemrev.9b00693
Chem. Rev. 2020, 120, 5798−5877

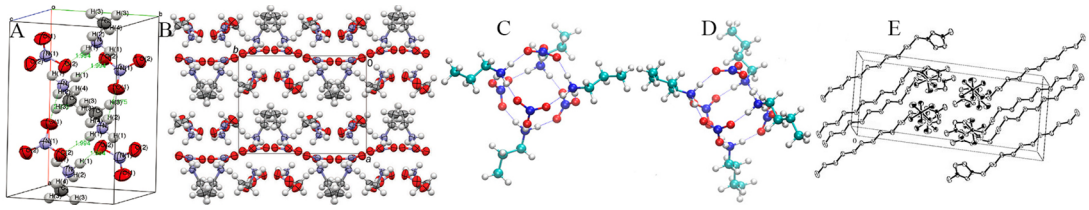

Figure 2. Molecular packing of (A) MAN and (B) EtAN crystal structures. Reproduced with permission from ref 186. Copyright 2011 American Chemical Society. Reproduced with permission from ref 196. Copyright 2012 Royal Society of Chemistry. Minimum energy structures of (C) PAN and (D) BAN ILs determined from atomistic simulations. Reproduced with permission from ref 188. Copyright 2012 American Chemical Society. (E) Unit cell of $[C_{12}MIM][PF_6]$ crystal structure. Reproduced with permission from ref 197. Copyright 1998 Royal Society of Chemistry.

present diverse ordering structures compared to conventional molecular liquids driven by a combination of short-range HB, vdW, and solvophobic interactions and long-range Coulombic associations among constituent ions. Generally, ion interactions impose a degree of short-range ordering structures (ion pairs, ion clusters, *etc.*) and result in distinct mesoscopic organization (HB networks, amphiphilic combinations of polar and apolar components, micelle-like and bicontinuous liquid morphologies) in IL matrixes. ILs exhibit structural heterogeneities at multiple length scales, which is one of the most distinctive properties of ILs, and therefore it is feasible to fine-tune ILs' physicochemical and structural properties with desirable macroscopic functionalities for promising applications.

2.1. IL Crystal Structures

IL crystal structures provide clues to their liquid structures especially for local intermolecular interactions. Alkylammonium nitrate ILs are the most studied ILs since they are the first ILs ever synthesized in laboratory.[1] Bodo et al. reported crystal structure of methylammonium nitrate (MAN) using experimental techniques and DFT calculations.[186] A solid phase existing at high temperatures is a polymorph and has a high degree of disorder, corresponding to an ionic plastic phase where both cations and anions retain a more or less fixed reticular position. $[NO_3]$ anions are asymmetrically coordinated with MA cations via HB interactions, that is, a given $[NO_3]$ anion is not engaged in three equally strong HBs; instead, one HB is significantly weaker than the other two (Figure 2A). Such an asymmetric HB structure was also observed in theoretical calculations of MAN ion clusters.[187,188] It should be noted that there is no nanoscale apolar segregation in MAN as methyl groups are too small. For alkylammonium cations with alkyl chains longer than C_1, the corresponding nitrate ILs present some long-range ordering structures over a nanometer length scale, which stem from self-assembly of hydrophobic alkyl chains within polar networks.[108,189−195]

The crystal structure of ethanolammonium nitrate (EtAN) consists of two lamellar-like layers composed of EtA cations taking vertical configurations (Figure 2B).[196] Half of $[NO_3]$ anions are located between neighboring ammonium moieties forming polar domains, and the other $[NO_3]$ anions are interspersed between ethyl chains. Lengthening alkyl chains in alkylammonium cations leads to distinct structures as observed in propylammonium nitrate (PAN) (Figure 2C) and butylammonium nitrate (BAN) ILs (Figure 2D).[188,198] Raman spectra revealed that PA cations exhibit *trans* conformations in low temperature crystalline phase and undertake a crystal polymorphism transition with increasing temperatures to a phase in which PA cations are characterized by *gauche* conformations. Such a structural rearrangement takes place both in polar domains, in which there is a dominance of Coulombic and HB interactions between ammonium groups and $[NO_3]$ anions and in apolar domains, where there are strong vdW interactions among alkyl groups. The distorted cation−anion structures remain in the liquid phase at high temperatures but can be arrested in isles with distinct microscopic heterogeneities at high pressures.

The temperature dependence of ethylammonium chloride (EAC) and propylammonium chloride (PAC) crystal structures was investigated by *in situ* X-ray powder diffraction spectroscopy.[199−201] A polymorphic transition, with a reconstructive character, was observed for PAC from a monoclinic phase formed at low temperatures to a tetragonal phase formed at high temperatures. For EAC polymorphs, the thermal expansion is small and anisotropic, which is attributed to EAC's liquid organization characterized by an anisotropic framework consisting of apolar and polar domains, whereas an isotropic thermal expansion was observed for PAC attributing to striking intermolecular interactions between nitrogen atoms in PA cations and Cl anions. In addition, microscopic isostructurality was reported for other PA halides (Br and I) at room temperature.[200]

In contrast to alkylammonium ILs, imidazolium ILs show different crystal structures depending on anion structures and cation alkyl chain lengths. $[C_2MIM]$ ILs were extensively studied because they exhibit low melting points and high ion conductivities. When $[C_2MIM]$ cations are coordinated with halides, $[C_2MIM]F$ is unstable and has never been isolated under ambient conditions.[202] $[C_2MIM]Cl$ exhibits an orthorhombic crystal structure containing four ion pairs in an asymmetric unit cell,[203] in which Cl anions are situated in positions with characteristic C−H···Cl HB interactions. Similar HB structures were also observed in $[C_2MIM]Br$ and $[C_2MIM]I$ crystals.[204] $[C_2MIM][BF_4]$ exhibits a peculiar monoclinic crystal structure in which $[C_2MIM]$ cations exhibit one-dimensional (1D) pillar structures with one imidazolium ring facing the next one, and they are linked by H-(methylene)···π interactions,[205] whereas in ILs consisting of $[C_2MIM]$ cations and hexafluorocomplex anions, $[C_2MIM]$ cations form a similar 1D pillar structure with anions positioned in a zigzag arrangement along the same direction.[195,202]

XRD spectra showed that multiple polymorphs with rotational cation isomers are obtained for ILs consisting of $[C_4MIM]$ cations coupled with Cl, Br, I, $[BF_4]$, and $[PF_6]$ anions at crystalline and liquid states.[206] Both monoclinic crystal structures with *trans*−*trans* configurations and orthorhombic crystal structures having *gauche*−*trans* configurations are available depending on conformations of butyl chains in cations and their delicate associations with anions. In

https://dx.doi.org/10.1021/acs.chemrev.9b00693
Chem. Rev. 2020, 120, 5798−5877

monoclinic [C_4MIM]Cl crystal structure, butyl chains take a *trans*−*trans* conformation, while in orthorhombic [C_4MIM]Cl and [C_4MIM]Br crystal structures, butyl chains exhibit *gauche*−*trans* conformations. Complementary Raman spectra[207] revealed that [C_4MIM] cations in these ILs form mesostructures in liquid regions that are similar to column structures found in crystals.[206] Two different mesoscopic rotational isomers coexist in IL matrixes and are crucial in hindering crystallization of [C_4MIM] ILs.[208,209]

Imidazolium cations with alkyl chains longer than C_{14} can form a thermotropic smectic liquid crystal phase between liquid and solid states, which is similar to that observed in alkylammonium ILs with cations having long alkyl chains and some other protic ILs with cations having intermediate alkyl chains.[10,210] ILs consisting of halide anions and 1-alkyl-3-methylimidazolium ([C_nMIM]) cations with n = 12−18 exhibit bilayer crystal lattices,[197] in which anion species and imidazolium rings form polar sheets that are separated by apolar domains consisting of interdigitated cation alkyl chains. The interlayer distance between polar sheets ranges from 2.4 to 3.3 nm depending on cation alkyl chain length (Figure 2E). The thermal behavior of a series of ILs consisting of [C_nMIM] cations (n = 12−18) and anions having different coordinating abilities and sizes from Cl to [NTF_2] was studied using small-angle X-ray scattering (SAXS) experiments and differential scanning calorimetry (DSC).[211] These ILs form lamellar, sheetlike arrays in crystalline phase and enantiomeric structures in the smectic liquid crystal phase at higher temperatures, except for ILs containing [NTF_2] anions which directly melt and form isotropic liquids. Layer spacing in crystal mesophase determined from SAXS spectra increases with cation alkyl chain length and with coordination ability of anions, following an order of Cl > Br > [BF_4] > [TFO] > [NTF_2].

Among many different anion species, [NTF_2] anions exhibit striking behavior due to their diffuse charge distribution. The delocalized negative charge along S−N−S core in [NTF_2] anion reduces ion−ion interactions and results in a suppression of liquid-crystallinity and fluidizes imidazolium ILs with low melting points.[212] XRD, vibrational spectra, and DFT calculations[213,214] showed that [NTF_2] anions adopt a higher energy, less stable *cis* geometry in [C_1MIM][NTF_2] constrained by bifurcated C−H···O and C−H···N HBs resulting in the formation of fluorous layers in solid state structures.

2.2. Hydrogen Bonding and π−π Stacking Structures

2.2.1. Hydrogen Bonding Structures and Dynamics.

When cations contain hydrogen atoms and anions have lone electron pairs, it is possible to form cation−anion HBs with cations being dominant HB donors and anions being dominant HB acceptors, respectively. It should be noted that HB in ILs is not a binary on−off phenomenon but occurs on a graduated scale, which makes demarking HB difficult. Because of a wide range of cations and anions constituting ILs, the characteristics and features of HB interactions are quite system dependent.[149,153,215−218] In protic cations, hydrogen atoms in HB donors are often covalently bonded to heavy atoms carrying formal charges, and aprotic cations tend to have C−H groups as primary HB donor units. A large range of potential HB acceptors exist in anions ranging from strong HB acceptors like halides to weak HB acceptors with minimal HB interactions. In many cases, alkyl chains in ions can be functionalized with, but not limited to, alcohol, amine, carboxylic acid, and ether groups.[219−228] These functional groups add further opportunities to fine-tune HB interactions in IL matrixes.

Evans and co-workers made the first suggestion that there are well-defined HB structures in alkylammonium ILs.[229] They found that transferring hydrocarbons and rare gases from cyclohexane to EAN has negative enthalpies and thus speculated that proton donors and acceptors in constituent ions form a three-dimensional (3D) HB network resembling water. While this speculation was never seriously disputed, HB interactions in EAN and its derivative IL systems were convincingly established by Ludwig and co-workers in 2009.[230] In combination with DFT calculations, the deconvoluted vibrational bands in FT-IR spectra for EAN, PAN, and dimethylammonium nitrate ILs are assigned to intermolecular stretching and bending modes of N−H···NO_3 HBs. In these ILs, the characteristic symmetric and asymmetric stretching modes, as well as bending modes in low-frequency region of FT-IR spectra, are consistent with those of pure liquid water. These observations are rationalized by the formation of similar HB structures in these protic ILs, while unlikely to be tetrahedral, are structurally reminiscent of water, owing to different ion structures and donor−acceptor capabilities of alkylammonium nitrate ILs.

By choosing specific cation−anion moieties and changing the number of alkyl chains in alkylammonium cations, it is feasible to tune dominant forces from HB to Coulombic interactions by switching from protic ILs consisting of primary, secondary, and tertiary ammonium cations to aprotic tetraalkylammonium ILs.[231−233] FT-IR spectrum of [$N_{1,1,1,1}$][NO_3] shows a broad vibrational band attributing to librational contributions of interacting ions, whereas FT-IR spectrum of [$N_{0,1,1,1}$][NO_3] exhibits a distinct vibrational band at approximately 170 cm^{-1}, which is associated with N−H···NO_3 HB interactions since no other intramolecular vibrational motion of alkylammonium or nitrate is observed in this frequency range. This interpretation was further supported by DFT calculated frequencies of [$N_{1,1,1,1}$][NO_3] and [$N_{0,1,1,1}$][NO_3] ion clusters. The energy per ion pair for [$N_{0,1,1,1}$][NO_3] (one HB donor) is ∼49 kJ/mol, higher than that for [$N_{1,1,1,1}$][NO_3] (no HB donor), demonstrating the formation of a single HB between [$N_{0,1,1,1}$] cation and [NO_3] anion. In addition, this value is 2 times larger than that of HBs in water (∼22 kJ/mol), indicating that [$N_{0,1,1,1}$][NO_3] possesses stronger HBs than water.[234]

Solid-state NMR spectra in combination with atomistic simulation results revealed that N-D deuterons in [$N_{0,2,2,2}$] cations have the lowest deuteron quadrupole coupling constants in all reported tetraalkylammonium cations and have strong HB interactions with anion species.[235] For hydroxyl-functionalized tetraalkylammonium ILs,[236] N-D deuterons have two types of HB interactions: a regular type Coulomb-enhanced cation−anion HBs and an unusual type cation−cation HBs. The formation of cation clusters prevents these ILs from crystallizing, and HBs between cation species persist at low temperatures, resulting in supercooling liquids and glass formation. Both neutron diffraction experiments and atomistic simulation results demonstrated that the elusive like-charge attraction is almost competitive with conventional ion-pair formation[104] and thus leads to enhanced ion pairing structures in comparison with dispersion forces between alkyl groups.[237] These findings revealed a new era of controlling IL nanostructures via HB interactions between like-charged ions, which impact diverse areas including electrochemical charge

https://dx.doi.org/10.1021/acs.chemrev.9b00693
Chem. Rev. 2020, 120, 5798−5877

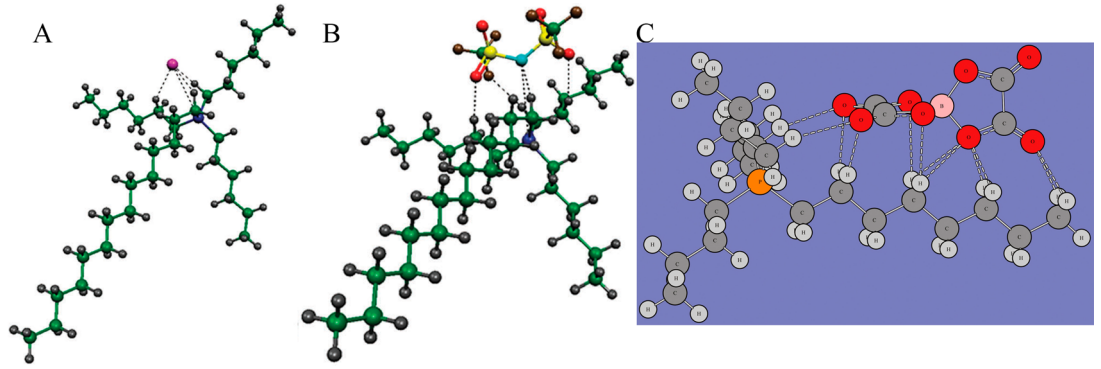

Figure 3. Optimized ion pair structures of (A) $[P_{6,6,6,14}]Cl$ and (B) $[P_{6,6,6,14}][NTF_2]$ ion pairs determined from quantum chemical calculations. Reproduced with permission from ref 144. Copyright 2011 Royal Society of Chemistry. (C) Optimized $[P_{4,4,4,8}][BOB]$ ion pair structure obtained from DFT calculations. Reproduced with permission from ref 164. Copyright 2014 American Chemical Society.

storage (batteries and catalysis), electrodeposition, and lubrication.

In addition, a number of DFT calculations and atomistic simulations indicated that hydrogen atoms in methylene units that are covalently bonded to central atoms in tetraalkylphosphonium cations assume preferential orientations toward electronegative atoms in anions via intermediate HB interactions.[142−144,238] In a representative $[P_{6,6,6,14}]Cl$, Cl anions interact with hydrogen atoms in central $P(CH_2)_4$ groups in cations, resulting in a cradlelike structure with Cl anions sitting in regions formed by three alkyl chains in $[P_{6,6,6,14}]$ cations (Figure 3A).[142−144,239,240] For large anions, like $[NTF_2]$ and orthoborates, the most negatively charged atoms are always coordinated with polar moieties in cations via strong electrostatic interactions and preferential HB coordinations (Figure 3B). A synergistic effect of these intermolecular interactions promotes a constrained orientation of large anion species around tetraalkylphosphonium cations, like the piggyback structure of bis(oxalato)borate ([BOB]) anion on $[P_{4,4,4,8}]$ cation (Figure 3C).[164]

When tetraalkylammonium cations are functionalized with hydroxyl groups, a subtle energy balance between Coulombic, HB interactions, and dispersion forces governs unique properties of ILs.[80,219] FT-IR spectra of $[CH][NTF_2]$ display a well-defined vibrational feature, which is assigned to a *jumping-and-pecking* motion of cations attributing to intermolecular vibrational modes between hydroxyl groups in [CH] cations and oxygen atoms in $[NTF_2]$ anions.[80,241] Repulsive Coulombic interactions between [CH] cations are replaced by cooperative HB interactions between cations, which are, in principle, similar to those of alcohol dimers.[241] Addition of alcohols to pure [CH] clusters results in enhanced "kinetic stability",[241] leading to the formation of ring structures with [CH] cations separated by neutral alcohols. The enhanced cooperative HB interactions and reduced Coulombic repulsions contribute to distinct thermodynamic stabilities of these ion clusters with increased melting temperatures and viscosities as well as decreased ion conductivities in comparison with those for $[N_{1,1,1,3}][NTF_2]$. Rotational dynamics and HB lifetimes for $[CH][NTF_2]$ consist of two time scales.[219] The short time contribution to rotational correlation times and HB lifetimes is around picoseconds, whereas the long time contribution decays with relaxation correlation times in nanosecond range, demonstrating importance and longevity of ion pairs stabilized by HBs.

HB interactions between imidazolium cations and paired anions were fairly debatable in early investigations since their contributions to ion arrangements are indistinguishable from strong electrostatic interactions. In addition, similar to other IL systems, the principle adopted to define a HB has a significant effect on its interpretation.[17,242] Nowadays, there is clear evidence of HB interactions in imidazolium ILs, and it is widely accepted that HB interactions between constituent ions in aprotic and protic imidazolium ILs behave as usual cation−anion interactions although sometimes HB interactions occur between ion species carrying the same charge.[243,244] Evidences of HB interactions in imidazolium ILs were reported via a variety of experimental characterizations (FT-IR,[81,245] NMR,[245] Raman spectroscopies,[244] *etc.*), DFT calculations,[81,245,246] and atomistic simulations.[153,215,216,247] Local and directional HB interactions in imidazolium ILs are indicated by short C−H···anion distances, downfield shifted C−H proton chemical shifts, red-shifted C−H frequencies, and by DFT calculated frequencies of IL clusters consisting of $[C_2MIM]$ cations paired with thiocyanate ([SCN]), dicyanamide ($[N(CN)_2]$), $[HSO_4]$, $[C_2SO_4]$, and $[NTF_2]$.[59,244,245] The observed differences in low frequency region of vibrational spectra of these ILs stem from specific cation−anion interactions, e.g., stretching and bending modes of C−H··· anion HB interactions.

Hunt and co-workers performed intensive DFT calculations to elucidate HB structures in imidazolium ILs.[17,149,248] HB donor sites in aprotic imidazolium cations are C−H units, which can be a C−H on ring moiety or a C−H from methylene or methyl groups of alkyl chains (Figure 4). DFT calculations revealed an array of different HB types between $[C_4MIM]$ cations and Cl anions.[249,250] The primary HB interaction is C(2)−H···Cl with a HB distance of ∼2 Å, which is very short considering the sum of vdW radii for Cl and H atoms.[250] It is noteworthy that this HB is not linear, as Cl sits slightly displaced, forming another weak HB with neighboring alkyl C−H unit. Large anions prefer to position over imidazolium rings.[251] These remarkable cation−anion configurations with anions sitting on top of imidazolium rings result in a slight blue-shift of computed C(2)−H vibration due to distinct anion-π donor−acceptor interactions.

HB interactions between imidazolium cations and their paired anions are affected by electronic characteristics and steric hindrance effects of alkyl chains. Alkyl chains can rotate to stabilize distributions of anions, and long alkyl chains can form secondary supporting HBs with anions. For all alkyl

https://dx.doi.org/10.1021/acs.chemrev.9b00693
Chem. Rev. 2020, 120, 5798−5877

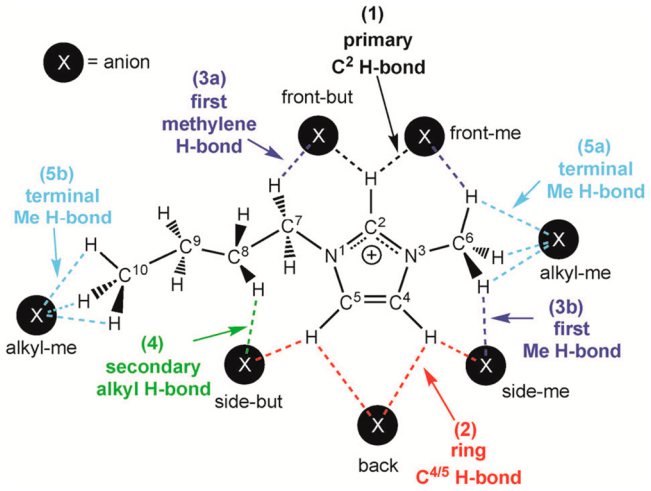

Figure 4. All possible HB donor sites in [C_4MIM] cation to coordinate anions denoted as filled black circles with a white X. Different HB types are color coded and numbered as primary (1) with C(2) of imidazolium ring (black), ring (2) with C(4) and C(5) at rear part of imidazolium ring (red), first methylene (3a) or first methyl (3b) with C(6) or C(7) groups in alkyl chain (dark blue), secondary (4) with lateral methylene groups in alkyl chain (green), and terminal methyl (5) with terminal C(6) or C(10) methyl groups in alkyl chain (light blue). Reproduced with permission from ref 17. Copyright 2015 Royal Society of Chemistry.

substituents in imidazolium cations, methylene groups bonded to nitrogen atoms on imidazolium rings have a distinctive electronic character and tend to form intermediate HBs, and the other methylene/methyl groups have varied weak HB capabilities depending on local conformations of alkyl chains.[17,165,248,250,252] Generally, multiple HBs are formed between imidazolium cations and anions via different HB donor and acceptor sites with a wide range of HB strengths (Figure 4). Secondary HBs of anions with cation alkyl chains are viewed as influencing primary ones via displacing anions from an ideal linear arrangement.[250] A key feature of these HB structures is that alkyl chains are able to reorient to maintain a more linear C−H HB interaction, while ring C−Hs cannot.[149] A chelating ability of these HBs is relevant; if one HB is broken, another can keep the anion in the local vicinity allowing the broken HB to reform.[61,217,248,253] These features are important for the formation of cation−anion HB networks in imidazolium ILs.[248]

Most imidazolium cations can be functionalized with various moieties, among which protonation of N(3) position and methylation of C(2) position hold specific significance.[220] The former can tune the cation's hydrophilicity from aprotic to protic. The hydrogen atom at N(3) position serves as a strong HB donor site and has significant and preferential HB interactions with anions and polar solutes in ILs.[75,94,163,254,255] A combination of OHD-OKE, NMR, Raman, and FT-IR spectra and atomistic simulations demonstrated that strong competitive HB interactions among cations, anions, and water molecules can significantly affect molecular mobilities and rotational dynamics of ion species as well as hydrodynamic behavior of ILs and IL−water mixtures.[75,94,254]

Methylation of C(2) position in imidazolium rings disrupts predominant cation−anion HB interactions, leading to surprising changes in physicochemical properties of ILs via adjusting respective contributions of Coulombic forces, vdW associations, and HB interactions to yield distinct cation−anion coordination patterns.[75,94,255,256] Elimination of C(2)-H···anion HBs by alkyl substitution tends to increase phase transition temperatures and liquid viscosities,[59,218] as manifested in experimental studies of [C_4C_1MIM]X (1-butyl-2,3-dimethylimidazolium) (X = Cl, Br, I, [BF_4], and [PF_6]) ILs in comparison with [C_4MIM]X ILs.[257] Based on computational results, it was argued that an increase in rotational barrier of butyl chains facilitates alkyl chain association, and an overcompensation of phase transition entropy decreases with increasing transition enthalpy. A so-called "'entropy theory"' was proposed, but it is still presumed that HBs stabilize imidazolium ILs.[221] Ludwig et al. suggested another explanation that directional cation−anion HBs destroy charge symmetry resulting in fluidized ILs.[230,233,258,259] HBs can be regarded as "defects" in Coulombic networks of ILs. These defects increase ion dynamics, leading to decreased melting

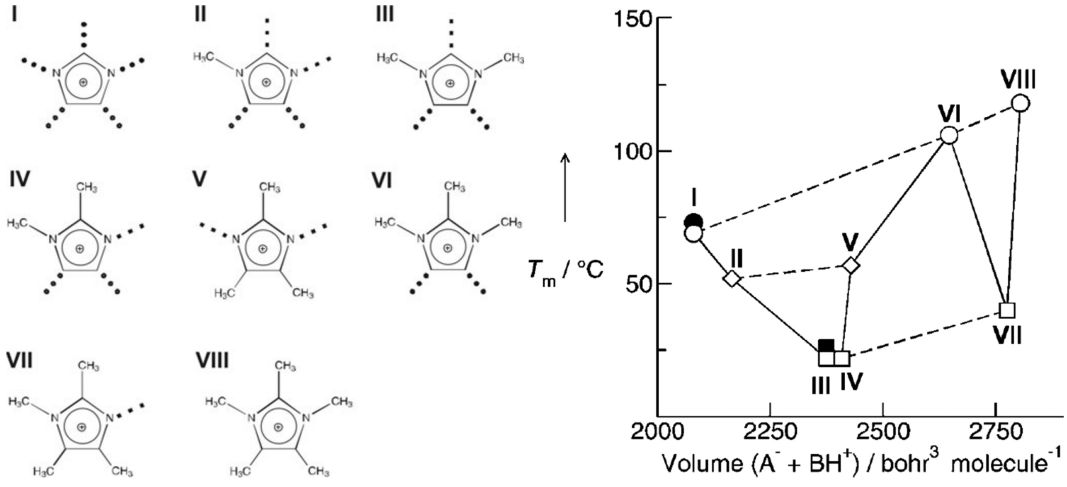

Figure 5. Left: Protonation and methylation of imidazolium rings at varied positions. Right: Plot of melting points (T_m) versus ion pair volumes for representative imidazolium [NTF_2] ILs. As indicated by dashed lines, there is an increase in T_m with increasing ion pair volumes for ILs with no specific interaction site (●), with one interaction site (□), and with two interaction sites (◊). Reproduced with permission from ref 261. Copyright 2011 Wiley-VCH Verlag GmbH & Co. KGaA.

https://dx.doi.org/10.1021/acs.chemrev.9b00693
Chem. Rev. 2020, 120, 5798−5877

points and viscosities, as observed in FT-IR spectra and DFT calculations of $[C_2MIM][NTF_2]$ and $[C_2C_1MIM][NTF_2]$ (1-ethyl-2,3-dimethylimidazolium) ion clusters. Additional studies showed that cation−anion interactions in imidazolium ILs are enhanced by HB interactions as indicated by frequency shifts to higher wavenumbers in FT-IR and terahertz spectra.[59,222,223,260]

A combination of these two effects, namely, protonation of N(3) position and methylation of C(2) position in imidazolium rings, leads to complex phase behaviors of imidazolium ILs. Ludwig and co-workers designed a series of polymethylated imidazolium cations with varied methyl groups and hydrogen atoms on imidazolium rings to reduce conformational flexibility of imidazolium cations (Figure 5).[222,223,261] By varying cation structures in a systematic way, it was shown that increasing interaction strength leads to a frequency shift to higher wavenumbers.[261] Supported by DFT calculations of IL clusters, a nearly linear relationship was observed between calculated binding energies per ion pair and the observed frequency shifts. These results are referred to enhanced cation−anion interactions. For protic imidazolium ILs, it was shown that the vibrational bands assigned to cation−anion interactions can be well separated from other low-frequency vibrational modes, which arise from librational and rattling motions of ions. Stronger HBs further shift vibrational energies to higher frequency and result in distinct vibrational bands which can be used for studying phase transitions of ILs and cation−anion interaction strengths as a function of temperature. HBs have significant influence on ILs' physicochemical properties, such as liquid viscosities, melting points, and enthalpies of vaporization (Figure 5).[59,218,262] In addition, Noack et al. performed experimental studies on similar ILs and found that changes in electron density can adjust locations and strengths of interionic interactions, leading to reduced configurational variations.[260] They suggested that neither "entropy theory"[221] nor "defect hypothesis"[59,222] alone is capable of explaining changes in physicochemical properties of ILs but complements each other.

There are other ideas discussing the relevance of inter- and intramolecular HB interactions on physicochemical properties of ILs.[263,264] Zahn et al. showed that the absence of HBs at C(2) position in imidazolium rings results in a reduced free movement of anions and an increased melting point of ILs, which is referred to flat energy landscapes of ion pairs.[264] Izgorodina et al. investigated two possible structural and energetic sources for decreased ion conductivities of imidazolium ILs due to methylation of C(2) position; first, ion associations, as suggested by the Walden rule, and second, variations of potential energy surface profiles that favor ion transport in non-C(2)-methylated imidazolium ILs.[263] It was shown that the increased liquid viscosities of C(2)-methylated-imidazolium ILs, attributing to a high potential energy barrier between energetically preferred conformations on potential energy surface, inhibit an overall ion transport.

It should be noted that methylation of C(2) position on imidazolium rings is also essential to improve chemical stabilities and tribological properties of ILs.[221,263] Trialkylimidazolium ILs are considered as promising electrolytes for electrochemical applications[265] due to the lack of an acidic proton at C(2) position and enhanced thermal and chemical stabilities[221] in comparison with dialkylimidazolium ILs. Thermal stability is an important property when it is necessary to select appropriate ILs for applications at high temperatures, such as thermal fluids and lubricants and solvents for organic reactions at elevated temperatures. ILs with low thermal and chemical stabilities have reduced efficiencies in some physicochemical processes, which may lead to hazardous byproducts.[266] Therefore, accurate data and knowledge of physicochemical properties of ILs are essential for engineering liquid flows for industrial applications and warrant extensive investigations combining experimental characterizations and computational studies.

Despite a wide range of anions, to date, HBs are formed with anions having a limited number of atom types. Anions, and their HB characteristics, can be classified by increasing structural complexity. The simplest anions are monatomic halides and small diatomics.[250,267] Then follows highly symmetric multiatomic anions which exhibit similar structures but weaker HB interactions compared with monatomic anions.[268] The next level of complexity includes small, less symmetric anions with an increasing number of strong HB acceptor sites, such as $[OAc]$, $[TFO]$, and $[HSO_4]$. The most complex anions have more than one type of HB acceptors. Nitrogen centered anion species such as $[NTF_2]$ and $[N(CN)_2]$ have both an electron rich central nitrogen atom and pendant groups containing oxygen and nitrogen atoms, respectively. In most cases, oxygen atoms in anions have preferential HB interactions, but in the liquid phase all electronegative atoms can form HBs with cation species.[269]

In typical ILs, ions assume configurations to maximize HB interactions, and there can be a fine balance between a small number of shorter stronger directional HB interactions and a large number of weaker looser HB interactions.[252,268,270] The density of HBs within ILs is very high, which facilitates networking. HB networking is expected to be maximized when the number of HB donor sites in cations is equal to the number of HB acceptor sites in anions. Perfectly matched HB donor and acceptor sites lead to the formation of "closed" rings and clusters or a rigid HB network in which all ions are held in place with well-defined configurations. A loss of HB sites or a restriction of alkyl chain rotation due to HB interactions can reduce entropy, which can be balanced by enhanced enthalpies of multiple HBs. A mismatch creates "'loose'" HB acceptors or HB donors, i.e., "defects" within a HB network, which tend to facilitate fluidity and enhance dynamic properties of HB networks.[187]

Recent investigations have featured the significance of time scales of HB interactions on ILs' physicochemical properties.[153,215,216,247,253] Both continuous and intermittent HB dynamics were examined for representative imidazolium ILs. For $[C_4MIM][PF_6]$, continuous HB lifetimes are related to rotations of anions leading to a rapid breaking and forming of HBs, and intermittent HB lifetimes are associated with caging and librational motions of ions in local heterogeneous environments,[271] respectively. Skarmoutsos et al. studied temperature dependence of HB dynamics in "hot" $[C_2MIM]Cl$ and "cold" $[C_4MIM]Cl$ ILs.[253] It was shown that HB dynamics change dramatically for an ∼100 °C temperature variation even though the average number of HBs remains constant. In "hot" $[C_2MIM]Cl$ IL, C(2)−H forms the strongest HB having the slowest intermittent HB dynamics with a time constant of ∼100−120 ps, which is similar to rotational dynamics of N−N vectors in imidazolium rings. These computational results indicate that in the time it takes the entire imidazolium ring to rotate, adjacent anions have moved away, breaking HB structures (Figure 6). In "cold"

https://dx.doi.org/10.1021/acs.chemrev.9b00693
Chem. Rev. 2020, 120, 5798−5877

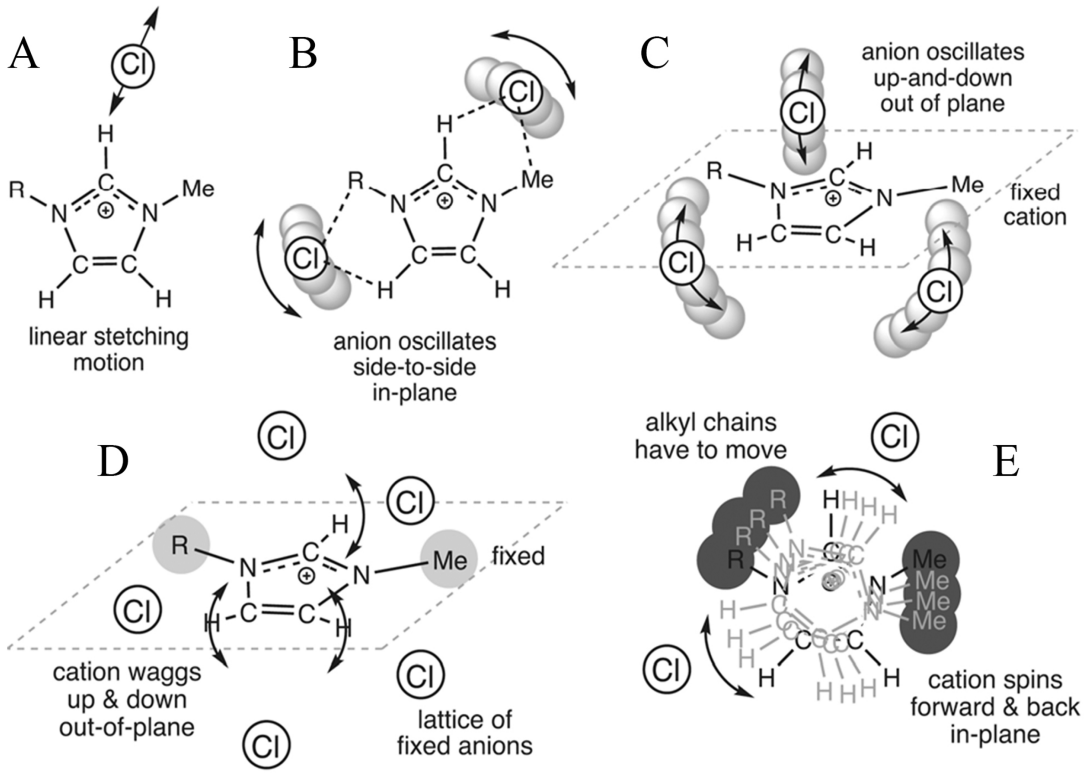

Figure 6. Cartoons indicating (A−C) movements of cations and anions for breaking and reforming cation−anion HBs, (D) out-of-plane wagging movements of anions around cations, and (E) cation in-plane spinning movements. Reproduced with permission from ref 253. Copyright 2014 Royal Society of Chemistry.

[C_4MIM]Cl IL, ring C−H sites dominate HB dynamics and intermittent HBs last for approximately 5 ns, whereas rotations of imidazolium ring planes occur on a much longer time scale. These HB dynamics can be intrinsically rationalized by underlying HB structures in these two ILs. In "hot" [C_2MIM]Cl IL, a dynamic HB network exists, which contains a large number of single HBs. Once one HB breaks, the respective ions forming this HB are less likely to remain colocated, and they will form new HBs with different ions. A high density of ions in IL matrix is likely to be important as ions should be sufficiently close together that new HB arrangements will be readily formed. Thus, in "hot" [C_2MIM]Cl IL, HBs are rapidly breaking and forming between different cations and anions. As this IL cools, a higher proportion of bifurcated HBs occurs. Ions are colocated for longer times, and lifetimes for individual HBs are extended (particularly for ring HBs). Even in "cold" [C_4MIM]Cl IL, HBs are still breaking and reforming, but it is much more likely that these are happened between the same ion pairs, and intermittent HB lifetimes are dramatically extended.

For imidazolium cations coupled with large anions, like [BOB], it was shown that the decay of continuous HB dynamics of C(2)−H in coordinating [BOB] anions is much faster than that of intermittent HB dynamics in a given IL matrix, which is consistent with computational results for [C_nMIM]Cl ILs at elevated temperatures.[253,272] It is noteworthy that residence lifetimes for HB dynamics, either ring C−H or alkyl C−H units, are much longer than those for water and alcohols under ambient conditions and are somewhat comparable with those of [C_2MIM]Cl, [C_2MIM]-[BF_4], and [C_2MIM][NTF_2] ILs at high temperatures and with those of [C_4MIM]Cl and [C_4MIM][BF_4] ILs over a wide temperature range.[156] The continuous and intermittent C(2)−H···O ([BOB]) HB dynamics are described by a stretched biexponential decay function, which are distinct to those of C(2)−H···Cl HB dynamics. Diffusive properties of Cl anions around cation species in [C_2MIM]Cl and [C_4MIM]Cl ILs are described by a correlation function with three decay components.[253] This observation is attributed to remarkable [BOB] anion structures compared with monatomic Cl anions in coordinating imidazolium cations.[156,253,272] [BOB] anions have multiple HB acceptor sites, promoting their constrained distributions in polar domains and the formation of HB networks in heterogeneous IL matrixes. Assuming that imidazolium cations are fixed on regular lattices, the rotational dynamics of [BOB] anions around imidazolium ring planes, either up-and-down or side-to-side angular motions, desire a large energy to break ion structures and HB networks and therefore are not favored in [C_nMIM][BOB] ILs. The fast decay of C(2)−H···O HB dynamics in [C_nMIM][BOB] ILs can be rationalized by a linear in-and-out stretching mode along C−H bonds in cations. The librational motions of Cl anions in IL matrixes, such as up-and-down and side-to-side angular motions relative to imidazolium ring planes and linear stretching vibration along the C−H bonds, lead to a fast decay of continuous C(2)−H···Cl HB dynamics (Figure 6).[253] Furthermore, lengthening cation alkyl chains leads to a substantial increase in residence lifetimes for both continuous and intermittent HB dynamics.[217]

2.2.2. π−π Stacking Structures. In addition to HB coupling, π-type interactions are correlated with preferential electrostatic interactions and favorable dispersion associations among heteroaromatic rings, such as imidazolium, triazolium, thiazolium, pyrazolium, pyridinium cations, orthoborate

https://dx.doi.org/10.1021/acs.chemrev.9b00693
Chem. Rev. 2020, 120, 5798−5877

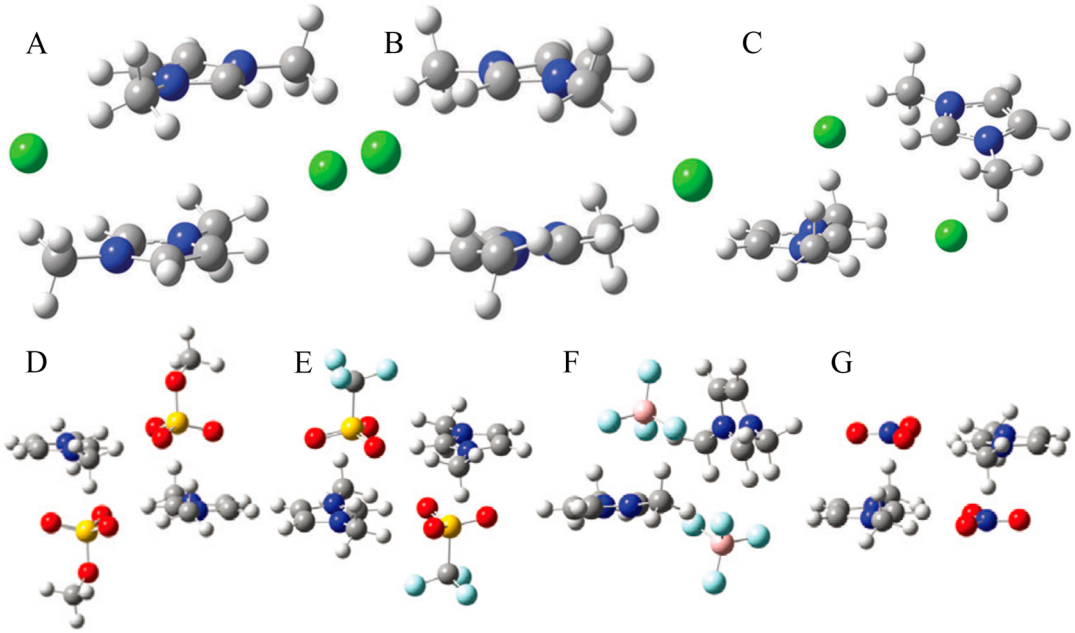

Figure 7. Optimized [C_1MIM]Cl ion pair dimer structures determined from quantum chemistry calculations ((A) and (B) are middle configurations, and (C) is the diagonal configuration). Reproduced with permission from ref 149. Copyright 2014 Royal Society of Chemistry. Ion pair dimer structures for (D) [C_1MIM][C_1SO4], (E) [C_1MIM][TFO], (F) [C_1MIM][BF_4], and (G) [C_1MIM][NO_3] obtained from DFT calculations. Reproduced with permission from ref 252. Copyright 2014 IOP Publishing.

anions, and their derivatives, despite the strong repulsive electrostatic forces between ring moieties having like charges.[6,60,273−278]

Matthews and Hunt performed DFT calculations to explore microstructural and energetic landscapes of $\pi-\pi$ stacking structures in [C_1MIM]Cl ion pair dimers.[149,252,279] Imidazolium ring stacking structures are described as electron deficient $\pi-\pi$ stacking interactions, and a competitive on-top ion pair structure is identified as a peculiar anion-donor π-acceptor coordination pattern between imidazolium ring planes and anions. Ion pair dimers display a subtle balance of varied microstructural features. The low-energy middle $\pi-\pi$ stacking conformer (Figure 7A) exhibits a front and side arrangement where imidazolium rings exhibit parallel-displaced and stacking structures, analogous to benzene dimers,[149,279] whereas in a low-energy diagonal conformer (Figure 7C) front and top arrangements dominate.[279] An energy barrier of ∼6.1 kJ/mol exists for conversion of a $\pi-\pi$ stacking structure (Figure 7B) to a diagonal conformer with no $\pi-\pi$ stacking (Figure 7C), indicating that such a structural conversion is a facile process in the liquid phase.[149,252] In addition, rotation of methyl groups within $\pi-\pi$ stacking structures facilitates the formation of linear secondary alkyl C−H···Cl HBs, which decay faster with distance than primary ring C−H···Cl HBs and C(2)···Cl anion$-\pi$ interactions. Theoretical analysis showed that a subtle structural difference of these stacking structures of [C_1MIM]Cl ion pair dimers is mainly attributed to an array of weak and strong HBs, anion$-\pi$, and $\pi-\pi$ stacking interactions. The energy differences between cation−anion HB interactions, anion$-\pi$ associations, and cation−cation $\pi-\pi$ stacking interactions are all very small (<10 kJ/mol), and their competition creates a very delicate balance of forces within liquid environments. These interactions fluctuate in strength, forming a small number of strong interactions and a larger number of moderate interactions with very little cost in energy. This is striking and in contrast to biological systems and some crystal structures where $\pi-\pi$ stacking, anion$-\pi$, and HB interactions impart remarkable secondary structures.[279]

Furthermore, the impact of anion electronic structures on disruption of $\pi-\pi$ stacking interactions was identified by a substitution of Cl with a range of large anions with diffuse charge (i.e., [NO_3], [C_1SO_4], [TFO], and [BF_4]).[252] A diagonal ion pair dimer structure is the most stable configuration in energy for large anions, reflecting a propensity of large multidentate [C_1SO_4] (Figure 7D), [TFO] (Figure 7E) and [BF_4] anions (Figure 7F) to favor top interactions. Based on analysis of molecular orbitals and electronic structures, it is evident that there is a subtle interplay between traditional in-plane HB coordinations and peculiar interplanar anion$-\pi$ interactions, the latter of which is particularly prominent for [C_1MIM][NO_3] ion pair dimers (Figure 7G). All these interactions have a significant impact on structural arrangements in ILs and highlight the influence of dispersion forces and the importance of HB interactions on the formation of $\pi-\pi$ stacking structures in imidazolium ILs.

Subsequent first-principles calculations also revealed preferential $\pi-\pi$ stacking interactions in [C_2MIM]Cl and [C_2MIM]-[SCN] ILs and their mixtures.[277] A weak $\pi-\pi$ ordering structure was observed in [C_2MIM][SCN] in comparison with that in [C_2MIM]Cl, and an intermediate $\pi-\pi$ stacking structure was observed in their mixture with an equimolar fraction. In addition, $\pi-\pi$ stacking dimer structure was also formed between imidazolium ring planes in [C_2MIM][NO_3],[6] [C_2MIM]$_2$[SO_4],[6] and [C_2MIM][NTF_2][275] crystal structures owing to a substantial screening of charge−charge repulsive forces among cation species mediated by anions. XRD data, complemented by atomistic simulations, revealed that Br anions in [C_2MIM]Br liquid phase are symmetrically distributed around [C_2MIM] cations and are more closer to ring moieties than those in crystal structures.[276] Thus, π-type interactions are recognized as a key component for local structuring of imidazolium ILs.

https://dx.doi.org/10.1021/acs.chemrev.9b00693
Chem. Rev. 2020, 120, 5798−5877

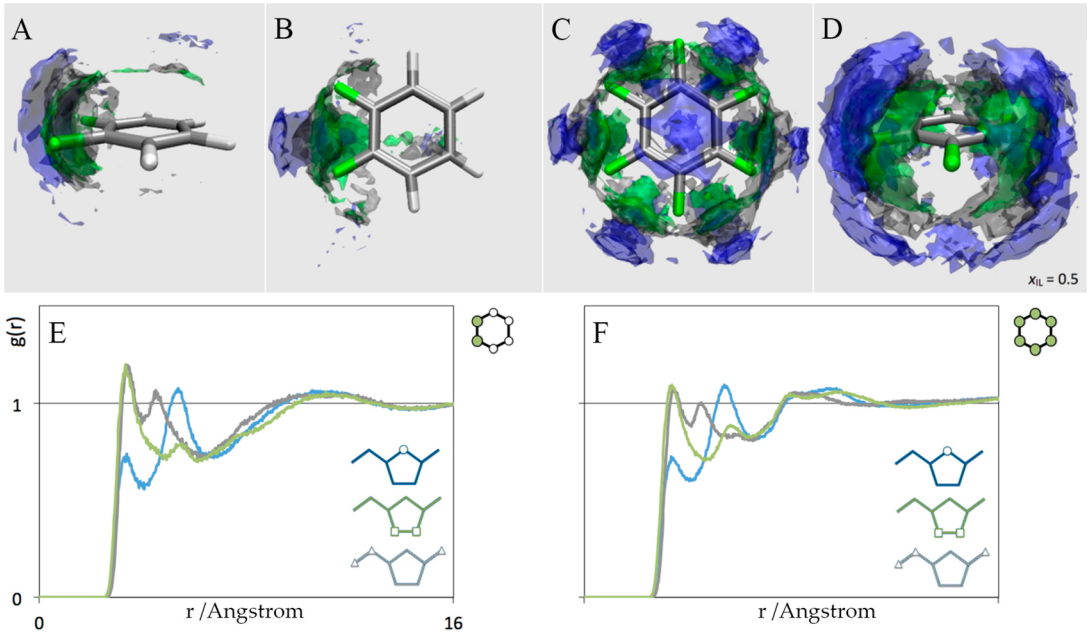

Figure 8. Spatial distributions of C(2) (blue), C(5) (green), and C(6) (gray) atoms around (A, B) 1,2-difluorobenzene and (C, D) hexafluorobenzene molecules in equimolar IL−aromatic mixtures. Radial distribution functions between carbon atoms in imidazolium cations (C(2), blue; C(5), green; C(7), gray) and fluorine atoms in (E) 1,2-difluorobenzene and (F) hexafluorobenzene in equimolar IL−aromatic mixtures. Reproduced with permission from ref 152. Copyright 2014 American Chemical Society.

For imidazolium cations with intermediate alkyl chains, dispersion interactions between alkyl chains play a dominant role.[280] Nuclear Overhauser effect experiments suggested a local short-ranged cation−cation stacking structure in $[C_4MIM][BF_4]$ and in its C(2)-methylated analogue.[281] A further lengthening cation alkyl chains results in the formation of ionic liquid crystals, in which interdigitation of alkyl chains facilitates alignment of imidazolium rings such that $\pi-\pi$ stacking interaction becomes more significant. Various lyotropic liquid crystalline phases were obtained in mixtures of $[C_nMIM]Br$ ILs (n = 12, 14, and 16) with p-xylene and water.[282] Strong $\pi-\pi$ stacking interactions of imidazolium rings and cation−π interactions with p-xylene have unique influences in determining structural properties, especially the thickness of water channels in mixtures. In addition, both rheological steady and dynamic moduli of these liquid crystalline phases increase with lengthening cation alkyl chains, leading to their promising applications in fabrication of nanomaterials.

Moreover, an incorporation of benzene (and its fluorinated derivatives) in imidazolium ILs can significantly alter microstructures and, in particular, cation−cation interactions.[152,283,284] Benzene molecules tend to displace anions by intercalation into high-charge density domains. This intercalation is attributed to $\pi-\pi$ stacking interactions between imidazolium ring planes and benzene molecules rationalized by attractive arrangements of quadrupole moments.[283,285−287] *Ab initio* and atomistic MD simulations showed that quadrupole moments of aromatics are an almost linear function of the number of fluorine substitutions,[89,152] which is fully reflected in spatial arrangements of imidazolium rings around aromatics. Cations are mainly located above/below benzene plane (Figure 8) because of strong diamagnetic influence of aromatic electrons. As benzene is progressively fluorinated, cations migrate to equatorial plane of aromatics, experiencing a milder paramagnetic effect. Lengthening alkyl chains in imidazolium cations contributes to a finite probability for benzene to be found both in apolar domains and in polar networks, indicating that benzene experiences different local environments in heterogeneous IL matrixes.[288] Concerning dynamic features, atomistic simulations showed that rotation of benzene in $[C_4MIM]Cl$ is controlled by vdW and $\pi-\pi$ interactions on short time scales (picoseconds) and by solvent charge associations on long time scales (hundreds of picoseconds).[289] OHD-OKE experiments on $[C_1MIM][NTF_2]$-benzene[89] and $[C_8MIM][BF_4]$-benzene[290] mixtures showed different intensities in comparison with their ideal mixing spectra, which is attributed to suppressed translational motions of benzene in mixtures.

2.2.3. Hydrogen Bonding vs $\pi-\pi$ Stacking Interactions. HB coordinations and $\pi-\pi$ stacking interactions have distinct effects on stabilization of liquid structures of ILs having heteroaromatic rings and multiple HB donor and acceptor sites.[252,279] For imidazolium cations paired with small anion species, such as Cl,[277,279] $[NO_3]$,[252] and [SCN],[277] $\pi-\pi$ stacking structures coexist with HB coupling between ion species, promoting the formation of decent microscopic ion structures in bulk ILs.[252,277,279] *Ab initio* molecular dynamics (AIMD) simulations revealed distinct $\pi-\pi$ stacking conformations in $[C_2MIM][SCN]$, which decrease dramatically in $[C_2MIM][N(CN)_2]$ and $[C_2MIM][B(CN)_4]$ (tetracyanoborate) ILs.[153] HB interactions are very pronounced in $[C_2MIM][N(CN)_2]$ and $[C_2MIM][SCN]$ ILs with anions taking in-plane configurations of imidazolium rings, while HB interactions are almost absent in $[C_2MIM][B(CN)_4]$ with $[B(CN)_4]$ anions taking on-top conformations above/below imidazolium rings.[291] The small size of [SCN] anion together with its strong HB capability stabilize local ion arrangements as was pointed out for $[C_nMIM]Cl$ ion pair dimers.[149,279] Cyano ILs are generally viscous and their liquid dynamics are well correlated with rotational dynamics of cyano groups.[292] Both microstructural and dynamical quantities of these ILs exhibit

https://dx.doi.org/10.1021/acs.chemrev.9b00693
Chem. Rev. 2020, 120, 5798−5877

similar sequence as their viscosities, inferring that high viscosity of [C_2MIM][SCN] might be related to enhanced $\pi-\pi$ stacking interactions between imidazolium rings.

For ILs composed of imidazolium cations paired with large anion species, like [C_1SO_4][252] and [NTF_2],[59,275,278] both $\pi-\pi$ stacking interactions and HB coordinations get weakened. These anions have multiple HB acceptors and have preferential HB coordinations with imidazolium cation hydrogen atoms, promoting the formation of HB networks with distinct HB strength and directionality. Additionally, these large anions prefer configurations above and below imidazolium rings or exhibit tilted orientations in equatorial region of imidazolium rings, leading to cation−cation π-type coordination being partially weakened or totally screened due to anion size effect. Therefore, HB networks overtake π-type interactions and have a significant effect on local ionic structures and complex liquid morphologies of ILs.

The subtle balance of HB and $\pi-\pi$ stacking interactions among ion species, either competitive or cooperative, will be more sophisticated if anions have planar rings, such as orthoborate anions.[61,217,293−296] For [C_nMIM][BOB] ILs, AIMD simulations revealed that preferential HB interactions and remarkable $\pi-\pi$ coordination among neighboring imidazolium and oxalato ring planes coexist in ILs (Figure 9).[61,217] HBs are formed between imidazolium cation hydrogen atoms and [BOB] anion oxygen atoms but with different HB features. At short radial distances, imidazolium rings exhibit $\pi-\pi$ stacking associations (Figure 9A) and present complicated orientational distributions at intermediate and large radial distances due to intervention of other ions. Spatial associations between imidazolium and oxalato ring planes are characterized by short-range $\pi-\pi$ stacking structures (Figure 9B) and displaced offset stacking conformations mediated by peculiar in-plane HB interactions (Figure 9C) and by distinct perpendicular distributions at intermediate radial distances because of attractive electrostatic interactions. The intermolecular interactions between oxalato ring planes are mediated by repulsive Coulombic interactions and steric hindrance effect, contributing to tilted orientations of oxalato ring planes to neighboring ones in local ionic environments (Figure 9D). A gradual lengthening of cation alkyl chains results in a substantial increase in interaction strength for all HBs. However, the strengthened HB interactions result in weakened $\pi-\pi$ stacking coordinations between imidazolium and oxalato ring planes, demonstrating significant competitive characteristics for HB and $\pi-\pi$ stacking interactions in [C_nMIM][BOB] ILs. In addition, intermittent and continuous HB dynamics exhibit a decent cooperative correlation feature with rotational and translational dynamics of ring moieties with increasing alkyl chains in imidazolium cations. The competitive structural trade-off and cooperative dynamical interplay of HB and $\pi-\pi$ stacking interactions in [C_nMIM][BOB] ILs are essentially correlated with preferential and collective associations among cation alkyl units and decisive Coulombic interactions among imidazolium and oxalate ring moieties in heterogeneous IL matrixes. These computational data may provide important physical insights for a thorough understanding of striking microstructures and dynamical quantities, and mesoscopic liquid morphologies of [C_nMIM][BOB] ILs as well as their macroscopic functionalities in industrial applications, for example, as promising solvent electrolytes in electrochemical devices or as alternative lubricants or lubricant additives in tribology.

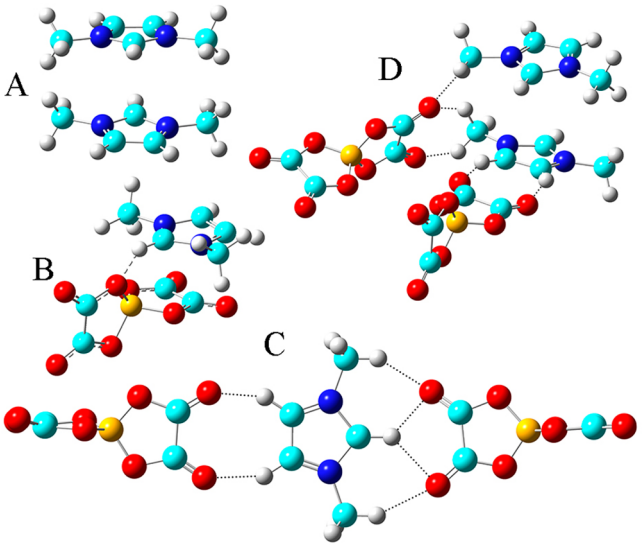

Figure 9. (A) Imidazolium ring pairs are featured with $\pi-\pi$ stacking orientation. Imidazolium and oxalate ring pairs are described by (B) $\pi-\pi$ stacking and (C) parallel displaced offset stacking configurations as well as hydrogen bonding interactions. (D) Intermolecular oxalato ring pairs are characterized by tilted distributions promoting their HB coordinations with cation hydrogen atoms. Reproduced with permission from ref 61. Copyright 2017 American Chemical Society.

2.3. Free Ions, Ion Pairs, and Ion Clusters

Since ILs are concentrated and solventless ion solutions, intimate ion pairs would be a natural expectation and many endeavors have been focused on describing bulk ILs as a large population of neutral ion pairs plus a small concentration of "free" ions or ion clusters.[18,135,271,297−303] Both mass spectrometric data and theoretical calculations suggested that distillation of ILs mainly occurs via neutral ion pair clusters of composition, followed by dissociation of large ion aggregates to lower order ion pairs and thereafter to small charged ion clusters in gas phase depending on the amount of internal energy for depositing charged clusters into neutral ion pairs upon evaporation.[304,305] These findings indicate that ion pairs might be available in bulk liquid phase, similar to that for a description of aqueous electrolyte solutions and Coulomb fluids. In addition, there are some postulations addressing that ILs form clustered supramolecular structures to maintain HB networks,[306] whereas other studies focused on ion cluster models including possible formation mechanism of IL ion clusters and effect of IL ion clusters on interfacial structures, liquid morphologies, and self-assembly processes of ILs in bulk liquids and in interfacial regions.[297] It should be noted that the concept of the ion cluster mainly comes from theoretical calculations and atomistic simulations. These studies should be carefully interpreted as there is no rigorous criteria to define an ion cluster and the distinction between different ion cluster models is arbitrary.[307]

Weingartner et al. suggested the formation of EAN ion pairs via measurement of critical behavior of EAN−octanol mixtures.[308] The obtained constant value describing ion pair associations from ion conductivity data is an order of magnitude larger than theoretical prediction of ion pairing behaviors in mixtures, suggesting that EAN may exist in a chemical equilibrium condition between "free" ions and ion

https://dx.doi.org/10.1021/acs.chemrev.9b00693
Chem. Rev. 2020, 120, 5798−5877

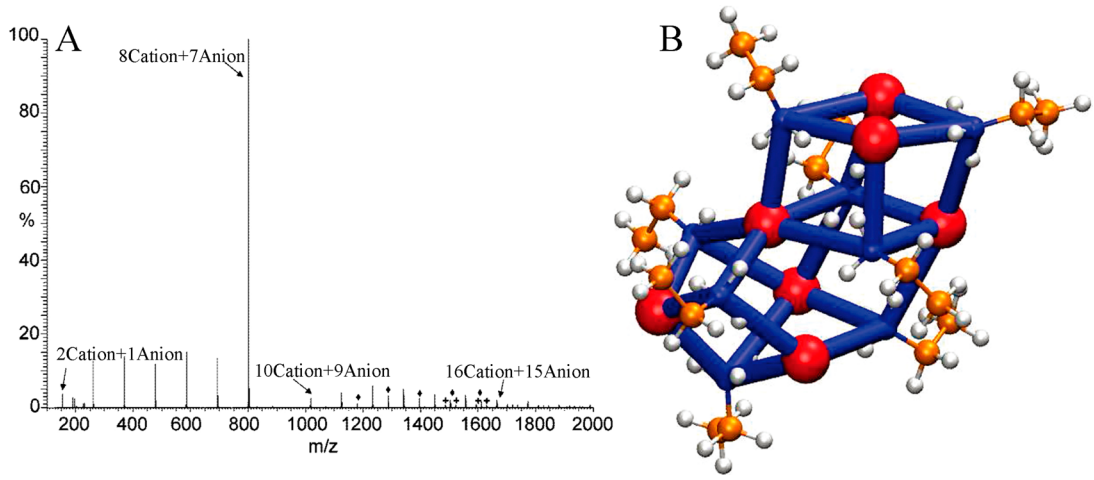

Figure 10. (A) Electrospray ionization mass spectrometry positive ion mode of EAN. Reproduced with permission from ref 299. Copyright 2009 American Chemical Society. (B) The most stable "8Cation+7Anion" model for EAN obtained from thermochemistry calculations. Hydrogen, carbon, and nitrogen atoms in EA cations are represented by white, orange, and blue spheres. [NO_3] anions are represented as red spheres. Reproduced with permission from ref 309. Copyright 2009 American Chemical Society.

pairs in the liquid region.[298] Ion pair lifetimes are close to those of ion coupling phenomena in alkali metal nitrate molten salts but are much larger than those for dilute aqueous electrolytes. Kennedy and Drummond proposed that protic ILs are composed of net charged ion clusters as they observed distinct ion aggregates with varied ion sizes from positive ion spectra of pure protic ILs, such as a dominant ion cluster consisting of eight cations and seven anions in EAN and PAN ILs (Figure 10A).[299] Therefore, it was suggested that EAN and PAN ILs are polydispersed mixtures consisting of aggregated ions and charged ion clusters. DFT calculations supported this hypothesis and showed that this particular ion cluster model is thermodynamically favorable for EAN in the gas phase and is the most stable species for entropic and enthalpic considerations because this ion cluster forms the most compact HB network in which all proton donors in EA cations and HB acceptors in [NO_3] anions are involved in an optimal way (Figure 10B).[309,310]

Dielectric spectra, theoretical calculations,[301,311] and atomistic simulations[271,300] on a range of aprotic imidazolium,[76,312] pyrrolidinium,[313] pyridinium,[313] and tetraalkylammonium[313] ILs did not display signatures of ion pair formation in bulk liquids. In an interesting work, Gebbie and co-workers provided a distinct view of bulk IL structures from DLVO (Derjaguin−Landau−Vervey−Overbeek) fits of SFA data.[135,136] For [C_4MIM[NTF_2] confined between two charged solid surfaces, a weak attractive force spanning from 3 to 30 nm was obtained, which is independent of applied electric potentials. The fitting of such a long-range force with DLVO theory predicts a negligible concentration of free ions in bulk liquids. Therefore, it was speculated that [C_4MIM]-[NTF_2] is a dilute electrolyte solution consisting of a large proportion of neutral ion pairs and a small fraction of dissociated free ion species, which is akin to the description of water consisting of an overwhelming majority of neutral water molecules plus some H_3O^+ and OH^- ions. It should be noted that while long-ranged forces might be real in IL matrixes,[314] the main conclusion of this work is conflict with many experimental and computational studies. An additional description indicated that DLVO theory is unsuitable to characterize phase behaviors of ILs because (1) ILs show complex association and dissociation equilibria,[315,316] (2) ion species change allegiances among neighboring counterions but not to single ion pairs or ion clusters in bulk liquids,[300,301] and (3) a long-range repulsive force was missing which should be accompanied by the long-ranged attractive force.

In another case, ion and electrical conductivities of [C_4MIM][PF_6] deviate from the Nernst−Einstein relationship,[271] which is attributed to correlated motion of ions having opposite charge and anticorrelated motion of ion species having the same charge over multiple timescales up to nanoseconds.[157,262,317,318] This scenario is distinct to that in electrolyte solutions, where positively correlated motion of ion species has a substantial contribution to decreased impedance conductivity.[318] On the basis of microstructural and dynamical analysis, this observation indicates that cation−anion interactions can be described using ion association instead of ion pair as each ion group is not solely paired to a single counterion nearby but to multiple counterions in ionic atmosphere. Additional atomistic simulations demonstrated that the formation of different ion associations is not so important to describe bulk IL structures as these ion units are weakly maintained together due to a small separation of ion species in bulk IL matrixes.[300] Therefore, it was suggested that the origin of destabilization of ion associations is caused by an overscreening of electrostatic charges in the first solvation shell.[301]

Modeling of bulk ILs as a continuum consisting of ion couples migrating together is not appropriate, which cannot be reconciled with their intrinsic character of low vapor pressure. It is known that the vapor pressure of liquid materials is correlated with ionicity, which is well represented in the Walden plot of molar conductivity against fluidity.[319] A separated neutral ion pairing unit does not have any contribution to ion conductivity and charge transferability. Therefore, ILs having a high proportion of neutral ion pairs or ion pairing aggregates should be "poor" liquids as ion conductivity and charge transferability will be less than expected from liquid viscosity. However, to some extent, most ILs are "good" liquids and have high ion conductivity, charge transferability, and low vapor pressure.[320] This might be attributed to the fact that spatial distributions of ion species in

https://dx.doi.org/10.1021/acs.chemrev.9b00693
Chem. Rev. 2020, 120, 5798−5877

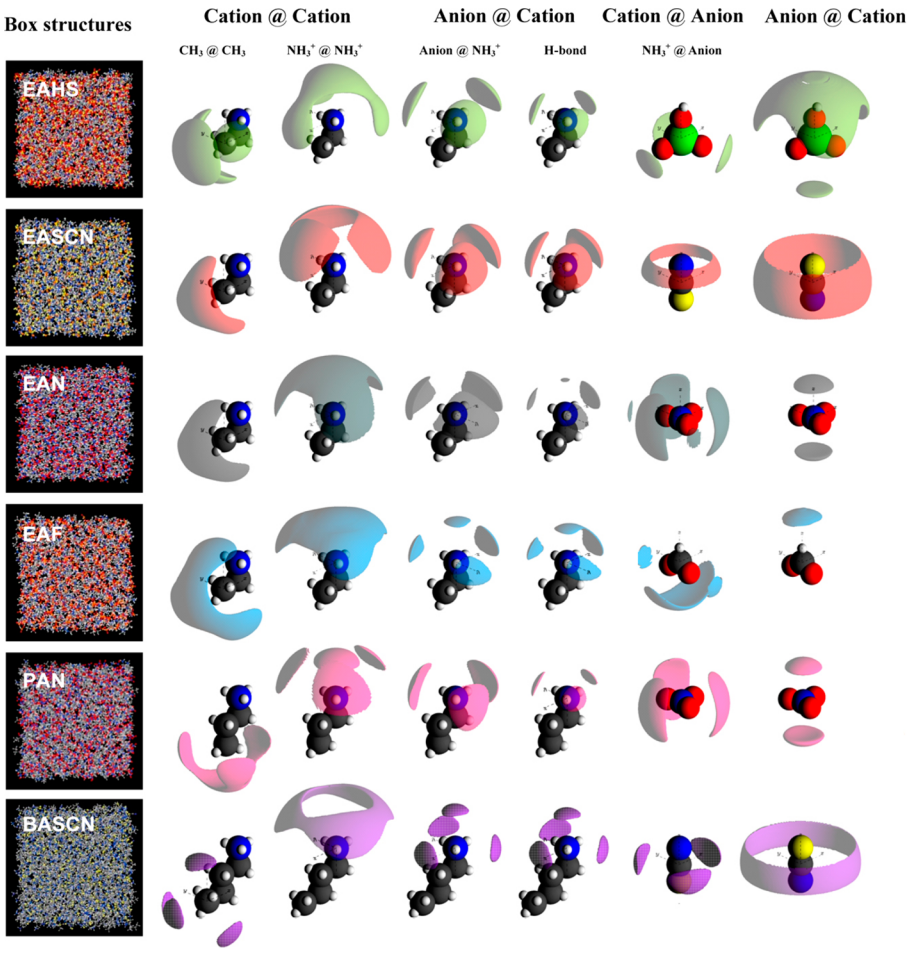

Figure 11. Nanostructures in primary alkylammonium protic ILs. Column 1 (left), box structures; column 2, uncharged groups in cations around uncharged groups in cations; column 3, charged groups in cations around charged groups in cations; column 4, charged groups in anions around charged groups in cations; column 5, HB acceptors in anions around HB donor sites in cations; column 6, charged groups in cations around charged groups in anions; and column 7, charged groups in anions around charged groups in anions. Reproduced with permission from ref 332. Copyright 2013 Wiley-VCH Verlag GmbH & Co. KGaA. Reproduced with permission from ref 190. Copyright 2014 American Chemical Society. Reproduced with permission from ref 18. Copyright 2015 American Chemical Society.

bulk ILs are highly heterogeneous with each ion surrounded by a shell of counterions exhibiting different configurations due to a delicate intermolecular interaction of central ion with neighboring counterions.

In contrast to pure ILs, some other investigations indicated that ILs may form ion pairing structures in IL−molecular solvent mixtures. The direct-contacted and solute-separated ion pairing structures were suggested in $[C_4MIM][BF_4]$−water and $[C_4MIM][BF_4]$−dimethyl sulfoxide mixtures.[321] In addition, $[C_4MIM][PF_6]$−naphthalene[322] and 1-methyl-4-cyanopyridinium $[NTF_2]$−methylnaphthalene[323] mixtures also exhibit cation−anion ion pairing and cation−aromatic pairing groups across a wide range of solute concentrations. Therefore, even the ion pairing concept is helpful to understand liquid structures in electrolyte solutions, it is not feasible to describe bulk IL structures. Transient ion pairing structures might exist in IL matrixes with their lifetimes shorter than picoseconds; however, it should be addressed that the overall liquid structures of bulk ILs are more complicated than a continuum of ion pairs, ion couples, and ion clusters in ion solutions.

2.4. Microstructures and Mesoscopic Liquid Morphologies

2.4.1. Alkylammonium ILs. Atkin and Warr[108] and Umebayashi et al.[189] investigated microstructures of EAN using complementary wide-angle X-ray scattering (WAXS) and small-angle neutron scattering (SANS) techniques, respectively. Both studies indicated that nanoscale heterogeneity exists in EAN with polar and apolar domains throughout the bulk liquid matrix, suggesting a disordered, locally smectic, or bicontinuous liquid structure. The solvophobic interactions among alkyl units are essentially responsible for production of nanostructural heterogeneity. In addition, both electrostatic and HB interactions between amine and $[NO_3]$ groups play a significant role in stabilizing microstructures in the EAN matrix.

Lengthening alkyl chains in alkylammonium cations leads to pronounced nanoscopic liquid structures in which apolar and polar domains are segregated and partially interdigitated, with ions in more precisely defined positions relative to one another.[108,192,195,324,325] HB networks are more stable and get stronger in ILs having longer cation alkyl chains owing to a distinct hydrophobic effect stemming from alkyl chain contacts. Equilibration within apolar domains, as evident from stretching dynamics of C−H bonds, is faster than that in

https://dx.doi.org/10.1021/acs.chemrev.9b00693
Chem. Rev. 2020, 120, 5798−5877

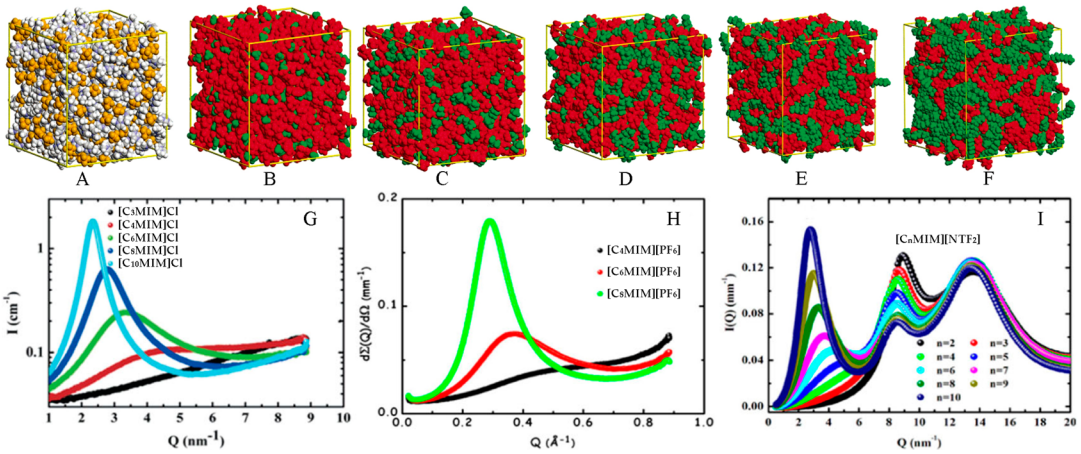

Figure 12. Snapshots of simulation systems containing 700 $[C_nMIM][PF_6]$ ion pairs. $[C_2MIM][PF_6]$ with (A) CPK color coding and (B) red (polar domain)-green (apolar domain) color coding, (C) $[C_4MIM][PF_6]$, (D) $[C_6MIM][PF_6]$, (E) $[C_8MIM][PF_6]$, and (F) $[C_{12}MIM][PF_6]$. Reproduced with permission from ref 343. Copyright 2006 American Chemical Society. (G) X-ray diffraction patterns for supercooled $[C_nMIM]Cl$ IL. Reproduced with permission from ref.[280] Copyright 2007 American Chemical Society. (H) X-ray diffraction patterns for $[C_nMIM][PF_6]$ ILs at 25 °C. Reproduced with permission from ref 345. Copyright 2008 Elsevier. (I) SWAXS data for $[C_nMIM][NTF_2]$ ILs at room temperature. Reproduced with permission from ref 346. Copyright 2009 IOP Publishing.

polar domains and shows a remarkably low thermal activation, indicating that ILs are not only structurally heterogeneous but also dynamics vary considerably among different substructures. Both ends of alkylammonium cations, namely, charged N−H head groups and hydrophobic tail C−H groups, exhibit rotational dynamics on different time scales. These rotational dynamics are heterogeneous and are governed by a local propellerlike motion of cations, which is intrinsically attributed to structural heterogeneity in IL matrixes.[187,193] The N−H head groups exhibit slow dynamics because of strong Coulombic interactions and preferential HB interactions with $[NO_3]$ anions, whereas the tail C−H groups exhibit fast dynamics due to their weaker vdW interactions with surrounding atoms. In particular, rotational dynamics of tail C−H groups show marginal dependence on cation alkyl chain length, while rotations of head N−H groups slow down with lengthening cation alkyl chains, demonstrating that dynamical heterogeneities are enhanced in ILs with longer alkyl chains in alkylammonium cations. Such a slowdown is mainly correlated with a decreased number of $[NO_3]$ anions near N−H groups, which presumably leads to an increase in energy barrier for their rotations and thus gives rise to a broad distribution of N−H rotation times. Furthermore, the relative free energy landscapes of cation−anion interactions exhibit a progressively deeper well as cation alkyl chains get longer.[192,326,327] These observations indicate that IL nanostructures are analogous to a surfactant mesophase, and thus the area ratio of polar and apolar domains will be useful to predict self-assembled liquid morphologies in alkylammonium ILs.[190]

Addition of hydroxyl groups to terminal methyl groups in EA cations leads to a disruption of solvophobic associations between alkyl chains in EtAN, resulting in small ion aggregates, rather than a spongelike liquid morphology with extended networks.[191,224] EtAN has a less ordered liquid arrangement than that of EAN since $[NO_3]$ anions are competitively coordinated with both ammonium and hydroxyl groups in EtA cations via strong HB interactions.[328,329] Generally, inclusion of additional HBs represents a source of defects in polar networks, leading to more disordered microstructures in ILs.[94,223,255,330] In addition, both translational and rotational dynamics of constituent ions slow down due to the formation of HB networks in IL matrixes. When an external electric field is applied, EtAN requires a lower electric field strength than that for EAN to emit ion pairs.[331] The applied electric field can effectively reduce the number of hydroxyl−$[NO_3]$ HBs but is less effective in disrupting HBs between N−H head groups and $[NO_3]$ anions.

Besides variations in cation structures, anions also have a significant effect on microstructures in a range of ILs consisting of primary alkylammonium cations coupled with Br, $[NO_3]$, [OAc], $[HSO_4]$, [SCN], formate, triflate ($[CF_3SO_3]$), and alkylsulfonate anions.[190,324,325,329,332−334] Representative spatial distributions of HB acceptors around donor sites are shown in Figure 11. Ion arrangements in these ILs are consequently attributed to a delicate balance of ion dimensions and varied intermolecular forces among constituent ions. While similar nanostructures characterized by bicontinuous liquid morphologies were formed in all these protic ILs, there is a substantial difference in HB features. More cation−anion HBs are formed when anions have multiple HB acceptors and build up a dense, cooperative HB network.[332] HB geometries are intrinsically related to capability of each ion to accommodate HBs in bicontinuous networks rather than creating a different structure in bulk liquids. When liquid structures are such that there is a high proportion of linear HBs, attractions between ion species increase and ILs exhibit solidlike phase behavior. In contrast, nanostructures with bifurcated or trifurcated HBs produce weak and bent HBs, leading to decreased cation−anion attractions, and therefore ILs are more fluidlike materials. These differences in HB interactions are reflected in macroscopic physicochemical properties, like melting points, glass transition temperatures, ion conductivities, and liquid viscosities of alkylammonium ILs.[18]

2.4.2. Imidazolium ILs. The first speculation of the existence of mesoscopic liquid structures in imidazolium ILs was suggested on the basis of experimental measurement of diffusive properties of electroactive solute molecules dissolved in imidazolium IL−water mixtures.[335] Neutral and charged solutes exhibit distinct diffusion coefficients, indicating that binary imidazolium IL−water mixtures should not be

https://dx.doi.org/10.1021/acs.chemrev.9b00693
Chem. Rev. 2020, 120, 5798−5877

considered as homogeneous liquids but have to be treated as nanostructured solvents consisting of polar and apolar domains. Later systematic measurements of physicochemical properties (densities, viscosities, diffusion coefficients, ion conductivities, *etc.*) of $[C_nMIM][NTF_2]$ ILs with cations having varied alkyl chains[262] and a suggestion of structural heterogeneity being the underlying microscopic origin of the "red-edge effect" observed in fluorescence spectroscopy[64] showed that experimental and computational studies are consistent with the hypothesis of microstructural and dynamical heterogeneities in imidazolium ILs.

Subsequent molecular simulations further suggested that aprotic imidazolium ILs can self-assemble and form solvent nanostructures. CG simulations of $[C_nMIM][NO_3]$ ILs demonstrated that imidazolium rings and $[NO_3]$ anions are relatively homogeneously distributed in bulk liquids. However, alkyl groups aggregate into spatially heterogeneous apolar domains, which is attributed to a competitive coordination between long-range electrostatic interactions among charged groups and short-range collective solvophobic associations between hydrophobic alkyl chains.[336,337] This observation is more significant for cations having long alkyl chains, contributing to the formation of liquid crystal-like structures.[184,338,339] The application of external electric fields can substantially affect spatial heterogeneities of ILs, which are first disordered from spatially heterogeneous to spatially homogeneous structures, and thereafter get reordered to nematic-like structures with a gradual increase in external electric field strength.[340,341] Translational diffusion of ions increases in the homogeneous regime and decreases in the nematic-like region, attributing to a competition between electrostatic interactions among ion species and the formation of ion cage structures under external electric fields.

ILs composed of imidazolium cations paired with varied spherical anions (F, Cl, Br, $[BF_4]$, and $[PF_6]$) present a similar picture of heterogeneous microstructures in IL matrixes but with a few important differences.[342,343] Polar domains in imidazolium ILs have heterogeneous distributions and form continuous ion channels in IL matrixes. Polar domains coexist with apolar domains consisting of hydrophobic alkyl groups. Simulation snapshots showed in Figure 12A−F, particularly those rendered under green (apolar domain) and red (polar domain) convention, provide a clear visualization on the evolution of heterogeneous liquid structures as cation alkyl chain length increases. For imidazolium cations with short alkyl chains, like C_1 and C_2, small and globular apolar "islands" are formed within interpenetrating polar networks. Lengthening cation alkyl chains enables apolar "islands" to aggregate into spongelike liquid nanostructures. $[C_4MIM]$ cation marks a microstructural transition between these two solvent morphologies.

Whether these computational results are interpreted as indications of micelle-like structures or bicontinuous liquid morphologies, X-ray scattering data are compelling evidence of self-assembled solvent nanostructures. S/WAXS spectra exhibit a well-defined peak at ∼0.3 $Å^{-1}$ for $[C_nMIM]Cl$ (Figure 12G) and $[C_nMIM][PF_6]$ (Figure 12H) ILs with cation alkyl chains longer than C_4.[280,344,345] Not only peak amplitudes increase but also peak positions shift toward low q values with lengthening cation alkyl chains. Enlarging anions from small Cl (Figure 12G) to intermediate $[PF_6]$ (Figure 12H) and then to large and asymmetric $[NTF_2]$ (Figure 12I) has no discernible effect on the dependence of characteristic size of nanoscale heterogeneity on cation alkyl chain length,[280] highlighting the importance of apolar aggregation in self-assembly of imidazolium ILs in bulk liquids.[280,346]

While these experimental studies provide valuable results, the model used to rationalize scattering data at low q values is minimalistic. It does not take into consideration privileged correlations between similar polar−polar, apolar−apolar, and different polar−apolar moieties. Hardacre et al. conducted SANS experiments on imidazolium ILs and elucidated local ion−ion distributions via an empirical potential structural refinement (EPSR) fitting of SANS spectra.[347,348] Microstructural arrangements in imidazolium ILs exhibit a remarkable charge ordering feature which, to some extent, resembles ion structures in crystalline state following an onionlike alternating cation−anion shells. $[C_1MIM]$ cation is not amphiphilic because of the very short methyl groups, and thus its bulk liquid structures are principally determined by electrostatic interactions.[348] This cation serves as a reference for description of bulk correlation peak changes with lengthening cation alkyl chains. SANS spectra showed that enhanced structural heterogeneities are mainly originated from decreased symmetry of imidazolium cations as alkyl chain length increases.[347] For $[C_nMIM][PF_6]$ ILs with cations having intermediate alkyl chains that are long enough to produce apolar segregations, an unambiguous scattering peak was observed in the low q region (Figure 12H).[345] This peak moves to low q values (large spatial distances), sharpens, and increases in intensity with lengthening cation alkyl chains. These results indicate that lattice expansion and correlation are entirely related to apolar domains with an increase of ∼2 Å per methylene unit.[344,347]

Margulis and co-workers[155] came to a similar conclusion to that of Hardacre et al.[347] via performing atomistic simulations of bulk $[C_6MIM]Cl$, $[C_8MIM][PF_6]$, and $[C_{10}MIM][PF_6]$ ILs. The first sharp diffraction peak (FSDP) at low q values in the scattering spectra is regarded as an indicator of the mesoscopic liquid structure, attributing to segregation of polar and apolar domains in IL matrixes. While cation anisotropy may be important for the formation of FSDPs, it appears that FSDPs can be described by a much simpler consideration of solvation shell asymmetry.[347] In addition, neutron scattering data for protic[190] and aprotic[347] ILs are generally consistent with the spatial distance of a spongelike liquid phase, and thus the scattering peak for a sponge phase formed in these ILs can be considered as a gauge of bulk self-assembly due to an amphiphilic feature of constituent ions.

For ILs composed of imidazolium cations paired with $[NTF_2]$ anions, neutron scattering data and theoretical calculations showed that $[C_1MIM][NTF_2]$ has a negligible long-range alternating counterion ordering.[275] Russina et al. conducted S/WAXS characterizations on a series of $[C_nMIM]$-$[NTF_2]$ ($1 < n < 10$) ILs and highlighted their microstructural heterogeneities.[346] Three decent diffraction peaks are observed with two peaks at high q values displaying marginal dependence on the cation alkyl chain length and one peak at a low q value showing strong dependence of amplitude and position on cation alkyl chain length (Figure 12I). The latter is a signature of microstructural heterogeneity with its size related to alkyl chain segregation in apolar domains,[349] similar to that observed in imidazolium ILs consisting of Cl, $[BF_4]$, and $[PF_6]$ anions.[344,346,348]

Mutating a methylene (methyl) group with specific atoms, like hydrogen,[94,254] oxygen,[225,350] fluorine,[278,351] silicon,[85,352]

https://dx.doi.org/10.1021/acs.chemrev.9b00693
Chem. Rev. 2020, 120, 5798−5877

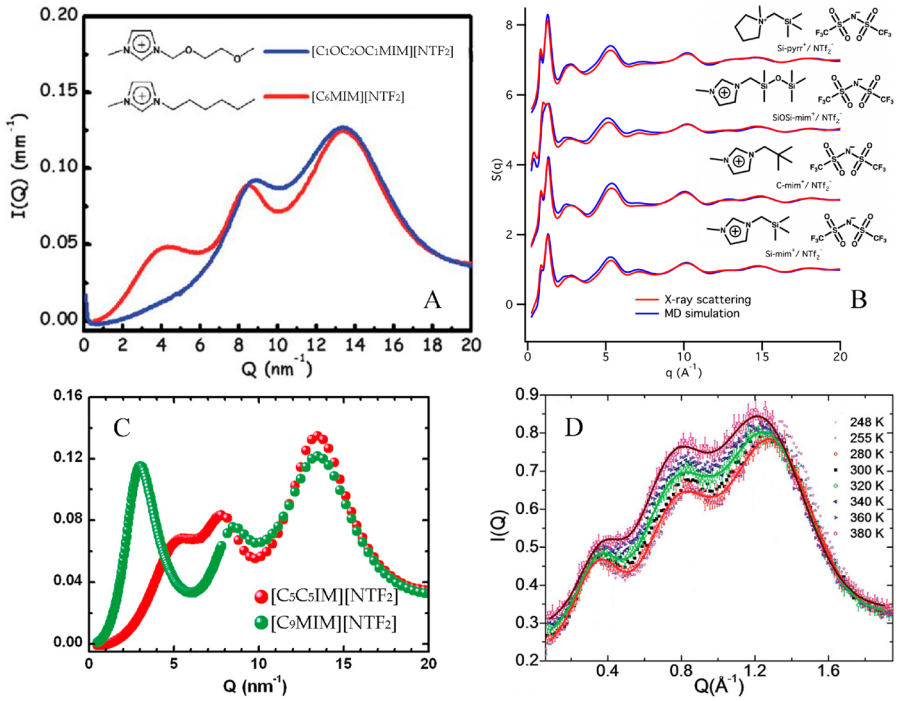

Figure 13. (A) SWAXS spectra for $[C_6MIM][NTF_2]$ and $[C_1OC_2OC_1MIM][NTF_2]$ ILs. Reproduced with permission from ref 225. Copyright 2012 Royal Society of Chemistry. (B) Experimental (red) and computational (blue) structure factors for four silicon-substituted imidazolium $[NTF_2]$ ILs. Reproduced with permission from ref 357. Copyright 2016 AIP Publishing LLC. (C) Comparison of SWAXS data for $[C_5C_5IM][NTF_2]$ and $[C_9MIM][NTF_2]$ ILs. Reproduced with permission from ref 358. Copyright 2011 American Chemical Society. (D) SWAX scattering intensities for double-headed $[C_{12}(MIM)_2][NTF_2]_2$ at varied temperatures. Reproduced with permission from ref 359. Copyright 2014 Royal Society of Chemistry.

selenium,[353] and even phenyl groups,[354−356] leads to distinct microstructural arrangements in heterogeneous IL matrixes.

Functionalization of alkyl chains using ether and hydroxyl groups disturbs a delicate balance of Coulombic, HB, and dispersion interactions, contributing to enhanced intermolecular interactions between constituent ions.[227,360,361] This has an overall effect on disrupting mesoscopic ordering structures, as revealed from peaks at low q values, which either have decreased scattering intensities or are totally disappeared. These changes in low q scattering are attributed to flexibility and increased polarity of alkoxy chains and favorable associations of ether and hydroxyl moieties with imidazolium rings via HB interactions.[225] Russina and Triolo compared SAXS data for $[C_6MIM][NTF_2]$ with its ether-substituted counterpart $[(C_1OC_1)_2MIM][NTF_2]$ (1-methoxyethoxymethyl-3methylimidazolium) and presented experimental evidence for mesoscopic liquid morphologies in these imidazolium ILs.[225] Later Shimizu et al. carried out a systematic study on $[C_nMIM][NTF_2]$ ILs (n = 3, 6, 9) and their ether-substituted $[(C_1OC_1)_{n/3}MIM][NTF_2]$ analogues.[350] A clear bulk structural peak is observed in the low q region for $[C_nMIM][NTF_2]$ ILs, but this does not occur when ether groups are present even though all ILs are isoelectronic (Figure 13A). SAXS data and atomistic simulations demonstrated that a suppression of nanostructures and the corresponding prepeaks in scattering structural functions for ether-substituted imidazolium cations occurs along the entire IL series, and this suppression of nanostructures is not due to any modification of ILs' polar networks but rather due to different morphologies of the surrounding apolar domains.[362] The microstructures in the apolar domains in $[C_nMIM][NTF_2]$ ILs are described by bulky segregated structures, which are transitioned to thin enveloping ones in $[(C_1OC_1)_{n/3}MIM][NTF_2]$ ILs. Such a microstructural transition is attributed to an inability of alkoxy chains for their effective side-by-side packing and the kinks along ether-substituted alkyl chains, which lead to scorpionlike intramolecular interactions among imidazolium rings and ether-substituted alkyl chains. As polyether chains are relatively polar, inter- and intramolecular driving forces are weak for spatial segregation of apolar moieties. This induces kinks along ether-substituted chains to form a clustered liquid morphology, which is similar to that in EtAN[224,363,364] and in ILs with imidazolium cations bearing hydroxyl and carboxyl terminal groups.[226,227,365,366]

The silicon-substituted imidazolium cations have advantages in some applications in comparison with carbon based imidazolium cations, and thus they are frequently used as solvent electrolytes and gas absorbents.[352] [SiMIM] (1-methyl-3-trimethylsilylmethylimidazolium) cation is very similar to $[C_nMIM]$ cations, in which the Si−C bond is slightly longer and more polar than the C−C bond, and therefore the [SiMIM] cation has a larger cation size and the Si atom has more excess charge than the corresponding carbon atom in $[C_nMIM]$ cation. Both electronic and size effects make intermolecular correlations in [SiMIM] ILs weaker than in $[C_nMIM]$ ILs,[357] leading to a low viscosity of [SiMIM]-$[NTF_2]$.[367−369] OHD-OKE spectroscopy revealed a generic correlation of low intermolecular vibrational frequencies for $[SiMIM][NTF_2]$ with its decreased liquid viscosity, which is distinct from that of $[C_nMIM][NTF_2]$ ILs.[367,368] An alkylsiloxy-substituted $[SiOSiMIM][NTF_2]$ (1-methyl-3-pentamethyldisiloxymethylimidazolium) has a decreased glass transition temperature and a low shear viscosity.[368] Despite its polar nature, pentamethyl-disiloxymethyl chains in

https://dx.doi.org/10.1021/acs.chemrev.9b00693
Chem. Rev. 2020, 120, 5798−5877

[SiOSiMIM] cations are long enough to display a distinct FSDP in X-ray scattering structural function (Figure 13B).[357] A dimethylphenylsilylmethyl substitution on imidazolium cations causes a substantial increase in liquid viscosities and glass transition temperatures.[368] It should be noted that [PhSiMIM][NTF_2] (1-dimethylphenylsilylmethyl-3-methylimidazolium) has higher shear viscosity and glass transition temperature than other silicon-substituted ILs, likely due to stronger intermolecular interactions. The diffusivities of small solutes in silicon-substituted ILs are faster than those in alkyl-substituted ILs with similar viscosities due to flexibilities of silicon-substituted alkyl chains and weak cation−solute interactions.[370]

Functionalizing imidazolium cations with aromatic moieties (benzyl groups) leads to significant and systematic changes in thermophysical properties of ILs. They have increased glass transition and melting temperatures arising from additional $\pi-\pi$ interactions.[371] Motivated by striking phase behaviors and distinct molecular dynamics of [C_nMIM][NTF_2]−benzene mixtures,[89,372] Xue et al. performed femtosecond optical-heterodyne-detected Raman-induced Kerr effect (OHD-RIKE) experiments and atomistic simulations on [BzMIM][NTF_2] (1-benzyl-3-methylimidazolium) and compared results with those for an equimolar [C_1MIM][NTF_2]−benzene mixture.[354] Kerr spectra showed marginal differences in spectral densities for phenyl and imidazolium rings, indicating a very similar local environment for these two ring moieties. Furthermore, intermolecular part of Kerr spectrum for [BzMIM][NTF_2] has lower intensity and higher frequency and is broader than that for the 1:1 [C_1MIM][NTF_2]−benzene mixture.[373] These results are rationalized as being a consequence of local liquid structures, which have $\pi-\pi$ stacking complexes involving a benzene molecule sandwiched between two imidazolium rings in 1:1 [C_1MIM][NTF_2]−benzene mixture. It should be noted that [BzMIM][NTF_2] is a glass-forming liquid,[355,371] whereas 1:1 [C_1MIM][NTF_2]−benzene mixture forms an inclusion crystal with a congruent melting temperature,[374] which is mainly maintained by $\pi-\pi$ stacking interactions between benzene and imidazolium ring planes and anion−π interactions of [NTF_2] with benzene π electrons.

For imidazolium ILs, most cations are characterized by an asymmetric feature with one nitrogen atom attached to either a hydrogen atom or a methyl group, and the other nitrogen is covalently bonded to an alkyl chain with varied chain length. It is known that cation symmetry provides distinct structural organizations that allow fine-tuning IL's physicochemical properties. There are two ways in tuning imidazolium cation symmetry. One is to bond two alkyl chains having the same number of carbon atoms to two nitrogen atoms in imidazolium rings.[358,375−378] The other is to functionalize terminal methyl group in long alkyl chain with an imidazolium ring.[379,380] The obtained symmetric imidazolium cations are described by double-tailed and double-headed structures, respectively.

For double-tailed imidazolium ILs, S/WAXS spectra showed that microstructural heterogeneity for an IL consisting of asymmetric imidazolium cations is larger than that for an IL consisting of double-tailed symmetric imidazolium cations.[358,375,376] Local liquid structures of double-tailed symmetric imidazolium ILs are more tightly packed and exhibit more solidlike behavior than ILs with asymmetric cations, as indicated by a high q peak being narrower for [C_5C_5IM][NTF_2] than that for [C_9MIM][NTF_2] (Figure 13C). Despite there are some controversies for the trend shift on enthalpies of vaporization, a nanostructuration effect in symmetric and asymmetric ILs is observed in their physicochemical properties.[262,358,375] [$C_{n/2}C_{n/2}$IM][NTF_2] ILs have higher volatilities and lower entropies of vaporization than [C_{n-1}MIM][NTF_2] ILs having the same number of carbon atoms in their alkyl substituents.[358,381] Moreover, [$C_{n/2}C_{n/2}$IM][NTF_2] ILs exhibit a striking odd−even feature in their enthalpies and entropies of vaporization.[381,382] With respect to intermolecular dynamics, OKE spectra for ILs having symmetric imidazolium cations are higher in frequency and broader than those for ILs having asymmetric imidazolium cations. In addition, an explicit difference was observed in the dependence of spectral parameters of the intermolecular part of the OKE spectrum of [C_nC_nIM][NTF_2] ILs on cation alkyl chains from ethyl to propyl groups,[358,375,376] indicating that alkyl chain segregation occurs at n = 3.

Besides distinct microstructural and dynamical heterogeneities in double-tailed imidazlium ILs, double-headed (divalent or dicationic) imidazolium ILs exhibit different microstructures,[359,383−385] dynamics,[385−387] and solvent properties.[380,386,387] S/WAXS experiments and atomistic simulations showed enhanced spatial heterogeneities in [C_n(MIM)$_2$][NTF_2]$_2$ ILs characterized by changes in scattering intensities and heterogeneity order parameters as the alkyl chain length increases from n = 3 to 6, and 12.[359] The bulk liquid structures and ion diffusivities of double-headed imidazolium ILs are substantially depend on the length of alkyl chain linkage separating two imidazolium rings.[383,385,388] Double-headed imidazolium ILs with short alkyl linkages exhibit almost identical mesostructural features as that for monovalent imidazolium ILs, regardless of anion types, whereas double-headed imidazolium ILs with long alkyl spacers between imidazolium rings display a very small prepeak and a low microstructural heterogeneity.[359,385,389] Moreover, anions have a weak effect on bulk liquid structures, but they are well organized around imidazolium rings with similar spatial distributions as in monovalent ILs,[389,390] leaving a low-density region around the alkyl linkage between two imidazolium rings in double-headed imidazolium ILs.[385,390] Variations in temperatures have a slight influence on locally assembled polar and apolar nanostructures for double-headed imidazolium ILs in comparison with monovalent ones. The scattering peaks at 0.9 $Å^{-1}$ and 1.4 $Å^{-1}$ are shifted toward lower q values as temperature increases (Figure 13D), which are reflected in variations in heterogeneity order parameters determined from atomistic simulations.[359,383−385,388] In addition, double-headed ILs are "subionic", relatively "superfragile", and moderately non-Newtonian fluids with positive Gibbs free energies of activation.[391]

In general, microstructural heterogeneity of ILs is accompanied by distinct dynamic heterogeneity of constituent ions.[11] Dynamic heterogeneity implies a distribution of spatial regions with varied relaxation rates, which are determined by a competition between short-range vdW interactions arising from hydrophobic alkyl chains and long-range Coulombic interactions from polar groups. This picture provides an appealing insight into microscopic origin of nonexponentiality that arises from ensembles of ions having fast and slow dynamics.[392] Indeed the diffusion mechanism of ions in IL matrixes is more complicated than originally expected,[393] which may have additional hints for rationalizing striking dynamical quantities in self-assembled IL matrixes.

https://dx.doi.org/10.1021/acs.chemrev.9b00693
Chem. Rev. 2020, 120, 5798−5877

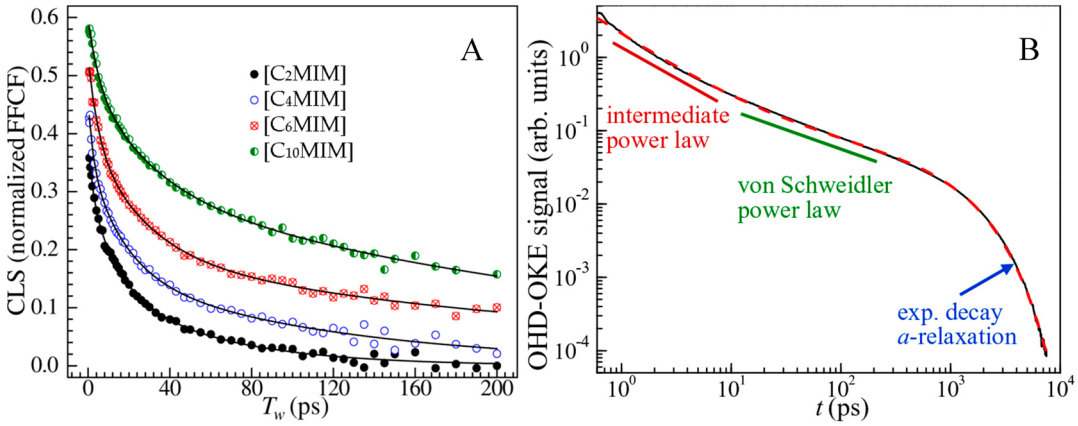

Figure 14. (A) Isotropic spectral diffusion of CO_2's asymmetric stretching in $[C_nMIM][NTF_2]$ ILs. Reproduced with permission from ref 394. Copyright 2016 American Chemical Society. (B) Representative OHD-OKE data for $[C_4MIM][BF_4]$. Reproduced with permission from ref 91. Copyright 2014 Elsevier.

The experimental data from ultrafast infrared spectroscopy and OHD-OKE spectroscopy are used as evidence to describe heterogeneous dynamics of ions in inhomogeneous ILs, which occur on different time scales. Fayer and co-workers performed ultrafast spectroscopy to study rotations and local structural fluctuation dynamics of CO_2 in $[C_nMIM][NTF_2]$ ILs, which are promising solvents for CO_2 capture.[91,92,394,395] The rotational dynamics of CO_2 occur on three time scales, corresponding to two different time scales of restricted wobbling-in-a-cone motions and a long-time complete diffusive rotational randomization. In addition, the complete rotational randomization of CO_2 and the structural fluctuation of ILs in supported IL membranes ($[C_2MIM][NTF_2]$ in poly(ether sulfone)) are slower than those in bulk liquids by approximately 2−3-fold in spite of large pore size (350 nm) in supported membranes. Experimental results indicated that variations of IL structures induced by polymer interface span more than hundred nanometers from the interfacial region, influencing dynamics of ion species and rotational dynamics of CO_2.[395,396] Furthermore, rotation of CO_2 slows down with lengthening cation alkyl chains but less than that in liquid viscosities of imidazolium ILs (Figure 14A).[394] These experimental results demonstrated that once there are substantial apolar regions in IL matrixes, making these regions larger does not change long-time-scale spectral diffusion dynamics experienced by CO_2. Therefore, if a process is to be optimized for carbon capture, liquid dynamics that actually influence CO_2 absorption should be systematically considered. OHD-OKE experiments showed that rotational relaxations of ILs have a complex time dependence that span from a few hundred femtoseconds to hundreds of nanoseconds with several power laws and a final exponential decay (Figure 14B).[90,91,93,397] The power laws reflect dynamics on time scales during which a molecule is "caged" by surrounding molecules, and the final exponential decay is the diffusive complete rotational randomization of ion species.

Related information on dynamical heterogeneities of ILs were obtained from NMR experiments,[87,262,398] atomistic[156−158] and CG[66−68,133,184,336] simulations on single (van Hove correlation function, incoherent intermediate scattering function, non-Gaussian parameter, diffusional anisotropy, *etc.*) and collective (self-diffusivity, thermal and ion conductivity, shear viscosity, rotation, *etc.*) dynamical quantities. Despite some discrepancies between NMR measurements and simulation results, the dynamical heterogeneities of ILs and changes in single and collective dynamical quantities with temperatures are qualitatively captured. In general, imidazolium cations have enhanced heterogeneous dynamical quantities in comparison with their paired anion species, and a small fraction of highly mobile cations contribute to their distinct self-diffusivities in IL matrixes.[66−68,185] Imidazolium cations structurally relax faster but rotationally relax slower than their coupled anion species at all temperatures. In addition, there is a distinct temperature dependence of rotational anisotropy for imidazolium cations but only a weak temperature dependence for anion species. Ion conductivities of ILs are significantly influenced not only by ion sizes but also by shapes of constituent ions. Variations in self-diffusion coefficients, viscosities, and ion conductivities with temperatures follow a Vogel−Fulcher−Tammann (VFT) equation.[262] All in all, the dynamical behaviors of ILs are extremely complex and consist of many different relaxation modes spanning multiple time scales. The sizes and shapes of IL ions and delicate interplay of interactions among constituent ions contribute to distinct dynamical heterogeneities of ILs in heterogeneous ionic environments.[156]

In addition to temperature changes,[399] effects of other external constraints, such as pressure,[400−405] shear flow,[406] and electric field,[407,408] on microstructural and dynamical heterogeneities of bulk ILs have been investigated via numerous experimental and computational studies. Imidazolium ILs consisting of either small halides (Cl,[409,410] Br[409]), $[BF_4]$,[401,411] $[PF_6]$,[404,412] or $[NTF_2]$ anions[400,405] exhibit complicated phase behaviors due to conformational flexibilities of alkyl chains. The external constraints can significantly affect conformational equilibrium of imidazolium cations and anions, like $[NTF_2]$,[400,405,409] which directly contribute to distinct IL structural transitions. For $[C_nMIM][NTF_2]$ ILs, the presence of sandwiched structures of $[NTF_2]$ anions between neighboring imidazolium rings leads to a substantial hindrance for alkyl chains to curl and consequently to dissolve polar−apolar alternations at high pressures.[400] This behavior is distinct from that of $[C_nMIM][BF_4]$ ILs where locations of $[BF_4]$ anions favor curling of alkyl chains and consequent changes in liquid structural organization.[411] In addition, $[C_nMIM][NTF_2]$ ILs with n = 3−10 form a glassy state at high pressures. Intriguingly, the glass transition pressure slightly increases up to n = 5, reaches a plateau at n = 8, and

https://dx.doi.org/10.1021/acs.chemrev.9b00693
Chem. Rev. 2020, 120, 5798−5877

increases again at n = 10.[405] This is completely different from high-pressure glass formation of $[C_nMIM][BF_4]$ ILs.[403] These findings are intrinsically correlated with the fact that $[C_nMIM][NTF_2]$ ILs are resistant to external pressures and prefer to retain their local liquid structures by essential conformational adjustments of $[C_nMIM]$ cations and $[NTF_2]$ anions at high pressures.[82]

2.4.3. Pyrrolidinium ILs. Pyrrolidinium ILs are widely used in electrochemical applications because of their wider electrochemical windows and higher electrochemical stabilities than imidazolium analogues.[413,414] SAXS and atomistic simulations showed that effects of alkyl chain lengths and temperatures on nanoscale organization of $[C_nMPYRR][NTF_2]$ ILs[415−418] are similar to those reported for $[C_nMIM][NTF_2]$ IL series even though imidazolium cations are planar and aromatic and pyrrolidinium cations are nonplanar and nonaromatic.[280,346,347] However, the FSDPs for $[C_nMPYRR][NTF_2]$ ILs with long cation alkyl chains display a remarkable shift to high q values with increasing temperatures,[417] which is rationalized by a competition between strong charge ordering associations of ions and vdW interactions between alkyl chains in $[C_nMPYRR]$ cations. This observation highlights a charge ordering pattern of polar moieties resulting from electrostatic ion ordering at short distances and a complex association among cation alkyl chain at long distances. The self-aggregation of alkyl chains and the dependence of polar group ordering on alkyl chain length provide a clear view of heterogeneous microstructures in $[C_nMPYRR][NTF_2]$ ILs. Rotation dynamics of $[C_nMPYRR]$ cations and $[NTF_2]$ anions are anisotropic, and the degree of anisotropy increases with decreasing temperatures. Electrostatic interactions between constituent ions are mainly responsible for decreased ion conductivities and increased viscosities of $[C_nMPYRR][NTF_2]$ ILs with larger effects at lower temperatures.[419]

In addition, constituent species (head and tail groups in cations and anions) of $[C_nMPYRR][NTF_2]$ ILs are structurally complex and can be conformationally modified by applying pressures.[419−422] The Margulis and Castner Jr. groups did comprehensive studies on microstructures of ILs consisting of a common $[NTF_2]$ anion coupled with varied pyrrolidinium cations (1-(cyclohexylmethyl)-1-methylpyrrolidinium, 1-(2-ethylhexyl)-1-methylpyrrolidinium, and 1-alkyl-1-methylpyrrolidinium) via SAXS experiments and atomistic simulations.[415,418,423] Both polarity and charge orderings decrease with increasing pressures as correlations of polar and apolar moieties are susceptible to applied pressures.[422] Alkyl tails in cations possess an increased number of gauche defects at higher pressures, leading to their increased bending and curling in heterogeneous ILs.[424] In addition, $[C_nMPYRR][NTF_2]$ ILs exhibit distinct changes in polarity and charge alternations upon pressuring these ILs with cations having branched and cyclic tails.[415,423]

Besides variations of pyrrolidinium cation alkyl chains, the inclusion of an additional methylene unit in pyrrolidinium ring leads to piperidinium and pyridinium ILs characterized by distinct microstructures and complex phase behaviors, as revealed from S/WAXS experiments.[126] Lengthening cation alkyl chains in $[C_nMPIP][NTF_2]$ ILs (n = 1−8) leads to a decrease in thermal stabilities and ion conductivities of ILs.[425] Although prominent peaks are observed in low q region in S/WAXS plots for $[C_nMPIP][NTF_2]$ ILs with alkyl chains ranging from C_2 to C_7, their peak positions are distinctly higher than those for imidazolium ILs, indicating a smaller characteristic length of microstructural heterogeneity in nonaromatic ILs than that in aromatic ILs.

Variations of cation structures from $[C_4MPYRR]$ to $[C_4HPYRI]$ and $[C_4MIM]$ lead to significant changes in low-frequency Kerr spectra when these cations are coupled with $[NTF_2]$ anions.[426] For ILs containing aromatic cations, such as $[C_4MIM][NTF_2]$ and $[C_4HPYRI][NTF_2]$, spectral intensities in the low-frequency region below 20 cm^{-1} increase and representative spectral peaks in the high-frequency region at around 80 cm^{-1} shift to lower frequencies with increasing temperatures. These shifts are attributed to distinct activation of translational and vibrational motions of ion species at high thermal energies and fast librational motions of aromatic rings due to large free volumes and weak intermolecular interactions at high temperatures. Small differences between imidazolium and pyridinium ILs are correlated with a delicate interplay of intermolecular interactions (vdW, HB, $\pi-\pi$ stacking, and Coulombic interactions) among constituent ions and, in particular, electronic structures of cations.[427] In contrast, ILs containing nonaromatic cations only exhibit an increase in spectral intensities at the low-frequency region, while spectra at the high-frequency region show little change with increasing temperatures, indicating that the presence of aromatic rings influences temperature-dependent spectral features, especially at the high-frequency region.

The presence of static microstructural heterogeneity of pyrrolidinium ILs leads to distinct solvation dynamics of (dye) solute molecules, either neutral or charged, in IL matrixes.[428,429] Solvatochromic measurements indicated that the extent of energetic heterogeneity of solutes in IL matrixes is significantly correlated not only with microstructural but also with dynamical heterogeneities arising from viscous glassy nature of ionic environments.[69,428,429] Small neutral and charged dye molecules explore locally "soft" (mostly apolar with low electrostriction) domains and locally "stiff" (mostly charged with high electrostriction) domains, respectively. These domains of low and high frictions are associated with jump and cage regimes. The enhanced diffusivities of neutral tracers in low friction domains, associated with apolar groups in constituent ions, have a substantial bearing on large positive deviations from the Stokes−Einstein hydrodynamics of ILs compared to conventional molecular solvents.[430] In contrast, the diminished mobilities of charged tracers involve lengthy caging dynamics separated by jump events, which are often caused by a recovery or loss of counterions. Charged solutes are strongly coupled with polar moieties of solvent ions and are not an innocent spectator of stiff and soft solvent regions but instead participate in creating electrostriction they experience.[428] As cations in less viscous ILs are often asymmetric, it is expected that a small positively charged probe will have stronger interactions with anions than with cations.[431,432] Therefore, small ion tracers will become an intrinsic component of polar networks and their diffusions are strongly correlated with that of ion groups comprising polar networks in IL matrixes.

2.4.4. Tetraalkylammonium and Tetraalkylphosphonium ILs. In protic alkylammonium ILs consisting of either primary, secondary, or tertiary ammonium cations, anions prefer to coordinate with N−H groups via preferential HB interactions, which are absent in aprotic tetraalkylammonium ILs.[433,434] SAXS[435,436] and atomistic simulations[437] of $[N_{1,n,n,n}][NTF_2]$ ILs (n = 4, 6, and 8) showed that low q peaks in scattering structural functions depend on alkyl chain length in

https://dx.doi.org/10.1021/acs.chemrev.9b00693
Chem. Rev. 2020, 120, 5798−5877

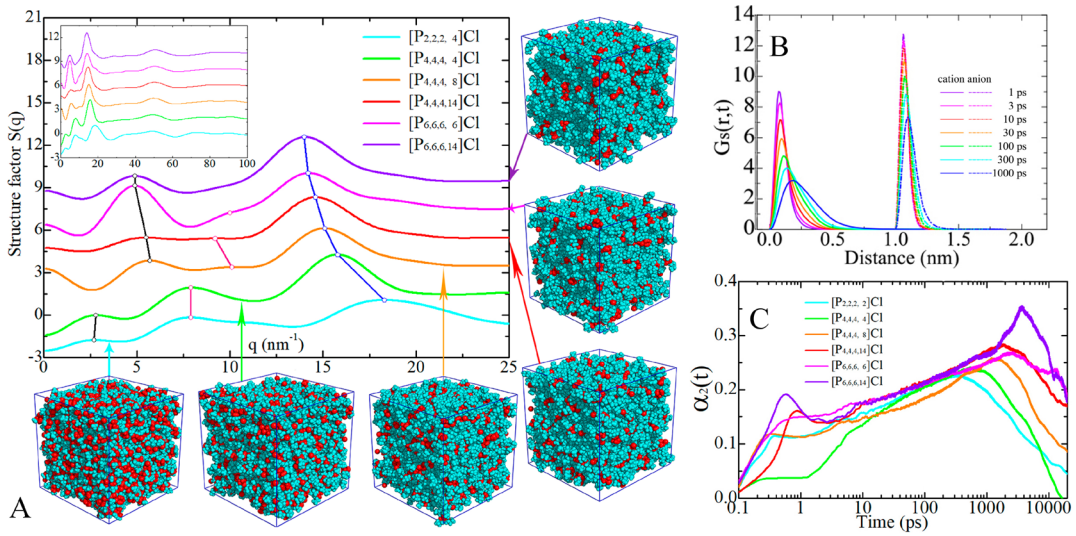

Figure 15. (A) Computational X-ray scattering structural functions and representative liquid morphologies of tetraalkylphosphonium Cl ILs. Polar domains (red) are composed of $P(CH_2)_4$ moieties in cations and anions, and the apolar entity (cyan) consists of the remaining alkyl groups in cations. (B) Self-part of van Hove correlation functions $G_s(r,t)$ for ion species in $[P_{6,6,6,14}]Cl$ at seven different times. (C) Non-Gaussian parameters $\alpha_2(t)$ for Cl anions in six tetraalkylphosphonium Cl IL matrixes. Reproduced with permission from ref 238. Copyright 2017 AIP Publishing LLC.

$[N_{1,n,n,n}]$ cations, while intermediate and high q peaks do not. These conjugated studies delineate the nature of marked nanoscale segregation of polar and apolar domains in ILs. Polar domains consist of 3D networks of ion channels, and apolar domains are arranged as a continuous microphase permeating polar networks. These results agree well with previous studies of $[C_nMIM][PF_6]$[438] and $[C_nMIM][NTF_2]$ ILs,[439] and provide another confirmation that not only ILs are nanostructured solvent media consisting of polar and apolar domains but also that their liquid structures can be further decomposed according to different categories of liquid morphologies.[440] In addition, $[N_{1,n,n,n}][NTF_2]$ ILs are not very viscous, but they exhibit a (low-frequency) macroscopic solidlike response to a low shear strain even at 100 °C above the glass transition temperature,[441] indicating collective elastic intermolecular interactions and long relaxation time scales. Therefore, the role of shear elasticity has to be considered for a better understanding of their odd properties, such as a non-Arrhenius temperature dependence of viscosities and ion conductivities as well as deviations of these dynamical properties from the Nernst−Einstein equation and their variations in the Walden plot, which are intrinsically ascribed to changes in high-frequency shear modulus with lengthening alkyl chains in tetraalkylammonium cations.[442]

Functionalization of the $[N_{1,1,1,2}]$ cation with a terminal hydroxyl group leads a good capability of [CH] cation in coordinating amino acid anions leading to a new type of ILs. These ILs are wholly composed of renewable biomaterials with inherent biocompatibility and low toxicity and hence can be used in enzymatic extraction and biocatalysis.[443] XRD and IR spectra as well as AIMD and atomistic MD simulations[444,445] revealed that amine groups in anions do not show strong interactions with [CH] cations, that is, amino acid anions are "more acid than amino", contributing to their similarities with alkylcarboxylate anions.[325] The liquid structures of [CH] amino acid ILs are substantially composed of two main docking interactions acting between different charge moieties: a strong HB feature connecting carboxyl terminals in amino acid anions to hydroxyl groups in [CH] cations, which determines short-range structural behavior and a substantial ion coupling as basic building blocks of IL matrixes.[446] A remarkable change was observed in translational and rotational responses of [CH] amino acid ILs to external electric fields.[447] Effective dipolar alignments of constituent ions with electric fields exhibit striking rotational mobilities of ions in the direction of electric field, which decrease with electric field frequency and increase with electric field strength.

SAXS experiments and atomistic simulations of ILs consisting of $[N_{2,2,2,8}]$, $[N_{2,2,2,(2O2O2)}]$ (2-ethoxyethoxy-ethyl-triethylammonium), and their phosphonium analogues showed that ILs with cations having four alkyl substituents exhibit FSDPs in their scattering structure functions, which are less intense or totally absent in diether-substituted analogues.[420,448,449] In ILs with cations having four alkyl substituents, anions are excluded from locations in which they are found in other types of ILs, eliminating long-range alternating polar−apolar patterns.[450] In addition, the inclusion of ether functionalities in tetraalkylammonium and tetraalkylphosphonium cations disturbs both long-ranged charge ordering and intermediate-ranged ordering in a rather subtle manner.[451] Ether groups have stronger interionic interactions with cation polar groups, resulting in larger surface tensions than ILs with hydrophobic alkyl groups and exhibiting a more flexible and less segregated polar domains in apolar networks in ILs.[452−454] These two structural features contribute to distinct transport properties of ether-substituted cations in comparison with their alkyl-substituted counterparts.

The specific effect of changing cation core from nitrogen to phosphorus atoms on cation−anion interactions, thermodynamics, microstructures, dynamical, and transport properties was investigated combining XPS,[114] femtosecond OHD-RIKES,[452] quasi-elastic light scattering spectroscopy, and broadband dielectric spectroscopy[83] as well as atomistic simulations.[453,455] Tetraalkylphosphonium ILs exhibit lower shear viscosities and glass transition temperatures and higher ion conductivities than the corresponding tetraalkylammonium ILs.[83,452,454,455] These properties are attributed to flexible molecular structures and weaker liquid structuring of

https://dx.doi.org/10.1021/acs.chemrev.9b00693
Chem. Rev. 2020, 120, 5798−5877

tetraalkylphosphonium cations in comparison with tetraalkylammonium homologues.[453] DFT calculations showed that phosphorus atoms in tetraalkylphosphonium cations carry more positive charge than nitrogen atoms in tetraalkylammonium cations, and a noticeable charge delocalization occurs in tetraalkylammonium cations in comparison with tetraalkylphosphonium congener.[455] These features contribute to a less ordered nanoscale aggregation of hydrophobic alkyl moieties and, consequently, inhibit cooperative relaxation dynamics in apolar networks in tetraalkylphosphonium ILs. Relative to α structural relaxation, these ILs present pronounced secondary structural relaxations that are strongly dependent on atomic identity of charged cation centers. $[P_{2,2,2,8}][NTF_2]$ exhibits faster secondary relaxations than $[N_{2,2,2,8}][NTF_2]$ at all measured temperatures, of which the former is characterized by an Arrhenius temperature dependence characteristic of local β relaxation, whereas the latter exhibits a mild non-Arrhenius thermal activation, which is indicative of molecular cooperativity.

Compared with imidazolium and pyrrolidinium ILs, the dependence of nanoscopic liquid morphologies of tetraalkylphosphonium ILs on alkyl chain length of cations is complicated as cations are composed of four alkyl chains and each one can be tuned by varying the chain length.[238,239,294,456] Tetraalkylphosphonium cations with short alkyl chains exhibit both liquid and solid states,[457,458] such as $[P_{1,2,2,4}][PF_6]$, in which the $[P_{1,2,2,4}]$ cation exhibits a distinct transport mechanism involving a crankshaft motion around the isobutyl group.[457,458] The microstructural liquid morphology of $[P_{2,2,2,4}]Cl$ is described by bicontinuous interpenetration of the polar and apolar networks (Figure 15A). Lengthening the cation alkyl chains results in a polar network composed of central polar moieties in cations and anions being partially fractured or totally partitioned within the apolar framework.[238] The variations of liquid morphologies and heterogeneous microstructures in the $[P_{n,n,n,m}]Cl$ IL matrixes are qualitatively manifested in decent adjacency correlation peaks and polarity alternation peaks observed at high and low q values in scattering structural functions, and their peak positions gradually shift to lower q values with lengthening alkyl chains in cations (Figure 15A). The peaks for charge alternations located in the intermediate q range present a complicated dependence on cation alkyl chain length due to a complete cancellation of positive contributions from ions having the same charge and negative contributions from ions having an opposite charge. These liquid structure changes are obviously manifested in dynamical properties. The terminal carbon atoms of alkyl chains exhibit an overall higher translational diffusivity than central phosphorus atoms in cations, which exhibit comparable translational diffusivities as Cl anions due to their decisive Coulombic associations in polar domains in IL matrixes. Lengthening cation alkyl chains leads to a concomitant shift of van Hove correlation functions to large radial distances (Figure 15B) and of non-Gaussian parameters to long time scales (Figure 15C), respectively, corresponding to increased translational diffusion heterogeneities of constituent ions in constrained ionic environments.

The $[P_{6,6,6,14}]$ ILs have been extensively investigated in experimental and computational studies due to a versatility of $[P_{6,6,6,14}]$ cations in coordinating various anions, from small spherical ones (halides, $[BF_4]$, $[PF_6]$, *etc.*)[459−462] to bulky asymmetrical ones with diffuse charges,[462,463] like $[NTF_2]$.[464,465] The FSDPs in scattering structural functions for $[P_{6,6,6,14}]$ ILs are independent of anion types and increase in intensity with decreasing temperatures.[462] In addition, charge and polarity orderings in $[P_{6,6,6,14}]$ ILs display appreciable sensitivity to external pressures.[460] Polarity ordering diminishes as pressure increases from ambient to a transition pressure. Upon further pressuring ILs, an additional peak corresponding to crystalline order emerges on a relatively short length scale. This observation is attributed to enhanced polar−polar and apolar−apolar correlations and decreased polar−apolar correlations. With increasing pressures, the probability of finding more gauche kinks along C_6 chains is systematically increased, whereas a mixed effect is observed for C_{14} chains in $[P_{6,6,6,14}]$ cations.

ILs consisting of $[P_{6,6,6,14}]$ cations coupled with chelated orthoborate anions have striking tribological features.[58,294,466] Atomistic simulations indicated that there are mainly four high probability regions for orthoborate anions to coordinate $[P_{6,6,6,14}]$ cations. Boron atoms in [BOB] anions exhibit dispersed tetrahedral distributions around $[P_{6,6,6,14}]$ cations. An increase in anion sizes from [BOB] to bis(malonato)borate ([BMLB]), bis(mandelato)borate ([BMB]) and bis(salicylato)borate ([BScB]) leads to an expansion of spatial distributions of boron atoms in these orthoborate anions around $[P_{6,6,6,14}]$ cations. Spatial distributions of oxygen atoms in orthoborate anions are characterized by a trefoil-like structure and follow a similar tendency as those of boron atoms as anion size increases. These distinct ion structures lead to significant changes in their liquid viscosities and rheological properties.[294,467,468]

3. IONIC LIQUID−MOLECULAR SOLVENT MIXTURES

3.1. Solvation Thermodynamics and Structures of Water in ILs

For IL related research in laboratory and industrial applications, an inevitable issue is the presence of residual impurities in ILs. As an omnipresent compound, water is one of the most common contaminants found in IL samples. On one side, this is caused by ILs' intrinsic hygroscopic feature, even those described by hydrophobic characteristics can absorb a considerable amount of water from atmosphere, and on the other side many processes including chemical synthesis and liquid extractions and purifications involve water. It has been well recorded that trace amounts of water can dramatically alter microstructures in ILs, resulting in significant changes in physicochemical and rheological properties of ILs as well as reactivities and selectivities of reactions taking place in IL matrixes.[469]

Water−ion interaction strength qualitatively determines the trend of excess chemical potentials and therefore miscibility of water in ILs.[470] Anthony et al. found that excess chemical potentials of water in $[C_4MIM][PF_6]$, $[C_8MIM][BF_4]$, and $[C_8MIM][PF_6]$ ILs lie between −15 kJ/mol and −20 kJ/mol and increase slowly with temperatures and cation alkyl chains.[471] Lynden-Bell et al. calculated excess chemical potentials of a series of solutes (water, methanol, dimethyl ether, acetone, and propane) dissolved in $[C_1MIM]Cl$ IL matrix using a thermodynamic integration method.[472] Water and methanol have large excess chemical potentials (−29 kJ/mol and −14 kJ/mol, respectively), which are attributed to specific HB interactions in stabilizing water and methanol in $[C_1MIM]Cl$. Apolar molecules like dimethyl ether and acetone

https://dx.doi.org/10.1021/acs.chemrev.9b00693
Chem. Rev. 2020, 120, 5798−5877

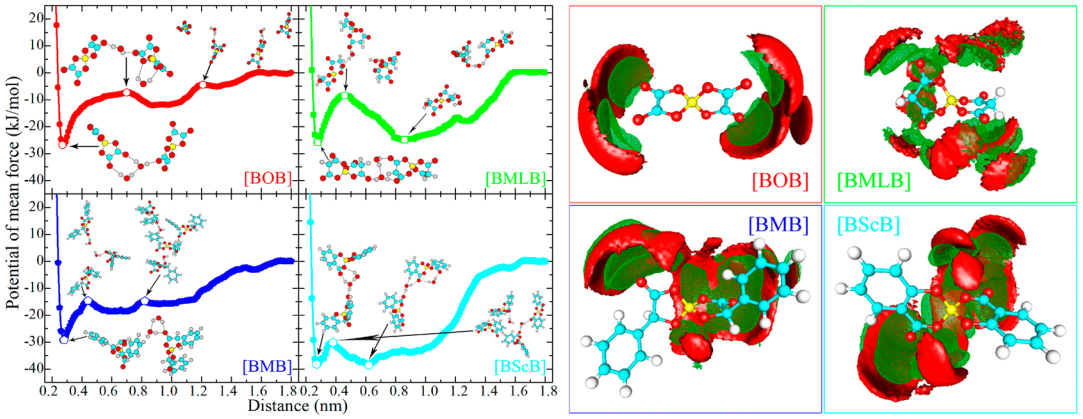

Figure 16. Left, potential of mean force curves of two solvated water molecules in IL matrixes, and representative configurations of solvated water molecules in coordinating neighboring anion species in $[P_{6,6,6,14}]$ orthoborate ILs. Right, spatial distributions of hydrogen (green contour) and oxygen (red contour) atoms in solvated water molecules around neighboring orthoborate anions. Reproduced with permission from ref 473. Copyright 2016 AIP Publishing LLC.

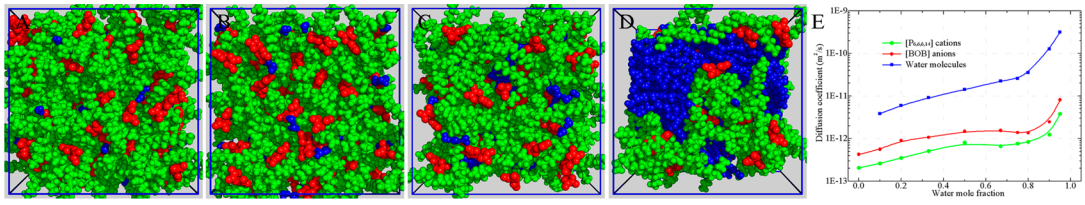

Figure 17. Representative snapshots of $[P_{6,6,6,14}][BOB]$–water mixtures containing varied water mole fractions of X_{water} = (A) 0.33, (B) 0.5, (C) 0.8, and (D) 0.95. Cations, anions, and water molecules are represented by green, red, and blue spheres, respectively. Reproduced with permission from ref 491. Copyright 2015 American Chemical Society. (E) Translational diffusion coefficients of all ion species in mixtures having different water concentrations at 333 K. Reproduced with permission from ref 293. Copyright 2016 American Chemical Society.

have excess chemical potentials of ~7 kJ/mol while the value for propane is of approximately 26 kJ/mol.

Wang et al. showed that free energies of solvating one water molecule from gas phase into bulk $[P_{6,6,6,14}]$ orthoborate IL matrixes are positive and exhibit linear dependence on temperatures.[473] At a given temperature, these solvation free energies are intrinsically related to orthoborate anion structures with an order of [BMLB] > [BScB] > [BMB] > [BOB], which is qualitatively consistent with experimentally determined residual water contents in the corresponding ILs. In addition, less solvation free energies are required to dissolve the second one within the first solvation shell of the first solvated water molecule, attributing to preferential pairwise intermolecular interactions between two water molecules and favorable multibody interactions of solvated water molecules with neighboring anion species at short and intermediate distances.

Seddon and co-workers provided guidelines on mutual miscibilities of ILs with water.[474] In general, ILs containing highly fluorinated and charge-delocalized anions, such as $[NTF_2]$, tricyanomethanide and $[PF_6]$, are hydrophobic and are immiscible with water.[475−477] ILs having hydrophilic ions, such as halides, ethanoate, $[NO_3]$, trifluoroacetate, and carboxylate, are totally miscible with water, and those consisting of $[BF_4]$, $[CF_3SO_3]$, and phosphate anions are either miscible or immiscible with water depending on cation substituents. In addition, cations also affect miscibilities of ILs in water with hydrophobicity of cations following an order of $[C_nMIM]$ < $[C_nMPYRI]$ < $[C_nMPYRR]$ < $[C_nMPIP]$ < tetraalkylammonium < tetraalkylphosphonium. Furthermore, hydrophobicity of cations increases with lengthening cation alkyl chains, indicating a decreased polarity of cations.[478]

It is understood that solvation structures of water in ILs depend primarily on strength of electrostatic ion–water interactions, which, in turn, are essentially determined by ion sizes and the amount of charge on the ion surface.[470] Interactions of water with small ions are favorable while those with large ions are much weak due to their delocalized charges.[470,475,477,479] In addition, HB interactions contribute to significant coordination of water with constituent ions due to a dual feature of water having HB interactions with both cations and anions, which further complicates solvation structures of multiple water molecules in ILs. The water–water potential of mean force profiles for $[P_{6,6,6,14}]$ orthoborate ILs indicate substantial interactions of solvated water molecules with neighboring ions depending on local ionic environments (Figure 16).[473] A characteristic deep potential minimum registered at ~0.28 nm corresponds to the formation of a water dimer complex, which has strong coordination with neighboring anions and forms stable ring structures via HB interactions. As the separation distance between solvated water molecules increases, there is not enough space between solvated water molecules for an ion to squeeze in, leading to the formation of unstable intermediates. These intermediates contribute to gradually enhanced water–water interactions until the formation of metastable ion-separated water association structures at intermediate separation distance. The association patterns for solvated water molecules at large separations are described by remarkable characteristics depending on specificities of anions and mild interactions of solvated water with surrounding ions, leading to remarkable spatial association

https://dx.doi.org/10.1021/acs.chemrev.9b00693
Chem. Rev. 2020, 120, 5798−5877

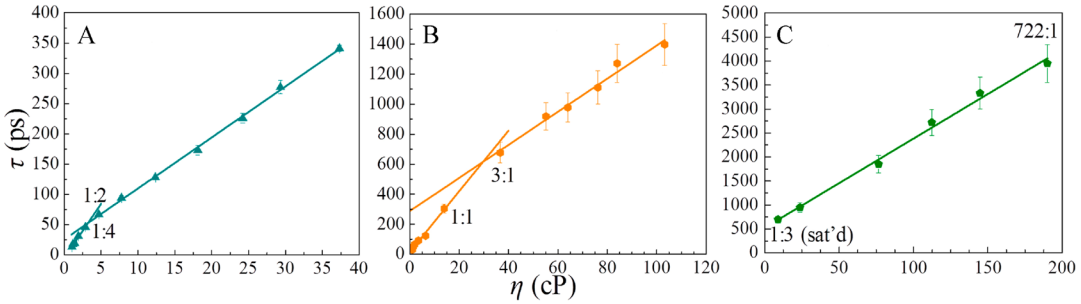

Figure 18. Debye–Stokes–Einstein plots for IL–water mixtures consisting of (A) $[C_2MIM][BF_4]$, (B) $[C_4MIM][BF_4]$, and (C) $[C_6MIM][BF_4]$ ILs with water at varied ratios of ion pairs:water. Reproduced with permission from ref 94. Copyright 2018 AIP Publishing LLC.

patterns of solvated water molecules around orthoborate anions (Figure 16).[473]

3.2. IL–Water Mixtures

Extensive experimental characterizations (NMR,[161,254,321,480−483] infrared and Raman spectroscopies,[151,230,482−488] X-ray and neutron scattering spectroscopies,[109,111,159,487,489] *etc.*), theoretical studies,[31,477] DFT calculations,[172,483,490] and atomistic simulations[72,160,162,167−169,171−174,178,180,491−493] have been performed to characterize phase behavior changes when mixing ILs with water. Variations in liquid structures, translational and rotational dynamics of ion species, and evolution of microscopic liquid morphologies of IL–water mixtures with a gradual increase of water concentration in ILs can be roughly classified into several compositional regimes. Representative changes of microstructural and dynamical quantities in $[P_{6,6,6,14}][BOB]$–water mixtures are illustrated in Figure 17.[164,293,491]

In IL–water mixtures with a small water mole fraction (generally $X_{water} \leq 0.2$), cation groups and anion species are strongly coupled together via decisive Coulombic interactions and preferential HB interactions and possibly $\pi-\pi$ stacking interactions in ILs containing heteroaromatic rings. Microscopic liquid organization is characterized by isolated polar domains dispersed in a connected apolar network or by interpenetrating polar and apolar networks. Most water molecules are scattered in IL matrixes and are preferentially coordinated with ion species nearby, leading to the local ionic structures described by solute-shared ion pairs[486] (Figure 17A). The restricted spatial configuration of water molecules in IL–water mixtures results in their constrained rotational relaxation within a cone of angles due to their dual feature in coordinating both cations and anions via HB interactions and a significant increase in translational diffusions of ion species in mixtures as water concentration increases (Figure 17E).[110,159,165,480,494]

For IL–water mixtures having intermediate water concentrations (generally $0.2 < X_{water} \leq 0.9$), small clusters, such as water dimers, trimers, and water channels, appear and dominate distribution of water aggregates in IL–water mixtures (Figure 17B,C). These water clusters serve as bridges connecting anions between isolated polar domains and mediating their distributions in mixtures.[485,495] The local ion structures in these IL–water mixtures are described by solute-mediated ion pairs, leading to increased spatial associations between ions and, thus, have a strong effect on translational and rotational dynamics of ion species in mixtures (Figure 17E).[111,151,166,488,496,497]

The further addition of water into IL–water mixtures results in a dynamic percolation of water molecules throughout the entire simulation box (Figure 17D). The local ionic environment is described by interpenetrating polar and apolar networks or loose micelle-like aggregates in a highly branched water network.[168,494] The formation of water networks promotes a rapid increase in ion dynamics in these water-concentrated mixtures. These IL–water mixtures are characterized by substantial spatiotemporal heterogeneities attributing to a competition between strong electrostatic and preferential HB interactions between polar moieties in ion species, and persistent dispersion associations between hydrophobic moieties in constituent ions.[482,484−486,490,496]

In addition to variations in microstructures and mesoscopic liquid morphologies determined from atomistic simulations, a combination of 2D IR spectroscopy,[72−75,488] OHD-OKE spectroscopy,[74,75,141,498] time-resolved ultrafast infrared spectroscopy,[93,102] and PSPP measurements[74,75,90] provides comprehensive characterizations on multi-time scale dynamics of ILs ranging from ultrafast vibrational motions of well-defined functional groups to rotational relaxation of constituent ions in IL–water mixtures at ground and excited states.[91,102,499] Take $[C_nMIM][BF_4]$–water mixtures for example, rotational dynamics of water in $[C_nMIM][BF_4]$ ILs (n = 4, 6, 8, and 10) characterized using 2D IR spectroscopy and PSPP experiments showed that water's hydroxyl absorption spectra are independent of cation alkyl chain length, indicating that dispersed water molecules feel fairly similar local ionic environments in all studied mixtures.[74] However, rotational relaxation (PSPP experiments) and spectral diffusion (structural dynamics using 2D IR experiments) measurements of hydroxyl groups display alkyl chain length dependence. These dynamics slow when cation alkyl chains become long enough to form apolar segregations in IL-water mixtures. At low water concentrations, all hydroxyls interact mainly with anions because of their dispersed distributions in heterogeneous IL matrixes. As water concentration increases, a water-associated water population forms, absorbing in a new spectral region red-shifted from absorption of isolated or anion-associated water populations. At sufficiently high water concentrations, water clusters grow and water molecules experience dynamics approach those of bulk water, and IL structures are fluidized by addition of water. Both rotations of hydroxyls and their spectral diffusions, tracking fluctuations in local structures and interactions, speed up noticeably with increasing water content in certain concentration ranges. The water concentration at which dilute water dynamics change to fluidized dynamics depends on cation alkyl chain length, which determines the extent and

https://dx.doi.org/10.1021/acs.chemrev.9b00693
Chem. Rev. 2020, 120, 5798−5877

ordering of apolar domains. Increasing water concentrations and lengthening cation alkyl chains tend to modify IL structural orderings but with opposite and competing effects on dissolved water dynamics.

It should be noted that water exhibits different solubilities in $[C_nMIM][BF_4]$ ILs depending on alkyl chain length in cations. Both $[C_2MIM][BF_4]$ and $[C_4MIM][BF_4]$ ILs are infinitely miscible with water, whereas in $[C_6MIM][BF_4]$ IL water saturates at X_{water} = 0.75.[94] The Debye−Stokes−Einstein (DSE) plot for $[C_2MIM][BF_4]$−water mixtures has two hydrodynamic regimes of $X_{water} < 0.67$ and $X_{water} > 0.80$ with a crossover region in between (Figure 18A).[94] Atomistic simulations showed that there is no connected apolar domains in $[C_2MIM]$ ILs. The local ionic environments in $[C_2MIM][BF_4]$ can restructure without paying a significant penalty for disrupting local ion structures in polar domains to accommodate more water molecules in the IL matrix. The DSE curve for $[C_6MIM][BF_4]$−water mixtures is linear, indicating that $[C_6MIM][BF_4]$−water mixtures do not substantially change local ionic environments as water concentration increases (Figure 18C).[90,94] $[C_6MIM][BF_4]$−water mixtures are hydrodynamic, likely due to favorable dispersion associations among cation alkyl chains, making it unfavorable for ion species to change local ionic structures to accommodate additional water molecules. Instead of disrupting the apolar framework in the IL matrix, $[C_6MIM][BF_4]$ saturates with water. $[C_4MIM][BF_4]$ is an intermediate item, in which apolar domains are interconnected and present to a limited extent. Similarly, two linear regimes, a low water content regime with a moderate slope and a high water content regime with a steep slope, are observed in the DSE curve for $[C_4MIM][BF_4]$−water mixtures (Figure 18B).[90,94] However, the transition point for $[C_4MIM][BF_4]$−water mixtures is between X_{water} = 0.25 and X_{water} = 0.50, which is lower than that for $[C_2MIM][BF_4]$−water mixtures. $[C_4MIM]$ cations are able to restructure local ionic environments to accommodate more water molecules, leading to two linear regimes in the DSE curve because apolar domains in $[C_4MIM][BF_4]$−water mixtures are less extensive than those in $[C_6MIM][BF_4]$−water mixtures.

It is known that protonation of N(3) position in imidazolium rings changes imidazolium cations from aprotic to protic. The hydrogen atoms in N(3)−H groups serve as strong HB donor sites and have preferential HB interactions with water molecules and anions.[75,94,163,254] OHD-OKE spectra showed that $[C_2MIM][NTF_2]$−water mixtures exhibit hydrodynamic behavior at all water concentrations up to saturation, whereas $[C_2HIM][NTF_2]$−water (1-ethyllimidazolium) mixtures display distinct phase behaviors at specific water concentrations.[75,94] Atomistic simulations demonstrated a substantial jump in the formation of $N(3)-H\cdots(H_2O)_n$ clusters in $[C_2HIM][NTF_2]$−water mixtures upon increasing water concentrations. Cluster formation contributes to significant deviations of rotational relaxations of $[C_2HIM][NTF_2]$−water mixtures from hydrodynamic behavior due to dominant HB interactions of water with N(3)−H groups over other HB donor sites in $[C_2HIM]$ and $[C_2MIM]$ cations. This structural variation is confirmed by FT-IR spectra showing an asymmetric O−D stretching that is indicative of water clusters in $[C_2HIM][NTF_2]$−water mixtures.

In addition to aprotic and protic imidazolium ILs, water exhibits distinct microstructures and dynamics in protic alkylammonium ILs.[154,230,500−503] AIMD simulations showed that HBs formed between MAN and water are characterized by distinct HB structures and dynamics, resulting in a significant incorporation of water into HB networks of MAN.[154,500] Water slows down rotational dynamics of cations and anions in MAN and, to some extent, changes polarization of IL ions. However, in EAN−water mixtures, water changes EAN nanostructures mainly due to its HB interactions with EA cations and $[NO_3]$ anions.[503] In addition to bicontinuous polar and apolar domains in the EAN IL matrix, separate EAN aggregations and water domains are also evident. Water neither dilutes molecularly dispersed IL ions nor does it swell polar networks of existing IL nanostructures. Instead, water is principally associated with ion polar groups, and its net effect is to increase effective cation headgroup size and to create an interfacial curvature around apolar domains. This changes EAN nanostructures in EAN−water mixtures from a near-zero mean curvature to a branched (locally cylindrical) network.[224,500,503]

S/WAXS and atomistic simulations were combined to explore liquid structures and dynamics of IL−water mixtures consisting of primary, secondary, and tertiary alkylammonium cations in conjunction with Cl, formate, and alkanoates anions.[199,502,504] For IL−water mixtures consisting of primary alkylammonium cations coupled with small anions, like EAC−water and PAC−water mixtures, there exists a complex liquid structure where cation groups and anion species do not possess a completely closed hydration shell of their own. In particular, a dominant percentage of solute-shared ion pair structures are formed in mixtures with low water concentrations, in which dispersed water molecules act as linkers between cations and anions via HB interactions. This percentage decreases with increasing water concentrations in mixtures, but in conditions of very high dilution, solvent-shared ion pair structures continue to survive.[199] Lengthening cation alkyl chains leads to distinct thermal behaviors in hexyl-, octyl-, and decylammonium Cl IL−water mixtures.[501] For ILs having large anions, liquid viscosities of IL−water mixtures exhibit characteristic behaviors of concentrated salt solutions, with water diluting protic ILs.[502,504] Ion conductivities of IL−water mixtures display complicated changes with a gradual increase of water concentrations due to a subtle interplay of available "free" ions in mixtures and changes in liquid viscosities of mixtures.

3.3. IL−Alcohol Mixtures

ILs are polar liquids, and polarities of pure ILs are higher than acetone, dimethyl sulfoxide, and dichloromethane but lower than water and close to short chain alcohols.[505] Mixtures of ILs with alcohols showed reduced viscosities and enhanced functionalities in chemical engineering applications.[9,18] In these processes, it is especially significant to understand how microstructures and molecular arrangements of ILs change upon mixing and in which way miscibility and physicochemical properties of IL−alcohol mixtures are related to their characteristics in applications.

3.3.1. Alkylammonium IL−Alcohol Mixtures. Both EAN and methanol are amphiphilic and their bulk liquid structures are characterized by extended HB networks. Hence, they are expected to exhibit ideal mixing characters.[506,507] However, though macroscopically homogeneous, EAN−methanol mixtures are heterogeneous fluids at the mesoscopic level.[194,508,509] Fluorescence anisotropy measurements, XRD spectra, and atomistic simulations revealed that even in methanol enriched mixtures, most EAN ion species are clustered and preserve their spongelike liquid organization,

https://dx.doi.org/10.1021/acs.chemrev.9b00693
Chem. Rev. 2020, 120, 5798−5877

and methanol molecules cannot fully dissociate EAN clusters.[510] Such heterogeneous liquid structures contribute to distinct dynamic heterogeneities of EAN−methanol mixtures as revealed from fluorescence anisotropy measurements.[510] Additional analysis of time-resolved anisotropy data together with DSE hydrodynamic theory predicts that reorientation times for EAN and methanol are comparable and close to the stick hydrodynamic line in mixtures with low EAN concentrations. EAN−methanol mixtures with intermediate EAN concentrations exhibit both Newtonian and Arrhenius behaviors, and their liquid viscosities are independent of temperatures.[510] Furthermore, SAXS spectra showed that strong cohesive forces in EAN and PAN ILs can induce intermediate chain length alcohols to self-organize into microemulsion-like and micelle-like structures in ILs, which is in contrast to their immiscibilities with EtA ILs and water.[191,194,511] This indicates that EA and PA cations act as cosurfactants and enable alcohols to aggregate, whereas EtA cations cannot serve this function because their terminating hydroxyl groups render EtA cations nonamphiphilic.

Shrivastav et al. performed additional atomistic simulations to explore the effect of alcohol alkyl chain length on liquid organization and HB interactions in equimolar mixtures of BAN with primary alcohols.[512] All BAN−alcohol mixtures exhibit two decent peaks in the low q region in structural functions, indicating the presence of bicontinuous heterogeneous ordering structures, which depend considerably on alcohol alkyl chain length.[191] Alcohols prefer to reside with their hydrophobic tails in apolar domains and their polar heads in polar domains in the IL matrixes.[194,511,513] This is distinct from distributions of polar solutes, like water, which reside in polar regions,[230,503,504] while apolar solutes prefer apolar domains.[191,513] Lengthening alcohol alkyl chains produces significant variations in microstructural ordering of polar and apolar domains in BAN−alcohol mixtures and exhibits enhanced HB interactions of hydroxyls in alcohols with anions and other alcohols.[326]

Both miscibility and liquid organization of binary alkylammonium IL−alcohol mixtures are structured on two distinct length scales: one is associated with self-assembled alcohol aggregates and the other is associated with the underlying IL nanostructures, both of which are primarily sensitive to the ratio of alcohol alkyl chain length to alkylammonium cation alkyl chain length.[191,509] Alcohols with alkyl chains shorter than twice that of alkylammonium cations disrupt intrinsic amphiphilic IL nanostructures and reduce periodic orders but do not generate a qualitatively different solution structures. Long chain alcohols cannot be accommodated within intrinsic IL nanostructures to any significant extent and instead are expelled into large amphiphilic aggregates. The self-assembled liquid structures depend on detailed chemical compositions of IL−alcohol mixtures. Globular micelles are formed at low alcohol concentrations, but micelles tend to percolate into bicontinuous structures at high alcohol concentrations, which are alcohol-rich but contain some cation groups acting as cosurfactants. EtA cations cannot act as cosurfactants to induce self-assembly of alcohols and therefore lead to immiscibility once alcohol alkyl chains exceed twice the EtA cation alkyl chains.[191,514] It should be noted that these liquid structural transitions are affected by anion structures and anion HB capacities.[326] Ethylammonium formate (EAF) has a less pronounced bulk nanostructure than EAN and PAN ILs,[190] and its miscibility with octanol results from a weak solvophobic driving force. Therefore, fewer and smaller aggregates are formed in EAF−octanol mixtures.

These observations provide valuable physical insights into microstructural features and general stabilization mechanisms of weakly structured mixtures and reveal new pathways for identifying molecules and ILs that are likely to generate weakly structured fluids for facilitating aggregations of nontraditional amphiphiles and for supporting self-assembly of nontraditional surfactants. Understanding these systems is an important step toward applications of functional ILs as solvent electrolytes for electrochemical devices and their effective utilization to assemble new forms of soft matter.[191,194,515]

3.3.2. Imidazolium and Pyrrolidinium IL−Alcohol Mixtures. The mutual solubility of imidazolium ILs and alcohols are intrinsically related to significant interactions of ILs with alcohols.[516,517] These interactions are important characters affecting physicochemical behaviors of IL−alcohol mixtures.[518,519] A general feature is that a gradual lengthening of alcohol alkyl chains leads to a systematic decrease in solubility of ILs in alcohols, which is deduced from solubility of $[C_2MIM][NTF_2]$ in propanol, butanol, and pentanol,[520] and of $[C_8MIM][BF_4]$ in butanol and pentanol,[521] as well as solubility of other ILs containing different cation−anion moieties in various alcohols.[516,522,523] Lengthening alcohol alkyl chains leads to a decrease in excess molar enthalpies and increases in molar excess volumes and in upper critical solution temperature (UCST) of IL−alcohol mixtures. These properties indicate that packing structures and interactions between unlike molecules become less important in mixtures containing long chain alcohols.[519,524] By contrast, an increase in alkyl chain length in imidazolium cations leads to enhanced hydrophobicity of ILs and therefore results in a decrease in UCST of IL−alcohol mixtures.[518,525,526] Decreasing HB opportunities of alcohols with C(2)-methylated imidazolium cations results in an increase in UCST, while the coupled anions have a significant impact on this property,[525,527] which diminishes with increasing alkyl chain length in cations.[522,523,528]

Calorimetric data together with computational results showed evidence of effects of anion's basicity on IL−alcohol interactions and of cation structures on the solvation process of alcohols in ILs.[16,529] The effect of anion basicity on molar enthalpies of solvation at infinite dilution of propanol in $[C_4MIM]$ ILs is described by a sequence of anion enthalpy values: $[PF_6]$ > tri(pentafluoroethyl)trifluorophosphate ([FAP]) > $[NTF_2]$ > $[N(CN)_2]$ > trifluoroacetic acid ([TFA]). This trend of increasing exothermic enthalpies from $[C_4MIM][PF_6]$ to $[C_4MIM][TFA]$ is rationalized by a decrease in cavitation energy (endothermic contribution) and an increase in IL−alcohol interaction strength (exothermic contribution). In addition, variations in molar enthalpies of solvation of propanol in $[C_4MIM]$ ILs are linearly correlated with HB interactions of anions with propanol in IL−propanol mixtures.[519,530] These experimental and computational results are generally consistent with previous findings on delicate interactions of different solutes with anions in protic and aprotic ILs.[513,531,532]

The aggregation process of alcohols in ILs and dynamical quantities of ion species in IL−alcohol mixtures are highly dependent on the nature of anions and size of alcohols as alcohols have predominant interactions with anions, particularly in halogenated IL−alcohol mixtures.[533,534] Atomistic

https://dx.doi.org/10.1021/acs.chemrev.9b00693
Chem. Rev. 2020, 120, 5798−5877

simulations suggested that the formation of apolar networks, as has been reported for IL−water mixtures, does not take place in IL−alcohol mixtures when halides are present,[533,534] as observed from a significant presence of locally ordered structures in $[C_nMIM]Cl$−alcohol mixtures.[535] However, in solvophobic IL−alcohol mixtures with fluorinated anions, the formation of apolar aggregates and polar networks depends on anion sizes.[533,536] Diffusivities of constituent ions in IL−alcohol mixtures increase with increasing alcohol concentrations. Two different regimes are observed: (i) at low alcohol concentrations, diffusion coefficients of alcohols increase very slowly, which is associated with viscosities of mixtures, and (ii) at high alcohol concentrations, diffusion coefficients of alcohols show a rapid increase, which is related to percolation of alcohol domains breaking IL polar networks.[536,537]

Concerning liquid dynamics of IL−alcohol mixtures, particularly those involving HB fluctuations, Kramer et al. conducted a series of 2D IR measurements of spectral diffusions and PSPP measurements of vibrational population dynamics and rotation relaxation of hydroxyl stretching mode of methanol and ethanol molecules in $[C_2MIM][NTF_2]$.[397] Long time scale spectral diffusion (structural evolution) observed in 2D IR spectra showed a clear but not dramatic slowing as alcohol alkyl chain increases: 28 ps for methanol and 34 ps for ethanol, both of which are larger than that for water (23 ps) in the same IL. Frequency−frequency correlation functions characterizing structural evolution in IL−alcohol mixtures reported a variety of time scales for HB dynamics and water rotation relaxation ranging from a few hundred femtoseconds to tens of picoseconds. Rotational correlation functions for these IL−alcohol mixtures exhibit several periods of restricted angular wobbling-in-a-cone motions before a complete rotational randomization. These experimental results suggest a weakening of angular potential from methanol to ethanol with decreased HB strength.[538]

Similar microstructural and dynamical changes were also observed in mixtures of alcohols with pyrrolidinium, pyridinium, and piperidinium ILs.[529,538] Molar enthalpies of solvation at infinite dilution of propanol in ILs consisting of $[NTF_2]$ and [FAP] anions coupled with $[C_4MPYRR]$, $[C_4PYRI]$, and $[C_4MPIP]$ cations were studied to examine the influence of cation structural factors (size, aromaticity, charge distribution, and acidity).[538] For $[NTF_2]$ ILs, there is no significant dependence of solvation enthalpies on cation structures, which is an indirect evidence of substantial interactions of alcohols with $[NTF_2]$ anions. Regarding [FAP] ILs, there is a significant difference in solvation enthalpies of propanol in $[C_4MPYRR][FAP]$ in comparison with that in $[C_4MIM][FAP]$.[539] This is attributed to an nonaromaticity of $[C_4MPYRR]$ cations and a decrease in their acidic character, leading to decreased cation−alcohol dispersive and HB interactions.[538]

In general, solvation of alcohols in ILs can be described as a two-step process: creation of a cavity in ILs and relaxation of ions in cavities to establish preferential IL−alcohol interactions.[519] Experimental and computational results of solvation enthalpies of alcohols in ILs are interpreted as a balance between an endothermic contribution of cavitation effect in IL solvents and an exothermic contribution of solute−solvent interactions. These results provide a detailed effect of cations and anions on solvation of alcohols in ILs.

3.3.3. Tetraalkylammonium and Tetraalkylphosphonium IL−Alcohol Mixtures. Mixing $[N_{1,1,1,4}][NTF_2]$ with ethanol and propanol is expected to result in a competition between ion−ion and ion−alcohol interactions.[540] Solubility data of ethanol and propanol in $[N_{1,1,1,4}][NTF_2]$ indicate that mixing enthalpy is positive for these two alcohols because they must overcome strong Coulombic ion pair interactions to solvate in IL matrix. In addition, structural and energetic properties of $[N_{1,1,1,4}][NTF_2]$−alcohol mixtures provide important molecular-level information that can be used to understand and predict solubility trends for other alcohols in ILs. Furthermore, small variations in alcohol structures lead to a wealth of microstructures and liquid morphologies in IL−alcohol mixtures, highlighting a resilience of IL polar networks to addition of alcohols with different polarities.[531] Charge ordering peaks for all IL−alcohol mixtures exhibit higher intensities than those for pure ILs and are all shifted to lower q values due to expansions of apolar networks in IL−alcohol mixtures. It is noteworthy that the expansion of apolar networks and the partial breakdown of polar networks (domains) in [CH] ILs are totally different from those in $[C_nMIM]$ ILs. The modified polar networks are more filamentous in the former case, whereas in the latter case they are more globular in shape (some portions are expanded or broken while others still retain a fairly degree of 3D connectivity). Microstructures and liquid morphologies of these IL−alcohol mixtures are, in fact, determined by an intricate balance between different types of interactions (electrostatic, solvophobic, vdW, HB, *etc.*) that are privileged among intervening species.

In another work, atomistic simulations revealed that $[P_{6,6,6,14}]Cl$−methanol mixtures exhibit a microstructural evolution from IL-like to methanol-like with a gradual addition of methanol into $[P_{6,6,6,14}]Cl$.[459] In mixtures with high methanol concentrations, cation−anion pairs are widely separated by methanol molecules. The central polar units in $[P_{6,6,6,14}]$ are overwhelmingly surrounded by Cl anions and subsequently by methanol molecules, and methanol hydroxyl groups are preferentially solvated by anion species. In addition, liquid viscosities of $[P_{6,6,6,14}]Cl$−methanol mixtures show a nonlinear dependence on mole fractions of ILs with $X_{IL} < 0.1$, which is in contrast to a linear data variation with mole fractions of ILs with $X_{IL} > 0.1$.[541]

For molecules interacting mainly via permanent dipole moments (1,2-difluorobenzene, ethers) or permanent electric quadrupole moments (benzene, hexafluorobenzene), molecules tend to swell existing IL apolar domains and prefer to locate near polar networks with orientations to maximize favorable multipole−charge interactions. Such a charge-template arrangement also works in the other sense: IL polar networks are generally flexible and can be rearranged to accommodate solute molecules, even if such rearrangement implies expanding polar networks. In the case of alcohol solutes, IL polar networks have to simultaneously accommodate alkyl moieties and hydroxyl groups in alcohols. This impact leads to a general loss of ion−ion interactions in close solvation shells and a ramification in polar networks. Nonetheless, IL polar networks can form well-organized string-like arrangements and exist up to fairly high solute concentrations. In IL−alcohol mixtures, a second network composed of alcohols and anions forms at intermediate alcohol concentrations. Such a secondary network causes a sheathing of original IL polar networks, and is probably responsible for neutron diffraction and X-ray scattering patterns at low q values.

https://dx.doi.org/10.1021/acs.chemrev.9b00693
Chem. Rev. 2020, 120, 5798−5877

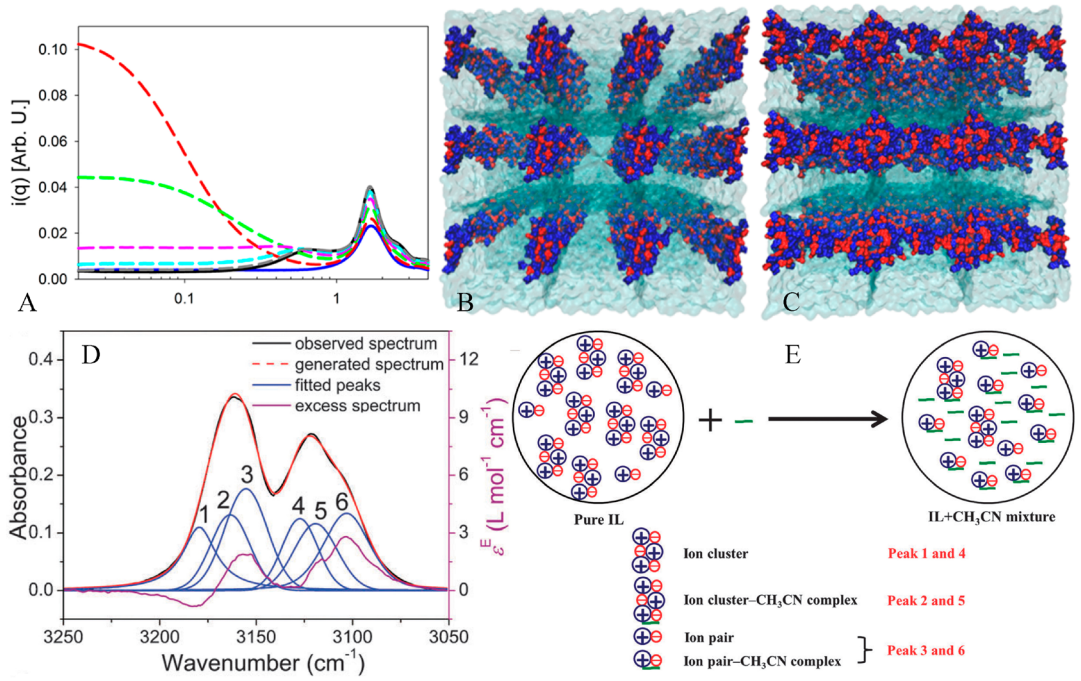

Figure 19. (A) SAXS patterns for EAN−ACN mixtures with EAN concentrations of 0.0 (blue), 0.1 (red), 0.3 (green), 0.5 (magenta), 0.7 (cyan), 0.9 (gray), and 1.0 (black). (B,C) Representative snapshots of EAN−ACN mixture with X_{EAN} = 0.1. Reproduced with permission from ref 544. Copyright 2017 American Chemical Society. (D) Deconvoluted IR spectrum in imidazolium ring C−H stretching region of a $[C_4MIM][BF_4]$−ACN mixture with X_{ACN} = 0.5. (E) Schematic model of a transformation of ion species in dilution process. Reproduced with permission from ref 245 Copyright 2013 Royal Society of Chemistry.

3.4. IL−Acetonitrile Mixtures

Acetonitrile (ACN) is an important organic solvent, and its mixtures with ILs have been utilized as reaction media for organic synthesis and thermally stable electrolytes in batteries and solar cells with low toxicity and high efficiency.[62,542] In addition, ACN is structurally similar to methanol but with different HB donation capability, which contributes to its intrinsic macroscopic functionalities in electrochemical applications.[62,543]

A large inhomogeneity was observed in EAN−ACN mixtures with EAN being a minority component, as identified from combined SAXS and atomistic simulations (Figure 19A).[544] It is EAN's wormlike liquid structure that is responsible for density fluctuations in EAN−ACN mixtures, which are even denser than pure EAN due to preferential HB interactions.[545] EAN and ACN have significant reciprocal effects: EAN ions orient toward dipolar ACN molecules and ACN effectively interacts with EA cations preventing self-association of EAN, which promotes mutual solubility of these two components (Figure 19B,C). Microstructural heterogeneities in EAN−ACN mixtures are manifested in their transport properties at micro- and mesoscopic levels.[546,547] Diffusion coefficients, ion conductivities of constituent ions, and shear viscosities of EAN−ACN mixtures exhibit strong deviations from ideal mixing, which is attributed to the formation of large ion clusters that behave similarly to colloidal aggregates. A similar inhomogeneity was also observed in PAN−ACN mixtures but with smaller magnitude than in EAN−ACN mixtures.[118]

Microstructrues and dynamics of $[C_4MIM]X$−ACN mixtures were extensively studied using S/WAXS,[220,245] IR,[82,548] NMR,[88,548] OHD-RIKE,[95] dielectric[77,549] and terahertz spectroscopies,[550] as well as theoretical[245,548] and computational[95,551−553] approaches. Ion species are nanostructurally organized into polar networks and apolar domains, and ACN molecules are localized in interfacial regions with nitrogen atoms pointing toward imidazolium rings because of HB interactions.[95] A gradual increase of IL concentration in mixtures leads to a structural transition of mixtures from "IL dissolved in ACN" to "ACN dissolved in IL", and a phase behavior transition of hydrodynamic boundary conditions from a "stick" regime to a "slip" regime. In IL−ACN mixtures with high IL concentrations, ACN diffuses much slower than expected due to strong ion−ACN interactions and the presence of ACN clusters in charge-enriched domains.[77,553] Another series of studies showed that dilution of $[C_4MIM][BF_4]$ by ACN results in a local structural transition from large ion clusters to small ion pairing structures (Figure 19D,E).[245,548] ACN cannot break apart strong electrostatic interactions among constituent ions, but they can separate large ion aggregates into small ion pairing clusters with a gradual increase of ACN concentration.[88,245,548,552] For $[C_4MIM]X$−ACN mixtures used as solvent electrolytes in electrochemical devices, microstructures and differential capacitances of pure ILs and IL−ACN mixtures can be described by a theoretical concept termed "counter-charge layer in generalized solvent".[551] An electrical double layer (EDL) structure is composed of a counter-charge layer consisting of polarized IL ions for balancing electrode charge, and the differential capacitances of EDLs are related to detailed interfacial ion structures that will be discussed comprehensively in section 5.

The microstructural and dynamical variations in IL−ACN mixtures further influence their solvent properties, especially in determining solvent−solute interactions. It was found that nitrogen-containing solutes (hexan-1-amine, dipropylamine)

https://dx.doi.org/10.1021/acs.chemrev.9b00693
Chem. Rev. 2020, 120, 5798−5877

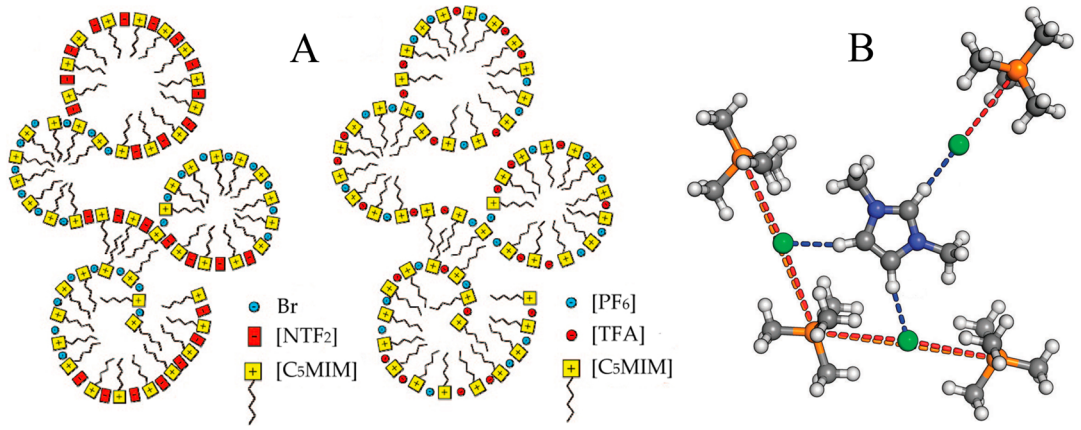

Figure 20. (A) Schematics of nanostructural organization in binary $[C_5MIM]Br_x[NTF_2]_{1-x}$ (left) and $[C_5MIM][PF_6]_x[TFA]_{1-x}$ (right) mixtures. Reproduced with permission from ref 561. Copyright 2008 American Chemical Society. (B) Ion cluster cage formed by one $[C_1MIM]$ cation, three Cl anions, and four $[P_{1,1,1,1}]$ cations obtained from DFT calculations. Reproduced with permission from ref 142. Copyright 2015 Royal Society of Chemistry.

diffuse more slowly than oxygen-containing solutes (1-hexanol and dipropylether) in $[C_4MIM][NTF_2]$–ACN mixtures, indicating enhanced IL–nitrogen interactions compared to IL–oxygen interactions in heterogeneous IL–ACN mixtures.[220] It should be noted that not only ACN but also other molecular components (water, dichloromethane, methanol, and *t*-butanol) with varied polarity, size, and isomerism can affect solvent power (dipolarity and polarizability) of ILs.[554] At low concentrations of molecular compounds, liquid properties of mixtures are dominated by properties of ILs. Conversely, when the quantity of molecular compound is increased, ILs become solute ions in a molecular medium, that is, an electrolyte solution. Between these two extremes, it is expected that there will be remarkable microstructural changes in mixtures with a gradual addition of molecular solutes into ILs, such as the swelling of IL networks, the formation of impetrating polar and apolar networks, and the disruption of large IL cluster into small ion pairs and then possibly solvated isolated ions in mixtures.

4. IONIC LIQUID–IONIC LIQUID MIXTURES

As ILs are solely consisting of cations and anion species, blending two or more ILs represents an important extension of ILs because IL mixtures have interesting physicochemical properties and may outperform pure IL components for a given process. A binary IL–IL mixture consists of either a common cation coupled with two different anions or a common anion coupled with two cations belonging to the same or different cation families. Molecular associations and liquid structures in IL–IL mixtures will be more complicated than those in respective pure IL matrixes and will have a significant effect on their macroscopic functional performance in specific applications.

4.1. IL–IL Mixtures Containing the Same Cation

Neutron and X-ray scattering spectra[327,329] showed that even small protic ILs can be nanostructured in the bulk liquid phase and have distinct rheological properties. Viscosities of pure protic alkylammonium ILs are strongly correlated with strength of HB networks and solvophobic nanostructures in ILs.[363] Pure alkylammonium ILs behave as Newtonian fluids at low shear rates but exhibit striking shear thinning feature at high shear rates. However, rheological properties of binary protic alkylammonium IL–IL mixtures demonstrated fundamental differences in cation–anion interactions due to an offsetting effect of HB interactions and the formation of solvophobic nanostructures in mixtures.[363,555] Mixtures containing the same protic alkylammonium cation coupled with formate and $[NO_3]$ anions can resist heavier flow fields than respective ILs due to different HB capabilities of two anions.[259,333] These protic alkylammonium IL mixtures are a representative demonstration of double-salt ILs in which constituent ions do not retain their individual nature.[556] Although pure alkylammonium ILs and their mixtures exhibit great similarities with respect to overall ion-alternating structures, each type of the statistically distributed ions experiences a completely different local ionic environments in heterogeneous IL matrixes.

For imidazolium IL–IL mixtures, it was found that $[C_4MIM][NTF_2]_x[C_1C_1PO_4]_{1-x}$ (dimethylphosphate) mixtures exhibit significant positive excess molar volumes, whereas $[C_4MIM][NTF_2]_x[TFO]_{1-x}$ mixtures show small deviations from ideality,[557,558] which is attributed to greater HB capability of $[C_1C_1PO_4]$ anions compared to that of $[TFO]$ anions in coordinating imidazolium cations. In addition, thermal and ion conductivities of imidazolium IL–IL mixtures exhibit either expected behavior upon mixing[559,560] or minor deviations from anticipated values[561,562] depending on a delicate interplay of interactions among constituent ions. Generally, deviations in phase behaviors of mixtures are related to variations in short-range interactions and ion asymmetries, the latter of which are crucial for ion associations and dissociations in mixtures.[315,563,564]

There are some experimental attempts to understand phase behaviors of imidazolium IL–IL mixtures.[558,561,565,566] OKE spectra for $[C_5MIM]Br_x[NTF_2]_{1-x}$ mixtures are well described by weighted sums of spectra for pure ILs, whereas OKE spectra for $[C_5MIM][PF_6]_x[TFA]_{1-x}$ mixtures are nonadditive.[561] Either additive or nonadditive of OKE spectra depends on relative sizes of anions in mixtures, assuming that mixtures are assembled into polar and apolar networks at the nanoscopic level.[336,564] For anions with similar sizes (i.e., $[PF_6]$ and $[TFA]$), polar networks in mixtures are described by random co-networks, whereas for anions that differ greatly in sizes (i.e., $[NTF_2]$ and Br), polar networks are characterized by "block co-networks", a nanostructural organization resembling that of

https://dx.doi.org/10.1021/acs.chemrev.9b00693
Chem. Rev. 2020, 120, 5798–5877

block copolymer (Figure 20A). Anion sizes and shapes have significant effects on spatial arrangements of ions in IL−IL mixtures in terms of interion distances and Coulombic attractions between oppositely charged ions.[563,567] NMR results showed that both static and dynamic free volumes are strongly correlated for imidazolium IL−IL mixtures.[558] Given a relationship between free volumes and transport properties such as liquid viscosities and ion conductivities, these results provide an intrinsic link between thermodynamics of mixing and liquid structures of IL−IL mixtures.

Focusing on electrochemical applications of pyrrolidinium and pyridinium IL−IL mixtures, the beneficial synergic effect on ion conductivities and electrochemical stabilities of mixtures was investigated combining experimental and computational studies.[568−570] Binary $[C_4MPYRI][BF_4]_x[N(CN)_2]_{1-x}$ mixtures exhibit two well-defined regions in which physicochemical properties resemble those of pure ILs, separated by a critical concentration of $[BF_4]$.[568] Liquid structures do not change remarkably once this critical concentration is reached, leading to an almost ideal mixing from a thermodynamic point of view. This points to a simple anion dilution effect leading to liquid regions dominated by interactions between $[C_4MPYRI]$ cations and $[N(CN)_2]$ anions with $[BF_4]$ anions being dispersed or liquid regions dominated by interactions between $[C_4MPYRI]$ cations and $[BF_4]$ anions with $[N(CN)_2]$ anions being dispersed.[568] Atomistic simulations indicated a weak structural change with an increase of $[C_4MPYRI][BF_4]$ concentration in mixtures, arising from decreased sizes of apolar domains. This structural change leads to positive excess molar volumes but without significant changes in energetic properties or in the manner in which ions interact.

4.2. IL−IL Mixtures Containing a Same Anion

IL−IL mixtures containing two substantially different cations and a common anion have a rich structural chemistry, even if these two cations belong to the same cation family.[571−573] Canongia Lopes et al. found very small positive excess volumes for binary imidazolium IL mixtures composed of cations with varied alkyl chains coupled with $[NTF_2]$ anions.[574] In addition, several thermophysical properties, such as liquid densities, enthalpies of mixing, conductivities, and viscosity data, also exhibit practically "ideal" (linear) mixing behavior with small excess deviations arising from structural differences between imidazolium cations.[559,575] For a $[C_2MIM]_{0.5}[C_6MIM]_{0.5}[NTF_2]$ mixture, microphase separation was observed between polar and apolar domains whose sizes are intermediate to those of two pure IL components.[572] SANS experiments and atomistic simulations of $[C_2MIM]_x[C_{12}MIM]_{1-x}[NTF_2]$ mixtures demonstrated that both physicochemical properties and liquid structures change substantially as a function of chemical composition of mixtures.[113,573] Liquid structures of mixtures with molar fractions of $[C_{12}MIM][NTF_2]$ less than 0.3 are described as aggregates of amphiphilic $[C_{12}MIM]$ cations in a relatively polar $[C_2MIM][NTF_2]$ solvent, whereas liquid structures of mixtures with molar fractions of $[C_{12}MIM][NTF_2]$ more than 0.3 are characterized by bicontinuous polar and apolar networks, where C_{12} chains percolate throughout mixtures forming a continuous apolar subphase. With a gradual increase of $[C_{12}MIM][NTF_2]$ concentration in mixtures, the length scale of apolar subphase increases and phase behaviors of mixtures become more reminiscent of pure $[C_{12}MIM][NTF_2]$. These $[C_2MIM]_x[C_{12}MIM]_{1-x}[NTF_2]$ mixtures become more disordered with increasing temperatures, but the fundamental liquid structures do not change substantially. In addition, these mixtures exhibit different response to the addition of water. For mixtures with less $[C_{12}MIM][NTF_2]$, water is incorporated into polar networks, whereas mixtures with more $[C_{12}MIM][NTF_2]$ are too hydrophobic to incorporate sufficient water and to change liquid structures.

In addition to aprotic IL−IL mixtures consisting of a common anion coupled with two imidazolium cations with varied alkyl chains, different mixing behaviors were observed in thermo-dynamical quantities of protic−aprotic mixtures with cations belonging to different cation families.[259,567,570,576,577] Atomistic simulations and experimental measurements showed that binary mixtures composed of alkylammonium protic ILs and imidazolium aprotic ILs exhibit almost ideal mixing behavior with a gradual microstructural transition between two pure IL components,[576,578] which is rationalized by a structural similarity of two ILs.[557,579] In particular, a noteworthy association was observed upon mixing PAN/BAN and $[C_2MIM][BF_4]$ ILs. In these mixtures, $[C_2MIM]$ cations are integrated into protic networks and $[BF_4]$ anions occupy previously empty regions near protic cation tails. It is significant that a subtle microstructural change in these mixtures leads to complicated variations in transport properties of constituent ions.[578] For EAN−$[C_2MIM][BF_4]$ mixtures, a novel conductivity curve exhibits pronounced deviations from the simple ideal mixing rule, with three different regions defined by a local maximum, reflecting enhanced translational dynamics relative to ideal mixing behavior, and a global minimum at intermediate concentrations. These regions are defined by the onset of the formation of EAN HB networks (X_{EAN} = 0.2) and the virtual disappearance of aprotic IL structures (X_{EAN} = 0.7), where long-range ordering for $[C_2MIM][BF_4]$ breaks down.

In addition to these mixing behaviors observed in protic−aprotic IL−IL mixtures where ions differ considerably in sizes and in HB forming abilities,[580] there are some mutually immiscible binary IL−IL mixtures,[570,581,582] which are in disagreement to the intuitive rule of thumb *similia similibus solvuntur*. Two phases were obtained for $[C_2MIM]_x[P_{6,6,6,14}]_{1-x}[NTF_2]$ mixtures over a wide temperature range.[581,583] In addition, mutually immiscible binary mixtures were also obtained if $[NTF_2]$ anions in $[C_nMIM]_x[P_{6,6,6,14}]_{1-x}[NTF_2]$ mixtures are replaced by Cl anions.[581,583] A large negative entropy of dissolving $[C_nMIM]Cl$ ILs in $[P_{6,6,6,14}]Cl$ was observed when imidazolium cation alkyl chains are shorter than C_5.[581] DFT calculations revealed that solvation of $[C_1MIM]Cl$ in $[P_{6,6,6,14}]Cl$ not only exhibits a large negative entropy but also leads to enhanced diffusion of $[P_{6,6,6,14}]$ cations compared to $[C_1MIM]$ cations in mixtures.[142] Both unexpected features are attributed to the formation of large symmetric ion cluster cages in which a $[C_1MIM]$ cation is surrounded by three Cl anions in the first solvation shell and four $[P_{6,6,6,14}]$ cations in the second solvation shell (Figure 20B). This cage structural motif illustrated that atoms involved in HB interactions in mixtures remain their positions similar to those in pure ILs because polar domains in $[C_1MIM]Cl$ and $[P_{6,6,6,14}]Cl$ ILs fit well with each other. Lengthening imidazolium cation alkyl chains disturbs cage structures and enhances $\pi-\pi$ stacking of imidazolium rings in $[C_nMIM]_x[P_{6,6,6,14}]_{1-x}Cl$ mixtures. Both aspects decrease liquid structural ordering in mixtures.

https://dx.doi.org/10.1021/acs.chemrev.9b00693
Chem. Rev. 2020, 120, 5798−5877

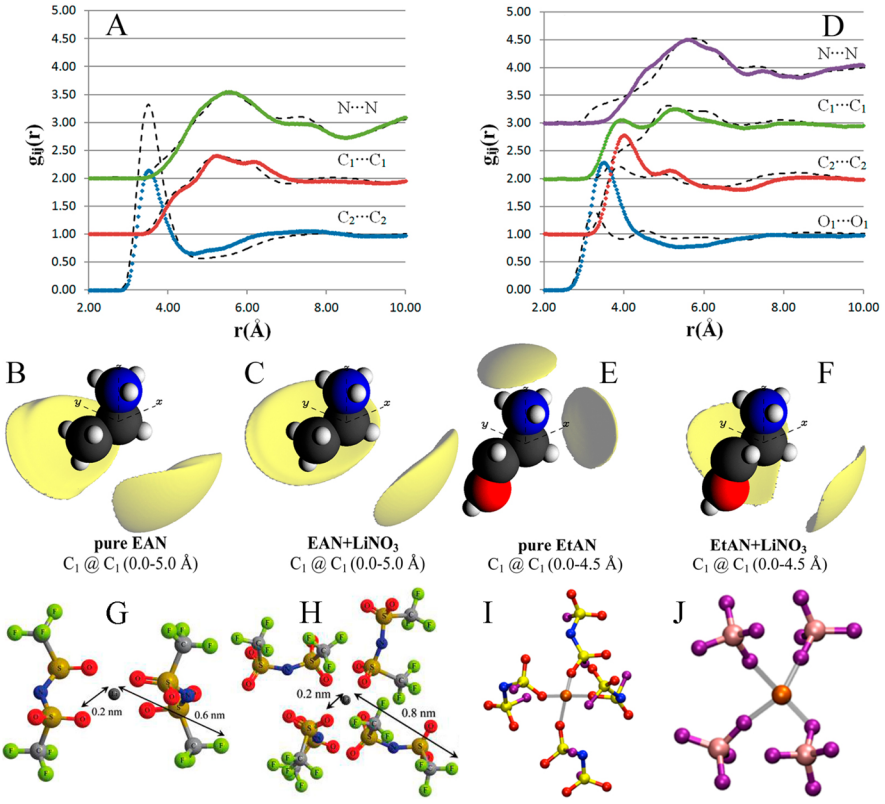

Figure 21. Local structures in apolar domains for IL−$LiNO_3$ mixtures. Comparison of radial distribution functions for (A) EAN−$LiNO_3$ and (D) EtAN−$LiNO_3$ mixtures (solid lines) with those for pure ILs (dashed lines). Spatial distribution function plots of carbon atoms bonded to nitrogen atoms in EA and EtA cations as a function of distance and angular position from a central cation for (B) EAN, (C) EAN−$LiNO_3$ mixture, (E) EtAN, and (F) EtAN−$LiNO_3$ mixture. Reproduced with permission from ref 596. Copyright 2014 American Chemical Society. Representative ion structures of (G) $[Li(NTF_2)_2]^-$ and (H) $[Li(NTF_2)_4]^{3-}$. Reproduced with permission from ref 598. Copyright 2008 American Chemical Society. Typical Li^+ coordination complexes of (I) $[Li(FSI)_4]^{3-}$ found in $[C_3MPYRR][FSI]$ and of (J) $[Li(BF_4)_4]^{3-}$ found in $[C_2MIM][BF_4]$ at 298 K and with X_{Li+} = 0.05. Reproduced with permission from ref 599. Copyright 2014 American Chemical Society.

Even though there are some variations for IL−IL mixtures consisting of a common anion and two cations, it is clear that these mixtures are distinct systems in comparison with pure IL components. Both experimental and computational studies showed that a range of microstructural and physicochemical properties can be controlled simply by fine-tuning chemical compositions of mixtures rather than by synthesizing a large number of pure ILs. These IL−IL mixtures provide a promising path for rational selection of appropriate ILs for particular applications.

4.3. Imidazolium IL−Imidazole Mixtures

For imidazolium ILs, there is a set of extraordinary binary mixtures consisting of imidazolium ILs and neutral amphoteric imidazole molecules.[163,584,585] Imidazole molecules provide both proton donor and acceptor sites to establish extended HB networks and facilitate proton transfer in ionic materials. AIMD simulations revealed that proton migration in imidazole involves two steps with a strong HB between two adjacent imidazole molecules (~0.3 ps) and thereafter a rotation of imidazole molecules because of HB cleavage (~30 ps). Imidazole molecules tend to form strong HBs with anions in mixtures, like selenocyanate ([SeCN]),[586] leading to a restricted short time angular wobbling-in-a-cone sampling of [SeCN] anions in heterogeneous solvent environments.

Mixing a protic $[C_2HIM][NTF_2]$ with imidazole perturbs the native HB networks in the IL matrix. Due to a structural similarity, imidazolium cations and imidazole molecules are interchangeable and exhibit competing features in coordinating $[NTF_2]$ anions.[163,585] These two species form HBs with $[NTF_2]$ anions with varied HB strengths depending on the detailed composition of IL−imidazole mixtures, leading to significant changes in microstructures and dynamics in binary mixtures. At low imidazole concentrations, HB network configurations promote proton transfer (Grotthuss mechanism) in mixtures where imidazole molecules act as base molecules pulling protons from neighboring imidazolium cations. In intermediate imidazole concentrations, mixtures display a nonideal mixing behavior rationalized by competitive ion−ion and ion−imidazole interactions and preferential HB interactions. For a $[C_2HIM][NTF_2]$−imidazole mixture with an equimolar fraction, a microstructural transition occurs from an ion network mainly stabilized by electrostatic forces among constituent ions to a mixed phase held together by site specific HB interactions. This composition marks a steep increase in ion conductivities resulting from the formation of HBs between neighboring imidazole molecules. Liquid structures of $[C_2HIM][NTF_2]$−imidazole mixtures with high imidazole concentrations are characterized by highly dissociated and rapidly diffusing ions in a neutral solvent. Charge transport in these imidazole-concentrated mixtures is characterized by a vehicular mechanism. These observations provide important physical insights into a potential usage of protic ILs as solvent electrolytes in electrochemical devices and demonstrate that

https://dx.doi.org/10.1021/acs.chemrev.9b00693
Chem. Rev. 2020, 120, 5798−5877

manipulation of HB networks is a valuable approach to fine-tune charge transport mechanisms in IL mixtures.

4.4. IL−Li Salt Mixtures

IL mixtures containing Li salts are useful systems for Li ion batteries in terms of safety, manufacturing cost, and performance.[560,587−590] Usually, Li salts containing IL anions are preferable because of a higher solubility with respect to mixtures with dissimilar anions. Therefore, IL−Li salt mixtures can be considered as a ternary component system consisting of IL cations, Li ions, and common anions.

Focusing on ILs as solvent electrolytes in batteries, representative studies were devoted to analysis of $LiNO_3$ in alkylammonium nitrate ILs. At ambient conditions, EAN and $LiNO_3$ are miscible up to ∼0.2 molar fraction of $LiNO_3$ in EAN.[591,592] An overall structural scenario in EAN−$LiNO_3$ mixtures, as determined from joint SAXS and atomistic simulations,[591,593] can be described as (1) EAN can essentially retain its nanostructure and liquid morphology upon addition of $LiNO_3$ and only interactions among ammonium groups and $[NO_3]$ anions being slightly perturbed and (2) Li ions are solvated in polar domains in IL matrixes, where they coordinate with $[NO_3]$ anions either in a monodentate or in a bidentate manner, leading to a solidlike short-range pseudolattice ordering structure.

However, it is noteworthy that solvated Li ions have distinct capabilities in coordinating ions in IL matrixes and can be described using a similar idea of "structure-making" and "structure-breaking", which are well-established concepts for description of dilute aqueous electrolytes.[594,595] $LiNO_3$ is a "structure-breaking" salt for EAN. Li ions are incorporated into polar domains of spongelike nanostructures. They disrupt alignments of ethyl chains in apolar domains and weaken cation−anion HB interactions, resulting in fewer linear HBs and a higher proportion of bifurcated HBs (Figure 21A−C).[596] Conversely, $LiNO_3$ is a "structure-making" salt for EtAN. Li ions induce a long-range rearrangement of EtAN ion species, such that a bicontinuous instead of a clustered nanostructure is formed, which is attributed to favorable *trans* conformations of EtA cations (Figure 21D−F).[596] In addition, heterogeneous structures in IL−Li salt mixtures are further corroborated by experimental characterizations of microstructural and rheological properties of EAN−$LiNO_3$ and EtAN−$LiNO_3$ mixtures in confined environments.[595] EAN is weakly dependent, with only small changes in structural forces, frictions, and liquid viscosities at low concentrations of Li ions,[592] whereas EtAN's behavior is strongly subjected to Li ion concentrations. At low Li ion concentrations, liquid viscosities of EtAN−$LiNO_3$ mixtures increase. Structural forces and the associated friction profiles deviate from those for pure EtAN, which has a direct consequence on boundary layers, as demonstrated from a large reduction in friction forces at high loads. A high Li ion concentration in EtAN leads to enhanced changes in liquid viscosities and structural forces. Lengthening alkyl chains in primary alkylammonium cations from EA to PA and BA and changes in cation structures from primary to secondary and tertiary ammonium cations have a significant impact on solvation structures of Li ions in mixtures as Li ions are preferentially accommodated into polar networks to coordinate anions.[597] With an increase of Li ion concentrations in mixtures, Li ions progressively erode HB networks, decreasing the extent of HB networks and inducing orientation disorders in polar domains. These effects are more pronounced for ILs having long cation alkyl chains due to a lower degree of cation−anion HB interactions. Large secondary and tertiary ammonium cations have sparsely packed 3D ion structures in IL matrixes, which are easily perturbed by Li salts.

OHD-OKE spectra demonstrated that addition of $LiNTF_2$ salt to $[C_4MIM][NTF_2]$ leads to an increase in liquid viscosity, a decrease in ion mobility, and distinct rotation relaxation dynamics of ions in IL−Li salt mixtures.[431,600,601] These changes are essentially correlated with distinct variations of microstructures in mixtures with a gradual addition of $LiNTF_2$ salt. Competitive binding of large cations to $[NTF_2]$ anions acts as an enhancer of Li ion diffusivities in mixtures by reducing $LiNTF_2$ aggregate sizes and keeping a tetra-coordination feature of Li ions.[598] IR and DFT calculations provided direct evidence supporting the presence of strongly coordinated $[Li(NTF_2)_2]^-$ structure being a major adduct in $[C_nMIM][NTF_2]$−$LiNTF_2$ mixtures (Figure 21G).[598,602,603] In general, $[Li(NTF_2)_{n+1}]^{n-}$ clusters are highly stable species due to strong Coulombic interactions between Li ions and oxygen atoms in $[NTF_2]$ anions (Figure 21H).[598,603−605]

A series of interesting works demonstrated that hybrid electrolytes consisting of imidazolium ILs and Li salts having different anions are promising electrolytes for Li ion batteries. For $[C_2MIM][NTF_2]$−$LiNTF_2$ mixtures, replacing $[NTF_2]$ with bis(fluorosulfonyl)imide ([FSI]) or combining both anions leads to enhanced ion conductivities in mixtures.[589] The $[C_2MIM][FSI]_{0.8}[LiNTF_2]_{0.2}$ electrolyte holds peculiar significance due to its high thermal stability, arising from a specific solvation structure of Li ions in coordinating $[NTF_2]$ and [FSI] anions.[606] In such a way, a remarkable EDL structure is formed on the electrode surface protecting $[C_2MIM]$ cations from decomposition and thereby improving cathodic stability. A nontrivial nature of these EDL structures together with their dependence on electrolytes and electrode materials[607] are on par with organic electrolytes in terms of viscosities, ion and electrical conductivities when taking into account their anticipated operating temperatures.[608]

The IL ion-Li coordination pattern in protic imidazolium ILs is very different to that in aprotic imidazolium ILs.[609,610] The coordination number of Li ions in protics is always smaller than that in aprotics, which makes Li ions more "free" to move in protic imidazolium ILs.[611,612] Furthermore, the charge valence of inorganic salt cations like Mg^{2+} and Ca^{2+} has a significant effect on HB networks in IL−salt mixtures than those in their monovalent counterparts.[590,613] Vibrational spectra and AIMD simulation results indicated that there are three different potential energy environments for $[NTF_2]$ anions in IL−Mg salt mixtures in contrast to the fact that there are only two coordination patterns in IL−Na and IL−Li salt mixtures.[614] Additional investigations revealed noteworthy coordination patterns of strontium, uranyl, and perrhenate salts with imidazolium ILs in IL−salt mixtures, which provide valuable clues for extraction of these salts in context of nuclear waste processing.[615]

In challenging electrochemical applications, pyrrolidinium ILs have prominence for their outstanding capabilities in dissolving Li salts, giving rise to IL−Li electrolytes for innovative uses in Li ion devices.[616,617] In comparison with those observed in imidazolium ILs, doping Li salts into pyrrolidinium analogues results in distinct microstructures.[599,618−620] For example, at low levels of Li salt doping, both $[C_4MPYRR][NTF_2]$ and $[C_3MPYRR][FSI]$ ILs exhibit stable Li solvation structures containing either two anions,

https://dx.doi.org/10.1021/acs.chemrev.9b00693
Chem. Rev. 2020, 120, 5798−5877

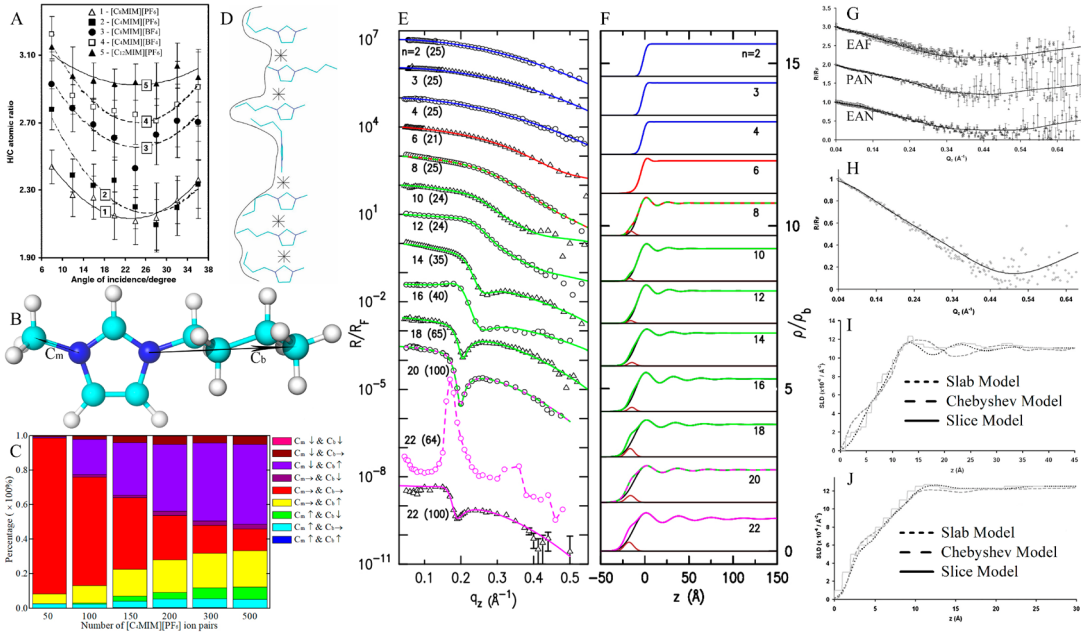

Figure 22. (A) Experimentally determined atomic H/C ratios for representative ILs at the IL−vapor interface. Reproduced with permission from ref 79. Copyright 2001 Royal Society of Chemistry. (B) Definition of C_m and C_b vectors in [C_4MIM] cation and (C) preferential distributions of [C_4MIM] cations, characterized with bivariate orientations of C_m and C_b vectors, at the IL−vapor interface for simulation systems containing varied numbers of [C_4MIM][PF_6] ion pairs on the graphene surface. The notations →, ↑, and ↓ correspond to C_m and C_b vectors being parallel and perpendicular to the IL−vapor interface with terminal carbon atoms protruded into the vapor phase and projected into bulk liquids, respectively. Reproduced with permission from ref 645. Copyright 2013 Royal Society of Chemistry. (D) Schematic conformation of [C_4MIM] in the IL−vapor interface. Reproduced with permission from ref 646. Copyright 2012 Royal Society of Chemistry. (E) Fresnel-normalized (symbols) and model-fitted (lines) XRR curves of the IL−vapor interface of [C_nMIM][NTF_2] ILs at specific temperatures. Different colors indicate different surface phases. Curves in two colors denote a transition between surface phases. (F) Electron density profiles (normalized to bulk electron density) obtained from model fits in part E. Reproduced with permission from ref 647. Copyright 2018 National Academy of Sciences. (G) XRR profiles for EAN (Δ), PAN (○), and EAF (□) IL−vapor interface, and for (H) EtAN−vapor interface. Reproduced with permission from ref 629. Copyright 2011 Royal Society of Chemistry. Scattering length density profiles for (I) EAN−vapor and (J) EtAN−vapor interfaces from the slab fit (dotted line), Chebyshev fit (dashed line), and slice fit (solid line) models. Reproduced with permission from ref 364. Copyright 2012 Royal Society of Chemistry.

both having bidentate ligand bonds, or three anions, one being bidentate and the other two being monodentate (Figure 21I), whereas [BF_4] ILs exhibit a tendency toward a solvation shell having four monodentate anions (Figure 21J).[599] A high level of Li doping leads to the formation of highly coordinated Li ion network structures where a single anion participates in multiple Li ion solvation shells. A similar $[Li(NTF_2)_{n+1}]^{n-}$ adduct structure is observed in [C_nMPYRR][NTF_2]−$LiNTF_2$ mixtures.[603,604,621] SAXS experiments showed a nonmonotonic variation of charge alternation distances with and without addition of Li salts into pyrrolidinium and imidazolium ILs as a function of cation alkyl chain length, highlighting a competitive feature of steric hindrance and vdW interactions of alkyl tails in cations and a reconfiguration of [NTF_2] anions in coordinating Li ions.[599,620,622]

It should be noted that transport and conductivities of Li ions in IL−Li salt mixtures are governed by their binding strength with anions and intrinsic liquid viscosities of ILs.[599,619,623,624] In a $[C_4MPYRR]_{0.9}Li_{0.1}[NTF_2]$ mixture, diffusivities of ion species are significantly smaller than those in pure IL matrix due to a larger viscosity of this IL−Li salt mixture and the formation of peculiar Li−anion adducts in this mixture.[604,625] These findings are rationalized by a hopping diffusion process of Li−anion adducts in mixture because of a disruption of adduct coordination shells by [NTF_2] anions (structure−diffusion mechanism) rather than a Brownian motion of the whole Li−anion adducts (vehicular mechanism).[593,618,625] Ion conductivities of IL−Li salt mixtures increase with increasing concentrations of Li ions, with this effect being greater at elevated temperatures. However, the contribution of Li ions to ion conductivities does not proportionally increase with Li ion concentrations but saturates at a high doping level.[604]

5. IONIC LIQUIDS IN INTERFACIAL REGIONS

Applications of ILs in gas separations, biphasic extractions, and in electrochemical devices involve their contact with gas, liquid, and solid materials. Microstructural and dynamical properties of ILs on surfaces and in interfacial regions determine their functionalities in physical and chemical processes occurring across phase boundaries. Given that interfacial regions are highly inhomogeneous, ILs exhibit fundamentally different physicochemical and structural quantities as that in bulk liquids. In the following subsections, we mainly focus on a description of heterogeneous microstructures and dynamics of ILs in varied interfacial regions and their effects on macroscopic functional performance of ILs in electrochemical and tribological applications.

5.1. IL−Vapor (Gas) Interface

The IL−vapor (gas) interface holds a special significance for particular applications of ILs involving adsorption and desorption of gas molecules.[626] In these applications, chemical compositions and molecular arrangements of ions in interfacial

https://dx.doi.org/10.1021/acs.chemrev.9b00693
Chem. Rev. 2020, 120, 5798−5877

regions are distinct to those in bulk liquids because ions experience unbalanced forces. A wide range of experimental techniques including DRS,[78,79,627] neutron reflectometry,[106,628−630] SFG,[96,98,100] XRR,[105,119,628,629] XPS,[115,626] and molecular simulations[631−633] have been employed to provide detailed information on surface compositions, interfacial structures, and dynamics of ions at the IL−vapor interface.

Watson et al. first reported experimental investigations of interfacial compositions and molecular orientations of imidazolium ILs using DRS spectroscopy.[79,627] Both imidazolium cations and anions in $[C_nMIM][PF_6]$ (n = 4, 8, and 12) and $[C_nMIM][BF_4]$ ILs (n = 4 and 8) are present at the IL−vapor interface with no significant segregation. Imidazolium rings in these two ILs exhibit similar orientations being perpendicular to the IL−vapor interface. However, butyl chains are positioned differently with those in $[C_4MIM][PF_6]$ being parallel to the IL−vapor interface and those in $[C_4MIM][BF_4]$ projecting into bulk liquids with a shift of $N-CH_3$ groups closer to the IL−vapor interface. Lengthening cation alkyl chains from C_4 to C_8 has little effect on the H/C ratio for all ILs at the IL−vapor interface, but a further increase to C_{12} results in a substantial increase in the H/C ratio for $[C_{12}MIM][PF_6]$ with methyl groups close to the IL−vapor interface (Figure 22A). In another series of studies, SFG spectra for hydrophobic $[C_4MIM][PF_6]$ and $[C_4MIM][NTF_2]$ ILs and hydrophilic $[C_4MIM][BF_4]$ IL suggested that imidazolium rings are most likely lying parallel to the IL−vapor interface with butyl chains projecting into the vapor phase with a tilt angle from the surface normal direction.[438,634] Moreover, SFG spectra illustrated that anions have a negligible effect on preferred orientations of $[C_4MIM]$ cations in the IL−vapor interfacial region.[97,635]

XRR and neutron reflectivity are complementary techniques in providing electron density profiles across the IL−vapor interface.[105,106,628,630] Bowers, Vergara-Gutierrez, and Webster carried out neutron reflectivity on $[C_4MIM][BF_4]$ and $[C_8MIM][PF_6]$ ILs.[636] A surface layering structural model was suggested with imidazolium rings and alkyl tail moieties being segregated at the IL−vapor interface forming a lamellar structure extending to two layers of the alkyl chains. On the other hand, XRR studies of $[C_4MIM][PF_6]$ and $[C_4MIM][BF_4]$ ILs reported by Deutsch et al. indicated the presence of surface layering structures at the IL−vapor interface.[630] Two types of molecular arrangements in the IL−vapor interfacial region were proposed, one with alkyl chains parallel to the IL−vapor interface and the other one with alkyl chains normal to the IL−vapor interface. In addition, XRR spectra revealed an increase in electron density (∼10−12%) at the IL−vapor interface, which is higher than that in bulk ILs and is mainly attributed to adsorption of anions at the IL−vapor interface. These experimental results indicate the presence of both cations and anions in the IL−vapor interfacial region, which is consistent with experimental data obtained from DRS spectra.[78,627]

Applications of external fields can significantly change interfacial ion structures.[637,638] An intriguing work conducted by Jurado et al. demonstrated that an extended SFA repeatedly imposing and releasing confinement on $[C_6MIM][C_2SO_4]$ IL film induced a phase transition that was not relieved by the final removal of such an external constraint.[639] Atomistic simulations of the $[C_8MIM][C_8SO_4]$ IL film indicated that a lamellar structure is not restricted to the IL−vapor interfacial region but instead extends across a slab of ∼9 nm.[640] A systematic variation of alkyl chain lengths in $[C_nMIM]$-$[C_mSO_4]$ ILs showed similar layering structures at the IL−vapor interface,[99,100,641,642] which is also supported by surface tension measurements with a decreased trend with increasing alkyl chain lengths of cations and anions if the corresponding counterion is fixed.[643] When $[C_nMIM]$ cations and $[C_mSO_4]$ anions are functionalized with ether groups in the alkyl chains, both of them still favor tail-outward orientations at the IL−vapor interface, and bulk liquid phase preserves an alternation of polar and apolar regions.[644] These experimental and computational observations indicate that different polymorphic phases of ILs can be "engineered" on the nanoscopic level via confinement perturbations or other external stimuli, and the observed liquid morphological transitions are very attractive for energy applications particularly for electrochemical devices.

It should be noted that not only IL ion structures but also IL film thickness can have a significant effect on distributions of cations in the IL−vapor interfacial region if the IL film is confined on a solid substrate.[645] With a gradual increase of the IL film thickness, preferential orientations of cations in $[C_4MIM][PF_6]$ at the IL−vapor interface exhibit a progressive transition from a dominant flat distribution in an IL monolayer to that described by multiple favorable orientations having varied proportions (Figure 22B,C).[645,648] In these favorable orientations, the main orientation of imidazolium rings is essentially perpendicular to the IL−vapor interface with some angular tilt (Figure 22D).[646] The formation of compact IL−vapor interfacial layering structures further complicates dynamical quantities of ILs in comparison with those in bulk liquids. In the IL−vapor interfacial region, translational mobilities of terminal carbon atoms in $[C_4MIM]$ butyl chains[648] and rotational dynamics of a short molecular axis in $[C_4MIM]$ cations[271] are faster than those in other layers of confined IL films and in bulk liquids of simulation systems without confinement. Rotational dynamics of $[C_4MIM]$ cations generally follow a Kohlrausch−Williams−Watts behavior in the IL−vapor interfacial region, whereas in bulk liquids of confined IL films, the temperature dependence of translational diffusions and rotational relaxations of $[C_4MIM]$ cations is characterized by a VFT feature over a wide temperature range.[271]

Systematic lengthening alkyl chains in imidazolium cations and enlarging anions from halides to $[BF_4]$, $[PF_6]$, [TFO], and complex anions containing perfluoroalkyl groups such as $[NTF_2]$, [FAP], and bis(perfluoroethylsulfonyl)imide lead to significant changes in interfacial structures and molecular arrangements in the IL−vapor interfacial region.[115,626,646,649] In general, lengthening the alkyl chains in the imidazolium cations and changing asymmetric $[C_nMIM]$ to symmetric $[C_nC_nIM]$ cations tend to increase the probability for alkyl chains to point into the vapor phase and the coverage of the IL−vapor interface by alkyl groups with an expense of imidazolium rings and anions.[633] However, this interfacial structural enhancement decreases with enlarging anion sizes, which promotes a disruption of interfacial alkyl layer structures, leading to cations with enhanced orientation freedom and more alkyl chains being able to point into liquid phase. In addition, no significant surface segregation of anions relative to imidazolium rings occurs in the IL−vapor interfacial layers, indicating that imidazolium rings and anions are located at similar distances from the interface, forming a densely packed polar layer due to strong Coulombic interactions. Temperature has a negligible influence on the overall density

https://dx.doi.org/10.1021/acs.chemrev.9b00693
Chem. Rev. 2020, 120, 5798−5877

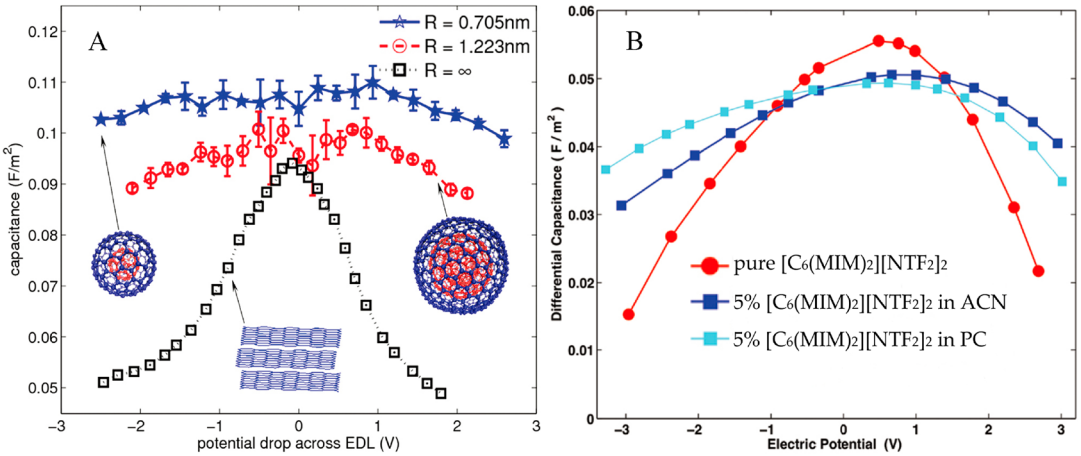

Figure 23. (A) Effect of electrode curvature on differential capacitance of ILs on OLCs and planar electrodes. *R* is the radius of an OLC, and it is infinity for a planar electrode. Reproduced with permission from ref 181. Copyright 2012 American Chemical Society. (B) Differential capacitance as a function of applied electric potential for pure $[C_6(MIM)_2][NTF_2]_2$, $[C_6(MIM)_2](NTF_2)_2$–ACN, and $[C_6(MIM)_2](NTF_2)_2$–PC mixtures with an IL concentration of 5%. Reproduced with permission from ref 674. Copyright 2014 IOP Publishing.

profiles and a relatively small effect on molecular orientations in the IL–vapor interfacial region. Ions stay considerably longer in the IL–vapor interfacial layers than they do in subinterfacial layers and ion exchange dynamics between consecutive layers are associated with distinct ion diffusions and rotational dynamics of ions within layers.

The evolution of IL–vapor interfacial structures with lengthening alkyl chains in imidazolium cations from Coulombic to vdW interaction domination was clarified in a systematic Angstrom-resolution synchrotron XRR study of $[C_nMIM][NTF_2]$ ILs.[647] A progressive change in electron density profiles was observed from a typical "simple liquid" for $n < 6$ (akin to that of simple liquids like water and organic solvents), through a nonmonotonic layered solvent for $8 < n < 20$ (single high-density surface-segregated monolayer), to a liquid crystal surface phase for $n = 22$ which reverts to a "conventional" layered surface phase at high temperatures (Figure 22E,F). The layered surface phase consists of alternating polar and apolar parallel slabs, and layer spacing is larger than extended alkyl chains in imidazolium cations but smaller than twice that length, indicating that alkyl chains in lateral packing slabs are flexible, kinked, and partially interdigitated.[375,650,651]

Compared to bulk liquid structures of protic ILs, XRR spectra showed that EAN, PAN, and EAF ILs exhibit extended IL–vapor interfacial structures spanning at least five ion pair diameters (Figure 22G,I).[119,629] All three ILs exhibit similar X-ray scattering length density profiles consisting of two parts. The top interfacial layer is a diffuse layer composed of multiple cations and anions arranged in such a way that polar groups are surrounded by cation alkyl chains, protecting hydrophilic species from the hydrophobic gaseous phase. Below this are layers enriched with apolar alkyl groups and polar domains consisting of cation ammonium moieties and anions, which gradually decay to bulk liquid structures. Lengthening cation alkyl chains from EA to PA results in pronounced interfacial structures. Alkyl chains in PA cations impart larger solvophobicity than those in EA cations, leading to well-defined segregation of polar and apolar domains in a heterogeneous PAN matrix. Conversely, replacing $[NO_3]$ with formate anions reduces HB interactions, and thus the interfacial region does not extend as far into bulk liquids. This suggests that solvophobicity determines the sharpness of segregation of interfacial structures while HB determines the extent of interfacial ordering.

The IL–vapor interfacial structures of EtAN (Figure 22H) are distinct from those of EAN, PAN, and EAF ILs.[364] A simple model used to fit XRR spectra revealed that electron densities increase from zero to bulk values over a distance of ~11 Å (Figure 22J), a distance of approximately twice the EtAN ion pair dimension. Polar head and tail moieties in EtA cations are internalized to form, along with $[NO_3]$ anions, the interior of the surface aggregates, which are coated by methyl moieties in contact with the vapor phase. However, surface orientations of alkyl groups in EtA cations are quite different from those of EA cations due to a less amphiphilic character of EtA than EA.[119] This is a clear illustration of how designer properties of ILs can be exploited to control interfacial nanostructures. If an (relatively) unstructured interface is desired, it is better to incorporate polar functional groups into alkyl chains to disrupt solvophobic interactions. This prevents the formation of a layered subsurface and facilitates a rapid adsorption and transport of species from the vapor phase through the interfacial region into bulk liquids, desirable for applications such as CO_2 absorption.

For ILs consisting of pyrrolidinium cations coupled with $[NTF_2]$ anions, experimental features observed in SFG and XPS spectra resemble those for imidazolium ILs with alkyl chains projecting into the vapor phase.[652,653] Pyrrolidinium rings appear to be parallel to the surface plane with alkyl chains taking tilted configurations relative to the surface normal direction. Atomistic simulations showed that $[C_4MPYRR][CF_3SO_3]$, $[C_4MPYRR][NTF_2]$, and $[C_4MPYRR][FAP]$ ILs exhibit distinct segregation of polar and apolar domains in the IL–vapor interfacial region, where liquid morphologies of apolar domains are independent of anion types.[654] The presence of a discontinuity in local density leads to a small charge segregation at the IL–vapor interface, which is less substantial for $[C_4MPYRR][FAP]$ as $[FAP]$ anions are voluminous and motivate a lack of interfacial ordering at the IL–vapor interface.

https://dx.doi.org/10.1021/acs.chemrev.9b00693
Chem. Rev. 2020, 120, 5798–5877

5.2. IL−Carbon Interface

Carbon materials span a wide range of active porous carbons with various ordering structures including C60,[655] onionlike carbons (OLCs),[181,656,657] carbon nanotubes (CNTs),[658−660] graphene/graphite,[661−663] and 3D ordered mesoporous carbon matrixes.[664−666] Carbon materials have distinct benefits, such as high hydrophobic surface areas, large pore volumes, and good thermal and mechanical stabilities and thus exhibit remarkable potential as promising materials for confining ILs. Interest in the IL−carbon interface has been fueled by the desire to understand the solvation structures of C60, CNTs, graphene/graphite, and their derivatives in ILs[659,667,668] as well as applications of ILs in supercapacitors, where ILs and carbon materials are used as solvent electrolytes and electrodes, respectively.[669,670]

5.2.1. IL−OLC Interface. Formed by vacuum annealing of nanodiamond powder, OLCs can be viewed as concentric graphene shells, and their surface is fully accessible for ion accumulation.[671] Therefore, OLCs are novel electrode materials for supercapacitors.[672] It was found that supercapacitors with OLC as an electrode and $[N_{2,2,2,2}][BF_4]$-PC (propylene carbonate) as an electrolyte have high energy density and ultrahigh power density.[672] Furthermore, EDL capacitance increases as OLC becomes smaller.[656] To understand the underlying physical origin of these striking phenomena, Cummings and co-workers performed intensive atomistic simulations to study interfacial structures of ILs near idealized spherical OLCs.[181,673] An almost linear relationship of surface charge density versus electrode potential applied over a large voltage range was found for EDLs of ILs near OLC electrodes,[181] leading to a differential capacitance versus electrode potential curve that is nearly flat (Figure 23A). These results are in contrast to the observed U-, bell-, and camel-shaped curves observed in many theoretical, computational, and experimental studies of ILs on planar electrodes. The flat capacitance−potential curve is ascribed to an almost constant charge overscreening behavior, and the normalized capacitance of EDLs on OLCs increases with curvatures of OLCs and decreases with sizes of OLCs, which is in good agreement with available experimental measurements.[672]

In addition, ILs consisting of double-headed imidazolium cations show distinct interfacial structures and enhanced capacitive performance over monovalent counterparts near OLC electrodes.[181,673] A high concentration of anions is accumulated near the OLC electrodes to neutralize the charge of the double-headed cations. For $[C_n(MIM)_2][BF_4]_2$ ILs, the average capacitance at the OLC electrode characterized by positive charges is higher than that at the OLC electrode characterized by negative charges, which is mainly attributed to the smaller size of $[BF_4]$ anions than $[C_n(MIM)_2]$ cations. In the latter case, differential capacitance decreases with increasing cation alkyl chain length. In order to facilitate the usage of double-headed imidazolium IL electrolytes in supercapacitors without compromising their power density, organic solvents such as PC and ACN are always used to increase ion conductivities, charging, and discharging rates (Figure 23B).[674] However, the reason for the underlying enhanced functionalities of the IL−solvent mixtures and the charging/discharging mechanisms are yet to be understood. This is an important direction of research for future electrochemical applications.

5.2.2. IL−CNT Interface. The confinement of ILs within CNT materials is of particular significance due to their fascinating surface structures. The initially empty CNTs can be filled spontaneously with ILs to reach a saturated state despite of their hydrophobic feature. The spontaneous diffusion of ILs into CNTs has been described with atomistic simulations.[658,675−677] The cations of $[C_4MIM][PF_6]$ are always faster than anions to enter CNTs in the filling process owing to favorable dispersion interactions of alkyl groups with CNT surface and preferential electronic interactions of imidazolium rings with CNT π-electrons.[658] Atomistic simulations showed that a single $[C_4MIM]$ cation can enter a CNT (9,9) from the bulk liquid region driven by a favorable free energy of −27 kJ/mol, whereas the corresponding value for a single $[PF_6]$ anion to enter this CNT is approximately 32 kJ/mol, indicating that it is very difficult for $[PF_6]$ anions to spontaneously enter this CNT.[658] However, for a $[C_4MIM][PF_6]$ ion pair, the obtained free energy value is around −27.6 kJ/mol, indicating that it is energetically favorable for ion pairs to enter CNTs. A hypothesis that a cation "pulls" an anion into CNT channels from bulk IL matrix gives a reasonable explanation for the insertion of $[C_4MIM][PF_6]$ into CNTs. Furthermore, CNTs with larger diameters can accommodate more ions and provide faster filling speed for ions entering CNTs.[658] It is noteworthy that the smallest diameter of CNTs capable of being filled by common ILs is around 0.95 nm, as revealed from atomistic simulations[677] and experiments.[678,679] This value is consistent with that determined from theoretical calculations considering the vdW radii of atoms constituting ions and sp^2 carbon atoms of CNTs.[679,680] Below this threshold, ILs do not spontaneously enter CNTs under normal conditions.

In addition to solvation of ILs inside CNTs, ILs are also good solvents to maintain dispersion of CNTs.[659,667,668] Weak vdW interactions between ILs and CNTs guide enthalpy alteration upon CNT solvation and increase monotonically with CNT diameters. Therefore, solvation of CNTs in ILs is strongly prohibited entropically. Functionalization of CNTs with hydrophilic groups is definitely helpful to enhance interactions of CNTs with ILs. At the macroscopic level, IL−CNT mixtures exhibit varied rheological and viscoelastic features depending on temperatures, concentrations, and types of CNTs dissolved in ILs.[681] Addition of multiwalled CNTs in the dilute regime of mixtures provokes a decrease in liquid viscosity at high flow fields, but concentrated dispersions of CNTs in ILs always have a high viscosity in comparison with that for pure ILs. Aligned multiwalled CNTs have a more pronounced effect on liquid viscosities than nonaligned CNTs in ILs.

The confinement of ILs in CNTs leads to anomalous variations of the ILs' phase behavior from the liquid phase to high-melting-point crystallites, which is attributed to ordered arrangements of ions inside CNTs.[678,682,683] The freezing behavior of ILs in CNTs is a nonequilibrium process that is fully suppressed in bulk liquids and only occurs in nanoconfinement or at very low temperatures.[682] Conversely, the presence of electrical charges at the IL−solid interface and changes in the local cation−anion ratio have a significant effect on a thawing thermal behavior.[684] For example, a downshift of melting point of confined $[C_3MPYRR][NTF_2]$ is attributed to high ion concentrations and nonstoichiometric local ion arrangements in the interfacial region impeding the formation of extended ionic liquid crystal structures. Both freezing and thawing phase transitions of ILs in CNTs are strongly influenced by geometric constraints and strong interactions of ILs with CNT walls.[685] The interior radius and chiralities of

https://dx.doi.org/10.1021/acs.chemrev.9b00693
Chem. Rev. 2020, 120, 5798−5877

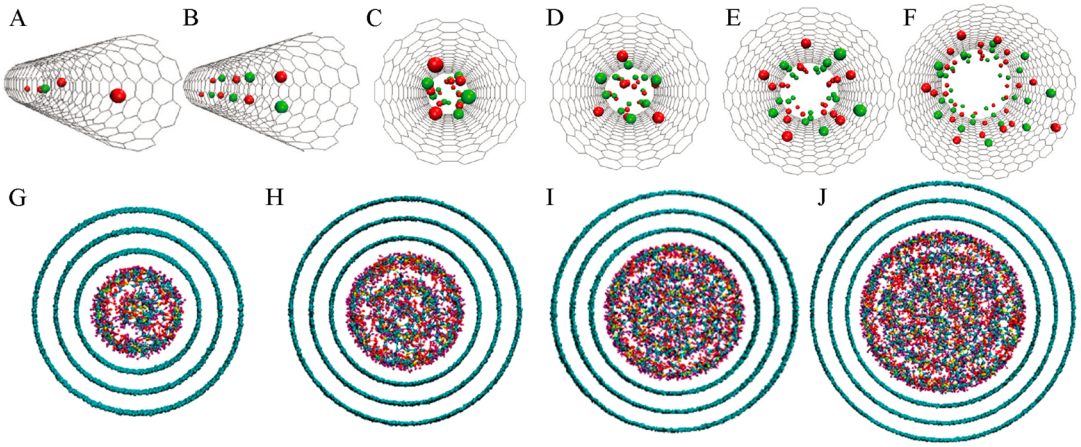

Figure 24. Snapshots of IL species in the first internal solvation shell of a CNT. Red and green spheres represent locations of center-of-mass of [C_2MIM] and [BF_4], respectively. (A) CNT (7,7), (B) CNT (8,8), (C) CNT (10,10), (D) CNT (12,12), (E) CNT (15,15), and (F) CNT (20,20). Reproduced with permission from ref 677. Copyright 2009 American Chemical Society. Snapshots of [C_4MIM][PF_6] confined inside multiwalled CNTs with diameters of (G) 2.0 nm, (H) 2.5 nm, (I) 3.0 nm, and (J) 3.7 nm. Reproduced with permission from ref 689. Copyright 2010 American Chemical Society.

CNTs and doping atoms in CNTs[686] can affect the melting temperatures of confined ILs.[687,688] ILs inside smaller CNTs are more stable than those in larger CNTs, which is attributed to enhanced interactions of ILs with CNT walls. In addition, ILs inside zigzag CNTs have lower energy and are more stable than those in armchair configurations and therefore have higher melting temperatures. Furthermore, the glass transition temperature of [C_2MIM][PF_6] encapsulated in a zigzag CNT is further increased when nitrogen atoms are doped into CNTs.[686]

ILs confined in CNTs are expected to display distinct microstructural characteristics that are not present in the bulk liquid phase. ILs exhibit diverse solvation structures in CNTs, resulting in heterogeneous density distribution along the radial[55,182,183,675,677,688−692] and axial directions of CNTs.[658,688−690] Atomistic simulations showed that internal solvation structures of [C_2MIM][BF_4] in CNTs are described by a single file distribution of ion species in CNT (7,7) (Figure 24A), zigzag distributions of cation−anion structures in CNT (8,8) (Figure 24B), chiral ion distributions in CNT (10,10) (Figure 24C), disordered ion structures in CNT (12,12) (Figure 24D), staggered pentagonal ion structures with alternating cation and anion layers in CNT (15,15) (Figure 24E), and staggered octagonal ion structures with disordered ion configurations in CNT (20,20) (Figure 24F).[677] Additionally, for [C_4MIM][PF_6] confined in CNTs, the number of ion layers increases from two to four with an increase of CNT diameters from 2.0 to 3.7 nm (Figure 24G−J).[689] The preferential ion structures inside CNTs are strongly associated with pore loading of [C_4MIM][PF_6] inside CNTs.[675,689,693] An increase in pore loading results in a concomitant increase in mass density distributions near the central regions of CNTs. Imidazolium cations prefer to align along CNTs and exhibit dense packing structures in the IL−CNT interfacial region compared to other layers farther from CNTs.[686] This behavior is attributed to hydrophobic interactions of CNTs with cation alkyl chains and $\pi-\pi$ stacking interactions between CNTs and imidazolium rings, whereas anions prefer to locate in the vicinity of imidazolium rings due to preferential intermolecular interactions.[675,677,689,693]

CNT diameters and pore loading of ILs inside CNTs have a remarkable influence on dynamic quantities of ILs, such as diffusion and ion conductivity.[676,680,686,688,694−697] An increase in diffusion coefficients, as observed for [C_8MIM][BF_4] in membranes consisting of vertically aligned CNTs (CNT forests consisting of multiwalled CNTs with 2 or 3 walls and with a 4 nm internal diameter),[697] is likely due to a frustration of self-organization of [C_8MIM][BF_4] on the nanoscopic scale. Ohba et al.[680,693] specified that a destruction of HB and electrostatically driven polar networks in [C_2MIM]Cl and frictionless movement of ions along CNT walls contribute to their enhanced mobilities inside CNTs. The hydrophobicity and HB structures of confined ILs in CNTs are assumed to play major roles, because some hydrophobic ILs, such as [C_4MIM][PF_6][689] and [C_4MIM][NTF_2] ILs,[694] characterized by hydrophobic features exhibit slow dynamics when they are confined within CNTs. Translational dynamics of confined IL ions are highly heterogeneous and depend on their relative distance from CNT walls.[678,698] Additionally, ion and electric conductivities of ILs increase with increasing temperatures[87] and decrease with lengthening imidazolium cation alkyl chains.[675]

Besides imidazolium ILs that are widely studied via experimental and computational characterizations, other ILs consisting of nonaromatic cations, such as EAN and its derivatives, can also form varied ion pair structures inside CNTs.[660,699] EAN exhibits peculiar, well-defined ion pair structures inside CNTs having various diameters[660] and has cylindrical double-shell solvation structures around the CNTs regardless of the CNT diameters.[699] In the first solvation shell, methyl groups in EA cations are closer to CNT walls than the amine groups, while [NO_3] anions tend to be in contact with CNT walls with three oxygen atoms facing bulk liquids. In addition, asymmetric stretching intensities of C−H in EA cations and N−O in [NO_3] anions at the EAN−CNT interface are slightly higher than those in bulk liquids owing to enhanced accumulation and significant orientation of cations and anions in interfacial regions.

5.2.3. IL−Graphene (Graphite) Interface. Besides CNTs, graphene and graphite provide another attractive confinement environments for ILs. Functional performance

https://dx.doi.org/10.1021/acs.chemrev.9b00693
Chem. Rev. 2020, 120, 5798−5877

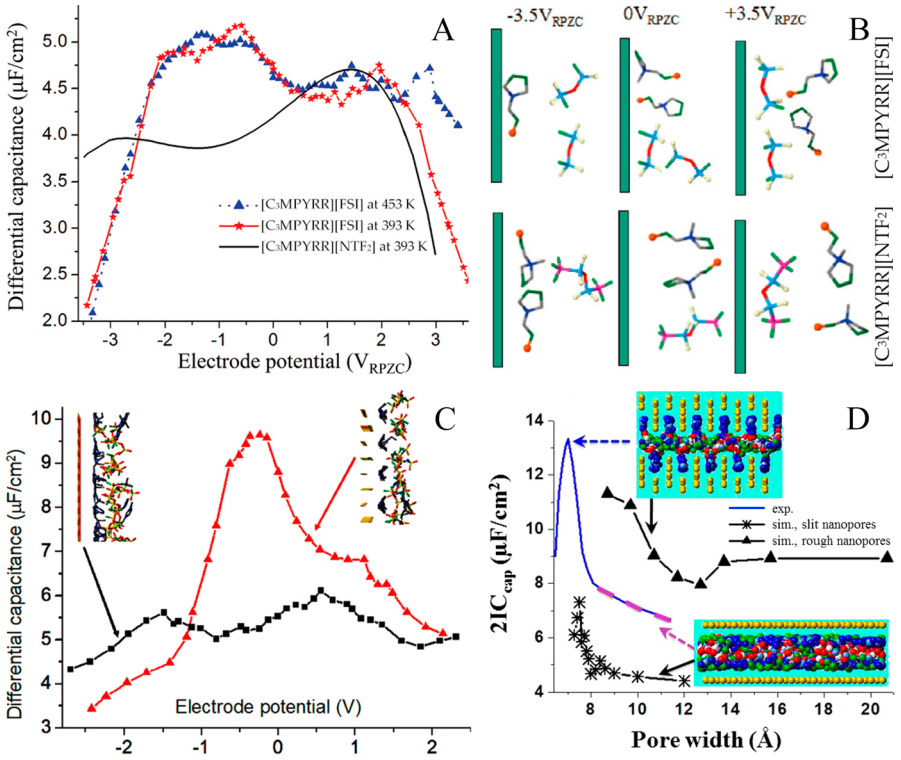

Figure 25. (A) Differential capacitance versus electrode potential for $[C_3MPYRR][NTF_2]$ and $[C_3MPYRR][FSI]$ ILs. (B) Representative snapshots of interfacial ion orientations for $[C_3MPYRR][NTF_2]$ and $[C_3MPYRR][FSI]$ ILs within 8 Å from the electrode surface (green vertical lines). Reproduced with permission from ref 746. Copyright 2011 American Chemical Society. (C) Differential capacitance versus EDL potential for varied electrode surfaces. Inserted image snapshots indicate electrolyte structures near flat (left) and rough (right) surfaces at ~2.5 V. Reproduced with permission from ref 747. Copyright 2011 American Chemical Society. (D) Comparison of absolute values of capacitances obtained from simulations in atomically flat and rough slit pores as a function of pore dimensions for $[C_2MIM][NTF_2]$ IL. Reproduced with permission from ref 745. Copyright 2015 American Chemical Society.

of ILs in IL−graphene systems, either in electrochemical devices or in lubrication, is strongly correlated with their wetting states on graphene surface.[700,701] Experimental characterizations showed that diverse wetting states of liquid droplets on graphene can be achieved by changing the thickness of graphene layers on substrates and by careful manipulation of IL−substrate interactions via a judicious selection of cations and anion species.[702,703]

SFG spectra for $[C_4MIM][C_1SO_4]$ on a graphene surface showed that methyl groups of $[C_1SO_4]$ anions align greater than 40° from the surface normal direction, while $[C_4MIM]$ cations exhibit a weak parallel alignment along the graphene surface, leading to a wetting state with a contact angle of 58 ± 2°.[101,704] Another SFG measurement of $[C_4MIM][N(CN)_2]$ demonstrated that only $[N(CN)_2]$ anions were aggregated on the bare barium fluoride substrate, whereas both $[C_4MIM]$ cations and $[N(CN)_2]$ anions were detected on barium fluoride substrate coated with graphene, which is accompanied by an increase of the contact angle from 57° for IL on bare barium fluoride substrate to 69° for IL on substrate covered by a single graphene layer. In addition, $[C_4MIM][N(CN)_2]$ forms ordered interfacial layers at different potentials, but concentrations and orientations of butyl chains exhibit negligible changes as the electrode potential varies.[705] More physical insights obtained from various experimental studies lay a solid foundation for a comprehensive understanding of interfacial IL structures on the electrified graphene surface and their utilities in specific applications.[130,663,706−711]

DFT calculations provided detailed microstructures of ILs at varied wetting states on the graphene surface.[146,147,274,712,713] Imidazolium cations interact more strongly with neutral graphene than anions due to $\pi-\pi$ stacking interactions between imidazolium ring planes and solvophobic associations of alkyl chains with graphene.[274,709,714,715] Imidazolium cations have a small band gap in comparison with pyrrolidinium analogues when they are paired with Br and $[BF_4]$ anions and a larger band gap when they are coupled with $[PF_6]$ and $[NTF_2]$ anions. These anions interact with graphene via different π type interactions.[145,714] Binding energies of representative ILs on neutral graphene surface follow an order of $[C_4MIM][PF_6]$ (−15.01 kcal/mol) > $[C_4MIM][N(CN)_2]$ (−14.38 kcal/mol) > $[N_{1,1,1,4}][N(CN)_2]$ (−13.53 kcal/mol) > $[C_4MIM][BF_4]$ (−13.04 kcal/mol) > $[N_{1,1,1,4}][PF_6]$ (−12.88 kcal/mol) > $[N_{1,1,1,4}][NTF_2]$ (−11.69 kcal/mol) > $[C_4MIM][NTF_2]$ (−10.53 kcal/mol) > $[N_{1,1,1,4}][BF_4]$ (−9.61 kcal/mol).[712,714,715] In addition, anions have stronger coordinations than cations with positively charged graphene surface. Interactions between halides and graphene are even stronger than those for molecular anions due to preferential and cooperative anion···π interactions.[715] However, at negatively charged graphene surface, cation alkyl chains prefer to align "epitaxially" along graphene lattice, which induces quasi-crystallization of (imidazolium) cations on graphene. Besides DFT calculations, atomistic and CG simulations showed that wetting graphene with ILs is essentially related to IL droplet size,[703] interaction strength between graphene and ILs,[716] coating materials,[703] temperatures,[710,716] and external electric

https://dx.doi.org/10.1021/acs.chemrev.9b00693
Chem. Rev. 2020, 120, 5798−5877

fields.[717,718] The interfacial energy of solid−liquid interface is a good indicator to describe affinity of ILs to graphene.[719] Imidazolium cations functionalized with benzyl groups have low interfacial energies due to favorable interactions between ring moieties and graphene and thus can easily wet the graphene surface. Imidazolium cations having long alkyl chains are characterized by low interfacial energies in comparison with those having short alkyl chains, but their affinities to graphene surface are weaker than that of pyrrolidinium analogues.

ILs confined in neutral graphene slits possess symmetric layering structures between graphene walls and exhibit distinct microstructural[720−725] and dynamical heterogeneities.[588,645,648,695,710,720,722,723,726,727] Ions in interfacial layers close to graphene walls exhibit slower dynamics than those in the central region of confined IL films. If graphene walls have a large slit width, ions in the central region of confined IL films usually have similar dynamical quantities and comparable relaxation times to those in bulk liquids without confinement. In addition, diffusions of ions in directions perpendicular to the pore walls are significantly slower than those along the pore walls as ions must traverse dense ion layers in the perpendicular direction.[695,722,723,728]

Heterogeneous microstructures and dynamical quantities of ILs in the IL−graphene interfacial region are essentially correlated with their functionalities in applications, such as in electrochemical devices[20,133,729−735] and in lubrication.[736−738] Yan and co-workers performed intensive atomistic simulations studying effects of anion structures,[739,740] temperatures,[741] and specific interactions of ions with graphene[742,743] on EDL structures and capacitive functionalities of imidazolium ILs confined between graphene electrodes. On one side, specific adsorption of imidazolium cations on the graphene electrode causes a positive potential of zero charge (PZC) on a positively charged electrode and a depression of capacitance at positive polarization.[742] On the other side, adsorption of imidazolium cations effectively lowers the surface charge and electrode potential on the negatively charged graphene electrode and thus raises capacitance at negative polarization.[742] For specifically absorbed ions, such as [C_1MIM], variations in the electrode potentials near PZC do not affect the cation absorption structures to a significant extent but alter the anion layer next to the absorbed cation interfacial layer.[742] Consequently, the local minimum of camel-shaped differential capacitance curve, though commonly observed in experiments and simulations, may not be related to PZC, whereas interfacial co-ion structures next to absorbed counterions may contribute to a striking relationship between differential capacitances and applied potentials by altering an effective EDL thickness.

For [C_3MPYRR] ILs near a graphite electrode, cations exhibit perpendicular orientations at potentials near the PZC, and anion species in the first interfacial layer exhibit increased parallel orientation to the electrode with a gradual increase in applied electrode potentials.[744,745] The asymmetry of the capacitance−electrode polarity curve for [C_3MPYRR][NTF_2] is attributed to strong interactions of fluorine atoms in [NTF_2] anions with a graphite electrode, with the relatively large footprint of [NTF_2] anions in comparison with [C_3MPYRR] cations and the tendency of C_3 chains in [C_3MPYRR] cations to reside in the IL−graphite interfacial region even at high positive potentials (Figure 25A). Replacing [NTF_2] with [FSI] does not lead to a significant increase in differential capacitance near a positively charged graphite electrode,[746] whereas a 30% higher differential capacitance is observed on a negatively charged graphite electrode for [C_3MPYRR][FSI] in comparison with [C_3MPYRR][NTF_2] (Figure 25A).[744] This behavior is correlated with two microstructural characteristics of EDL: (a) a closer approach of [FSI] to the electrode surface than [NTF_2] (Figure 25B) and (b) a faster anion desorption rate (vs potential decrease) for [FSI] from the electrode surface than [NTF_2]. An observed decrease in capacitance and a disappearance of the minimum in the capacitance−potential curve near PZC with increasing temperatures are most probably attributed to an enhanced crowding effect of ions in IL−graphite interfacial layers.

Further atomistic simulations indicated that the atomic level roughness of the graphene electrode can qualitatively change the dependence of capacitance on the applied potentials.[747,748] ILs on an atomically flat basal plane of the graphite surface exhibit camel-shaped differential capacitance curves, whereas those on an atomically corrugated prismatic face of the graphite surface have large differential capacitances characterized by bell shapes at low double-layer potentials (Figure 25C,D). Both bell-shaped and camel-shaped capacitance−potential curves are correlated with variations of the EDL structures as a function of the applied potential due to a strong dependence of electrolyte packing structures on the surface and a large difference in the intermolecular potential energies of electrolyte ions near the flat and rough graphene surfaces. In addition, ILs on an atomically flat graphene electrode exhibit a slight decrease in capacitance with increasing temperatures due to thicker EDL structures,[739,749] whereas the influence of temperatures on differential capacitance is more pronounced for ILs confined on atomically corrugated graphene surface with ion dimension comparable to the size of corrugation pattern on graphene surface. Therefore, interpretation of experimental capacitance data should take detailed knowledge of the electrode topography and roughness into consideration, and it should go beyond the typical route of considering electrolyte behavior near a flat surface. These computational studies further indicate that controlling the electrode surface roughness might be an effective route to improve energy densities of EDL capacitors.

Addition of ACN into imidazolium and tetraalkylphosphonium ILs improves ion conductivities and thus enhances power and energy densities of supercapacitors as ACN facilitates dissociation of cation−anion pairs in EDL.[674,750,751] However, addition of PC into imidazolium ILs results in distinct changes in interfacial ion structures and capacitances of supercapacitors. PC molecules exhibit outstanding co-ion expulsion capabilities due to their strong absorption onto the graphite surface in contrast to ACN. In addition, doping inorganic salts (Li^+,[752−754] K^+,[753] Mg^{2+},[752] Ca^{2+},[755] and Al^{3+}[755]) and molecular solvents (water,[754,756] methanol,[757] ethanol[757]) in ILs and generating vacancy sites on the graphene surface[757,758] leads to significant variations in interfacial structures and dynamics of confined ions in comparison with those in bulk liquids and thereafter variations in capacitance−potential curves.

A significant experimental observation showed that the energy density of supercapacitors can be significantly increased by confining ILs in the graphene slits with pore widths at the subnanometer scale, but this reduces their power density and compromises the key advantage of supercapacitors.[728,745,759−766] Molecular simulations using a phenomenological model revealed that charging ionophilic pores with pore widths comparable to ion diameters is a

https://dx.doi.org/10.1021/acs.chemrev.9b00693
Chem. Rev. 2020, 120, 5798−5877

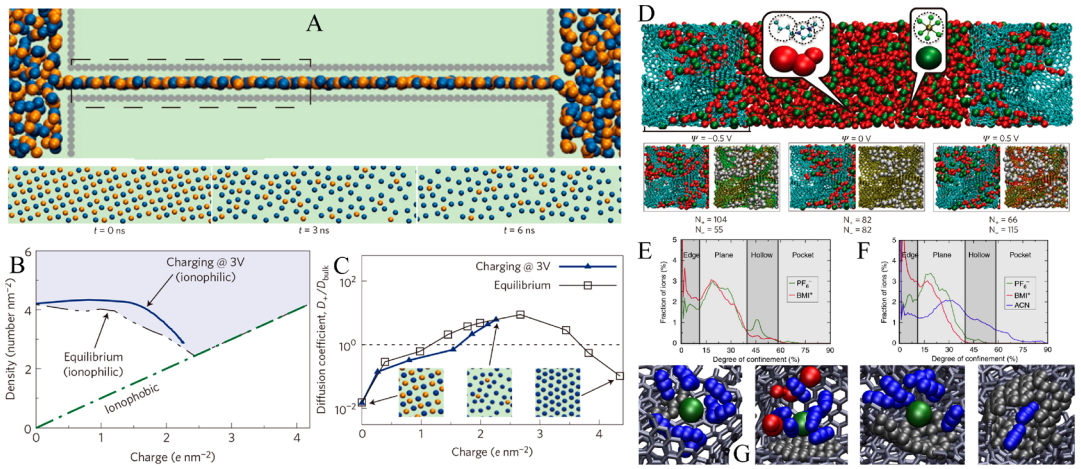

Figure 26. (A) Side-view snapshot of simulation system for charging narrow electrode pores with ILs, and top-view perspectives of ion species inside a negatively charged electrode pore when a voltage of 3 V is applied between electrodes. Blue and orange spheres represent cations and anions, respectively. (B) A plot showing averaged total and charge densities during instant charging (blue solid line) and in equilibrium conditions (black dash-dot-dot line). Green dash-dot line corresponds to an ionophobic pore. (C) Normalized diffusion coefficients of cations along an equilibrium path and along charge densities corresponding to instant charging at 3 V. Reproduced with permission from ref 759. Copyright 2014 Nature Publishing Group. (D) EDLC simulation cell consists of CG $[C_4MIM][PF_6]$ electrolyte confined between two porous electrodes. The same configuration at each potential is shown twice: ion distribution (left) and degree of charging of electrode atoms (right), in which carbon atoms are color coded according to partial charge q they carry (green, $q < 0$; yellow, $q \approx 0$; and red, $q > 0$). Reproduced with permission from ref 765. Copyright 2012 Nature Publishing Group. Adsorption of ion species in a nanoporous carbon electrode at null potential, and distribution of degree of confinement experienced by ion species in (E) pure $[C_4MIM][PF_6]$ and in (F) $[C_4MIM][PF_6]$–ACN mixtures. (G) Representative configurations of ion species for their four adsorption modes (gray rods for C–C bonds, gray spheres for carbon atoms that are in a coordination sphere of central molecules, red for $[C_4MIM]$ cations, green for $[PF_6]$ anions, and blue for ACN molecules, respectively.). Reproduced with permission from ref 766. Copyright 2013 Nature Publishing Group.

complex process (Figure 26A).[759] It is adsorption-driven at high potentials but depend on the ion concentrations, and it is dominated either by co-ion desorption or by adsorption of both types of ions at low potentials (Figure 26B). Diffusivities of ions in subnanometer pores exhibit a strong dependence on ion densities and local chemical compositions (Figure 26C) during charging over a few orders of magnitude and can exceed a few times the bulk liquid ion diffusion under similar conditions.[759,767] A fast demixing transition inside narrow pores due to an instant expulsion of co-ions from the pores above a certain electrode potential threshold and the ability of conductive pores to maintain elevated densities of counterions after demixing lead to distinct capacitance enhancement.[728,760] During cyclic charging and discharging, a nanopore system is driven far from the equilibrium state. Indeed, the internal state of nanopores, in particular, total ion densities, not only deviates from those under quasi-static charging and discharging conditions but also varies greatly as the scan rate changes.

For supercapacitors, the charge storage mechanism is a complicated process intrinsically correlated with multiple factors such as relative ratios of pore sizes over ion dimensions[669] and desolvation effects of ILs in confined environments.[670] For negative polarization, the adsorption of cations onto solid substrates dominates, whereas for positive polarization, charging proceeds by an ion exchange effect with anions replacing cations in the interfacial regions. Experimental measurements using NMR and *in situ* electrochemical quartz crystal microbalance indicated that adsorbed ions are partially solvated.[768] Atomistic simulations demonstrated that charge screening,[20,761,769] ion rearrangement and confinement (Figure 26D),[765,766] and pore surface properties[21,733,759,770−773] have significant effects on charging dynamics and differential capacitances. ILs absorbed onto solid electrodes exhibit varied configurations and have striking coordinations with different adsorption sites like edge sites (concave curvature), plane sites (graphene sheetlike structure), hollow sites (convex curvature), and pocket sites (inside a subnanometer carbon pore) (Figure 26E–G).[766] These different adsorption sites have distinct effects on power performance of electrochemical devices.[774]

It should be noted that molecular dynamics of ions near electrified nanoporous electrode are described by multiple time scales arising from solvation, electrosorption, and ion confinement effects.[775] Diffusivities of confined ions are always slower than those of bulk electrolytes due to the confinement effect and strong electrostatic attractions with pore walls when a potential is applied, which significantly hinder their utilizations as electrolytes for ensuring fast charging supercapacitors.[776] Therefore, molecular simulations with effective prescreening methods will be an economical procedure for selection and design appropriate IL candidates with enhanced properties to meet specific application requirements.[777,778]

5.2.4. IL–3D Mesoporous Carbon Interface. In addition to cylindrical CNTs and graphene slits, confinement of ILs within 3D carbon materials having complicated pore sizes and pore geometries, such as CMK-3[664] and CMK-5,[665,666] was also investigated via atomistic simulations. These CMKs are amorphous carbon materials characterized as interconnected mesoporous but with different pore size, shape, and surface roughness, which have a significant effect on microstructural and dynamical quantities of confined ILs. Large spatial structural heterogeneities of confined ILs are observed in the axial direction of CMK-3 at a pore loading below bulk IL density, suggesting that ions tend to cluster together to create domains with similar local densities as those of bulk liquids (Figure 27A,C).[664] For the same ILs confined

https://dx.doi.org/10.1021/acs.chemrev.9b00693
Chem. Rev. 2020, 120, 5798−5877

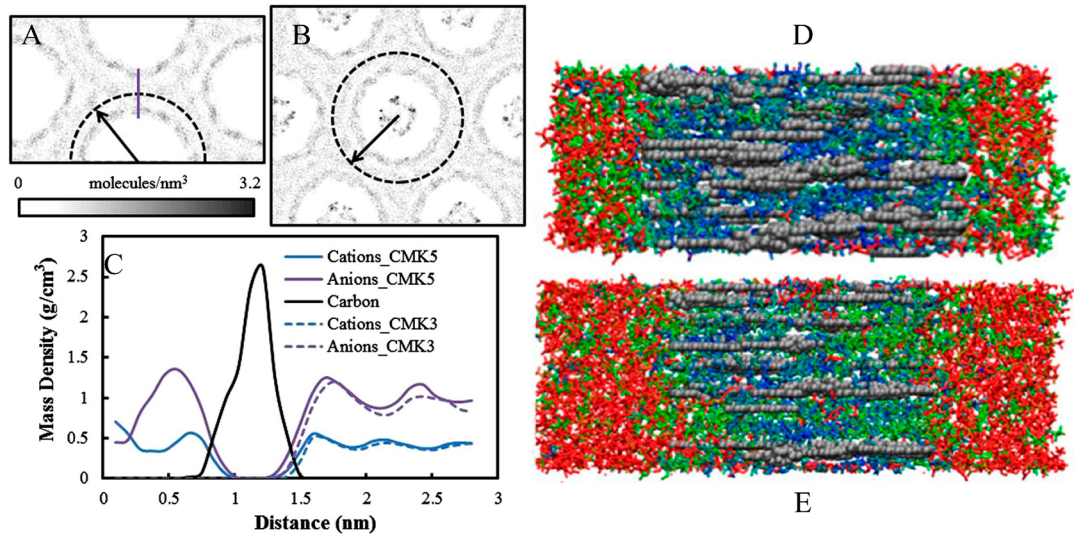

Figure 27. Density profiles of $[C_2MIM][NTF_2]$ IL inside (A) CMK-3 and (B) CMK-5 carbon materials. Areas with high cation densities are depicted in dark shades of gray. (C) Density distributions of $[C_2MIM]$ cations and $[NTF_2]$ anions outside CMK-3 nanorods and inside/outside CMK-5 nanopipes along the direction indicated by solid arrows up to distances indicated by dashed circles. Reproduced with permission from ref 666. Copyright 2016 Taylor & Francis. Representative snapshots of $[C_2MIM][NTF_2]$ IL inside a coconut shell carbon material with pore sizes of (D) 0.75 nm and (E) 1.23 nm. Reproduced with permission from ref 727. Copyright 2014 American Chemical Society.

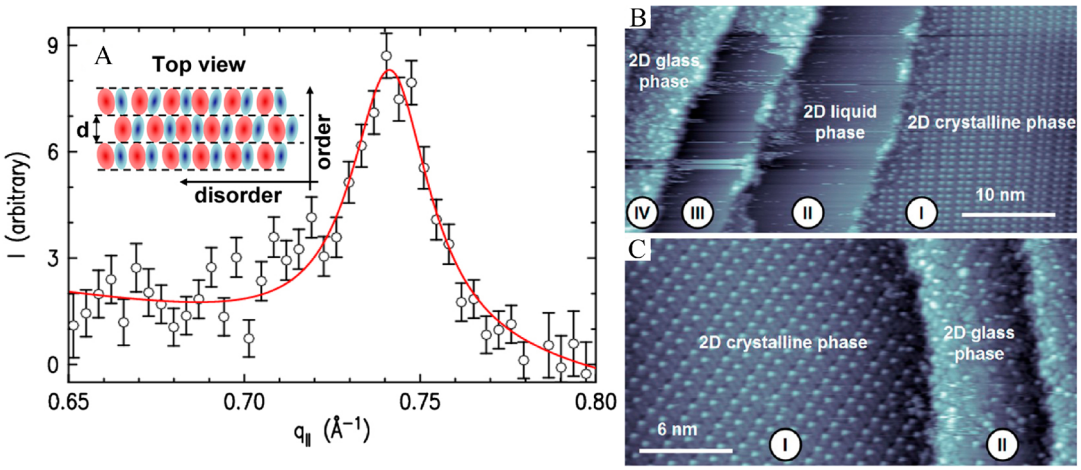

Figure 28. (A) Measured (symbols) and Lorentzian-plus-linear background fitted (line) diffraction peak for $[C_4MPYRR][FAP]$ on the Hg surface at a surface coverage of 50 $Å^2$/molecule. Reproduced with permission from ref 122. Copyright 2011 American Physical Society. STM images of $[C_4MPYRR][NTF_2]$ on Ag(111) surface recorded at 100 K. (B) Image at submonolayer coverage exhibits four Ag terraces. (C) At monolayer coverage, large Ag terrace is covered by an ordered 2D crystalline phase, while small Ag terraces are occupied by a disordered 2D glass phase. Reproduced with permission from ref 781. Copyright 2013 American Chemical Society.

within CMK-5, ILs adsorbed at the outer surface of carbon nanopipes have a dramatic effect on density distributions of ILs confined inside carbon nanopipes (Figure 27B,C).[665,666] Ions are more closer to carbon walls in CMK-5 than those in the CMK-3 matrix due to preferential interactions of IL ions inside CMK-5 nanopipes with those outside CMK-5 nanopipes. The surface curvature and mesoporous arrangement in CMK-3 and CMK-5 result in different confinement effects on dynamical properties of ILs. ILs adsorbed outside CMK-5 nanopipes have faster dynamics than those outside CMK-3 having a similar pore size.[664] Exterior ion absorption can affect dynamics of ions inside nanopipes, but this effect is IL-specific. It should be noted that all confined ions inside CMK carbon materials exhibit slower translational and rotational dynamics compared to those in bulk IL matrixes.[664,666]

Compared with constrained microstructures of ILs within carbon matrixes having regular nanopores, it was shown that ILs exhibit bulk liquidlike microstructures inside porous carbon materials having varied pore size and pore geometry.[727] $[C_2MIM][NTF_2]$ prefers to form ion layers on a coconut shell carbon surface with ions parallel to surface walls.[727] Different to well-defined ion layering structures in slit pores, confined ion species exhibit significant spatiotemporal heterogeneities in coconut shell carbon materials due to complex pore geometries of carbon materials (Figure 27D,E), wherein ions near pore walls move more slowly than those in central regions of the pores, similar to observations in other slit pores.[722,725] Furthermore, a gradual increase in averaged pore size in carbon materials leads to small and nonmonotonic variations in ion transport properties which, in turn, leads to a nonuniform and weakened confinement effect of irregular

https://dx.doi.org/10.1021/acs.chemrev.9b00693
Chem. Rev. 2020, 120, 5798−5877

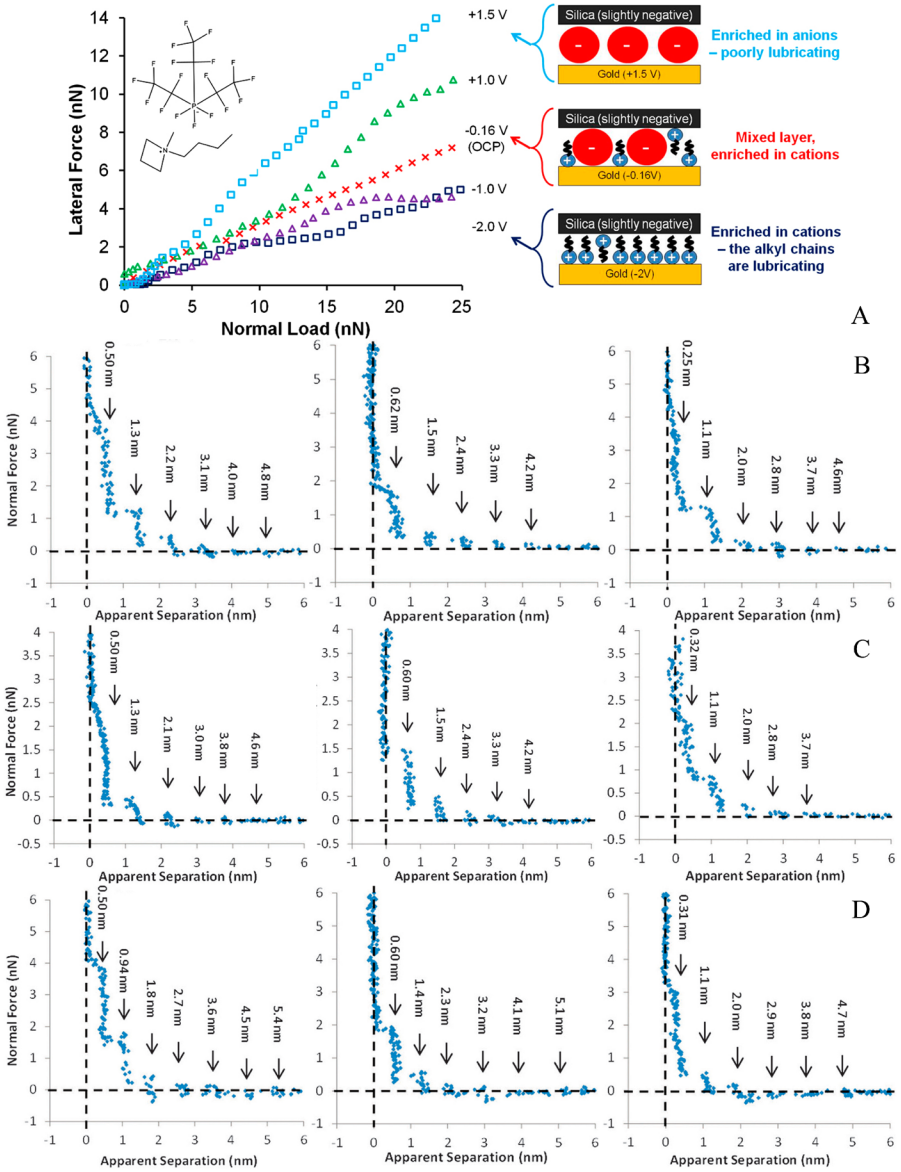

Figure 29. (A) Lateral force against normal load for different surface potentials for $[C_4MPYRR][FAP]$ confined between the Au(111) electrode surface and a silica colloid probe. Reproduced with permission from ref 805. Copyright 2012 American Physical Society. Typical force versus apparent separation distance for the silica colloid probe approaching the Au (111) surface in (B) $[C_2MIM][FAP]$, (C) $[C_4MIM][FAP]$, and (D) $[C_6MIM][FAP]$. Left column, ILs at negative potentials (−2.0 V for $[C_2MIM][FAP]$, −1.0 V for $[C_4MIM][FAP]$, and −2.0 V for $[C_6MIM][FAP]$). Middle column, ILs at null potential. Right column, ILs at positive potentials (1.5 V for $[C_2MIM][FAP]$, 1.0 V for $[C_4MIM][FAP]$, and 1.5 V for $[C_6MIM][FAP]$). Reproduced with permission from ref 803. Copyright 2013 Royal Society of Chemistry.

carbon materials compared with those with regular pore geometries.

5.3. IL−Metal Interface

5.3.1. IL−Hg Interface. Mercury provides a very smooth liquid surface which enables one to carry out XRR experiments at sub-Angstrom resolution, as demonstrated by investigations of a mercury-supported $[C_4MPYRR][FAP]$ IL Langmuir film in both the lateral and longitudinal directions.[122] At a low surface coverage (90 $Å^2$/molecule), a monolayer ion pair structure is formed at the IL−Hg interface, whereas a bilayer surface-parallel ion pair structure is formed at a high surface coverage (50 $Å^2$/molecule) (Figure 28A). Surface-parallel ion pairs self-organize into stripes, exhibiting 1D, smecticlike order, implying a checkerboard-like tilted ion surface structure. This checkerboard pattern at the IL−Hg interface has similarities with interfacial structures of Hg-supported Langmuir films of alcohols, thiols, and fatty acids.[779] In these Langmuir films, full 2D lateral ordering structures eventually emerge upon increasing cation alkyl chain lengths, irrespective of irregular ion shapes and strong Coulombic interactions between constituent ions. However, XRR spectra for $[C_nMIM][NTF_2]$ ILs demonstrated that IL−Hg interfacial structures are highly disordered, and diffuse surface-normal electron density profiles exhibit gradual Hg penetration into IL films and surface-normal structural evolution over a period of hours.[780] Unlike localized charges in pyrrolidinium cations, charge delocalizations in imidazolium cations and $[NTF_2]$ anions increase their affinities to Hg atoms, leading to a lateral segregation of ions into polar and apolar domains at the IL−Hg interface with residual Hg in apolar domains.

https://dx.doi.org/10.1021/acs.chemrev.9b00693
Chem. Rev. 2020, 120, 5798−5877

In electrochemical applications of the IL−Hg interface, a thorough understanding of the dependence of differential capacitance and charging curves of the IL EDL structures on constituent ions is important.[782,783] Costa et al. found that interactions of positively charged imidazolium rings with the Hg surface gradually diminish with lengthening cation alkyl chains due to preferential hydrophobic interactions of alkyl chains with the Hg surface. Variations in cation alkyl chains lead to remarkable changes in capacitance−potential curves for $[C_nMIM][NTF_2]$ ILs (n = 2, 4, and 6) on Hg electrode.[430,782,783] In addition, differential capacitance of ILs increases with increasing temperatures.[784] Both noncoincidence and positive temperature coefficients of PZC are distinct to predictions of classical Gouy−Chapman theory, which is suitable for description of phase behaviors of dilute aqueous electrolytes.[785,786]

5.3.2. IL−Au Interface. Potential-induced surface reconstruction of single-crystalline Au electrode is always an important issue in electrochemical surface science. Concentrated solvent electrolytes (ILs) interact strongly with Au atoms and destroy the long-range order of a single-crystal Au surface at certain potentials.[787−790] STM characterizations of $[C_4MPYRR][NTF_2]$ and $[C_nMIM]$ ILs on Au(hkl) substrates demonstrated that Au(111) and Au(100) can be reconstructed into the usual surface structures at sufficiently negative potentials,[134,791] indicating that solvent adsorption of ILs has a remarkable influence on electrode processes compared to aqueous electrolytes.

A comprehensive investigation of adsorption of ILs on an unreconstructed Au(100) surface in a wide potential range revealed that $[C_4MIM][PF_6]$ exhibits a 2D phase transition upon cathodic excursion.[792] For $[C_4MIM][BF_4]$, ordered adsorption of $[BF_4]$ anions occurs at the anodic side of the bell-shaped capacitance maximum, while adsorption of $[C_4MIM]$ cations is on the cathodic side of the capacitance maximum and follows a potential-promoted disorder−order transition.[134] However, $[C_2MIM][NTF_2]$ and $[C_8MIM][NTF_2]$ ILs absorb onto the Au(111) surface and form a 2D liquid phase at ambient temperature, whereas they condense into 2D islands with short-range ordering glasslike structures at lower temperatures.[793] These findings indicate that (1) the formation of IL−Au interfacial structures is dominated by a tendency to optimize anion adsorption geometries and (2) cation alkyl chains prefer standing upright rather than lying flat along the Au surface.[134,793−801] A close similarity was found in the adlayer structures of $[C_4MPYRR][NTF_2]$ on the Au(111) surface.[795,796] At room temperature, the growth of 2D IL film occurs up to one monolayer coverage, with both anions and cations in direct contact with the Au substrate. At lower temperatures, ion mobilities in the IL−Au interfacial region are frozen. Both a 2D crystalline phase with long-range order and a disordered 2D glass state are formed. Annealing experiments revealed that the 2D crystalline phase is thermally more stable than the 2D glass state against melting, and its stability is strongly influenced by coverage of adsorbates on the underlying Au(111) surface.[795,796]

Atkin and co-workers elucidated interfacial structures of various ILs on charged Au electrodes via AFM experiments.[802,803] At null potential, interfacial behaviors of ILs are consistent with a discontinuous sliding process. This effect is less pronounced when a positive or negative potential is applied. ILs consisting of imidazolium cations coupled with [FAP] anions exhibit similar lubrication behavior: a high friction at positive potentials and a low friction at negative potentials, suggesting that imidazolium cations are more lubricating than [FAP] anions.[802,804−807] The lateral force varies as a function of applied potential and ion structures because of changes in interfacial compositions of confined ion layers from anion-enriched (at positive potentials) to mixed (at null potential) and then to cation-enriched (at negative potentials) structures (Figure 29A). The length of alkyl chains in imidazolium cations has a significant influence on lubricity at similar negative potentials. C_6 chains in $[C_6MIM]$ cations produce a well-formed interfacial layer that provides a lubricating sliding plane (left column in Figure 29D), whereas C_4 chains in $[C_4MIM]$ cations lead to a less defined interfacial layer and reduced lubricity (left column in Figure 29C). When the cation alkyl chain length is further reduced to C_2, imidazolium rings in $[C_2MIM]$ cations orientate parallel to the Au surface, and lubricity is increased relative to $[C_4MIM]$ cations (left column in Figure 29B). However, when interfacial layers are [FAP] enriched, imidazolium cations become irrelevant and a same friction coefficient is obtained at positive potentials independent of cation alkyl chain length (right columns in Figure 29B−D).

A combined AFM-STM investigation provides a comprehensive understanding of EDL structures in the IL−Au interfacial region.[133,808] Both $[C_2MIM][NTF_2]$ and $[C_4MPYRR][NTF_2]$ ILs form multiple ion pair layers (3−5 layers) on the Au(111) surface at an open circuit potential.[809] The $[C_4MPYRR][NTF_2]$−Au interface appears highly structured (in part wormlike), while the $[C_2MIM][NTF_2]$−Au interface exhibits weak interfacial structuring. Therefore, it requires a large force to rupture the innermost IL solvation layer for $[C_4MPYRR][NTF_2]$ in comparison with that for $[C_2MIM][NTF_2]$. This remarkable difference is ascribed to stronger interactions of $[C_4MPYRR]$ cations than $[C_2MIM]$ cations with the Au(111) surface. Similar experimental features were also observed for ILs consisting of [FAP] anions coupled with either imidazolium or pyrrolidinium cations.[810−812]

Addition of inorganic salt precursors[810,813−818] or water[819−821] can significantly affect the IL−Au interfacial structures. AFM investigations revealed that typical multilayered IL interfacial structures are retained only at quite low salt concentrations. IL EDL structures will be disturbed when a large amount of salt is introduced into the IL−Au interfacial region, where new EDL structures consisting of salt ions will be formed. The width of the innermost layer is dependent on salt concentrations and applied electrode potentials. For IL−water mixtures, a clear transition from "water in IL" to "IL in water" was observed with a gradual increase of water concentration in ILs.[819] Above a certain water concentration, cation−anion intermolecular interactions are drastically weakened, and a transition from a multilayered interfacial structure to a classic double-layer structure occurs at specific electrode potentials. As more water molecules adsorb onto the Au surface, the thickness of the interior EDL structures increases and the thickness of the neutral exterior layers (beyond the first two layers in the IL−Au interfacial region) remain constant.[820]

In addition to heterogeneous microstructures in the IL−Au interfacial region, the dynamic evolution of these interfacial structures upon charging Au electrodes was studied using various experimental techniques including surface-enhanced infrared absorption spectroscopy (SEIRAS),[822−824] surface plasmon resonance,[825] STM,[131,132] and AFM measurements.[826,827] Distinct stepwise transitions were observed in

https://dx.doi.org/10.1021/acs.chemrev.9b00693
Chem. Rev. 2020, 120, 5798−5877

the IL−Au interfacial region with increasing electrode charge density. SEIRAS measurements revealed hysteretic cation−anion exchanges and rotations of ions in the first IL−Au interfacial layer.[822,823] During potential scans for ILs consisting of sufficiently large ion groups, a fast and barrierless change in the local ionic environment occurs first in the overlayers, and thereafter a slow replacement of ions with their counterions occurs in the IL−Au interfacial layers to compensate the surface charge when an overpotential exceeding a critical value is applied. These results highlight the significance of a steric hindrance effect of ion species on their replacement in the interfacial layers.[826,828,829]

Extensive experimental and computational investigations were performed to address effects of IL ion structures and EDL interfacial structures on differential capacitance of ILs upon charging Au electrodes.[748,830−834] It was revealed that IL capacities follow an order of $[C_4MIM][PF_6]$ < $[C_4MIM][NTF_2]$ < $[C_4MIM][BF_4]$. Lengthening the cation alkyl chains does not obviously affect the general shape of capacitance−potential curves but influences capacitances in a systematic way due to constrained distributions of alkyl chains in the IL−Au interfacial region. In addition, enlarging anions from small spherical ones (Cl, $[BF_4]$, and $[PF_6]$ *etc.*) to large nonspherical and multidendate species ($[NTF_2]$, [FAP] *etc.*) further complicates the dependence of differential capacitances of ILs on cation alkyl chain lengths and potentials required for a transition from overscreening to overcrowding IL−Au interfacial layers due to distinct interactions between confined ions and Au atoms. It is noteworthy that an IL composed of tetramer imidazolium cations and $[NTF_2]$ anions exhibits outstanding electrochemical properties in EDL devices.[835] Furthermore, an introduction of ether spacers to the imidazolium ring moieties makes these oligomers fluidic, and multivalent electrostatic interactions ensured by their oligomeric structures play a vital role in their functional performance in electrochemical devices.

5.3.3. IL−Ag Interface. Metallic silver is a catalyst in oxygen-assisted coupling reactions.[836] Potential applications of Ag alloys in heterogeneous catalysis raise additional interest in understanding interactions of Ag with ILs. Research on ultrathin IL layers on the Ag substrate showed that both $[C_nMIM]$ cations and $[NTF_2]$ anions adsorb in a checkerboard arrangement with both ions in contact with the Ag(111) surface,[837] similar to that observed in the IL−Au(111) interfacial region.[838] Deposition of a large amount of $[C_1MIM][NTF_2]$ on Ag(111) revealed an initial 3D IL film morphology.[839,840] In contrast, a quasi 2D film morphology was found from the beginning of depositing $[C_8MIM][NTF_2]$ on the Ag(111) substrate, indicating a remarkable effect of imidazolium cation alkyl chain length on IL film growth kinetics. In addition, STM investigations reported that $[C_2MIM][NTF_2]$ and $[C_8MIM][NTF_2]$ ILs exhibit similar ion mobilities at submonolayer coverage on the Ag(111) surface as that on the Au(111) substrate.[793] When $[C_8MIM][NTF_2]$ and $[C_8MIM][PF_6]$ ILs are sequentially deposited onto the Ag(111) surface, a pronounced enrichment of $[NTF_2]$ anions was observed at the IL−vapor interface due to a rapid anion exchange at the IL−Ag interface.[841] It is the larger adsorption energy and surface tension of $[C_8MIM][PF_6]$ than those of $[C_8MIM][NTF_2]$ that contribute to exchange of $[NTF_2]$ with $[PF_6]$ anions in the IL−Ag interfacial region.

For deposition of $[C_4MPYRR][NTF_2]$ on the Ag(111) surface at room temperature followed by a gradual cool-down to ∼100 K, a coexistence of a 2D liquid phase, a disordered 2D glass phase, and an ordered 2D crystalline phase was observed (Figure 28B).[781] Dynamic STM measurements at low temperatures resolved exchanges of adspecies at crystalline−liquid and disordered glass−liquid phase boundaries (Figure 28C). In addition, a dynamic equilibrium between the liquid phase and the crystalline phase is attributed to weak adsorbate−adsorbate associations and a low surface diffusion barrier. DFT calculations revealed an equal adsorption of $[C_4MPYRR]$ cations and $[NTF_2]$ anions laterally placed side by side with $[NTF_2]$ anions exhibiting *cis* configurations, SO_2 groups binding to the Ag surface, and CF_3 groups pointing toward the IL−vapor interface. ILs interact with the Ag surface through weak electrostatic (dipole induced dipole) interactions and preferential dispersion interactions, leading to a distinct electron solvation behavior of $[C_4MPYRR][NTF_2]$ at the IL−Ag(111) interface.[842]

Besides these extensive studies of ILs confined on Hg, Au, and Ag surfaces, there are some other metals that are used as substrates to support ILs for specific applications, such as Li,[843] Cu,[116,799,844,845] Ti,[466,846] Fe,[847,848] Ni,[847] Ru,[849] Pd,[850] Cd,[851] In,[852] Pt,[853,854] and Bi.[855] ILs exhibit varied interfacial structures and dynamical quantities in IL−metal interfacial regions depending on the delicate interplay of interactions among constituent ions and metal atoms that are in direct contact with confined ILs. These IL−metal interfacial systems have distinct electrochemical applications.

5.4. IL−Al_2O_3 Interface

Mezger et al. reported temperature-dependent microstructures of [FAP] ILs on a charged Al_2O_3 substrate using XRR spectroscopy.[121] A pronounced interfacial layering structure with the innermost layer spacing of ∼8 Å was observed for $[C_4MPYRR][FAP]$ at the IL−Al_2O_3 interface, indicating a double-layer interfacial structure with $[C_4MPYRR]$ cations being in contact with the Al_2O_3 surface (Figure 30A). [FAP] anions are repelled from the negatively charged Al_2O_3 surface and form a second anion layer on the interfacial cation layer. Such an EDL structure is totally distinct from those of dilute aqueous electrolytes near charged substrates, owing to strong correlations between oppositely charged ions. This EDL structure leads to some apparently counterintuitive observation like charge inversion and attraction between like-charged objects.[856,857] A gradual addition of PC solutes in $[C_4MPYRR][FAP]$ leads to reduced ion−ion correlations and a decreased correlation length of interfacial layer structures. At high concentrations, PC molecules accumulate laterally within the IL−Al_2O_3 interfacial layers and reduce Coulombic repulsions between like-charged ions.

Replacing $[C_4MPYRR]$ with $[C_6MIM]$ and $[N_{4,4,4,4}]$ cations leads to negligible variations in molecular layer structures at the IL−Al_2O_3 interface, but there are distinct changes in the interfacial electron densities (Figure 30B,C).[121] However, additional experimental characterizations showed that $[C_4MIM][PF_6]$ and $[C_4MIM][BF_4]$ ILs exhibit different IL−Al_2O_3 interfacial behaviors.[858] The former exhibits strong, exponentially decaying, and alternate-charge layering structures at the IL−Al_2O_3 interface, whereas the latter does not show interfacial layer structures but only a single dense layer at the IL−Al_2O_3 interface. This interfacial structural discrepancy is attributed to different correlations between constituent ions of these two ILs. In additional, preferential HB interactions between Al_2O_3 interfacial groups and ILs can also induce

https://dx.doi.org/10.1021/acs.chemrev.9b00693
Chem. Rev. 2020, 120, 5798−5877

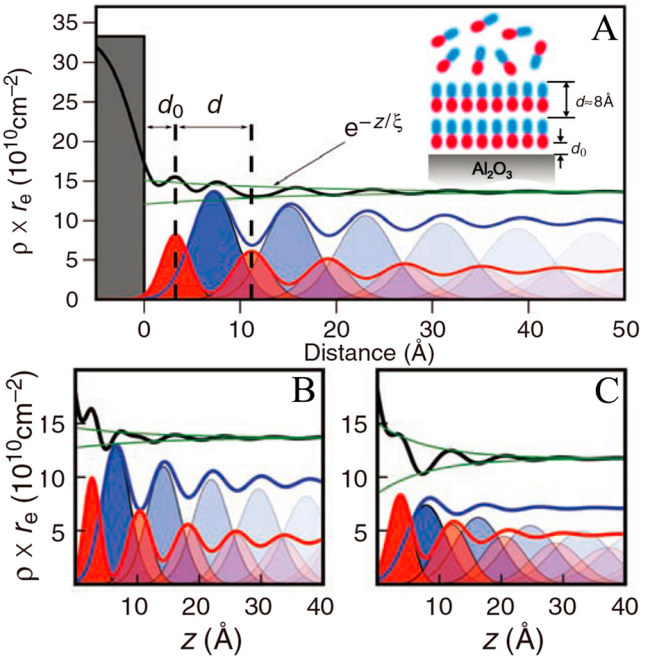

Figure 30. Total (black) and individual (red for cations and blue for anions) electron densities for (A) [C_4MPYRR][FAP], (B) [C_6MIM]-[FAP], and (C) [$N_{4,4,4,4}$][FAP] at the IL−Al_2O_3 interface. Red and blue lines indicate Gaussian distributions for cations and anions contributing to their respective partial electron density profiles. The gray bar corresponds to the electron density of the Al_2O_3 substrate without roughness. Reproduced with permission from ref 121. Copyright 2008 American Association for the Advancement of Science.

lateral ordering structures characterized by an excess of cations in the IL−Al_2O_3 interfacial region.[121,858]

Saramago and co-workers characterized the wetting properties of [C_8MIM][BF_4] IL films on representative solid substrates (silicon, boron-silicate glass, and aluminum) and found that only aluminum substrate is wetted and the corresponding interfacial structures are strongly dependent on time and IL ion concentrations in ethanol solution.[859,860] IL films deposited from highly diluted IL in ethanol exhibit liquidlike lamellar structures, whereas IL films deposited from concentrated IL in ethanol present solidlike or solid−liquid coexistence structures.[128] These interfacial structures are mainly determined by London dispersion forces between confined ion species and substrates. For [C_8MIM][BF_4], its reduced surface tension is well described by Guggenheim's universal curve for simple, purely dispersive fluids. However, for [C_2OH-MIM][BF_4] (1-(2-hydroxyethyl)-3-methylimidazolium), there is a distinct deviation of reduced surface tension toward lower values, which is a typical behavior of molecular fluids having strong HB interactions.

SEIRAS spectra showed that adsorption of [C_4MIM]-[NTF_2] on a well-ordered Al_2O_3 surface is molecular and reversible.[861] Strong changes in relative intensities of [NTF_2] anion related vibrational bands were observed in the submonolayer region due to distinct accumulation of [NTF_2] anions in the IL−Al_2O_3 interfacial region, indicating a pronounced interfacial orientation of [NTF_2] anions. DFT calculations demonstrated that [NTF_2] anions predominately adopt a *cis* conformation with slightly tilted orientation with respect to the IL−Al_2O_3 interface, preferentially interacting with interfacial atoms via SO_2 groups. In addition, characteristic differences were observed in monolayer adsorption spectra of [C_2MIM][TFO] on a bare Al_2O_3/NiAl(110) surface and that covered by Pd nanoparticles.[862] [TFO] anions are less oriented on the Al_2O_3 surface, while they appear to stand up on the Pd nanoparticles with CF_3 groups directed toward the

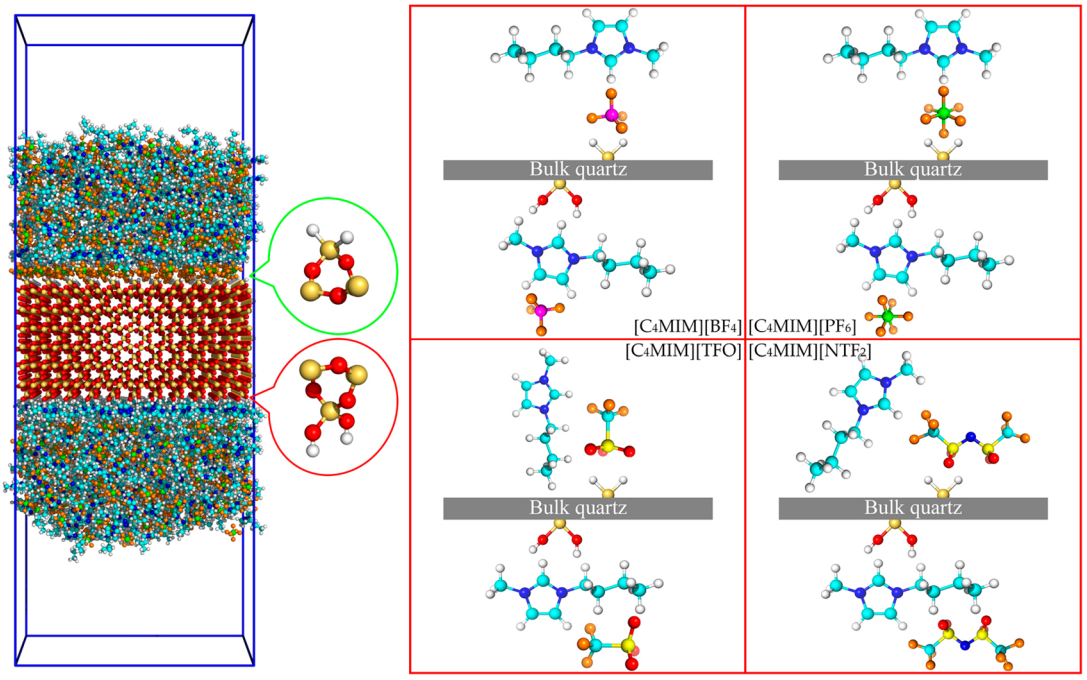

Figure 31. Representative configurations of ILs consisting of [C_4MIM] cations coupled with [BF_4], [PF_6], [TFO], and [NTF_2] anions confined on silica surfaces covered by positively charged SiH_2 (top) and negatively charged $Si(OH)_2$ (bottom) interfacial groups. Reproduced with permission from ref 63. Copyright 2014 Royal Society of Chemistry.

https://dx.doi.org/10.1021/acs.chemrev.9b00693
Chem. Rev. 2020, 120, 5798−5877

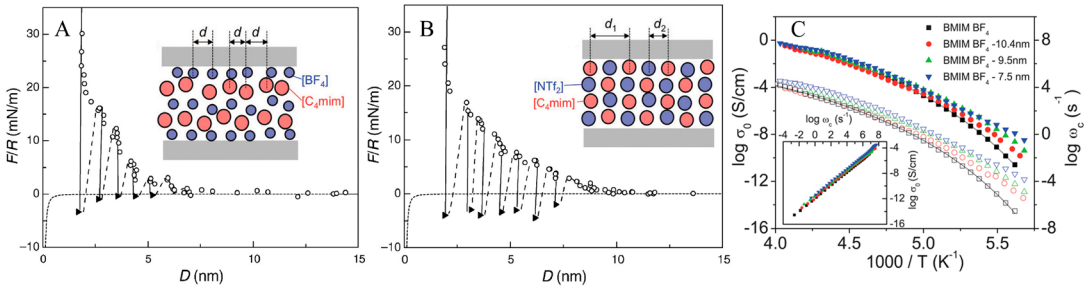

Figure 32. Normal force rescaled with the radius of the surface curvature (F/R) as a function of surface separation distance between two silica surfaces in (A) $[C_4MIM][BF_4]$ and (B) $[C_4MIM][NTF_2]$ ILs. Open circles and closed triangles correspond to data on approach and on retraction, respectively. Dotted lines represent vdW attractions between silica surfaces calculated from the Lifshitz theory. Solid and dashed lines correspond to stable and unstable regions, respectively, in the force profiles. Reproduced with permission from ref 884. Copyright 2010 Royal Society of Chemistry. Schematic spatial distributions of ion species between silica surfaces are shown in the insets. Reproduced with permission from ref 125. Copyright 2018 Royal Society of Chemistry. (C) Temperature dependence of ion conductivity $\sigma_0(T)$ (open symbols) and characteristic rate of charge transport ω_c (filled symbols) for $[C_4MIM][BF_4]$ in the bulk liquid region and in confined silica nanopores. Lines represent VFT fitting of the bulk data. Inset: ion conductivity σ_0 versus charge transport ω_c for bulk and confined $[C_4MIM][BF_4]$ IL. Reproduced with permission from ref 889. Copyright 2012 Royal Society of Chemistry.

vapor phase due to stronger intermolecular interactions of SO_3 groups with Pd atoms.

5.5. IL–Silica Interface

A microporous silica matrix is a promising framework for confining ILs because of its simple synthesis procedure and nontoxicity. When ILs are confined in silica matrixes, an obvious difference is observed in melting points of ILs in comparison with those in bulk liquids. The effect of silica confinement on melting points of ILs, either increases[863] or decreases,[864,865] is contradictory from different reports. Most studies stated that melting endotherms of confined ILs are detected at relatively lower temperatures and sometimes disappear compared to bulk ILs, resulting in liquidlike phase behavior of ILs below their solidification temperatures.[865−868] ILs consisting of $[C_2MIM]$ cations coupled with $[N(CN)_2]$, $[C_2SO_4]$, [SCN], and [TFO] anions have decreased melting temperatures when they are confined within mesoporous silica monoliths, in which melting temperatures of $[C_2MIM][N(CN)_2]$ and $[C_2MIM]$[TFO] ILs are depressed by approximately 14 and 8 °C, respectively.[868] $[C_4MIM][C_8SO_4]$ shows significant changes in melting, crystallization, and glass transition temperatures in a nanoporous silica matrix.[864] In addition, melting temperature depression for ILs confined within a porous silica matrix shows a linear variation with the inverse of the mean pore diameter of the microporous silica matrix.[864,868] Furthermore, immobilization of imidazolium cations on the silica surface can also lead to a melting point depression for confined ILs depending on the weight proportion of immobilized ions and the loading amount of ILs on the silica surface.[869] In contrast to melting temperature depression, it was shown that compressed gases play an important role in increasing melting temperatures of imidazolium ILs entrapped within mesoporous silica matrixes.[863,870]

These nonbulk thermodynamic phase behaviors of ILs confined in silica matrixes are essentially correlated with delicate interactions of silica surface atoms with confined ion species. The silica surface contains Si atoms, Si−O, silanol SiOH, and silane SiH_2 groups.[63,127,871,872] Depending on the specificity of the ion species and their relative positions in confined environments, ILs exhibit varied coordination features with these interfacial groups, as revealed from combined SFG, FT-IR spectra, and theoretical calculations.[127,864,866,873,874] In general, strong charge-balancing and electrostatic interactions and preferential HB interactions between confined ion species and silica interfacial groups contribute to remarkable microstructures and distinct orientations of ILs on the silica surface.[63,125,871,873,875−877] For ILs consisting of $[C_4MIM]$ cations coupled with $[BF_4]$, $[PF_6]$, [TFO], and $[NTF_2]$ anions, atomistic simulations showed that $[C_4MIM]$ cations attach exclusively onto the negatively charged silica surface covered by $Si(OH)_2$ surface groups, with imidazolium ring planes perpendicular to the interfacial $Si(OH)_2$ groups and butyl chains elongated above the $Si(OH)_2$ groups along the silica surface (Figure 31).[63] Anions exhibit random orientation distributions in subsequent anion layers because interactions between the adsorbed anion species and interfacial $Si(OH)_2$ groups are partially screened.[63,864,875,878,879] However, anions are particularly absorbed onto positively charged silica surface covered by silane SiH_2 groups. The main axes of asymmetric $[NTF_2]$ and [TFO] anions are parallel and perpendicular to interfacial SiH_2 groups, respectively (Figure 31).[63] Additional simulations demonstrated that silica surface with irregularly distributed SiOH groups is less efficient in trapping anions such that confined ILs are less localized on the amorphous SiO_2 surface.[878] In addition, there are significant positive dipole determined short-range SiOH-anion interactions in the IL−SiO_2 interfacial region, which can be perturbed by strong external fields. Therefore, an effective way to control interfacial structures of ILs on the silica surface is to regulate the concentration of interfacial hydroxyl groups via appropriate physicochemical treatments of the SiO_2 surface.

Owing to substantial interactions of ILs with silica surface groups, confined ions with flexible structures usually have distinct conformations near the silica surface.[867,878,880−882] Even though the *trans* conformer is dominant for $[NTF_2]$ anions in bulk ILs, both Raman spectroscopy[330,881] and atomistic simulations[880] indicated that $[NTF_2]$ anions preferably adopt a *cis* conformation, allowing efficient packing of $[NTF_2]$ anions in the IL−SiO_2 interfacial region.[881] An increase in degree of confinement[880] or loading amount of ILs[330] into silica matrix leads to a gradual increase in the *cis*/*trans* ratio, and the *cis* conformer becomes dominant. In addition, conformational changes of $[NTF_2]$ anions resulting from the confinement effect lead to prominent variations in

https://dx.doi.org/10.1021/acs.chemrev.9b00693
Chem. Rev. 2020, 120, 5798−5877

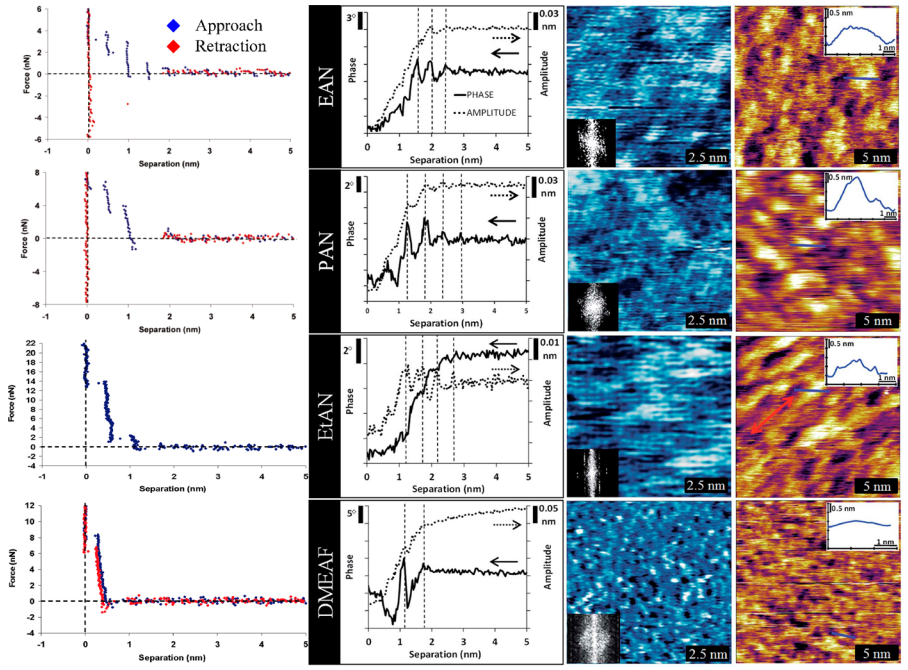

Figure 33. Interfacial data for EAN−, PAN−, EtAN−, and dimethylethylammonium formate (DMEAF)−mica systems. Column 1 (left) shows forces versus separation distances for an AFM tip to approach and to retract from the mica surface. Reproduced with permission from ref 129. Copyright 2007 American Chemical Society. Reproduced with permission from ref 908. Copyright 2009 American Chemical Society. Column 2 shows typical amplitude (dotted) and phase (black) data documented when an oscillating AFM tip approaching a mica surface dispersed in ILs. Column 3 shows topographic images of the innermost ion layer adsorbed to a mica surface. Column 4 (right) shows topographic images of the first near-surface layer of IL−mica systems. Insets present section analysis of interfacial IL structures near mica surfaces indicated by a blue line. Reproduced with permission from ref 912. Copyright 2015 Royal Society of Chemistry.

spectroscopic properties, especially fluorescence,[865] FT-IR,[864,867,873] and Raman vibrational spectra of anion species.[330,873,881,883]

Because of the distinct confinement effect and preferential distributions of ions on the silica surface, ILs exhibit remarkable interfacial layering structures.[869,875,878,884] $[C_4MIM][NTF_2]$ and $[C_4MIM][BF_4]$ ILs confined between two silica surfaces display considerable oscillatory solvation force profiles with varied features depending on ion pair dimensions and structure-forming abilities of ILs (Figure 32A,B).[884] $[C_4MIM][NTF_2]$ in a confined silica matrix shows two XRD peaks, indicating that both cations and anions coexist in the interfacial layer with a checkerboard ion arrangement.[125,878,885] Force−distance profiles revealed that interfacial structures of $[C_4MPYRR][NTF_2]$ are much weaker than those of $[C_4MIM][NTF_2]$, and addition of $LiNTF_2$ salt can further abate interfacial IL nanostructures. Similar interfacial layering structures of ILs confined within porous silica materials were also observed in extensive atomistic simulations.[125,875,877,882,886−888]

Besides distinct interfacial layering structures, dynamical quantities of confined ILs and the intrinsic response of interfacial structures to external variables, such as shear and electric fields, are important for their usage in lubrication and electrochemical applications. Studies have been mainly focused on addressing translational[873,875,878,879,883,890,891] and rotational dynamics,[876,890] shear viscosities,[880,892] ion and thermal conductivities,[877,889] and tribological[884,892] and dielectric relaxations[869] of ILs in confined environments. Unlike ILs in bulk liquids, dynamics of confined ILs, either increase[882,893] or decrease[873,877,880,894] with different trends and extents, depend on the delicate interplay of interactions among constituent ions and interfacial groups and the loading fraction of ILs in confined environments.[330,877,880,886] Jacob et al. measured self-diffusion coefficients of $[C_6MIM][PF_6]$ and $[C_4MIM][BF_4]$ ILs confined within micro- and mesoporous silica membranes.[889,895] NMR data exhibit a distinct temperature dependence of translational diffusion data of hydrophilic $[C_4MIM][BF_4]$ on pore sizes in silica matrixes.[889] Ion conductivities of $[C_4MIM][BF_4]$ in mesopores silica matrixes present a peculiar thermal activation described by VTF character, exhibiting a stepwise increase in ion conductivities with decreasing pore diameters of silica matrixes at low temperatures (Figure 32C).[889]

A silica surface functionalized with various chemical groups, such as tributylsilyls,[893] metal carbonyls,[896] and even IL groups,[897,898] offers additional pathways for tuning heterogeneous dynamics of confined ions in silica matrixes. Diffusion coefficients of hydrophobic $[C_6MIM][PF_6]$ IL in untreated silica membranes (hydrophilic) decrease by approximately 1 order of magnitude compared to that in bulk liquids. However, a remarkable increase in diffusion coefficients is observed upon decorating silica membranes with hexamethyldisilazane groups.[889,895] In another case, both $[C_6MIM][NTF_2]$ and diethylmethylammonium methanesulfonate ILs display higher ion conductivities in silica matrixes functionalized with tributylsilyl groups as compared with those in untreated silica nanopores.[893] A similar feature with enhanced proton conductivity is observed in $[C_8HIM][NTF_2]$−imidazole mixtures confined in nanopores of silica particles.[899] Proton conductivity occurs due to an establishment of new N···H−N HBs and fast proton exchange events in polar domains, which are decoupled from molecular diffusions of constituent ions in heterogeneous IL matrixes.

https://dx.doi.org/10.1021/acs.chemrev.9b00693
Chem. Rev. 2020, 120, 5798−5877

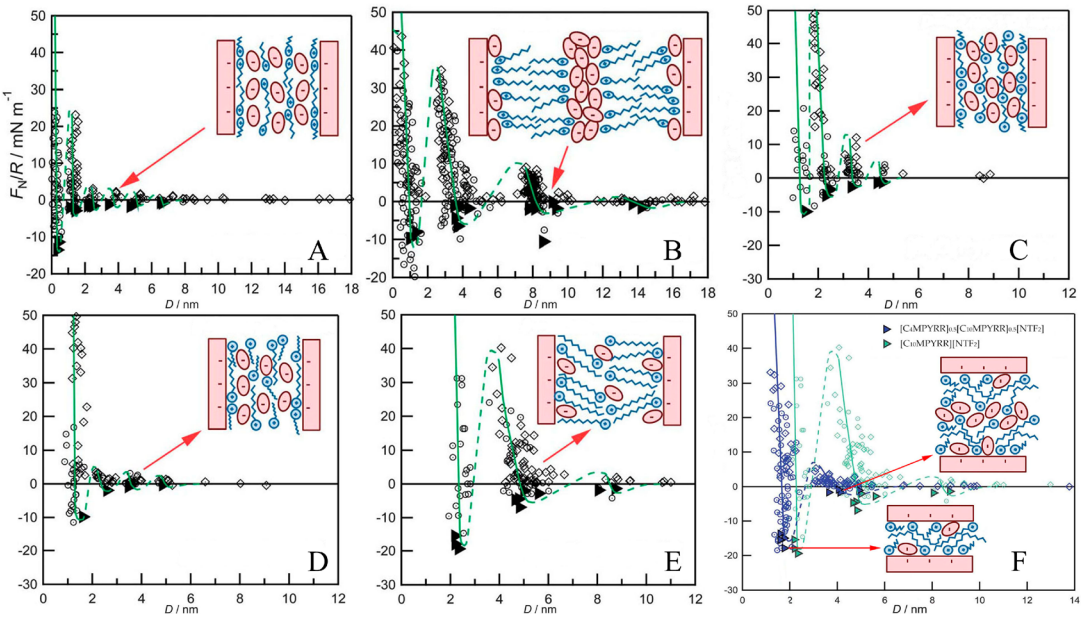

Figure 34. Normal force (F_N) renormalized with curvature radius (R) between mica surfaces across (A) $[C_4MIM][NTF_2]$, (B) $[C_6MIM][NTF_2]$, (C) $[C_4MPYRR][NTF_2]$, (D) $[C_8MPYRR][NTF_2]$, (E) $[C_{10}MPYRR][NTF_2]$, and (F) $[C_4MPYRR]_{0.5}[C_{10}MPYRR]_{0.5}[NTF_2]$ mixture as a function of separation distance between mica surfaces. Open diamond points were measured on approach and open circles on retraction of mica surfaces. Schematics indicate possible layering structures for pure ILs and IL−IL mixtures. Reproduced with permission from ref 920. Copyright 2013 Royal Society of Chemistry.

For ILs used as lubricants or lubricant additives, their tribological and antiwear properties are intrinsically correlated with a balance of molecular shapes of ILs and atomic structures of solid surfaces and possible residual impurities (such as water) in ILs.[892,900−905] Spencer and co-workers studied representative tribological behaviors of silica/silicon tribopairs lubricated with fluorinated ILs.[901,902,906] XPS and Raman spectra showed that a mechanical form of wear dominates within a wide speed range for $[C_2MIM][NTF_2]$ and $[C_6MIM][NTF_2]$ ILs.[906] In contrast, the corresponding [FAP] ILs exhibit significantly different XPS and Raman spectra, suggesting a different boundary lubrication mechanism depending on contact pressure.[901,902] Furthermore, effect of water on antiwear properties of IL lubricants depends on hydrophilicities of anions and surface types.[903,904] Addition of water into hydrophilic $[C_4MIM][BF_4]$ results in a disruption of solvation IL layers and thereafter the formation of an interfacial water phase on silica via HB interactions of water with IL ions and silica interfacial groups.[904]

5.6. IL−Mica Interface

Mica is a layered alumina silicate with two layers of silica tetrahedra sandwiching a layer of alumina octahedra. Mica has been extensively used as a model surface to gain insights into microstructures and dynamical properties of liquids and solutions in confined environments.[107] Horn and co-workers measured oscillatory forces between atomically smooth mica surfaces immersed in EAN and EAN−water mixtures.[907] Four to five oscillations are obtained for EAN before strong repulsion is observed, which prevents a closer approach of mica surfaces. The step period of 0.5−0.6 nm is consistent with the EAN ion pair diameter, indicating that EA cations and $[NO_3]$ anions are present in approximately equal numbers at the IL−mica interface. For EAN−water mixtures with low EAN concentrations, EAN behaves as a simple electrolyte and EDL force between mica surfaces decreases with a gradual increase of EAN concentration, consistent with DLVO theoretical prediction.[856] As EAN concentration increases, EA cations adsorb to mica surfaces in a manner that is described by an ion-exchange model, and the EDL force becomes weak and is completely replaced by a short-range solvation force extending up to several nanometers.

Atkin and co-workers studied interfacial structural quantities of alkylammonium ILs confined between a Si_3N_4 AFM tip and a mica surface.[129,130,908,909] Two significant features, a series of repeating "push-through" at discrete separations on the AFM tip approach and retraction and a significant increase in the rupture force closer to the mica surface, were consistently obtained from extensive AFM measurements (Figure 33). In addition, oscillatory force profiles for EAN−mica systems exhibit a significant temperature dependence. An increase in temperature leads to a decrease in the number of solvation layers in the EAN−mica interfacial region and a decreased force that is required to rupture the innermost solvation layer due to reduced liquid viscosity.[910] However, the force barriers associated with interfacial ordering structures are largely unaffected by temperatures, indicating that boundary IL layers remain in the interfacial region even at high temperatures.

Lengthening the alkyl chains in alkylammonium cations from C_2 to C_3 leads to notable changes in the solvation forces for alkylammonium nitrate ILs confined on a mica surface.[129,908,911,912] C_3 chains in PA cations pack efficiently without layering as they confer more orientation freedom than C_2 chains in EA cations, and thus fewer and more compressible interfacial layers are detected in the PAN−mica interfacial region (Figure 33). Additional AFM characterization of the PAN−alcohol mixtures on the mica surface showed that butanol can pack into the native PAN nanostructural region and causes swelling of polar and apolar networks with minimal structural variation.[913] Alkyl chains in octanol and dodecanol are too long to simply accommodate themselves alongside PA

https://dx.doi.org/10.1021/acs.chemrev.9b00693
Chem. Rev. 2020, 120, 5798−5877

cations. Even if hydroxyl groups in octanol and dodecanol are solvated in polar domains, alkyl chains in these two alcohols can transverse apolar domains in PAN. In addition, dissolved inorganic ions (Li^+, Na^+, Mg^{2+}, and Al^{3+}) compete effectively with PA cations in coordinating negatively charged sites on mica surface even at low ion concentrations, leading to distinct interfacial structures at the IL−mica interface.[914]

Covalently tethering a hydroxyl group to the terminal methyl unit in the EA cation leads to a dramatic change in the oscillatory force profile for EtAN on the mica surface.[908,911,912] EtAN exhibits less ordered interfacial structures and fewer interfacial layers than EAN and PAN near the mica surface (Figure 33). In addition, substitution of primary alkylammonium cations with secondary and tertiary ones reduces the number of solvation layers at the IL−mica interface and weakens adsorption of cations onto the mica surface (Figure 33).[908,912] These two variations are intrinsically related to intermolecular cohesive forces between ions and preferential coordinations of ions with the mica surface.

In comparison with EAN, $[C_2MIM][NTF_2]$ exhibits distinct interfacial structures as revealed by AFM experiments, which are correlated with intrinsic molecular structures of constituent ions and their abilities to self-assemble at the mica surface.[909,915−917] AFM imaging revealed that EAN self-assembles in a wormlike liquid morphology at the mica surface, whereas $[C_2MIM]$ cations adsorb in a more isolated fashion but still in rows templated by the mica surface. In addition, EA cations remain adsorbed to mica surface at high forces, whereas $[C_2MIM]$ cations desorb at a relatively low pressure, which is attributed to electrostatic attractions of charged atoms on the mica surface with localized charges in the EA cations being stronger than that with delocalized charges in $[C_2MIM]$ cations. This indicates that for applications where strong surface adsorption is desirable, such as in tribology, ions with localized charges are preferred; however, for applications where access to the solid interfacial region is required, such as in electrochemical devices like dye-sensitized solar cells (DSSCs), ions with delocalized charges should be employed as the solutes are more readily diffused from the solution to solid surfaces.

In another series of systematic studies, interfacial microstructures of $[C_nMIM][NTF_2]$ ILs confined between negatively charged mica sheets were studied using the SFB technique,[107,137−140] neutron reflectivity,[107] X-ray scattering spectroscopy,[124,125] and atomistic simulations.[124,125,918,919] Both $[C_4MIM[NTF_2]$ and $[C_6MIM][NTF_2]$ ILs exhibit clear oscillatory forces with alternating repulsive and attractive regions and increased amplitude with decreasing relative distance between the two mica surfaces.[137,920] The oscillation period for $[C_4MIM][NTF_2]$ is close to one ion pair dimension, indicating that ions are arranged in alternating cation−anion monolayers between mica surfaces (Figure 34A). $[C_6MIM]$-$[NTF_2]$ is more structured between mica surfaces with a larger repeat distance although alkyl chain length is merely and incrementally increased relative to $[C_4MIM][NTF_2]$, indicating a structural transition from alternating cation−anion monolayers for $[C_4MIM][NTF_2]$ to *tail-to-tail* cation bilayers for $[C_6MIM][NTF_2]$ driven by solvophobic self-assembly of $[C_6MIM]$ cations in confined environments (Figure 34B). Furthermore, a combination of SFB and neutron reflectivity experiments demonstrated that $[C_{10}MIM][NTF_2]$ exhibits clear evidence of interfacial layering structures between mica surfaces. These results were later reproduced by atomistic simulations[138,919] and are rationalized by delicate electrostatics and chemical interactions controlling interfacial structures of ILs in confined environments.[139,639,921]

One thing should be mentioned is that the mica surface is very reactive and readily adsorbs hydrocarbons and water species, leading to the formation of a few Angstrom thick contamination layer on the mica surface.[904,915,922,923] XPS data revealed that $[C_1MIM][NTF_2]$ and $[C_4MIM][NTF_2]$ ILs exhibit complete dewetting behavior on a clean mica surface, but they form thin IL films on a fully carbon-covered mica surface.[924] A considerable surface enhancement of $[NTF_2]$ anions is detected at submonolayer coverage in the IL−mica interfacial region, where $[NTF_2]$ anions are located above imidazolium rings that are parallel to the mica surface. $[NTF_2]$ anions adopt a *cis* conformation with CF_3 groups pointing away from the mica surface. These film growth and interfacial structural features strongly differ from that found for submonolayer coverage of ILs on the Au surface, where confined cations and anions in $[C_nMIM][NTF_2]$ ILs adsorb next to each other.[838,925] The presence of water in $[C_nMIM]$-$[NTF_2]$ ILs alters not only interfacial layering structures but also lateral and orientation ordering and aggregation of cation hydrophobic tails in the interfacial region. For $[C_4MIM]$-$[NTF_2]$ confined between mica surfaces, water weakens adsorption of $[C_4MIM]$ cations onto mica surfaces and displaces ions from mica surfaces, and therefore interfacial layering structures nearly diminish. A general feature concerning the effect of water on the IL interfacial structures can be understood based on available experimental and computational studies of IL−water−mica systems.[915,922,923] In the presence of water, interfacial structures near the mica surface are electrifiable via surface atom dissociation. Electrification of the mica surface is correlated with self-organization of interfacial ions and adsorption of water at the IL−mica interface. Water often, but not always, weakens interfacial layering structures, which can be traced back to the fact that water is both a dielectric solvent and a molecular liquid.[918,926] For water-stable ILs, water may be leveraged to improve functional performance of ILs in applications. Therefore, adopting interfacial water is promising to manipulate IL interfacial structures (and dynamics) and potentially allows more flexibility in specific applications. In this regard, encouraging results have already been reported for using interfacial water to improve capacitive energy storage and lubrication.[756,927,928]

Novel interfacial behaviors were also observed in a homologous series of $[C_nMPYRR][NTF_2]$ ILs.[421,920,926,929,930] $[C_nMPYRR]$ cations (n = 4, 6, and 8) exhibit consistent stable alternating cation−anion layers, akin to $[C_nMIM][NTF_2]$ ILs with very similar film thickness.[920,931] This implies a tendency for alkyl chains to lie more or less parallel along the mica surface, leading to a decrease in the number density of cations within the interfacial layers as the alkyl chain length increases, a gradually increased mismatch in maximum possible ion concentration of anion and cation layers, and a frustration of overscreened alternating cation−anion interfacial layering structures. These mismatches contribute to a substantial lowering of oscillatory forces for $[C_8MPYRR][NTF_2]$ (Figure 34D) compared to $[C_4MPYRR]$-$[NTF_2]$ (Figure 34C) confined between mica surfaces. A substantially different oscillatory force is observed in $[C_{10}MPYRR][NTF_2]$, which is attributed to a flip from monolayer to bilayer interfacial structures (Figure 34E). This

https://dx.doi.org/10.1021/acs.chemrev.9b00693
Chem. Rev. 2020, 120, 5798−5877

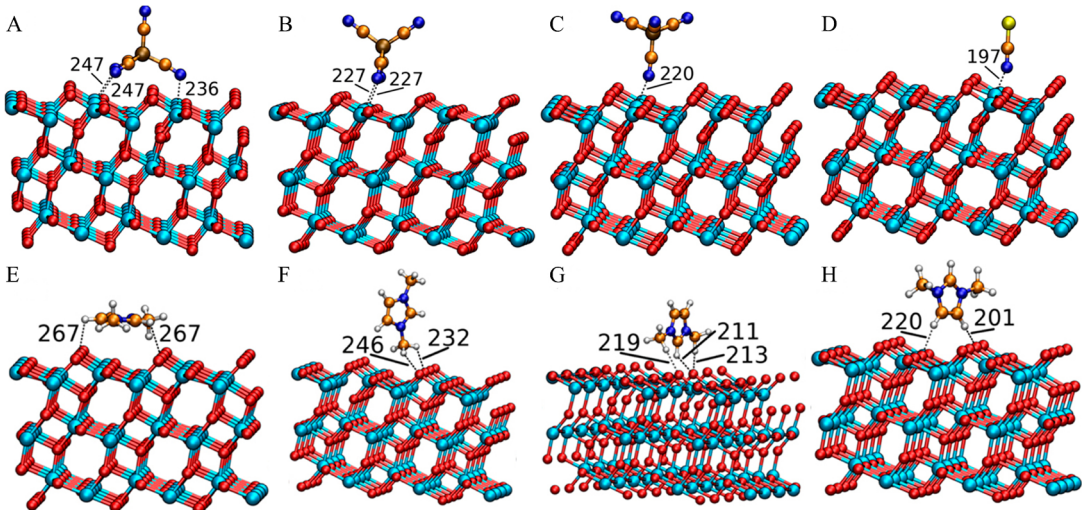

Figure 35. Adsorption geometries of ion species on the anatase(101) surface determined from DFT calculations. $[B(CN)_4]$ with (A) face conformation, (B) edge conformation, and (C) vertex conformation. (D) [SCN] with "N coordination" conformation. $[C_1MIM]$ with (E) "flat" conformation, (F) "vertical" conformation, (G) "H5 coordination" conformation, and (H) "H4 coordination" conformation. Labeled distances are in picometers. Reproduced with permission from ref 943. Copyright 2015 American Chemical Society.

change is different from that for $[C_6MIM][NTF_2]$ as C_{10} chains of $[C_{10}MPYRR]$ cations interdigitate and $[NTF_2]$ anions reside between neighboring pyrrolidinium rings.[926,929]

It is noteworthy that the monolayer-to-bilayer transition and the resulting bilayer architectures for $[C_nMIM][NTF_2]$ and $[C_nMPYRR][NTF_2]$ ILs are intrinsically different in alkyl chain length transition and interfacial bilayer thickness.[920] Crossover from the anion−cation monolayer to cation bilayer structures occurs between C_4 and C_6 for $[C_nMIM][NTF_2]$ ILs and between C_8 and C_{10} for $[C_nMPYRR][NTF_2]$ ILs. This difference is attributed to distinct cation−cation interactions. Planar imidazolium rings with delocalized charges can interact favorably via $\pi-\pi$ stacking interactions, allowing a close approach of alkyl chains and favorable dispersion interactions in apolar domains. Pyrrolidinium cations, on the other hand, cannot stack at such close distances and, therefore, require long alkyl chains to drive bilayer formation.[932] In addition, $[C_nMIM][NTF_2]$ and $[C_nMPYRR][NTF_2]$ ILs exhibit qualitatively different interfacial bilayer architectures in the IL−mica interfacial region. A *toe-to-toe* bilayer structure is proposed for confined $[C_6MIM][NTF_2]$ with $[NTF_2]$ anions sitting on top of imidazolium rings; however, C_{10} chains of $[C_{10}PYRR]$ cations are significantly interdigitated with $[NTF_2]$ anions positioned with pyrrolidinium polar groups in the same plane in the bilayer structures.[920]

Furthermore, oscillatory structural forces for a $[C_4MPYRR]_{0.5}[C_{10}MPYRR]_{0.5}[NTF_2]$ mixture confined between mica surfaces are distinct to those for pure IL components with both $[C_4MPYRR]$ and $[C_{10}MPYRR]$ cations being present in the confined IL film, rather than one component being more substantially surface active than the other and thus segregating from the bulk mixture in the thin IL film (Figure 34F).[920] The interfacial layer thickness of this mixture differs appreciably from that of alternating ion layers (monolayers) and is more similar to that of a bilayer structural motif for $[C_{10}MPYRR][NTF_2]$, indicating the formation of bilayer-like interfacial structures in the $[C_4MPYRR]_{0.5}[C_{10}MPYRR]_{0.5}[NTF_2]$ mixture. However, this bilayer-like interfacial structure is slightly thinner than that for pure $[C_{10}MPYRR][NTF_2]$ and is substantially more compressible and requires a low force to rupture or squeeze-out. In this mixture, $[C_{10}MPYRR]$ cations dictate interfacial structures, which are reminiscent of the effect of mixtures on bulk nanostructures, where cations with long alkyl chains are predominant in determining apolar domain sizes.[225]

It should be addressed that both anion sizes and shapes (halides, $[BF_4]$, $[PF_6]$, $[N(CN)_2]$, [FSI], $[NTF_2]$, [FAP], *etc.*) have a significant influence on oscillatory force profiles for ILs confined between mica surfaces.[140,237,916,917,933−935] $[PF_6]$ anions appear to be more conducive to nanostructure formation than $[NTF_2]$, $[NO_3]$, and formate anions, underlining the importance of anion features related to their symmetries and charge distributions. This points to a new avenue for molecularly designing IL architectures and, thereafter, tuning interfacial phenomena for particular applications, such as adhesion, lubrication, and electrokinetic flows.[917] Where mobility and transfer of ion species to and from solid interface is desirable (heterogeneous catalysis, batteries, supercapacitors, DSSCs, *etc.*), IL containing multiple sterically hindered allylic functional groups can be considered to maximize compressibility of IL solvation layers and minimize IL−substrate associations in interfacial regions. Conversely, in situations where adsorption of ILs to solid surface is required (*e.g.*, electrode surface restructuring and lubrication), ions with symmetric shapes having localized charge centers are preferable.[934]

5.7. IL−TiO_2 Interface

TiO_2 is a representative photoanode material in DSSCs,[936] and the IL−TiO_2 interface is of particular interest in DSSC research as detailed knowledge of interfacial structures may shed light on device differences in regard to function and durability.[936] A combination of XPS and extended X-ray absorption fine structure spectra showed that $[C_4MIM][BF_4]$ absorbs onto the anatase(101) surface, the most thermodynamically stable and dominant surface exposed in the TiO_2 substrate,[937] in an ordering manner via electrostatic interactions at a low coverage with imidizolium rings oriented at 32 ± 4° from the anatase surface.[938,939] With an increase in coverage of $[C_4MIM][BF_4]$ on the anatase(101) surface, the influence of the TiO_2 surface on interfacial orientations of

https://dx.doi.org/10.1021/acs.chemrev.9b00693
Chem. Rev. 2020, 120, 5798−5877

confined ions at the uppermost IL−vapor layers is reduced and interfacial ordering structures are partially or totally lost. Above specific temperatures, both cations and anions undergo surface-induced degradation on the anatase(101) surface, leading to a production of varied ion species detected by XPS.[938,940] The decomposition mechanism of ILs on the anatase(101) surface is distinct depending on ion structures and temperatures. $[BF_4]$ anions most likely react with interfacial atoms at oxygen-vacancy sites resulting in an incorporation of fluorine atoms into oxygen vacancies at the anatase surface.[938]

Atomistic simulations provided complementary results for a thorough understanding of interfacial structures at the IL−TiO_2 interface.[941−944] It was found that layering effect for $[C_2MIM][NTF_2]$ confined inside a rutile(110) slit is more pronounced compared to its confinement in a graphitic slit having the same slit width.[725] Both $[C_2MIM]$ cations and $[NTF_2]$ anions adopt multiple orientations and exhibit significantly slower diffusion rates near rutile walls than near graphite walls,[725] which is attributed to specific interactions between confined ion species and interfacial atoms of the rutile walls. Strong electrostatic and dispersion interactions are present between individual atoms in $[C_2MIM][NTF_2]$ and Ti and oxygen atoms on rutile walls, whereas only vdW interactions are present between confined ions and carbon atoms at graphitic walls.

Barbara and co-workers performed AIMD simulations to study interfacial structures of $[C_2MIM][SCN]$ and $[C_2MIM]$-$[B(CN)_4]$ ILs on the anatase(101) surface.[942−944] These two ILs exhibit dense interfacial layers at the IL−TiO_2 interface with $[C_2MIM]$ cations being perpendicular to the anatase surface because of HB interactions of C(2)−H atoms with interfacial oxygen atoms on the anatase surface. Most $[B(CN)_4]$ anions exhibit face conformation (Figure 35A), where three CN groups have preferential interactions with the anatase(101) surface. The less populated edge (Figure 35B) and vertex (Figure 35C) conformations with two and one CN groups in contact with the anatase(101) surface are also observed. Favorable N−Ti interactions of [SCN] anions with the anatase(101) surface result primarily in perpendicular distributions of [SCN] anions with nitrogen atoms closest to the anatase(101) surface (Figure 35D). In addition, absorbed imidazolium cations exhibit varied adsorption geometries on the anatase(101) surface (Figure 35E−H) and tend to cause an energetic downward shift of TiO_2 band levels by accepting electron density from the anatase surface. Anions are observed to raise energy levels by donating electron density to the anatase surface.[942] Both effects take place simultaneously and counteract each other, leaving a complicated charge transfer phenomenon at the IL−TiO_2 interface. In general, if it aims to achieve a maximum energetic upward shift, the adopted ILs should consist of cations with highly delocalized or screened positive charges, and their interactions with the TiO_2 surface should be minimal. Additionally, ILs can be changed systematically to increase or decrease the band edge position to match the band levels appropriately. If alignment of the band levels is satisfactory, different ILs that yield similar band shifts can be employed to improve other aspects for peculiar applications, such as compatibilities of electrolytes with dye molecules, redox mediators, and solar cell sealing materials.[945]

Furthermore, there are some sporadic experimental and computational investigations on absorption of ILs on various metal oxide surfaces including CeO_2,[946,947] ZnO,[948,949] VO_2,[950,951] $SrTiO_3$,[952,953] CoO/Co_3O_4,[954] FeO,[955,956] ZrO_2,[957] and even on some metal sulfide surfaces, like GeS_2[958] and MoS_2.[959,960] These studies illustrated that delicate intermolecular interactions between IL ions and metal oxide surfaces and acidity of the metal oxide surfaces have a significant effect on short- and long-term thermal stabilities of supported ILs. A detailed elucidation of these interactions offers new opportunities for rational design of materials, such as solid catalysts on supported IL layers for heterogeneous catalysis and supported IL membranes for gas separation.

6. CONCLUSIONS AND OUTLOOK

Over the last 2 decades, ILs have attracted increasing attention in academia and industrial communities owing to their numerous useful physicochemical and structural properties. Due to a countless number of combinations of cation−anion moieties and mixtures with cosolvents, a thorough understanding of their hierarchical structures and dynamics is highly significant for rational selection and design of ILs with desired properties and thereafter maximizing their functionalities in applications including catalysis, gas capture and separation, energy storage and harvesting, and lubrication. This is a uniting theme across different IL types including alkylammonium, imidazolium, pyrrolidinium, pyridinium, piperidinium, and tetraalkylammonium and tetraalkylphosphonium cations with either organic or inorganic anions. An important feature of these ILs is that they are more complex than molecular solvents and show rich diversities in various aspects ranging from molecular structures of constituent ions, intra- and intermolecular interactions, dynamical quantities, and self-assembled liquid morphologies of ILs in bulk liquids. Therefore, ILs have been extensively investigated in different ways including free ions, ion pairs, ion clusters, ion continuum, HB networks, and bicontinuous sponge structures with interpenetrating polar and apolar networks via advanced experimental techniques and molecular simulations. In addition, nanoconfined ILs, owing to distinct spatial confinement and dominant surface forces at short length scale, offer new and attractive features, such as distinct phase transitions and depressed transport properties. These microstructural, dynamical, and transport properties are attributed to a complex interplay of constituent ions with surrounding ions in bulk liquids, with cosolvent molecules and inorganic salts in IL mixtures, and with solid surfaces in confined environments. A specific feature of ILs, either in bulk liquids or in interfacial regions, is microstructural and dynamical heterogeneities, which are hallmark characteristics of their unique properties. These heterogeneities of ILs arise because ILs are composed of cations and anions or, alternatively, polar and apolar groups, leading to repeating and correlated microstructures in bulk liquids and in interfacial regions on nanometer dimensions. The diversified solvent structures of ILs are the origin of much past, current, and future interest in ILs, which are implicated in almost all aspects of their chemistry.

At the current stage, the IL research field has reached an astonishing level, enriched with an unexpected diversity of ions with distinct capacities for self-assembly in bulk liquids and in confined environments. This diversity has catalyzed IL research, and their chemical and self-assembled structures can be used to unlock their potential to impact many areas of scientific research and technological applications. As this field matures, there needs to be increasing economic cost/benefit analysis of ILs, how to select and how to design appropriate

https://dx.doi.org/10.1021/acs.chemrev.9b00693
Chem. Rev. 2020, 120, 5798−5877

ions to achieve peculiar microstructures, distinctive mesoscopic liquid morphologies, and specific macroscopic functions, which will be critical for ILs to compete with established liquids and materials. Multiscale modeling approaches, including *first principle* calculations and *ab initio*, atomistic, and CG MD simulations, provide not only complementary results but also critical physical insights for understanding spectacular phenomena taking place in bulk liquids and in interfacial regions under harsh conditions. In future work, molecular simulations will be generally adopted in two modes within the IL community: accurate prediction of physicochemical and structural quantities of IL systems and providing qualitative insights into the structure−property relationship for maximizing their utilization in applications. It is anticipated that in a long period of time in the future, multiscale modeling simulations will be on an equal footing with experimental investigations to explore important properties of ILs in a wide range of applications. An integration of multiscale simulation results and experimental characterizations is expected to unveil fundamental mechanisms governing distinct microstructural and dynamical heterogeneities of ILs in a wide range of physical and chemical environments and to fine-tune these properties in an intelligent fashion. A comprehensive understanding of fundamental properties of ILs can provide unprecedented guidance for preselection and design of appropriate IL candidates and advancing their functionalities in industrial applications while minimizing environmental effects for a sustainable future.

AUTHOR INFORMATION

Corresponding Author

Yong-Lei Wang − *Department of Materials and Environmental Chemistry, Arrhenius Laboratory, Stockholm University, SE-106 91 Stockholm, Sweden;* orcid.org/0000-0003-3393-7257; Phone: +46 70 254 9882; Email: yonglei.wang@mmk.su.se, wangyonl@gmail.com

Authors

Bin Li − *School of Chemical Engineering and Technology, Sun Yat-sen University, Zhuhai 519082, P. R. China;* orcid.org/0000-0002-5103-0790

Sten Sarman − *Department of Materials and Environmental Chemistry, Arrhenius Laboratory, Stockholm University, SE-106 91 Stockholm, Sweden*

Francesca Mocci − *Department of Chemical and Geological Sciences, University of Cagliari, I-09042 Monserrato, Italy*

Zhong-Yuan Lu − *State Key Laboratory of Supramolecular Structure and Materials, Institute of Theoretical Chemistry, Jilin University, Changchun 130021, P. R. China;* orcid.org/0000-0001-7884-0091

Jiayin Yuan − *Department of Materials and Environmental Chemistry, Arrhenius Laboratory, Stockholm University, SE-106 91 Stockholm, Sweden;* orcid.org/0000-0003-1016-5135

Aatto Laaksonen − *Department of Materials and Environmental Chemistry, Arrhenius Laboratory, Stockholm University, SE-106 91 Stockholm, Sweden; State Key Laboratory of Materials-Oriented and Chemical Engineering, Nanjing Tech University, Nanjing 210009, P. R. China; Centre of Advanced Research in Bionanoconjugates and Biopolymers, Petru Poni Institute of Macromolecular Chemistry, 700487 Iasi, Romania; Department of Engineering Sciences and Mathematics, Division of Energy Science, Luleå University of Technology, SE-97187 Luleå, Sweden;* orcid.org/0000-0001-9783-4535

Michael D. Fayer − *Department of Chemistry, Stanford University, Stanford, California 94305, United States;* orcid.org/0000-0002-0021-1815

Complete contact information is available at: https://pubs.acs.org/10.1021/acs.chemrev.9b00693

Notes

The authors declare no competing financial interest.

Biographies

Yong-Lei Wang received his Ph.D. in 2012 from Jilin University, China, and in 2013 from Stockholm University, Sweden, under the joint supervision of Prof. Zhong-Yuan Lu and Prof. Aatto Laaksonen. From 2013 to 2016, he worked as a postdoctoral fellow with Prof. Aatto Laaksonen at Stockholm University and with Prof. Lars Kloo at KTH Royal Institute of Technology. In 2016, he received financial support from the Knut and Alice Wallenberg Foundation and worked as a Wallenberg Fellow with Prof. Michael D. Fayer at Stanford University and with Prof. Jiayin Yuan at Stockholm University. His research mainly focuses on numerical algorithm development for efficient handling of long-range Coulombic interactions, multiscale modelling of ionic liquids and polymeric fluids (charged soft matter systems), and computational studies of luminescent properties of transition-metal complexes in biological systems.

Bin Li was born in Siping, Jilin, China. He received his Ph.D. in 2013 from the Institute of Theoretical Chemistry, Jilin University, under the supervision of Prof. Zhong-Yuan Lu. Then he performed research as a postdoc at Technical University of Darmstadt, Germany, in the group of Prof. Nico van der Vegt (2013−2014), and Lund University, Sweden, in the group of Prof. Jan Forsman (2015−2017). After that, he moved to the National Center for Nanoscience and Technology, China, as an Assistant Professor. Currently he is an Assistant Professor at the School of Chemical Engineering and Technology, Sun Yat-sen University, China (2019−present). He mainly focuses on molecular simulations of soft matter systems, including ionic liquids properties and applications on supercapacitors as well as self-assembly of polymers and colloids.

Sten Sarman received his Ph.D. degree in physical chemistry at KTH Royal Institute of Technology, Sweden. Thereafter, he has worked at Australian National University in Canberra, Australia and Göteborg University and Stockholm University in Sweden. His main interest is various aspects of statistical thermodynamics and transport properties of liquids, including flow properties of ionic liquids, liquid crystals, and integral equation theory of inhomogeneous liquids close to walls or in narrow slits.

Francesca Mocci graduated in Chemistry in 1999 at Cagliari University, where she obtained her Ph.D. in Chemistry in 2002, under the supervision of Prof. Giuseppe Saba. She has been Aggr. Prof. in Physical Methods in Organic Chemistry at the Faculty of Pharmacy of Cagliari University since 2007. She has been a visiting professor for several years at Stockholm University (2011−2016). Her scientific activity is mainly directed at the study of conformational preferences and structural organization of organic and bio-organic systems, with particular attention to the interactions in highly charged systems.

Zhong-Yuan Lu received his Ph.D. from Jilin University, China, in 1999, with Professor Ze-Sheng Li as the advisor. After receiving a Ph.D., he stayed in the group of Professor Reinhard Hentschke as a postdoc at Bergische Universitaet-Gesamthochshule Wuppertal,

https://dx.doi.org/10.1021/acs.chemrev.9b00693
Chem. Rev. 2020, 120, 5798−5877

Germany, until 2003. He then moved back to Jilin University and started his own research group as an Associate Professor. In 2010, he was awarded with the National Nature Science Foundation for Outstanding Youth Scholars of China. Now he is a Full Professor at Jilin University. His research interest is multiscale simulation of polymers.

Jiayin Yuan studied chemistry at Shanghai Jiao Tong University (1998−2002), China. He received a M.Sc. degree from University of Siegen (Germany) in 2004 and a Ph.D. from Bayreuth University (Germany) in 2009. He joined the Max Planck Institute of Colloids and Interfaces in Potsdam as a postdoc and then became a group leader. He received the European Research Council Starting Grant in 2014, Dr. Hermann-Schnell Award in 2015, the Dozentenpreis from the Fund of Chemical Industry in 2016, and a Wallenberg Academy Fellow in Sweden in 2017. From December 2018, he is a Full Professor at Stockholm University (Sweden). He is interested in functional polymers and carbon materials.

Aatto Laaksonen is a Professor of Physical Chemistry at Stockholm University. He received a Ph.D. in 1981 from Stockholm University and was a postdoctoral fellow at Daresbury Laboratory (U.K.) in 1982 with Vic Saunders and at IBM Poughkeepsie/Kingston (U.S.) from 1983 to 1985 with Enrico Clementi. He had a sabbatical at Dalhousie University 1993−1995 (Canada) with Rod Wasylishen. He has been a visiting professor at JAERI 2002, 2005 (Japan), at Cagliari University 2008, 2009, 2011, 2015 (Sardinia), at Nanjing Tech University 2018−present (China), and at Petru Poni Institute for Macromolecular Chemistry 2018−present (Romania). Research areas include multiscale modelling/simulations including method and model development in bio and materials sciences and green chemical engineering.

Michael D. Fayer received a B.S. degree in Chemistry from University of California at Berkeley where he was Phi Beta Kapa. He also received his Ph.D. from University of California at Berkeley in 1974, working with Professor Charles B. Harris. After graduate school, Fayer went directly to Stanford University as an Assistant Professor of Chemistry in 1974. He has been a Full Professor since 1984 and became the David Mulvane Ehrsam and Edward Curtis Franklin Professor of Chemistry in 2000. Fayer pioneered the development and use of ultrafast nonlinear optical spectroscopy for studying dynamics in complex condensed matter molecular systems. Over the last 45 years, he has advanced the field, expanding from visible to infrared and to multidimensional techniques as he pursued a wide array of fundamentally important problems ranging from water to proteins. Fayer also developed detailed theoretical descriptions of nonlinear experiments and molecular systems. In 1979, Fayer performed the first picosecond (ultrafast at the time) photon echoes on molecular crystals. In 1993, the Fayer group conducted the first ultrafast infrared echo experiments, dubbed vibrational echoes, using an infrared free electron laser. These initial experiments set the stage for the current widespread field of ultrafast 2D IR spectroscopy. By the early 2000s, Fayer was using 2D IR spectroscopy to study hydrogen bonding, leading to a detailed understanding of water hydrogen bond dynamics. Fayer opened a new era of spectroscopic research on the dynamics of complex molecular system through his ground-breaking development and application of ultrafast nonlinear optical experiments. His work in both visible and IR has spread widely and stimulated a vast amount of research around the world that has amplified and extended the fields. Fayer has received many honors for his scientific work. He was elected to the National Academy of Sciences of U.S.A. in 2007 and the American Academy of Arts and Sciences in 1999. He received the Pittsburgh Spectroscopy Award from SSP in 2018, the Ahmed Zewail Award in Ultrafast Science and Technology from ACS in 2014, the Arthur L. Schawlow Prize in Laser Science from APS in 2012, the Ellis R. Lippincott Award from OSA in 2009, the E. Bright Wilson Award for Spectroscopy from ACS in 2007, and the Earl K. Plyler Prize for Molecular Spectroscopy from APS in 2000.

ACKNOWLEDGMENTS

Y.-L. Wang gratefully acknowledges financial support from the Knut and Alice Wallenberg Foundation (Grant KAW 2018.0380). F. Mocci acknowledges financial support from Progetto Fondazione di Sardegna (Grant CUP F71I17000170002). Z.-Y. Lu acknowledges financial support from the National Science Foundation of China (Grants 21534004 and 21833008). J. Yuan is grateful for financial support from ERC Starting Grant NAPOLI-639720 from the European Research Council, Swedish Research Council Grant 2018-05351, Dozentenpreis 15126 from Verband der Chemischen Industrie e.V. (VCI) in Germany, and the Wallenberg Academy Fellow program (Grant KAW 2017.0166) in Sweden. A. Laaksonen acknowledges the Swedish Science Council for financial support and partial support from a grant from the Ministry of Research and Innovation of Romania (CNCS−UEFISCDI, Project Number PN-III-P4-ID-PCCF-2016-0050, within PNCDI III). M. D. Fayer acknowledges the Division of Chemical Sciences, Geosciences, and Biosciences, Office of Basic Energy Sciences of the U.S. Department of Energy through Grant No. DEFG03-84ER13251 and Air Force Office of Scientific Research under AFOSR Award No. FA9550-16-1-0104 for support of this research.

ABBREVIATIONS

1D	one-dimensional
2D	two-dimensional
3D	three-dimensional
AIMD	*ab initio* molecular dynamics
ACN	acetonitrile
AFM	atomic force microscopy
BAN	butylammonium nitrate
$B(CN)_4$	tetracyanoborate
BF_4	tetrafluoroborate
BMB	bis(mandelato)borate
BMLB	bis(malonato)borate
BOB	bis(oxalato)borate
BScB	bis(salicylato)borate
BzMIM	1-benzyl-3-methylimidazolium
$C_1C_1PO_4$	dimethylphosphate
$(C_1OC_1)_2MIM$	1-methoxyethoxymethyl-3-methylimidazolium
C_2C_1MIM	1-ethyl-2,3-dimethylimidazolium
C_2HIM	1-ethyllimidazolium
C_2OH-MIM	1-(2-hydroxyethyl)-3-methylimidazolium
C_4C_1MIM	1-butyl-2,3-dimethylimidazolium
CF_3SO_3	triflate
CG	coarse-grained
CH	2-hydroxyethyl-trimethylammonium (cholinium)
C_nC_mIM	dialkylimidazolium
C_nC_mPYRR	dialkylpyrrolidinium
C_nMIM	1-alkyl-3-methylimidazolium
$C_n(MIM)_2$	di-imidazolium
C_nMPIP	1-alkyl-methylpiperidinium
C_nPYRI	*N*-alkylpyridinium
C_nSO_4	alkylsulfate

https://dx.doi.org/10.1021/acs.chemrev.9b00693
Chem. Rev. 2020, 120, 5798−5877

CNT	carbon nanotube
DFT	density functional theory
DLVO	Derjaguin-Landau-Vervey-Overbeek
DMEAF	dimethylethylammonium formate
DRS	direct recoil spectroscopy
DSC	differential scanning calorimetry
DSE	Debye−Stokes−Einstein
DSSCs	dye-sensitized solar cells
EAC	ethylammonium chloride
EAF	ethylammonium formate
EAN	ethylammonium nitrate
EDL	electrical double layer
EPSR	empirical potential structure refinement
EtAN	ethanolammonium nitrate
FAP	tris(pentafluoroethyl)trifluorophosphate
FSDP	first sharp diffraction peak
FSI	bis(fluorosulfonyl)imide
FT	Fourier transform
HB	hydrogen bonding
IL	ionic liquid
IR	infrared
MAN	methylammonium nitrate
MD	molecular dynamics
$N_{2,2,2,(2O2O2)}$	2-ethoxyethoxy-ethyltriethylammonium
$N(CN)_2$	dicyanamide
$N_{i,j,k,l}$	tetraalkylammonium
NMR	nuclear magnetic resonance
NO_3	nitrate
NTF_2	bis(trifluoromethanesulfonyl)imide
OAc	acetate
OHD-OKE	optical-heterodyne-detected optical Kerr effect
OHD-RIKE	optical-heterodyne-detected Raman-induced Kerr effect
OLC	onion like carbon
PAC	propylammonium chloride
PAN	propylammonium nitrate
PC	propylene carbonate
PF_6	hexafluorophosphate
PhSiMIM	1-dimethylphenylsilylmethyl-3-methylimidazolium
$P_{i,j,k,l}$	tetraalkylphosphonium
PSPP	polarization sensitive pump−probe
PZC	potential of zero charge
SANS	small-angle neutron scattering
SAXS	small-angle X-ray scattering
SCN	thiocyanate
SeCN	selenocyanate
SEIRAS	surface-enhanced infrared absorption spectroscopy
SFA	surface force apparatus
SFB	surface force balance
SFG	sum frequency generation
SiMIM	1-methyl-3-trimethylsilylmethylimidazolium
SiOSiMIM	1-methyl-3-pentamethyldisiloxymethylimidazolium
STM	scanning tunneling microscopy
TFA	trifluoroacetic acid
TFO	trifluoromethylsulfonate
UCST	upper critical solution temperature
vdW	van der Waals
VFT	Vogel−Fulcher−Tammann
WAXS	wide-angle X-ray scattering
XPS	X-ray photoelectron spectroscopy
XRD	X-ray diffraction
XRR	X-ray reflectivity

REFERENCES

(1) Walden, P. Molecular Weights and Electrical Conductivity of Several Fused Salts. *Bull. Acad. Imper. Sci. (St. Petersburg)* **1914**, *8*, 405−422.

(2) Sugden, S.; Wilkins, H. CLXVII.—The Parachor and Chemical Constitution. Part XII. Fused Metals and Salts. *J. Chem. Soc.* **1929**, *0*, 1291−1298.

(3) Hurley, F. H.; Wier, T. P. The Electrodeposition of Aluminum from Nonaqueous Solutions at Room Temperature. *J. Electrochem. Soc.* **1951**, *98*, 207−212.

(4) Welton, T. Ionic liquids: A Brief History. *Biophys. Rev.* **2018**, *10*, 691−706.

(5) Wilkes, J. S. A. Short History of Ionic Liquids—From Molten Salts to Neoteric Solvents. *Green Chem.* **2002**, *4*, 73−80.

(6) Wilkes, J. S.; Zaworotko, M. J. Air and Water Stable 1-Ethyl-3-methylimidazolium Based Ionic Liquids. *J. Chem. Soc., Chem. Commun.* **1992**, *13*, 965−967.

(7) Cooper, E. I.; Angell, C. A. Versatile Organic Iodide Melts and Glasses with High Mole Fractions of LiI: Glass Transition Temperatures and Electrical Conductivities. *Solid State Ionics* **1983**, *9*, 617−622.

(8) Poole, S. K.; Shetty, P. H.; Poole, C. F. Chromatographic and Spectroscopic Studies of Solvent Properties of A New Series of Room-temperature Liquid Tetraalkylammonium Sulfonates. *Anal. Chim. Acta* **1989**, *218*, 241−264.

(9) Plechkova, N. V.; Seddon, K. R. Applications of Ionic Liquids in the Chemical Industry. *Chem. Soc. Rev.* **2008**, *37*, 123−150.

(10) Binnemans, K. Ionic Liquid Crystals. *Chem. Rev.* **2005**, *105*, 4148−4204.

(11) Ediger, M. D. Spatially Heterogeneous Dynamics in Supercooled Liquids. *Annu. Rev. Phys. Chem.* **2000**, *51*, 99−128.

(12) Welton, T. Room-Temperature Ionic Liquids. Solvents for Synthesis and Catalysis. *Chem. Rev.* **1999**, *99*, 2071−2084.

(13) Dong, K.; Liu, X.; Dong, H.; Zhang, X.; Zhang, S. Multiscale Studies on Ionic Liquids. *Chem. Rev.* **2017**, *117*, 6636−6695.

(14) MacFarlane, D. R.; Forsyth, M.; Howlett, P. C.; Kar, M.; Passerini, S.; Pringle, J. M.; Ohno, H.; Watanabe, M.; Yan, F.; Zheng, W.; Zhang, S.; Zhang, J. Ionic Liquids and Their Solid-State Analogues as Materials for Energy Generation and Storage. *Nat. Rev. Mater.* **2016**, *1*, 15005.

(15) Zhang, S.; Zhang, J.; Zhang, Y.; Deng, Y. Nanoconfined Ionic Liquids. *Chem. Rev.* **2017**, *117*, 6755−6833.

(16) Podgorsek, A.; Jacquemin, J.; Pádua, A. A.; Costa Gomes, M. F. Mixing Enthalpy for Binary Mixtures Containing Ionic Liquids. *Chem. Rev.* **2016**, *116*, 6075−6106.

(17) Hunt, P. A.; Ashworth, C. R.; Matthews, R. P. Hydrogen Bonding in Ionic Liquids. *Chem. Soc. Rev.* **2015**, *44*, 1257−1288.

(18) Hayes, R.; Warr, G. G.; Atkin, R. Structure and Nanostructure in Ionic Liquids. *Chem. Rev.* **2015**, *115*, 6357−6426.

(19) Zhang, S.; Sun, J.; Zhang, X.; Xin, J.; Miao, Q.; Wang, J. Ionic Liquid-Based Green Processes for Energy Production. *Chem. Soc. Rev.* **2014**, *43*, 7838−7869.

(20) Burt, R.; Birkett, G.; Zhao, X. S. A Review of Molecular Modelling of Electric Double Layer Capacitors. *Phys. Chem. Chem. Phys.* **2014**, *16*, 6519−6538.

(21) Fedorov, M. V.; Kornyshev, A. A. Ionic Liquids at Electrified Interfaces. *Chem. Rev.* **2014**, *114*, 2978−3036.

(22) Somers, A. E.; Howlett, P. C.; MacFarlane, D. R.; Forsyth, M. A Review of Ionic Liquid Lubricants. *Lubricants* **2013**, *1*, 3−21.

(23) Niedermeyer, H.; Hallett, J. P.; Villar-Garcia, I. J.; Hunt, P. A.; Welton, T. Mixtures of Ionic Liquids. *Chem. Soc. Rev.* **2012**, *41*, 7780−7802.

https://dx.doi.org/10.1021/acs.chemrev.9b00693
Chem. Rev. 2020, 120, 5798−5877

(24) Hallett, J. P.; Welton, T. Room-Temperature Ionic Liquids: Solvents for Synthesis and Catalysis. 2. *Chem. Rev.* **2011**, *111*, 3508−3576.
(25) Castner, E. W., Jr; Margulis, C. J.; Maroncelli, M.; Wishart, J. F. Ionic Liquids: Structure and Photochemical Reactions. *Annu. Rev. Phys. Chem.* **2011**, *62*, 85−105.
(26) Armand, M.; Endres, F.; MacFarlane, D. R.; Ohno, H.; Scrosati, B. Ionic-Liquid Materials for the Electrochemical Challenges of the Future. *Nat. Mater.* **2009**, *8*, 621−629.
(27) Wang, Y. L.; Hedman, F.; Porcu, M.; Mocci, F.; Laaksonen, A. Non-Uniform FFT and Its Applications in Particle Simulations. *Appl. Mathematics* **2014**, *5*, 520−541.
(28) Santos, C. S.; Baldelli, S. Gas-Liquid Interface of Room-Temperature Ionic Liquids. *Chem. Soc. Rev.* **2010**, *39*, 2136−2145.
(29) Soukup-Hein, R. J.; Warnke, M. M.; Armstrong, D. W. Ionic Liquids in Analytical Chemistry. *Annu. Rev. Anal. Chem.* **2009**, *2*, 145−168.
(30) Zhou, F.; Liang, Y.; Liu, W. Ionic Liquid Lubricants: Designed Chemistry for Engineering Applications. *Chem. Soc. Rev.* **2009**, *38*, 2590−2599.
(31) Ma, C.; Laaksonen, A.; Liu, C.; Lu, X.; Ji, X. The Peculiar Effect of Water on Ionic Liquids and Deep Eutectic Solvents. *Chem. Soc. Rev.* **2018**, *47*, 8685−8720.
(32) Yuan, J.; Antonietti, M. Poly(ionic liquid)s: Polymers Expanding Classical Property Profiles. *Polymer* **2011**, *52*, 1469−1482.
(33) Fellinger, T. P.; Thomas, A.; Yuan, J.; Antonietti, M. 25th Anniversary Article:"Cooking Carbon with Salt": Carbon Materials and Carbonaceous Frameworks From Ionic Liquids and Poly(Ionic Liquid)s. *Adv. Mater.* **2013**, *25*, 5838−5855.
(34) Men, Y.; Kuzmicz, D.; Yuan, J. Poly(Ionic Liquid) Colloidal Particles. *Curr. Opin. Colloid Interface Sci.* **2014**, *19*, 76−83.
(35) Endres, F. Interfaces of Ionic Liquids. *Phys. Chem. Chem. Phys.* **2012**, *14*, 5008−5009.
(36) Endres, F. Physical Chemistry of Ionic Liquids. *Phys. Chem. Chem. Phys.* **2010**, *12*, 1648.
(37) Muldoon, M. J.; Nockemann, P.; Lagunas, M. C. Crystal Engineering with Ionic Liquids. *CrystEngComm* **2012**, *14*, 4873.
(38) Austen Angell, C.; Ansari, Y.; Zhao, Z. Ionic Liquids: Past, Present and Future. *Faraday Discuss.* **2012**, *154*, 9−27.
(39) Perkin, S.; Salanne, M. Interfaces of Ionic Liquids. *J. Phys.: Condens. Matter* **2014**, *26*, 280301.
(40) Rogers, R. D.; Voth, G. A. Ionic Liquids. *Acc. Chem. Res.* **2007**, *40*, 1077−1078.
(41) Perkin, S.; Kirchner, B.; Fayer, M. D. Preface: Special Topic on Chemical Physics of Ionic Liquids. *J. Chem. Phys.* **2018**, *148*, 193501.
(42) Castner, E. W., Jr; Wishart, J. F. Spotlight on Ionic Liquids. *J. Chem. Phys.* **2010**, *132*, 120901.
(43) Marcus, Y. *Ionic Liquid Properties: From Molten Salts to RTILs*; Springer-Verlag: Berlin-Heidelberg, 2016.
(44) *Electrodeposition From Ionic Liquids*; Endres, F., Abbott, A., MacFarlane, D. R., Eds.; John Wiley & Sons, 2017.
(45) *The Structure of Ionic Liquids*; Caminiti, R., Gontrani, L., Eds.; Springer-Verlag: Berlin-Heidelberg, 2014.
(46) *Electrochemistry in Ionic Liquids*. Vol. 1: Fundamentals; Torriero, A. A. J., Eds.; Springer-Verlag: Berlin-Heidelberg, 2015.
(47) *Structures and Interactions of Ionic Liquids*; Zhang, S., Wang, J., Lu, X., Zhou, Q., Eds.; Springer-Verlag: Berlin-Heidelberg, 2013.
(48) Wang, Y.-L.; Sarman, S.; Golets, M.; Mocci, F.; Lu, Z.-Y.; Laaksonen, A. Multigranular Modeling of Ionic Liquids. In *Ionic Liquids: Synthesis, Properties, Technologies and Applications*; Fehrmann, R., Santini, C., Eds.; De Gruyter, 2019.
(49) Mocci, F.; Laaksonen, A.; Wang, Y.-L.; Saba, G.; Lai, A.; Marincola, F. C. CompChem and NMR Probing Ionic Liquids. In *The Structure of Ionic Liquids*; Caminiti, R., Gontrani, L., Eds.; Springer-Verlag: Berlin-Heidelberg, 2014.
(50) Wood, N.; Stephens, G. Accelerating the Discovery of Biocompatible Ionic Liquids. *Phys. Chem. Chem. Phys.* **2010**, *12*, 1670−1674.
(51) Chauvin, Y.; Mussmann, L.; Olivier, H. A Novel Class of Versatile Solvents for Two-Phase Catalysis: Hydrogenation, Isomerization, and Hydroformylation of Alkenes Catalyzed by Rhodium Complexes in Liquid 1,3-Dialkylimidazolium Salts. *Angew. Chem., Int. Ed. Engl.* **1996**, *34*, 2698−2700.
(52) Lei, Z.; Dai, C.; Chen, B. Gas Solubility in Ionic Liquids. *Chem. Rev.* **2014**, *114*, 1289−1326.
(53) Watanabe, M.; Thomas, M. L.; Zhang, S.; Ueno, K.; Yasuda, T.; Dokko, K. Application of Ionic Liquids to Energy Storage and Conversion Materials and Devices. *Chem. Rev.* **2017**, *117*, 7190−7239.
(54) MacFarlane, D. R.; Tachikawa, N.; Forsyth, M.; Pringle, J. M.; Howlett, P. C.; Elliott, G. D.; Davis, J. H.; Watanabe, M.; Simon, P.; Angell, C. A. Energy Applications of Ionic Liquids. *Energy Environ. Sci.* **2014**, *7*, 232−250.
(55) Li, B.; Ma, K.; Wang, Y.-L.; Turesson, M.; Woodward, C. E.; Forsman, J. Fused Coarse-Grained Model of Aromatic Ionic Liquids and Their Behaviour at Electrodes. *Phys. Chem. Chem. Phys.* **2016**, *18*, 8165−8173.
(56) Zhang, W.; Wei, S.; Wu, Y.; Wang, Y.-L.; Zhang, M.; Roy, D.; Wang, H.; Yuan, J.; Zhao, Q. Poly(Ionic Liquid)-Derived Graphitic Nanoporous Carbon Membrane Enables Superior Supercapacitive Energy Storage. *ACS Nano* **2019**, *13*, 10261−10271.
(57) Bi, S.; Banda, H.; Chen, M.; Niu, L.; Chen, M.; Wu, T.; Wang, J.; Wang, R.; Feng, J.; Chen, T.; Dinca, M.; Kornyshev, A. A.; Feng, G. Molecular Understanding of Charge Storage and Charging Dynamics in Supercapacitors with MOF Electrodes and Ionic Liquid Electrolytes. *Nat. Mater.* **2020**, DOI: 10.1038/s41563-019-0598-7.
(58) Hjalmarsson, N.; Bergendal, E.; Wang, Y.-L.; Munavirov, B.; Wallinder, D.; Glavatskih, S.; Aastrup, T.; Atkin, R.; Furó, I.; Rutland, M. W. Electro-Responsive Surface Composition and Kinetics of an Ionic Liquid in a Polar Oil. *Langmuir* **2019**, *35*, 15692−15700.
(59) Fumino, K.; Wulf, A.; Ludwig, R. Strong, Localized, and Directional Hydrogen Bonds Fluidize Ionic Liquids. *Angew. Chem., Int. Ed.* **2008**, *47*, 8731−8734.
(60) Geronimo, I.; Jiten Singh, N.; Kim, K. S. Nature of Anion-Templated $\pi^+-\pi^+$ Interactions. *Phys. Chem. Chem. Phys.* **2011**, *13*, 11841−11845.
(61) Wang, Y.-L.; Laaksonen, A.; Fayer, M. D. Hydrogen Bonding versus π-π Stacking Interactions in Imidazolium-Oxalatoborate Ionic Liquid. *J. Phys. Chem. B* **2017**, *121*, 7173−7179.
(62) Gao, N.; He, Y.; Tao, X.; Xu, X.-Q.; Wu, X.; Wang, Y. Crystal-Confined Freestanding Ionic Liquids for Reconfigurable and Repairable Electronics. *Nat. Commun.* **2019**, *10*, 547.
(63) Wang, Y.-L.; Laaksonen, A. Interfacial Structure and Orientation of Confined Ionic Liquids on Charged Quartz Surfaces. *Phys. Chem. Chem. Phys.* **2014**, *16*, 23329−23339.
(64) Hu, Z.; Margulis, C. J. Heterogeneity in a Room-Temperature Ionic Liquid: Persistent Local Environments and the Red-Edge Effect. *Proc. Natl. Acad. Sci. U. S. A.* **2006**, *103*, 831−836.
(65) Habasaki, J.; Ngai, K. Heterogeneous Dynamics of Ionic Liquids from Molecular Dynamics Simulations. *J. Chem. Phys.* **2008**, *129*, 194501.
(66) Roy, D.; Patel, N.; Conte, S.; Maroncelli, M. Dynamics in an Idealized Ionic Liquid Model. *J. Phys. Chem. B* **2010**, *114*, 8410−8424.
(67) Karimi-Varzaneh, H. A.; Müller-Plathe, F.; Balasubramanian, S.; Carbone, P. Studying Long-Time Dynamics of Imidazolium-Based Ionic Liquids with a Systematically Coarse-Grained Model. *Phys. Chem. Chem. Phys.* **2010**, *12*, 4714−4724.
(68) Wang, Y.-L.; Zhu, Y.-L.; Lu, Z.-Y.; Laaksonen, A. Electrostatic Interactions in Soft Particle Systems: Mesoscale Simulations of Ionic Liquids. *Soft Matter* **2018**, *14*, 4252−4267.
(69) Hu, Z.; Margulis, C. J. A Study of the Time-Resolved Fluorescence Spectrum and Red Edge Effect of ANF in a Room-Temperature Ionic Liquid. *J. Phys. Chem. B* **2006**, *110*, 11025−11028.
(70) Karmakar, S.; Dasgupta, C.; Sastry, S. Growing Length and Time Scales in Glass-Forming Liquids. *Proc. Natl. Acad. Sci. U. S. A.* **2009**, *106*, 3675−3679.

(71) Kim, J.; Kim, C.; Sung, B. J. Simulation Study of Seemingly Fickian but Heterogeneous Dynamics of Two Dimensional Colloids. *Phys. Rev. Lett.* **2013**, *110*, 047801.
(72) Terranova, Z.; Corcelli, S. Molecular Dynamics Investigation of the Vibrational Spectroscopy of Isolated Water in an Ionic Liquid. *J. Phys. Chem. B* **2014**, *118*, 8264−8272.
(73) Ren, Z.; Brinzer, T.; Dutta, S.; Garrett-Roe, S. Thiocyanate as a Local Probe of Ultrafast Structure and Dynamics in Imidazolium-Based Ionic Liquids: Water-Induced Heterogeneity and Cation-Induced Ion Pairing. *J. Phys. Chem. B* **2015**, *119*, 4699−4712.
(74) Giammanco, C. H.; Kramer, P. L.; Wong, D. B.; Fayer, M. D. Water Dynamics in 1-Alkyl-3-methylimidazolium Tetrafluoroborate Ionic Liquids. *J. Phys. Chem. B* **2016**, *120*, 11523−11538.
(75) Bailey, H. E.; Wang, Y.-L.; Fayer, M. D. Impact of Hydrogen Bonding on the Dynamics and Structure of Protic Ionic Liquid/Water Binary Mixtures. *J. Phys. Chem. B* **2017**, *121*, 8564−8576.
(76) Ridings, C.; Lockett, V.; Andersson, G. Effect of the Aliphatic Chain Length on Electrical Double Layer Formation at the Liquid/Vacuum Interface in the $[C_n mim][BF_4]$ Ionic Liquid Series. *Phys. Chem. Chem. Phys.* **2011**, *13*, 17177−17184.
(77) Stoppa, A.; Hunger, J.; Hefter, G.; Buchner, R. Structure and Dynamics of 1-N-alkyl-3-N-methylimidazolium Tetrafluoroborate +Acetonitrile Mixtures. *J. Phys. Chem. B* **2012**, *116*, 7509−7521.
(78) Gannon, T. J.; Law, G.; Watson, P. R.; Carmichael, A. J.; Seddon, K. R. First Observation of Molecular Composition and Orientation at the Surface of a Room-Temperature Ionic Liquid. *Langmuir* **1999**, *15*, 8429−8434.
(79) Law, G.; Watson, P. R.; Carmichael, A. J.; Seddon, K. R. Molecular Composition and Orientation at Surface of Room-Temperature Ionic Liquids: Effect of Molecular Structure. *Phys. Chem. Chem. Phys.* **2001**, *3*, 2879−2885.
(80) Knorr, A.; Fumino, K.; Bonsa, A.-M.; Ludwig, R. Spectroscopic Evidence of 'Jumping and Pecking'of Cholinium and H-bond Enhanced Cation-Cation Interaction in Ionic Liquids. *Phys. Chem. Chem. Phys.* **2015**, *17*, 30978−30982.
(81) Zaitsau, D. H.; Emel'yanenko, V. N.; Stange, P.; Schick, C.; Verevkin, S. P.; Ludwig, R. Dispersion and Hydrogen Bonding Rule: Why the Vaporization Enthalpies of Aprotic Ionic Liquids are Significantly Larger Than Those of Protic Ionic Liquids. *Angew. Chem., Int. Ed.* **2016**, *55*, 11682−11686.
(82) Umebayashi, Y.; Jiang, J.-C.; Lin, K.-H.; Shan, Y.-L.; Fujii, K.; Seki, S.; Ishiguro, S.-I.; Lin, S. H.; Chang, H.-C. Solvation and Microscopic Properties of Ionic Liquid/Acetonitrile Mixtures Probed by High-Pressure Infrared Spectroscopy. *J. Chem. Phys.* **2009**, *131*, 234502.
(83) Griffin, P. J.; Holt, A. P.; Tsunashima, K.; Sangoro, J. R.; Kremer, F.; Sokolov, A. P. Ion Transport and Structural Dynamics in Homologous Ammonium and Phosphonium-Based Room Temperature Ionic Liquids. *J. Chem. Phys.* **2015**, *142*, 084501.
(84) Aliotta, F.; Ponterio, R. C.; Saija, F.; Salvato, G.; Triolo, A. Excess Ehermodynamic Properties in Mixtures of a Representative Room-Temperature Ionic Liquid and Acetonitrile. *J. Phys. Chem. B* **2007**, *111*, 10202−10207.
(85) Chung, S. H.; Lopato, R.; Greenbaum, S. G.; Shirota, H.; Castner, E. W., Jr.; Wishart, J. F. Nuclear Magnetic Resonance Study of the Dynamics of Imidazolium Ionic Liquids with $CH_2Si(CH_3)_3$ vs $CH_2C(CH_3)_3$ Substituents. *J. Phys. Chem. B* **2007**, *111*, 4885−4893.
(86) Borodin, O.; Gorecki, W.; Smith, G. D.; Armand, M. Molecular Dynamics Simulation and Pulsed-Field Gradient NMR Studies of Bis(fluorosulfonyl)imide (FSI) and Bis[(trifluoromethyl)sulfonyl]-imide (TFSI)-Based Ionic Liquids. *J. Phys. Chem. B* **2010**, *114*, 6786−6798.
(87) Mbondo Tsamba, B. E.; Sarraute, S.; Traïkia, M.; Husson, P. Transport Properties and Ionic Association in Pure Imidazolium-Based Ionic Liquids as a Function of Temperature. *J. Chem. Eng. Data* **2014**, *59*, 1747−1754.
(88) Marekha, B. A.; Kalugin, O. N.; Bria, M.; Idrissi, A. Probing Structural Patterns of Ion Association and Solvation in Mixtures of Imidazolium Ionic Liquids with Acetonitrile by Means of Relative ^1H and ^{13}C NMR Chemical Shifts. *Phys. Chem. Chem. Phys.* **2015**, *17*, 23183−23194.
(89) Lynden-Bell, R. M.; Xue, L.; Tamas, G.; Quitevis, E. L. Local Structure and Intermolecular Dynamics of an Equimolar Benzene and 1,3-Dimethylimidazolium Bis[(trifluoromethane)sulfonyl]amide Mixture: Molecular Dynamics Simulations and OKE Spectroscopic Measurements. *J. Chem. Phys.* **2014**, *141*, 044506.
(90) Sturlaugson, A. L.; Fruchey, K. S.; Fayer, M. D. Orientational Dynamics of Room Temperature Ionic Liquid/Water Mixtures: Water-Induced Structure. *J. Phys. Chem. B* **2012**, *116*, 1777−1787.
(91) Fayer, M. D. Dynamics and Structure of Room Temperature Ionic Liquids. *Chem. Phys. Lett.* **2014**, *616*, 259−274.
(92) Giammanco, C. H.; Kramer, P. L.; Yamada, S. A.; Nishida, J.; Tamimi, A.; Fayer, M. D. Carbon Dioxide in an Ionic Liquid: Structural and Rotational Dynamics. *J. Chem. Phys.* **2016**, *144*, 104506.
(93) Shin, J. Y.; Yamada, S. A.; Fayer, M. D. Influence of Water on Carbon Dioxide and Room Temperature Ionic Liquid Dynamics: Supported Ionic Liquid Membrane vs the Bulk Liquid. *J. Phys. Chem. B* **2018**, *122*, 2389−2395.
(94) Bailey, H. E.; Wang, Y.-L.; Fayer, M. D. The Influence of Hydrophilicity on the Orientational Dynamics and Structures of Imidazolium-Based Ionic Liquid/Water Binary Mixtures. *J. Chem. Phys.* **2018**, *149*, 044501.
(95) Bardak, F.; Xiao, D.; Hines, L. G., Jr; Son, P.; Bartsch, R. A.; Quitevis, E. L.; Yang, P.; Voth, G. A. Nanostructural Organization in Acetonitrile/Ionic Liquid Mixtures: Molecular Dynamics Simulations and Optical Kerr Effect Spectroscopy. *ChemPhysChem* **2012**, *13*, 1687−1700.
(96) Shultz, M. J.; Baldelli, S.; Schnitzer, C.; Simonelli, D. Aqueous Solution/Air Interfaces Probed with Sum Frequency Generation Spectroscopy. *J. Phys. Chem. B* **2002**, *106*, 5313−5324.
(97) Rivera-Rubero, S.; Baldelli, S. Surface Characterization of 1-Butyl-3-methylimidazolium Br^-, I^-, PF_6^-, BF_4^-, $(CF_3SO_2)_2N^-$, SCN^-, $CH_3SO_3^-$, $CH_3SO_4^-$, and $(CN)_2N^-$ Ionic Liquids by Sum Frequency Generation. *J. Phys. Chem. B* **2006**, *110*, 4756−4765.
(98) Peñalber-Johnstone, C.; Adamová, G.; Plechkova, N. V.; Bahrami, M.; Ghaed-Sharaf, T.; Ghatee, M. H.; Seddon, K. R.; Baldelli, S. Sum Frequency Generation Spectroscopy of Tetraalkylphosphonium Ionic Liquids at the Air-Liquid Interface. *J. Chem. Phys.* **2018**, *148*, 193841.
(99) Santos, C. S.; Baldelli, S. Alkyl Chain Interaction at the Surface of Room Temperature Ionic Liquids: Systematic Variation of Alkyl Chain Length (R = C_1−C_4, C_8) in Both Cation and Anion of $[RMIM][ROSO_3]$ by Sum Frequency Generation and Surface Tension. *J. Phys. Chem. B* **2009**, *113*, 923−933.
(100) Martinez, I. S.; Santos, C.; Baldelli, S. Structural Study at the Gas-Liquid Interface of 1-Alkyl-3-methylimidazolium Alkylsulfates Using Surface Potential Measurements. *ChemPhysChem* **2012**, *13*, 1818−1824.
(101) Baldelli, S. Interfacial Structure of Room-Temperature Ionic Liquids at the Solid−Liquid Interface as Probed by Sum Frequency Generation Spectroscopy. *J. Phys. Chem. Lett.* **2013**, *4*, 244−252.
(102) Yan, C.; Thomaz, J. E.; Wang, Y.-L.; Nishida, J.; Yuan, R.; Breen, J. P.; Fayer, M. D. Ultrafast to Ultraslow Dynamics of a Langmuir Monolayer at the Air/Water Interface Observed with Reflection Enhanced 2D IR Spectroscopy. *J. Am. Chem. Soc.* **2017**, *139*, 16518−16527.
(103) Humphreys, E. K.; Allan, P. K.; Welbourn, R. J. L.; Youngs, T. G. A.; Soper, A. K.; Grey, C. P.; Clarke, S. M. A Neutron Diffraction Study of the Electrochemical Double Layer Capacitor Electrolyte Tetrapropylammonium Bromide in Acetonitrile. *J. Phys. Chem. B* **2015**, *119*, 15320−15333.
(104) Niemann, T.; Neumann, J.; Stange, P.; Gärtner, S.; Youngs, T. G.; Paschek, D.; Warr, G. G.; Atkin, R.; Ludwig, R. The Double-Faced Nature of Hydrogen Bonding in Hydroxy-Functionalized Ionic Liquids Shown by Neutron Diffraction and Molecular Dynamics Simulations. *Angew. Chem., Int. Ed.* **2019**, *58*, 12887−12892.

https://dx.doi.org/10.1021/acs.chemrev.9b00693
Chem. Rev. 2020, 120, 5798−5877

(105) Daillant, J.; Gibaud, A. *X-ray and Neutron Reflectivity: Principles and Applications*; Springer-Verlag: Berlin-Heidelberg, 2008.
(106) Mars, J.; Hou, B.; Weiss, H.; Li, H.; Konovalov, O.; Festersen, S.; Murphy, B. M.; Rütt, U.; Bier, M.; Mezger, M. Surface Induced Smectic Order in Ionic Liquids − An X-ray Reflectivity Study of $[C_{22}C_1im][NTf_2]$. *Phys. Chem. Chem. Phys.* **2017**, *19*, 26651−26661.
(107) Griffin, L. R.; Browning, K. L.; Clarke, S. M.; Smith, A. M.; Perkin, S.; Skoda, M.; Norman, S. E. Direct Measurements of Ionic Liquid Layering at a Single Mica-Liquid Interface and in Nano-Films Between Two Mica-Liquid Interfaces. *Phys. Chem. Chem. Phys.* **2017**, *19*, 297−304.
(108) Atkin, R.; Warr, G. G. The Smallest Amphiphiles: Nanostructure in Protic Room-Temperature Ionic Liquids with Short Alkyl Groups. *J. Phys. Chem. B* **2008**, *112*, 4164−4166.
(109) Abe, H.; Takekiyo, T.; Shigemi, M.; Yoshimura, Y.; Tsuge, S.; Hanasaki, T.; Ohishi, K.; Takata, S.; Suzuki, J.-I. Direct Evidence of Confined Water in Room-Temperature Ionic Liquids by Complementary Use of Small-Angle X-ray and Neutron Scattering. *J. Phys. Chem. Lett.* **2014**, *5*, 1175−1180.
(110) Migliorati, V.; Zitolo, A.; D'Angelo, P. Using a Combined Theoretical and Experimental Approach to Understand the Structure and Dynamics of Imidazolium-Based Ionic Liquids/Water Mixtures. 1. MD Simulations. *J. Phys. Chem. B* **2013**, *117*, 12505−12515.
(111) Gao, J.; Wagner, N. J. Water Nanocluster Formation in the Ionic Liquid 1-Butyl-3-methylimidazolium Tetrafluoroborate $([C_4mim][BF_4])$−D_2O Mixtures. *Langmuir* **2016**, *32*, 5078−5084.
(112) Bier, M.; Mars, J.; Li, H.; Mezger, M. Salt-Induced Microheterogeneities in Binary Liquid Mixtures. *Phys. Rev. E: Stat. Phys., Plasmas, Fluids, Relat. Interdiscip. Top.* **2017**, *96*, 022603.
(113) Cabry, C. P.; D'Andrea, L.; Shimizu, K.; Grillo, I.; Li, P.; Rogers, S.; Bruce, D. W.; Canongia Lopes, J. N.; Slattery, J. M. Exploring the Bulk-Phase Structure of Ionic Liquid Mixtures Using Small-Angle Neutron Scattering. *Faraday Discuss.* **2018**, *206*, 265−289.
(114) Blundell, R. K.; Licence, P. Quaternary Ammonium and Phosphonium Based Ionic Liquids: A Comparison of Common Anions. *Phys. Chem. Chem. Phys.* **2014**, *16*, 15278−15288.
(115) Lovelock, K.; Kolbeck, C.; Cremer, T.; Paape, N.; Schulz, P.; Wasserscheid, P.; Maier, F.; Steinruck, H.-P. Influence of Different Substituents on the Surface Composition of Ionic Liquids Studied Using ARXPS. *J. Phys. Chem. B* **2009**, *113*, 2854−2864.
(116) Olschewski, M.; Gustus, R.; Höfft, O.; Lahiri, A.; Endres, F. Monochromatic X-ray Photoelectron Spectroscopy Study of Three Different Ionic Liquids in Interaction with Lithium-Decorated Copper Surfaces. *J. Phys. Chem. C* **2017**, *121*, 2675−2682.
(117) Jeon, Y.; Vaknin, D.; Bu, W.; Sung, J.; Ouchi, Y.; Sung, W.; Kim, D. Surface Nanocrystallization of an Ionic Liquid. *Phys. Rev. Lett.* **2012**, *108*, 055502.
(118) Campetella, M.; Mariani, A.; Sadun, C.; Wu, B.; Castner, E. W., Jr; Gontrani, L. Structure and Dynamics of Propylammonium Nitrate-Acetonitrile Mixtures: An Intricate Multi-Scale System Probed with Experimental and Theoretical Techniques. *J. Chem. Phys.* **2018**, *148*, 134507.
(119) Niga, P.; Wakeham, D.; Nelson, A.; Warr, G. G.; Rutland, M.; Atkin, R. Structure of Ethylammonium Nitrate Surface: An X-ray Reflectivity and Vibrational Sum Frequency Spectroscopy Study. *Langmuir* **2010**, *26*, 8282−8288.
(120) Uysal, A.; Zhou, H.; Feng, G.; Lee, S. S.; Li, S.; Fenter, P.; Cummings, P. T.; Fulvio, P. F.; Dai, S.; McDonough, J. K.; Gogotsi, Y. Structural Origins of Potential Dependent Hysteresis at the Electrified Graphene/Ionic Liquid Interface. *J. Phys. Chem. C* **2014**, *118*, 569−574.
(121) Mezger, M.; Schroder, H.; Reichert, H.; Schramm, S.; Okasinski, J. S.; Schoder, S.; Honkimaki, V.; Deutsch, M.; Ocko, B. M.; Ralston, J.; Rohwerder, M.; Stratmann, M.; Dosch, H. Molecular Layering of Fluorinated Ionic Liquids at a Charged Sapphire(0001) Surface. *Science* **2008**, *322*, 424−428.
(122) Tamam, L.; Ocko, B.; Reichert, H.; Deutsch, M. Checkerboard Self-Patterning of an Ionic Liquid Film on Mercury. *Phys. Rev. Lett.* **2011**, *106*, 197801.
(123) Nemoto, F.; Kofu, M.; Nagao, M.; Ohishi, K.; Takata, S.-i.; Suzuki, J.-i.; Yamada, T.; Shibata, K.; Ueki, T.; Kitazawa, Y.; Watanabe, M.; Yamamuro, O. Neutron Scattering Studies on Short- and Long-Range Layer Structures and Related Dynamics in Imidazolium-Based Ionic Liquids. *J. Chem. Phys.* **2018**, *149*, 054502.
(124) Zhou, H.; Rouha, M.; Feng, G.; Lee, S. S.; Docherty, H.; Fenter, P.; Cummings, P. T.; Fulvio, P. F.; Dai, S.; McDonough, J.; Presser, V.; Gogotsi, Y. Nanoscale Perturbations of Room Temperature Ionic Liquid Structure at Charged and Uncharged Interfaces. *ACS Nano* **2012**, *6*, 9818−9827.
(125) Tomita, K.; Mizukami, M.; Nakano, S.; Ohta, N.; Yagi, N.; Kurihara, K. X-ray Diffraction and Resonance Shear Measurement of Nano-Confined Ionic Liquids. *Phys. Chem. Chem. Phys.* **2018**, *20*, 13714−13721.
(126) Triolo, A.; Russina, O.; Fazio, B.; Appetecchi, G. B.; Carewska, M.; Passerini, S. Nanoscale Organization in Piperidinium-Based Room Temperature Ionic Liquids. *J. Chem. Phys.* **2009**, *130*, 164521.
(127) Hoffmann, V.; Lahiri, A.; Borisenko, N.; Carstens, T.; Pulletikurthi, G.; Borodin, A.; Atkin, R.; Endres, F. Nanostructure of the H-Terminated p-Si(111)/Ionic Liquid Interface and the Effect of Added Lithium Salt. *Phys. Chem. Chem. Phys.* **2017**, *19*, 54−58.
(128) Bovio, S.; Podesta, A.; Lenardi, C.; Milani, P. Evidence of Extended Solidlike Layering in $[Bmim][NTf_2]$ Ionic Liquid Thin Films at Room-Temperature. *J. Phys. Chem. B* **2009**, *113*, 6600−6603.
(129) Atkin, R.; Warr, G. G. Structure in Confined Room-Temperature Ionic Liquids. *J. Phys. Chem. C* **2007**, *111*, 5162−5168.
(130) Werzer, O.; Cranston, E. D.; Warr, G. G.; Atkin, R.; Rutland, M. W. Ionic Liquid Nanotribology: Mica-Silica Interactions in Ethylammonium Nitrate. *Phys. Chem. Chem. Phys.* **2012**, *14*, 5147−5152.
(131) Müller, C.; Németh, K.; Vesztergom, S.; Pajkossy, T.; Jacob, T. The Interface Between HOPG and 1-Butyl-3-methyl-imidazolium Hexafluorophosphate. *Phys. Chem. Chem. Phys.* **2016**, *18*, 916−925.
(132) Wen, R.; Rahn, B.; Magnussen, O. M. Potential-Dependent Adlayer Structure and Dynamics at the Ionic Liquid/Au (111) Interface: A Molecular-Scale in situ Video-STM Study. *Angew. Chem., Int. Ed.* **2015**, *54*, 6062−6066.
(133) Merlet, C.; Limmer, D. T.; Salanne, M.; van Roij, R.; Madden, P. A.; Chandler, D.; Rotenberg, B. The Electric Double Layer Has a Life of Its Own. *J. Phys. Chem. C* **2014**, *118*, 18291−18298.
(134) Su, Y. Z.; Fu, Y. C.; Yan, J. W.; Chen, Z. B.; Mao, B. W. Double Layer of Au(100)/Ionic Liquid Interface and Its Stability in Imidazolium-Based Ionic Liquids. *Angew. Chem., Int. Ed.* **2009**, *48*, 5148−5151.
(135) Gebbie, M. A.; Valtiner, M.; Banquy, X.; Fox, E. T.; Henderson, W. A.; Israelachvili, J. N. Ionic Liquids Behave as Dilute Electrolyte Solutions. *Proc. Natl. Acad. Sci. U. S. A.* **2013**, *110*, 9674−9679.
(136) Gebbie, M. A.; Valtiner, M.; Banquy, X.; Henderson, W. A.; Israelachvili, J. N. Experimental Observations Demonstrate that Ionic Liquids Form Both Bound (Stern) and Diffuse Electric Double Layers. *Proc. Natl. Acad. Sci. U. S. A.* **2013**, *110*, E4122.
(137) Perkin, S.; Crowhurst, L.; Niedermeyer, H.; Welton, T.; Smith, A. M.; Gosvami, N. N. Self-Assembly in the Electrical Double Layer of Ionic Liquids. *Chem. Commun.* **2011**, *47*, 6572−6574.
(138) Dragoni, D.; Manini, N.; Ballone, P. Interfacial Layering of a Room-Temperature Ionic Liquid Thin Film on Mica: A Computational Investigation. *ChemPhysChem* **2012**, *13*, 1772−1780.
(139) Lhermerout, R.; Perkin, S. Nanoconfined Ionic Liquids: Disentangling Electrostatic and Viscous Forces. *Phys. Rev. Fluids* **2018**, *3*, 014201.
(140) Smith, A. M.; Perkin, S. Influence of Lithium Solutes on Double-Layer Structure of Ionic Liquids. *J. Phys. Chem. Lett.* **2015**, *6*, 4857−4861.

https://dx.doi.org/10.1021/acs.chemrev.9b00693
Chem. Rev. 2020, 120, 5798−5877

(141) Sturlaugson, A. L.; Arima, A. Y.; Bailey, H. E.; Fayer, M. D. Orientational Dynamics in a Lyotropic Room Temperature Ionic Liquid. *J. Phys. Chem. B* **2013**, *117*, 14775−14784.
(142) Zahn, S.; Stark, A. Order in the Chaos: The Secret of the Large Negative Entropy of Dissolving 1-Alkyl-3-methylimidazolium Chloride in Trihexyltetradecylphosphonium Chloride. *Phys. Chem. Chem. Phys.* **2015**, *17*, 4034−4037.
(143) Wang, Y.-L.; Sarman, S.; Li, B.; Laaksonen, A. Multiscale Modeling of the Trihexyltetradecylphosphonium Chloride Ionic Liquid. *Phys. Chem. Chem. Phys.* **2015**, *17*, 22125−22135.
(144) Thompson, D.; Coleman, S.; Diamond, D.; Byrne, R. Electronic Structure Calculations and Physicochemical Experiments Quantify the Competitive Liquid Ion Association and Probe Stabilisation Effects for Nitrobenzospiropyran in Phosphonium-Based Ionic Liquids. *Phys. Chem. Chem. Phys.* **2011**, *13*, 6156−6168.
(145) Yu, C.-J.; Ri, U.-S.; Ri, G.-C.; Kim, J.-S. Revealing the Formation and Electrochemical Properties of Bis-(trifluoromethanesulfonyl)imide Intercalated Graphite with *First-Principles* Calculations. *Phys. Chem. Chem. Phys.* **2018**, *20*, 14124−14132.
(146) Atilhan, M.; Aparicio, S. Theoretical Study of Low Viscous Ionic Liquids at the Graphene Interface. *J. Phys. Chem. C* **2018**, *122*, 1645−1656.
(147) Pensado, A. S.; Malberg, F.; Gomes, M. F. C.; Pádua, A. A. H.; Fernández, J.; Kirchner, B. Interactions and Structure of Ionic Liquids on Graphene and Carbon Nanotubes Surfaces. *RSC Adv.* **2014**, *4*, 18017−18024.
(148) Li, H.; Atkin, R.; Page, A. J. Combined Friction Force Microscopy and Quantum Chemical Investigation of Tribotronic Response at Propylammonium Nitrate-Graphite Interface. *Phys. Chem. Chem. Phys.* **2015**, *17*, 16047−16052.
(149) Matthews, R. P.; Welton, T.; Hunt, P. A. Competitive π Interactions and Hydrogen Bonding within Imidazolium Ionic Liquids. *Phys. Chem. Chem. Phys.* **2014**, *16*, 3238−3253.
(150) Dong, D.; Hooper, J. B.; Bedrov, D. Structural and Dynamical Properties of Tetraalkylammonium Bromide Aqueous Solutions: A Molecular Dynamics Simulation Study Using a Polarizable Force Field. *J. Phys. Chem. B* **2017**, *121*, 4853−4863.
(151) Voss, J. M.; Marsh, B. M.; Zhou, J.; Garand, E. Interaction Between Ionic Liquid Cation and Water: Infrared Predissociation Study of $[bmim]^+(H_2O)_n$ Clusters. *Phys. Chem. Chem. Phys.* **2016**, *18*, 18905−18913.
(152) Dias, N.; Shimizu, K.; Morgado, P.; Filipe, E. J.; Canongia Lopes, J. N.; Vaca Chávez, F. N. Charge Templates in Aromatic Plus Ionic Liquid Systems Revisited: NMR Experiments and Molecular Dynamics Simulations. *J. Phys. Chem. B* **2014**, *118*, 5772−5780.
(153) Weber, H.; Kirchner, B. Complex Structural and Dynamical Interplay of Cyano-Based Ionic Liquids. *J. Phys. Chem. B* **2016**, *120*, 2471−2483.
(154) Zahn, S.; Wendler, K.; Delle Site, L.; Kirchner, B. Depolarization of Water in Protic Ionic Liquids. *Phys. Chem. Chem. Phys.* **2011**, *13*, 15083−15093.
(155) Annapureddy, H. V.; Kashyap, H. K.; De Biase, P. M.; Margulis, C. J. What is the Origin of the Prepeak in the X-ray Scattering of Imidazolium-Based Room-Temperature Ionic Liquids? *J. Phys. Chem. B* **2010**, *114*, 16838−16846.
(156) Sha, M.; Liu, Y.; Dong, H.; Luo, F.; Jiang, F.; Tang, Z.; Zhu, G.; Wu, G. Origin of Heterogeneous Dynamics in Local Molecular Structures of Ionic Liquids. *Soft Matter* **2016**, *12*, 8942−8949.
(157) Liu, H.; Maginn, E. A Molecular Dynamics Investigation of the Structural and Dynamic Properties of the Ionic Liquid 1-n-Butyl-3-methylimidazolium Bis(trifluoromethanesulfonyl)imide. *J. Chem. Phys.* **2011**, *135*, 124507.
(158) Kowsari, M.; Alavi, S.; Ashrafizaadeh, M.; Najafi, B. Molecular Dynamics Simulation of Imidazolium-Based Ionic Liquids. II. Transport Coefficients. *J. Chem. Phys.* **2009**, *130*, 014703.
(159) Price, D. L.; Borodin, O.; González, M. A.; Kofu, M.; Shibata, K.; Yamada, T.; Yamamuro, O.; Saboungi, M.-L. Relaxation in a Prototype Ionic Liquid: Influence of Water on Dynamics. *J. Phys. Chem. Lett.* **2017**, *8*, 715−719.
(160) D'Angelo, P.; Zitolo, A.; Aquilanti, G.; Migliorati, V. Using a Combined Theoretical and Experimental Approach to Understand the Structure and Dynamics of Imidazolium-Based Ionic Liquids/Water Mixtures. 2. EXAFS Spectroscopy. *J. Phys. Chem. B* **2013**, *117*, 12516−12524.
(161) Moreno, M.; Castiglione, F.; Mele, A.; Pasqui, C.; Raos, G. Interaction of Water with the Model Ionic Liquid $[Bmim][BF_4]$: Molecular Dynamics Simulations and Comparison with NMR Data. *J. Phys. Chem. B* **2008**, *112*, 7826−7836.
(162) Mariani, A.; Caminiti, R.; Gontrani, L. Water and Hexane in an Ionic Liquid: Computational Evidence of Association Under High Pressure. *Phys. Chem. Chem. Phys.* **2017**, *19*, 8661−8666.
(163) Yaghini, N.; Gómez-González, V.; Varela, L. M.; Martinelli, A. Structural Origin of Proton Mobility in a Protic Ionic Liquid/Imidazole Mixture: Insights From Computational and Experimental Results. *Phys. Chem. Chem. Phys.* **2016**, *18*, 23195−23206.
(164) Wang, Y.-L.; Shah, F. U.; Glavatskih, S.; Antzutkin, O. N.; Laaksonen, A. Atomistic Insight into Orthoborate-Based Ionic Liquids: Force Field Development and Evaluation. *J. Phys. Chem. B* **2014**, *118*, 8711−8723.
(165) Spickermann, C.; Thar, J.; Lehmann, S.; Zahn, S.; Hunger, J.; Buchner, R.; Hunt, P.; Welton, T.; Kirchner, B. Why Are Ionic Liquid Ions Mainly Associated in Water? A Car-Parrinello Study of 1-Ethyl-3-methyl-imidazolium Chloride Water Mixture. *J. Chem. Phys.* **2008**, *129*, 104505.
(166) Brehm, M.; Weber, H.; Pensado, A. S.; Stark, A.; Kirchner, B. Proton Transfer and Polarity Changes in Ionic Liquid-Water Mixtures: A Perspective on Hydrogen Bonds from *ab Initio* Molecular Dynamics at the Example of 1-Ethyl-3-methylimidazolium Acetate−Water Mixtures—Part 1. *Phys. Chem. Chem. Phys.* **2012**, *14*, 5030−5044.
(167) Bhargava, B.; Klein, M. L. Formation of Interconnected Aggregates in Aqueous Dicationic Ionic Liquid Solutions. *J. Chem. Theory Comput.* **2010**, *6*, 873−879.
(168) Liu, X.; Zhou, G.; Huo, F.; Wang, J.; Zhang, S. Unilamellar Vesicle Formation and Microscopic Structure of Ionic Liquids in Aqueous Solutions. *J. Phys. Chem. C* **2016**, *120*, 659−667.
(169) Heid, E.; Docampo-Álvarez, B.; Varela, L. M.; Prosenz, K.; Steinhauser, O.; Schröder, C. Langevin Behavior of the Dielectric Decrement in Ionic Liquid Water Mixtures. *Phys. Chem. Chem. Phys.* **2018**, *20*, 15106−15117.
(170) Kobayashi, T.; Reid, J. E.; Shimizu, S.; Fyta, M.; Smiatek, J. The Properties of Residual Water Molecules in Ionic Liquids: A Comparison Between Direct and Inverse Kirkwood−Buff Approaches. *Phys. Chem. Chem. Phys.* **2017**, *19*, 18924−18937.
(171) Wu, Y.; Wang, X.; Liu, Q.; Ma, X.; Fang, D.; Jiang, X.; Guan, W. Dynamic Phase Change and Local Structures in IL-Containing Mixtures: Classical MD Simulations and Experiments. *Phys. Chem. Chem. Phys.* **2017**, *19*, 3028−3038.
(172) Borodin, O.; Price, D. L.; Aoun, B.; González, M. A.; Hooper, J. B.; Kofu, M.; Kohara, S.; Yamamuro, O.; Saboungi, M.-L. Effect of Water on the Structure of a Prototype Ionic Liquid. *Phys. Chem. Chem. Phys.* **2016**, *18*, 23474−23481.
(173) Sha, M.; Dong, H.; Luo, F.; Tang, Z.; Zhu, G.; Wu, G. Dilute or Concentrated Electrolyte Solutions? Insight From Ionic Liquid/Water Electrolytes. *J. Phys. Chem. Lett.* **2015**, *6*, 3713−3720.
(174) Méndez-Morales, T.; Carrete, J.; Cabeza, O.; Gallego, L. J.; Varela, L. M. Molecular Dynamics Simulation of the Structure and Dynamics of Water-1-Alkyl-3-methylimidazolium Ionic Liquid Mixtures. *J. Phys. Chem. B* **2011**, *115*, 6995−7008.
(175) Annapureddy, H. V.; Dang, L. X. Pairing Mechanism Among Ionic Liquid Ions in Aqueous Solutions: A Molecular Dynamics Study. *J. Phys. Chem. B* **2013**, *117*, 8555−8560.
(176) Hegde, G. A.; Bharadwaj, V. S.; Kinsinger, C. L.; Schutt, T. C.; Pisierra, N. R.; Maupin, C. M. Impact of Water Dilution and Cation Tail Length on Ionic Liquid Characteristics: Interplay Between Polar and Non-polar Interactions. *J. Chem. Phys.* **2016**, *145*, 064504.

https://dx.doi.org/10.1021/acs.chemrev.9b00693
Chem. Rev. 2020, 120, 5798−5877

(177) Bernardes, C. E.; Minas da Piedade, M. E.; Canongia Lopes, J. N. The Structure of Aqueous Solutions of a Hydrophilic Ionic Liquid: The Full Concentration Range of 1-Ethyl-3-methylimidazolium Ethylsulfate and Water. *J. Phys. Chem. B* **2011**, *115*, 2067−2074.
(178) Martins, V. L.; Nicolau, B. G.; Urahata, S. M.; Ribeiro, M. C.; Torresi, R. M. Influence of the Water Content on the Structure and Physicochemical Properties of an Ionic Liquid and Its Li^+ Mixture. *J. Phys. Chem. B* **2013**, *117*, 8782−8792.
(179) Pal, T.; Biswas, R. Composition Dependence of Dynamic Heterogeneity Time- and Length Scales in [Omim][BF_4]/Water Binary Mixtures: Molecular Dynamics Simulation Study. *J. Phys. Chem. B* **2015**, *119*, 15683−15695.
(180) Sharma, A.; Ghorai, P. K. Effect of Water on Structure and Dynamics of [BMIM][PF_6] Ionic Liquid: An All-Atom Molecular Dynamics Simulation Investigation. *J. Chem. Phys.* **2016**, *144*, 114505.
(181) Feng, G.; Jiang, D.-E.; Cummings, P. T. Curvature Effect on the Capacitance of Electric Double Layers at Ionic Liquid/Onion-Like Carbon Interfaces. *J. Chem. Theory Comput.* **2012**, *8*, 1058−1063.
(182) Richey, F. W.; Dyatkin, B.; Gogotsi, Y.; Elabd, Y. A. Ion Dynamics in Porous Carbon Electrodes in Supercapacitors Using in situ Infrared Spectroelectrochemistry. *J. Am. Chem. Soc.* **2013**, *135*, 12818−12826.
(183) Deschamps, M.; Gilbert, E.; Azais, P.; Raymundo-Piñero, E.; Ammar, M. R.; Simon, P.; Massiot, D.; Béguin, F. Exploring Electrolyte Organization in Supercapacitor Electrodes with Solid-State NMR. *Nat. Mater.* **2013**, *12*, 351−358.
(184) Saielli, G.; Bagno, A.; Wang, Y. Insights on the Isotropic-to-Smectic a Transition in Ionic Liquid Crystals from Coarse-Grained Molecular Dynamics Simulations: The Role of Microphase Segregation. *J. Phys. Chem. B* **2015**, *119*, 3829−3836.
(185) Wang, Y.-L.; Lyubartsev, A.; Lu, Z.-Y.; Laaksonen, A. Multiscale Coarse-Grained Simulations of Ionic Liquids: Comparison of Three Approaches to Derive Effective Potentials. *Phys. Chem. Chem. Phys.* **2013**, *15*, 7701−7712.
(186) Bodo, E.; Postorino, P.; Mangialardo, S.; Piacente, G.; Ramondo, F.; Bosi, F.; Ballirano, P.; Caminiti, R. Structure of the Molten Salt Methylammonium Nitrate Explored by Experiments and Theory. *J. Phys. Chem. B* **2011**, *115*, 13149−13161.
(187) Zahn, S.; Thar, J.; Kirchner, B. Structure and Dynamics of the Protic Ionic Liquid Monomethylammonium Nitrate ([CH_3NH_3]-[NO_3]) from *ab Initio* Molecular Dynamics Simulations. *J. Chem. Phys.* **2010**, *132*, 124506.
(188) Bodo, E.; Mangialardo, S.; Ramondo, F.; Ceccacci, F.; Postorino, P. Unravelling the Structure of Protic Ionic Liquids with Theoretical and Experimental Methods: Ethyl-, Propyl- and Butylammonium Nitrate Explored by Raman Spectroscopy and DFT Calculations. *J. Phys. Chem. B* **2012**, *116*, 13878−13888.
(189) Umebayashi, Y.; Chung, W.-L.; Mitsugi, T.; Fukuda, S.; Takeuchi, M.; Fujii, K.; Takamuku, T.; Kanzaki, R.; Ishiguro, S.-I. Liquid Structure and the Ion-Ion Interactions of Ethylammonium Nitrate Ionic Liquid Studied by Large Angle X-ray Scattering and Molecular Dynamics Simulations. *J. Comput. Chem., Jpn.* **2008**, *7*, 125−134.
(190) Hayes, R.; Imberti, S.; Warr, G. G.; Atkin, R. Effect of Cation Alkyl Chain Length and Anion Type on Protic Ionic Liquid Nanostructure. *J. Phys. Chem. C* **2014**, *118*, 13998−14008.
(191) Greaves, T. L.; Kennedy, D. F.; Kirby, N.; Drummond, C. J. Nanostructure Changes in Protic Ionic Liquids (PILs) Through Adding Solutes and Mixing PILs. *Phys. Chem. Chem. Phys.* **2011**, *13*, 13501−13509.
(192) Campetella, M.; Macchiagodena, M.; Gontrani, L.; Kirchner, B. Effect of Alkyl Chain Length in Protic Ionic Liquids: An AIMD Perspective. *Mol. Phys.* **2017**, *115*, 1582−1589.
(193) Usui, K.; Hunger, J.; Bonn, M.; Sulpizi, M. Dynamical Heterogeneities of Rotational Motion in Room Temperature Ionic Liquids Evidenced by Molecular Dynamics Simulations. *J. Chem. Phys.* **2018**, *148*, 193811.
(194) Jiang, H. J.; FitzGerald, P. A.; Dolan, A.; Atkin, R.; Warr, G. G. Amphiphilic Self-Assembly of Alkanols in Protic Ionic Liquids. *J. Phys. Chem. B* **2014**, *118*, 9983−9990.
(195) Mariani, A.; Caminiti, R.; Campetella, M.; Gontrani, L. Pressure-Induced Mesoscopic Disorder in Protic Ionic Liquids: First Computational Study. *Phys. Chem. Chem. Phys.* **2016**, *18*, 2297−2302.
(196) Henderson, W. A.; Fylstra, P.; De Long, H. C.; Trulove, P. C.; Parsons, S. Crystal Structure of the Ionic Liquid $EtNH_3NO_3$—Insights into the Thermal Phase Behavior of Protic Ionic Liquids. *Phys. Chem. Chem. Phys.* **2012**, *14*, 16041−16046.
(197) Gordon, C. M.; Holbrey, J. D.; Kennedy, A. R.; Seddon, K. R. Ionic Liquid Crystals: Hexafluorophosphate Salts. *J. Mater. Chem.* **1998**, *8*, 2627−2636.
(198) Faria, L. F.; Penna, T. C.; Ribeiro, M. C. Raman Spectroscopic Study of Temperature and Pressure Effects on the Ionic Liquid Propylammonium Nitrate. *J. Phys. Chem. B* **2013**, *117*, 10905−10912.
(199) Migliorati, V.; Ballirano, P.; Gontrani, L.; Triolo, A.; Caminiti, R. Thermal and Structural Properties of Ethylammonium Chloride and Its Mixture with Water. *J. Phys. Chem. B* **2011**, *115*, 4887−4899.
(200) King, M. V.; Lipscomb, W. The Low-Temperature Modification of n-Propyl-ammonium Chloride. *Acta Crystallogr.* **1950**, *3*, 227−230.
(201) Migliorati, V.; Ballirano, P.; Gontrani, L.; Russina, O.; Caminiti, R. Crystal Polymorphism of Propylammonium Chloride and Structural Properties of Its Mixture with Water. *J. Phys. Chem. B* **2011**, *115*, 11805−11815.
(202) Matsumoto, K.; Hagiwara, R.; Yoshida, R.; Ito, Y.; Mazej, Z.; Benkič, P.; Žemva, B.; Tamada, O.; Yoshino, H.; Matsubara, S. Syntheses, Structures and Properties of 1-Ethyl-3-methylimidazolium Salts of Fluorocomplex Anions. *Dalton Trans* **2004**, 144−149.
(203) Dymek, C.J.; Grossie, D. A.; Fratini, A. V.; Wade Adams, W. Evidence for the Presence of Hydrogen-Bonded Ion-Ion Interactions in the Molten Salt Precursor, 1-Methyl-3-ethylimidazolium Chloride. *J. Mol. Struct.* **1989**, *213*, 25−34.
(204) Elaiwi, A.; Hitchcock, P. B.; Seddon, K. R.; Srinivasan, N.; Tan, Y.-M.; Welton, T.; Zora, J. A. Hydrogen Bonding in Imidazolium Salts and Its Implications for Ambient-Temperature Halogenoaluminate(III) Ionic Liquids. *J. Chem. Soc., Dalton Trans.* **1995**, 3467−3472.
(205) Matsumoto, K.; Hagiwara, R.; Mazej, Z.; Benkič, P.; Žemva, B. Crystal Structures of Frozen Room Temperature Ionic Liquids, 1-Ethyl-3-methylimidazolium Tetrafluoroborate (EMImBF_4), Hexafluoroniobate (EMImNbF_6) and Hexafluorotantalate (EMImTaF_6), Determined by Low-Temperature X-ray Diffraction. *Solid State Sci.* **2006**, *8*, 1250−1257.
(206) Hamaguchi, H.-O.; Saha, S.; Ozawa, R.; Hayashi, S. Raman and X-ray Studies on the Structure of [Bmim]X (X = Cl, Br, I, [BF_4], [PF_6]): Rotational Isomerism of the $[Bmim]^+$ Cation. *ACS Symp. Ser.* **2005**, Chapter 5, *90*168−78.
(207) Berg, R. W.; Deetlefs, M.; Seddon, K. R.; Shim, I.; Thompson, J. M. Raman and *ab Initio* Studies of Simple and Binary 1-Alkyl-3-methylimidazolium Ionic Liquids. *J. Phys. Chem. B* **2005**, *109*, 19018−19025.
(208) Ozawa, R.; Hayashi, S.; Saha, S.; Kobayashi, A.; Hamaguchi, H.-O. Rotational Isomerism and Structure of the 1-Butyl-3-methylimidazolium Cation in the Ionic Liquid State. *Chem. Lett.* **2003**, *32*, 948−949.
(209) Hayashi, S.; Ozawa, R.; Hamaguchi, H.-O. Raman Spectra, Crystal Polymorphism, and Structure of a Prototype Ionic-Liquid [BMIM]Cl. *Chem. Lett.* **2003**, *32*, 498−499.
(210) Tschierske, C. Molecular Self-Organization of Amphotropic Liquid Crystals. *Prog. Polym. Sci.* **1996**, *21*, 775−852.
(211) Bradley, A.; Hardacre, C.; Holbrey, J.; Johnston, S.; McMath, S.; Nieuwenhuyzen, M. Small-Angle X-ray Scattering Studies of Liquid Crystalline 1-Alkyl-3-methylimidazolium Salts. *Chem. Mater.* **2002**, *14*, 629−635.
(212) Faria, L. F.; Matos, J. R.; Ribeiro, M. C. Thermal Analysis and Raman Spectra of Different Phases of the Ionic Liquid Butyltrime-

https://dx.doi.org/10.1021/acs.chemrev.9b00693
Chem. Rev. 2020, 120, 5798−5877

thylammonium Bis(trifluoromethylsulfonyl)imide. *J. Phys. Chem. B* **2012**, *116*, 9238−9245.
(213) Holbrey, J. D.; Reichert, W. M.; Rogers, R. D. Crystal Structures of Imidazolium Bis(trifluoromethanesulfonyl)imide Ionic Liquid Salts: The First Organic Salt with a *cis*-TFSI Anion Conformation. *Dalton Trans* **2004**, 2267−2271.
(214) Dhumal, N. R.; Noack, K.; Kiefer, J.; Kim, H. J. Molecular Structure and Interactions in the Ionic Liquid 1-Ethyl-3-Methylimidazolium Bis(trifluoromethylsulfonyl)imide. *J. Phys. Chem. A* **2014**, *118*, 2547−2557.
(215) Kohagen, M.; Brehm, M.; Lingscheid, Y.; Giernoth, R.; Sangoro, J.; Kremer, F.; Naumov, S.; Iacob, C.; Karger, J.; Valiullin, R.; Kirchner, B. How Hydrogen Bonds Influence the Mobility of Imidazolium-Based Ionic Liquids. A Combined Theoretical and Experimental Study of 1-n-Butyl-3-methylimidazolium Bromide. *J. Phys. Chem. B* **2011**, *115*, 15280−15288.
(216) Sun, Q.; Harvey, J. A.; Greco, K. V.; Auerbach, S. M. Molecular Simulations of Hydrogen Bond Cluster Size and Reorientation Dynamics in Liquid and Glassy Azole Systems. *J. Phys. Chem. B* **2016**, *120*, 10411−10419.
(217) Wang, Y.-L. Competitive Microstructures vs. Cooperative Dynamics of Hydrogen Bonding and π Type Stacking Interactions in Imidazolium Bis(oxalato)borate Ionic Liquids. *J. Phys. Chem. B* **2018**, *122*, 6570−6585.
(218) Fumino, K.; Reimann, S.; Ludwig, R. Probing Molecular Interaction in Ionic Liquids by Low Frequency Spectroscopy: Coulomb Energy, Hydrogen Bonding and Dispersion Forces. *Phys. Chem. Chem. Phys.* **2014**, *16*, 21903−21929.
(219) Strate, A.; Neumann, J.; Overbeck, V.; Bonsa, A.-M.; Michalik, D.; Paschek, D.; Ludwig, R. Rotational and Translational Dynamics and Their Relation to Hydrogen Bond Lifetimes in an Ionic Liquid by Means of NMR Relaxation Time Experiments and Molecular Dynamics Simulation. *J. Chem. Phys.* **2018**, *148*, 193843.
(220) Keaveney, S. T.; Greaves, T. L.; Kennedy, D. F.; Harper, J. B. Understanding the Effect of Solvent Structure on Organic Reaction Outcomes When Using Ionic Liquid/Acetonitrile Mixtures. *J. Phys. Chem. B* **2016**, *120*, 12687−12699.
(221) Hunt, P. A. Why Does a Reduction in Hydrogen Bonding Lead to an Increase in Viscosity for the 1-Butyl-2,3-dimethylimidazolium Based Ionic Liquids? *J. Phys. Chem. B* **2007**, *111*, 4844−4853.
(222) Wulf, A.; Fumino, K.; Ludwig, R. Spectroscopic Evidence for an Enhanced Anion-Cation Interaction From Hydrogen Bonding in Pure Imidazolium Ionic Liquids. *Angew. Chem., Int. Ed.* **2010**, *49*, 449−453.
(223) Fumino, K.; Peppel, T.; Geppert-Rybczyńska, M.; Zaitsau, D. H.; Lehmann, J. K.; Verevkin, S. P.; Köckerling, M.; Ludwig, R. The Influence of Hydrogen Bonding on the Physical Properties of Ionic Liquids. *Phys. Chem. Chem. Phys.* **2011**, *13*, 14064−14075.
(224) Hayes, R.; Imberti, S.; Warr, G. G.; Atkin, R. Amphiphilicity Determines Nanostructure in Protic Ionic Liquids. *Phys. Chem. Chem. Phys.* **2011**, *13*, 3237−3247.
(225) Russina, O.; Triolo, A. New Experimental Evidence Supporting the Mesoscopic Segregation Model in Room Temperature Ionic Liquids. *Faraday Discuss.* **2012**, *154*, 97−109.
(226) Katsyuba, S. A.; Vener, M. V.; Zvereva, E. E.; Fei, Z.; Scopelliti, R.; Laurenczy, G.; Yan, N.; Paunescu, E.; Dyson, P. J. How Strong is Hydrogen Bonding in Ionic Liquids? Combined X-ray Crystallographic, Infrared/Raman Spectroscopic, and Density Functional Theory Study. *J. Phys. Chem. B* **2013**, *117*, 9094−9105.
(227) Fakhraee, M.; Zandkarimi, B.; Salari, H.; Gholami, M. R. Hydroxyl-Functionalized 1-(2-Hydroxyethyl)-3-methylimidazolium Ionic Liquids: Thermodynamic and Structural Properties Using Molecular Dynamics Simulations and *ab Initio* Calculations. *J. Phys. Chem. B* **2014**, *118*, 14410−14428.
(228) Knorr, A.; Stange, P.; Fumino, K.; Weinhold, F.; Ludwig, R. Spectroscopic Evidence for Clusters of Like-Charged Ions in Ionic Liquids Stabilized by Cooperative Hydrogen Bonding. *ChemPhysChem* **2016**, *17*, 458−462.
(229) Evans, D. F.; Chen, S.-H.; Schriver, G. W.; Arnett, E. M. Thermodynamics of Solution of Nonpolar Gases in a Fused Salt. Hydrophobic Bonding Behavior in a Nonaqueous System. *J. Am. Chem. Soc.* **1981**, *103*, 481−482.
(230) Fumino, K.; Wulf, A.; Ludwig, R. Hydrogen Bonding in Protic Ionic Liquids: Reminiscent of Water. *Angew. Chem., Int. Ed.* **2009**, *48*, 3184−3186.
(231) Fumino, K.; Reichert, E.; Wittler, K.; Hempelmann, R.; Ludwig, R. Low-Frequency Vibrational Modes of Protic Molten Salts and Ionic Liquids: Detecting and Quantifying Hydrogen Bonds. *Angew. Chem., Int. Ed.* **2012**, *51*, 6236−6240.
(232) Fumino, K.; Ludwig, R. Analyzing the Interaction Energies Between Cation and Anion in Ionic Liquids: The Subtle Balance Between Coulomb Forces and Hydrogen Bonding. *J. Mol. Liq.* **2014**, *192*, 94−102.
(233) Stange, P.; Fumino, K.; Ludwig, R. Ion Speciation of Protic Ionic Liquids in Water: Transition from Contact to Solvent-Separated Ion Pairs. *Angew. Chem., Int. Ed.* **2013**, *52*, 2990−2994.
(234) Steiner, T. The Hydrogen Bond in the Solid State. *Angew. Chem., Int. Ed.* **2002**, *41*, 48−76.
(235) Khudozhitkov, A. E.; Stange, P.; Golub, B.; Paschek, D.; Stepanov, A. G.; Kolokolov, D. I.; Ludwig, R. Characterization of Doubly Ionic Hydrogen Bonds in Protic Ionic Liquids by NMR Deuteron Quadrupole Coupling Constants: Differences to H-bonds in Amides, Peptides, and Proteins. *Angew. Chem., Int. Ed.* **2017**, *56*, 14310−14314.
(236) Khudozhitkov, A.; Neumann, J.; Niemann, T.; Zaitsau, D.; Stange, P.; Paschek, D.; Stepanov, A.; Kolokolov, D.; Ludwig, R. Hydrogen Bonding Between Ions of Like Charge in Ionic Liquids Characterized by NMR Deuteron Quadrupole Coupling Constants-Comparison with Salt Bridges and Molecular Systems. *Angew. Chem., Int. Ed.* **2019**, *58*, 17863−17871.
(237) Niemann, T.; Li, H.; Warr, G. G.; Ludwig, R.; Atkin, R. Influence of Hydrogen Bonding Between Ions of Like Charge on the Ionic Liquid Interfacial Structure at a Mica Surface. *J. Phys. Chem. Lett.* **2019**, *10*, 7368−7373.
(238) Wang, Y.-L.; Li, B.; Sarman, S.; Laaksonen, A. Microstructures and Dynamics of Tetraalkylphosphonium Chloride Ionic Liquids. *J. Chem. Phys.* **2017**, *147*, 224502.
(239) Liu, X.; Zhao, Y.; Zhang, X.; Zhou, G.; Zhang, S. Microstructures and Interaction Analyses of Phosphonium-Based Ionic Liquids: A Simulation Study. *J. Phys. Chem. B* **2012**, *116*, 4934−4942.
(240) Zhou, G.; Liu, X.; Zhang, S.; Yu, G.; He, H. A Force Field for Molecular Simulation of Tetrabutylphosphonium Amino Acid Ionic Liquids. *J. Phys. Chem. B* **2007**, *111*, 7078−7084.
(241) Strate, A.; Niemann, T.; Ludwig, R. Controlling the Kinetic and Thermodynamic Stability of Cationic Clusters by the Addition of Molecules or Counterions. *Phys. Chem. Chem. Phys.* **2017**, *19*, 18854−18862.
(242) Desiraju, G. R. A Bond by Any Other Name. *Angew. Chem., Int. Ed.* **2011**, *50*, 52−59.
(243) Ribeiro, M. C. High Viscosity of Imidazolium Ionic Liquids with the Hydrogen Sulfate Anion: A Raman Spectroscopy Study. *J. Phys. Chem. B* **2012**, *116*, 7281−7290.
(244) Faria, L. F.; Lima, T. A.; Ferreira, F. F.; Ribeiro, M. C. Ultraslow Phase Transitions in an Anion-Anion Hydrogen-Bonded Ionic Liquid. *J. Phys. Chem. B* **2018**, *122*, 1972−1980.
(245) Zheng, Y.-Z.; Wang, N.-N.; Luo, J.-J.; Zhou, Y.; Yu, Z.-W. Hydrogen-Bonding Interactions Between [BMIM][BF_4] and Acetonitrile. *Phys. Chem. Chem. Phys.* **2013**, *15*, 18055−18064.
(246) Dong, K.; Song, Y.; Liu, X.; Cheng, W.; Yao, X.; Zhang, S. Understanding Structures and Hydrogen Bonds of Ionic Liquids at the Electronic Level. *J. Phys. Chem. B* **2012**, *116*, 1007−1017.
(247) Ramya, K.; Kumar, P.; Venkatnathan, A. Molecular Simulations of Anion and Temperature Dependence on Structure and Dynamics of 1-Hexyl-3-methylimidazolium Ionic Liquids. *J. Phys. Chem. B* **2015**, *119*, 14800−14806.

https://dx.doi.org/10.1021/acs.chemrev.9b00693
Chem. Rev. 2020, 120, 5798−5877

(248) Skarmoutsos, I.; Dellis, D.; Matthews, R. P.; Welton, T.; Hunt, P. A. Hydrogen Bonding in 1-Butyl- and 1-Ethyl-3-methylimidazolium Chloride Ionic Liquids. *J. Phys. Chem. B* **2012**, *116*, 4921−4933.
(249) Dong, K.; Zhang, S.; Wang, D.; Yao, X. Hydrogen Bonds in Imidazolium Ionic Liquids. *J. Phys. Chem. A* **2006**, *110*, 9775−9782.
(250) Hunt, P. A.; Gould, I. R. Structural Characterization of the 1-Butyl-3-methylimidazolium Chloride Ion Pair Using *ab Initio* Methods. *J. Phys. Chem. A* **2006**, *110*, 2269−2282.
(251) Malberg, F.; Pensado, A. S.; Kirchner, B. The Bulk and the Gas Phase of 1-Ethyl-3-methylimidazolium Ethylsulfate: Dispersion Interaction Makes the Difference. *Phys. Chem. Chem. Phys.* **2012**, *14*, 12079−12082.
(252) Matthews, R. P.; Ashworth, C.; Welton, T.; Hunt, P. A. The Impact of Anion Electronic Structure: Similarities and Differences in Imidazolium Based Ionic Liquids. *J. Phys.: Condens. Matter* **2014**, *26*, 284112.
(253) Skarmoutsos, I.; Welton, T.; Hunt, P. A. The Importance of Timescale for Hydrogen Bonding in Imidazolium Chloride Ionic Liquids. *Phys. Chem. Chem. Phys.* **2014**, *16*, 3675−3685.
(254) Yaghini, N.; Nordstierna, L.; Martinelli, A. Effect of Water on the Transport Properties of Protic and Aprotic Imidazolium Ionic Liquids−An Analysis of Self-Diffusivity, Conductivity, and Proton Exchange Mechanism. *Phys. Chem. Chem. Phys.* **2014**, *16*, 9266−9275.
(255) Yaghini, N.; Pitawala, J.; Matic, A.; Martinelli, A. Effect of Water on the Local Structure and Phase Behavior of Imidazolium-Based Protic Ionic Liquids. *J. Phys. Chem. B* **2015**, *119*, 1611−1622.
(256) Martinelli, A.; Matic, A.; Johansson, P.; Jacobsson, P.; Börjesson, L.; Fernicola, A.; Panero, S.; Scrosati, B.; Ohno, H. Conformational Evolution of $TFSI^-$ in Protic and Aprotic Ionic Liquids. *J. Raman Spectrosc.* **2011**, *42*, 522−528.
(257) Endo, T.; Kato, T.; Nishikawa, K. Effects of Methylation at the 2 Position of the Cation Ring on Phase Behaviors and Conformational Structures of Imidazolium-Based Ionic Liquids. *J. Phys. Chem. B* **2010**, *114*, 9201−9208.
(258) Fumino, K.; Wulf, A.; Ludwig, R. The Potential Role of Hydrogen Bonding in Aprotic and Protic Ionic Liquids. *Phys. Chem. Chem. Phys.* **2009**, *11*, 8790−8794.
(259) Fumino, K.; Bonsa, A. M.; Golub, B.; Paschek, D.; Ludwig, R. Non-Ideal Mixing Behaviour of Hydrogen Bonding in Mixtures of Protic Ionic Liquids. *ChemPhysChem* **2015**, *16*, 299−304.
(260) Noack, K.; Schulz, P. S.; Paape, N.; Kiefer, J.; Wasserscheid, P.; Leipertz, A. The Role of the C_2 Position in Interionic Interactions of Imidazolium Based Ionic Liquids: A Vibrational and NMR Spectroscopic Study. *Phys. Chem. Chem. Phys.* **2010**, *12*, 14153−14161.
(261) Peppel, T.; Roth, C.; Fumino, K.; Paschek, D.; Köckerling, M.; Ludwig, R. The Influence of Hydrogen-Bond Defects on the Properties of Ionic Liquids. *Angew. Chem., Int. Ed.* **2011**, *50*, 6661−6665.
(262) Tokuda, H.; Hayamizu, K.; Ishii, K.; Susan, M. A. B. H.; Watanabe, M. Physicochemical Properties and Structures of Room Temperature Ionic Liquids. 2. Variation of Alkyl Chain Length in Imidazolium Cation. *J. Phys. Chem. B* **2005**, *109*, 6103−6110.
(263) Izgorodina, E. I.; Maganti, R.; Armel, V.; Dean, P. M.; Pringle, J. M.; Seddon, K. R.; MacFarlane, D. R. Understanding the Effect of the C_2 Proton in Promoting Low Viscosities and High Conductivities in Imidazolium-Based Ionic Liquids: Part I. Weakly Coordinating Anions. *J. Phys. Chem. B* **2011**, *115*, 14688−14697.
(264) Zahn, S.; Bruns, G.; Thar, J.; Kirchner, B. What Keeps Ionic Liquids in Flow? *Phys. Chem. Chem. Phys.* **2008**, *10*, 6921−6924.
(265) Liao, C.; Shao, N.; Han, K. S.; Sun, X.-G.; Jiang, D.-E.; Hagaman, E. W.; Dai, S. Physicochemical Properties of Imidazolium-Derived Ionic Liquids with Different C-2 Substitutions. *Phys. Chem. Chem. Phys.* **2011**, *13*, 21503−21510.
(266) Cao, Y.; Mu, T. Comprehensive Investigation on the Thermal Stability of 66 Ionic Liquids by Thermogravimetric Analysis. *Ind. Eng. Chem. Res.* **2014**, *53*, 8651−8664.
(267) Hunt, P. A.; Kirchner, B.; Welton, T. Characterising the Electronic Structure of Ionic Liquids: An Examination of the 1-Butyl-3-methylimidazolium Chloride Ion Pair. *Chem. - Eur. J.* **2006**, *12*, 6762−6775.
(268) Dong, K.; Zhang, S. Hydrogen Bonds: A Structural Insight into Ionic Liquids. *Chem. - Eur. J.* **2012**, *18*, 2748−2761.
(269) Tsuzuki, S.; Tokuda, H.; Hayamizu, K.; Watanabe, M. Magnitude and Directionality of Interaction in Ion Pairs of Ionic Liquids: Relationship with Ionic Conductivity. *J. Phys. Chem. B* **2005**, *109*, 16474−16481.
(270) Niedermeyer, H.; Ashworth, C.; Brandt, A.; Welton, T.; Hunt, P. A. A Step Towards the a Priori Design of Ionic Liquids. *Phys. Chem. Chem. Phys.* **2013**, *15*, 11566−11578.
(271) Zhao, W.; Leroy, F.; Heggen, B.; Zahn, S.; Kirchner, B.; Balasubramanian, S.; Müller-Plathe, F. Are There Stable Ion-Pairs in Room-Temperature Ionic Liquids? Molecular Dynamics Simulations of 1-n-Butyl-3-methylimidazolium Hexafluorophosphate. *J. Am. Chem. Soc.* **2009**, *131*, 15825−15833.
(272) Qiao, B.; Krekeler, C.; Berger, R.; Delle Site, L.; Holm, C. Effect of Anions on Static Orientational Correlations, Hydrogen Bonds, and Dynamics in Ionic Liquids: A Simulational Study. *J. Phys. Chem. B* **2008**, *112*, 1743−1751.
(273) Ramírez-González, P. E.; Ren, G.; Saielli, G.; Wang, Y. Effect of Ion Rigidity on Physical Properties of Ionic Liquids Studied by Molecular Dynamics Simulation. *J. Phys. Chem. B* **2016**, *120*, 5678−5690.
(274) Tang, F.; Ohto, T.; Hasegawa, T.; Bonn, M.; Nagata, Y. $\pi^+-\pi^+$ Stacking of Imidazolium Cations Enhances Molecular Layering of Room Temperature Ionic Liquids at Their Interfaces. *Phys. Chem. Chem. Phys.* **2017**, *19*, 2850−2856.
(275) Deetlefs, M.; Hardacre, C.; Nieuwenhuyzen, M.; Padua, A. A.; Sheppard, O.; Soper, A. K. Liquid Structure of the Ionic Liquid 1,3-Dimethylimidazolium Bis{(trifluoromethyl)sulfonyl}amide. *J. Phys. Chem. B* **2006**, *110*, 12055−12061.
(276) Aoun, B.; Goldbach, A.; Kohara, S.; Wax, J.-F.; González, M. A.; Saboungi, M.-L. Structure of a Prototypic Ionic Liquid: Ethylmethylimidazolium Bromide. *J. Phys. Chem. B* **2010**, *114*, 12623−12628.
(277) Brüssel, M.; Brehm, M.; Pensado, A. S.; Malberg, F.; Ramzan, M.; Stark, A.; Kirchner, B. On the Ideality of Binary Mixtures of Ionic Liquids. *Phys. Chem. Chem. Phys.* **2012**, *14*, 13204−13215.
(278) Weber, H.; Hollóczki, O.; Pensado, A. S.; Kirchner, B. Side Chain Fluorination and Anion Effect on the Structure of 1-Butyl-3-methylimidazolium Ionic Liquids. *J. Chem. Phys.* **2013**, *139*, 084502.
(279) Matthews, R. P.; Welton, T.; Hunt, P. A. Hydrogen Bonding and $\pi-\pi$ Interactions in Imidazolium-Chloride Ionic Liquid Clusters. *Phys. Chem. Chem. Phys.* **2015**, *17*, 14437−14453.
(280) Triolo, A.; Russina, O.; Bleif, H.-J.; Di Cola, E. Nanoscale Segregation in Room Temperature Ionic Liquids. *J. Phys. Chem. B* **2007**, *111*, 4641−4644.
(281) Mele, A.; Romanò, G.; Giannone, M.; Ragg, E.; Fronza, G.; Raos, G.; Marcon, V. The Local Structure of Ionic Liquids: Cation-Cation NOE Interactions and Internuclear Distances in Neat $[BMIM][BF_4]$ and $[BDMIM][BF_4]$. *Angew. Chem., Int. Ed.* **2006**, *45*, 1123−1126.
(282) Li, X.-W.; Zhang, J.; Dong, B.; Zheng, L.-Q.; Tung, C.-H. Characterization of Lyotropic Liquid Crystals Formed in the Mixtures of 1-Alkyl-3-methylimidazolium Bromide/p-Xylene/Water. *Colloids Surf., A* **2009**, *335*, 80−87.
(283) Deetlefs, M.; Hardacre, C.; Nieuwenhuyzen, M.; Sheppard, O.; Soper, A. K. Structure of Ionic Liquid-Benzene Mixtures. *J. Phys. Chem. B* **2005**, *109*, 1593−1598.
(284) Shimizu, K.; Costa Gomes, M. F.; Pádua, A. L. A.; Rebelo, L. S. P. N.; Canongia Lopes, J. N. On the Role of the Dipole and Quadrupole Moments of Aromatic Compounds in the Solvation by Ionic Liquids. *J. Phys. Chem. B* **2009**, *113*, 9894−9900.
(285) Harper, J. B.; Lynden-Bell, R. Macroscopic and Microscopic Properties of Solutions of Aromatic Compounds in an Ionic Liquid. *Mol. Phys.* **2004**, *102*, 85−94.
(286) Blesic, M.; Lopes, J. N. C.; Pádua, A. L. A.; Shimizu, K.; Gomes, M. F. C.; Rebelo, L. S. P. N. Phase Equilibria in Ionic Liquid-

https://dx.doi.org/10.1021/acs.chemrev.9b00693
Chem. Rev. 2020, 120, 5798−5877

Aromatic Compound Mixtures, Including Benzene Fluorination Effects. *J. Phys. Chem. B* **2009**, *113*, 7631−7636.
(287) Holbrey, J. D.; Reichert, W. M.; Nieuwenhuyzen, M.; Sheppard, O.; Hardacre, C.; Rogers, R. D. Liquid Clathrate Formation in Ionic Liquid-Aromatic Mixtures. *Chem. Commun.* **2003**, 476−477.
(288) Shimomura, T.; Takamuku, T.; Yamaguchi, T. Clusters of Imidazolium-Based Ionic Liquid in Benzene Solutions. *J. Phys. Chem. B* **2011**, *115*, 8518−8527.
(289) Yasaka, Y.; Klein, M. L.; Nakahara, M.; Matubayasi, N. Exploring the Reorientation of Benzene in an Ionic Liquid via Molecular Dynamics: Effect of Temperature and Solvent Effective Charge on the Slow Dynamics. *J. Chem. Phys.* **2011**, *134*, 191101.
(290) Shirota, H. Intermolecular/Interionic Vibrations of 1-Methyl-3-n-octylimidazolium Tetrafluoroborate Ionic Liquid and Benzene Mixtures. *J. Phys. Chem. B* **2013**, *117*, 7985−7995.
(291) Fumino, K.; Wittler, K.; Ludwig, R. The Anion Dependence of the Interaction Strength Between Ions in Imidazolium-Based Ionic Liquids Probed by Far-Infrared Spectroscopy. *J. Phys. Chem. B* **2012**, *116*, 9507−9511.
(292) Penna, T. C.; Faria, L. F.; Ribeiro, M. C. Raman Band Shape Analysis of Cyanate-Anion Ionic Liquids. *J. Mol. Liq.* **2015**, *209*, 676−682.
(293) Wang, Y.-L.; Shimpi, M. R.; Sarman, S.; Antzutkin, O. N.; Glavatskih, S.; Kloo, L.; Laaksonen, A. Atomistic Insight into Tetraalkylphosphonium Bis(oxalato)borate Ionic Liquid/Water Mixtures. 2. Volumetric and Dynamic Properties. *J. Phys. Chem. B* **2016**, *120*, 7446−7455.
(294) Shah, F. U.; Glavatskih, S.; MacFarlane, D. R.; Somers, A.; Forsyth, M.; Antzutkin, O. N. Novel Halogen-Free Chelated Orthoborate-Phosphonium Ionic Liquids: Synthesis and Tribophysical Properties. *Phys. Chem. Chem. Phys.* **2011**, *13*, 12865−12873.
(295) Golets, M.; Shimpi, M. R.; Wang, Y.-L.; Antzutkin, O. N.; Glavatskih, S.; Laaksonen, A. Understanding the Thermal Decomposition Mechanism of a Halogen-Free Chelated Orthoborate-Based Ionic Liquid: A Combined Computational and Experimental Study. *Phys. Chem. Chem. Phys.* **2016**, *18*, 22458−22466.
(296) Wang, Y.-L.; Golets, M.; Li, B.; Sarman, S.; Laaksonen, A. Interfacial Structures of Trihexyltetradecylphosphonium-Bis(mandelato)borate Ionic Liquid Confined Between Gold Electrodes. *ACS Appl. Mater. Interfaces* **2017**, *9*, 4976−4987.
(297) Chen, S.; Zhang, S.; Liu, X.; Wang, J.; Wang, J.; Dong, K.; Sun, J.; Xu, B. Ionic Liquid Clusters: Structure, Formation Mechanism, and Effect on the Behavior of Ionic Liquids. *Phys. Chem. Chem. Phys.* **2014**, *16*, 5893−5906.
(298) Weingärtner, H.; Knocks, A.; Schrader, W.; Kaatze, U. Dielectric Spectroscopy of the Room Temperature Molten Salt Ethylammonium Nitrate. *J. Phys. Chem. A* **2001**, *105*, 8646−8650.
(299) Kennedy, D. F.; Drummond, C. J. Large Aggregated Ions Found in Some Protic Ionic Liquids. *J. Phys. Chem. B* **2009**, *113*, 5690−5693.
(300) Lynden-Bell, R. Screening of Pairs of Ions Dissolved in Ionic Liquids. *Phys. Chem. Chem. Phys.* **2010**, *12*, 1733−1740.
(301) Lee, A. A.; Vella, D.; Perkin, S.; Goriely, A. Are Room-Temperature Ionic Liquids Dilute Electrolytes? *J. Phys. Chem. Lett.* **2015**, *6*, 159−163.
(302) Lu, H.; Li, B.; Nordholm, S.; Woodward, C. E.; Forsman, J. Ion Pairing and Phase Behaviour of an Asymmetric Restricted Primitive Model of Ionic Liquids. *J. Chem. Phys.* **2016**, *145*, 234510.
(303) Feng, G.; Chen, M.; Bi, S.; Goodwin, Z. A. H.; Postnikov, E. B.; Brilliantov, N.; Urbakh, M.; Kornyshev, A. A. Free and Bound States of Ions in Ionic Liquids, Conductivity, and Underscreening Paradox. *Phys. Rev. X* **2019**, *9*, 021024.
(304) Armstrong, J. P.; Hurst, C.; Jones, R. G.; Licence, P.; Lovelock, K. R. J.; Satterley, C. J.; Villar-Garcia, I. J. Vapourisation of Ionic Liquids. *Phys. Chem. Chem. Phys.* **2007**, *9*, 982−990.
(305) Neto, B. A. D.; Meurer, E. C.; Galaverna, R.; Bythell, B. J.; Dupont, J.; Cooks, R. G.; Eberlin, M. N. Vapors From Ionic Liquids: Reconciling Simulations with Mass Spectrometric Data. *J. Phys. Chem. Lett.* **2012**, *3*, 3435−3441.
(306) Dupont, J. On the Solid, Liquid and Solution Structural Organization of Imidazolium Ionic Liquids. *J. Braz. Chem. Soc.* **2004**, *15*, 341−350.
(307) Weingaertner, H. NMR Studies of Ionic Liquids: Structure and Dynamics. *Curr. Opin. Colloid Interface Sci.* **2013**, *18*, 183−189.
(308) Weingärtner, H.; Merkel, T.; Käshammer, S.; Schröer, W.; Wiegand, S. The Effect of Short-Range Hydrogen-Bonded Interactions on the Nature of the Critical Point of Ionic Fluids. Part I: General Properties of the New System Ethylammonium Nitrate + n-Octanol with an Upper Consolute Point Near Room Temperature. *Ber. Bunsenges. Phys. Chem.* **1993**, *97*, 970−975.
(309) Ludwig, R. A Simple Geometrical Explanation for the Occurrence of Specific Large Aggregated Ions in Some Protic Ionic Liquids. *J. Phys. Chem. B* **2009**, *113*, 15419−15422.
(310) Addicoat, M. A.; Stefanovic, R.; Webber, G. B.; Atkin, R.; Page, A. J. Assessment of the Density Functional Tight Binding Method for Protic Ionic Liquids. *J. Chem. Theory Comput.* **2014**, *10*, 4633−4643.
(311) Kirchner, B.; Malberg, F.; Firaha, D. S.; Hollóczki, O. Ion Pairing in Ionic Liquids. *J. Phys.: Condens. Matter* **2015**, *27*, 463002.
(312) Bren, U.; Martínek, V.; Florián, J. Decomposition of the Solvation Free Energies of Deoxyribonucleoside Triphosphates Using the Free Energy Perturbation Method. *J. Phys. Chem. B* **2006**, *110*, 12782−12788.
(313) Weingärtner, H.; Sasisanker, P.; Daguenet, C.; Dyson, P. J.; Krossing, I.; Slattery, J. M.; Schubert, T. The Dielectric Response of Room-Temperature Ionic Liquids: Effect of Cation Variation. *J. Phys. Chem. B* **2007**, *111*, 4775−4780.
(314) Perkin, S.; Salanne, M.; Madden, P.; Lynden-Bell, R. M. Is a Stern and Diffuse Layer Model Appropriate to Ionic Liquids at Surfaces? *Proc. Natl. Acad. Sci. U. S. A.* **2013**, *110*, E4121.
(315) Lui, M. Y.; Crowhurst, L.; Hallett, J. P.; Hunt, P. A.; Niedermeyer, H.; Welton, T. Salts Dissolved in Salts: Ionic Liquid Mixtures. *Chem. Sci.* **2011**, *2*, 1491−1496.
(316) Bodo, E.; Gontrani, L.; Triolo, A.; Caminiti, R. Structural Determination of Ionic Liquids With Theoretical Methods: C_8mimBr and C_8mimCl. Strength and Weakness of Current Force Fields. *J. Phys. Chem. Lett.* **2010**, *1*, 1095−1100.
(317) Afandak, A.; Eslami, H. Ion-Pairing and Electrical Conductivity in the Ionic Liquid 1-n-Butyl-3-methylimidazolium Methylsulfate [Bmim][$MeSO_4$]: Molecular Dynamics Simulation Study. *J. Phys. Chem. B* **2017**, *121*, 7699−7708.
(318) Kashyap, H. K.; Annapureddy, H. V. R.; Raineri, F. O.; Margulis, C. J. How is Charge Transport Different in Ionic Liquids and Electrolyte Solutions? *J. Phys. Chem. B* **2011**, *115*, 13212−13221.
(319) Earle, M. J.; Esperanca, J. M.S.S.; Gilea, M. A.; Canongia Lopes, J. N.; Rebelo, L. P.N.; Magee, J. W.; Seddon, K. R.; Widegren, J. A. The Distillation and Volatility of Ionic Liquids. *Nature* **2006**, *439*, 831−834.
(320) Ueno, K.; Tokuda, H.; Watanabe, M. Ionicity in Ionic Liquids: Correlation With Ionic Structure and Physicochemical Properties. *Phys. Chem. Chem. Phys.* **2010**, *12*, 1649−1658.
(321) Mele, A.; Tran, C. D.; De Paoli Lacerda, S. H. The Structure of A Room-Temperature Ionic Liquid With and Without Trace Amounts of Water: The Role of C-H-O and C-H-F Interactions in 1-n-Butyl-3-methylimidazolium Tetrafluoroborate. *Angew. Chem.* **2003**, *115*, 4500−4502.
(322) Del Popolo, M. G.; Mullan, C. L.; Holbrey, J. D.; Hardacre, C.; Ballone, P. Ion Association in [Bmim][PF_6]/Naphthalene Mixtures: An Experimental and Computational Study. *J. Am. Chem. Soc.* **2008**, *130*, 7032−7041.
(323) Hardacre, C.; Holbrey, J. D.; Mullan, C. L.; Nieuwenhuyzen, M.; Youngs, T. G. A.; Bowron, D. T.; Teat, S. J. Solid and Liquid Charge-Transfer Complex Formation Between 1-Methylnaphthalene and 1-Alkyl-cyanopyridinium Bis{(trifluoromethyl)sulfonyl}imide Ionic Liquids. *Phys. Chem. Chem. Phys.* **2010**, *12*, 1842−1853.
(324) McDonald, S.; Murphy, T.; Imberti, S.; Warr, G. G.; Atkin, R. Amphiphilically Nanostructured Deep Eutectic Solvents. *J. Phys. Chem. Lett.* **2018**, *9*, 3922−3927.

https://dx.doi.org/10.1021/acs.chemrev.9b00693
Chem. Rev. 2020, 120, 5798−5877

(325) Reddy, T. D. N.; Mallik, B. S. Protic Ammonium Carboxylate Ionic Liquids: Insight into Structure, Dynamics and Thermophysical Properties by Alkyl Group Functionalization. *Phys. Chem. Chem. Phys.* **2017**, *19*, 10358−10370.
(326) Song, X.; Hamano, H.; Minofar, B.; Kanzaki, R.; Fujii, K.; Kameda, Y.; Kohara, S.; Watanabe, M.; Ishiguro, S.-I.; Umebayashi, Y. Structural Heterogeneity and Unique Distorted Hydrogen Bonding in Primary Ammonium Nitrate Ionic Liquids Studied by High-Energy X-ray Diffraction Experiments and MD Simulations. *J. Phys. Chem. B* **2012**, *116*, 2801−2813.
(327) Hayes, R.; Imberti, S.; Warr, G. G.; Atkin, R. Pronounced Sponge-Like Nanostructure in Propylammonium Nitrate. *Phys. Chem. Chem. Phys.* **2011**, *13*, 13544−13551.
(328) Thummuru, D. N. R.; Mallik, B. S. Structure and Dynamics of Hydroxyl-Functionalized Protic Ammonium Carboxylate Ionic Liquids. *J. Phys. Chem. A* **2017**, *121*, 8097−8107.
(329) Greaves, T. L.; Kennedy, D. F.; Mudie, S. T.; Drummond, C. J. Diversity Observed in the Nanostructure of Protic Ionic Liquids. *J. Phys. Chem. B* **2010**, *114*, 10022−10031.
(330) Nayeri, M.; Aronson, M. T.; Bernin, D.; Chmelka, B. F.; Martinelli, A. Surface Effects on the Structure and Mobility of the Ionic Liquid C_6C_1ImTFSI in Silica Gels. *Soft Matter* **2014**, *10*, 5618−5627.
(331) Mehta, N. A.; Levin, D. A. Comparison of Two Protic Ionic Liquid Behaviors in the Presence of an Electric Field Using Molecular Dynamics. *J. Chem. Phys.* **2017**, *147*, 234505.
(332) Hayes, R.; Imberti, S.; Warr, G. G.; Atkin, R. The Nature of Hydrogen Bonding in Protic Ionic Liquids. *Angew. Chem.* **2013**, *125*, 4721−4725.
(333) Paschek, D.; Golub, B.; Ludwig, R. Hydrogen Bonding in a Mixture of Protic Ionic Liquids: A Molecular Dynamics Simulation Study. *Phys. Chem. Chem. Phys.* **2015**, *17*, 8431−8440.
(334) Zheng, Z. P.; Fan, W. H.; Roy, S.; Mazur, K.; Nazet, A.; Buchner, R.; Bonn, M.; Hunger, J. Ionic Liquids: Not Only Structurally But Also Dynamically Heterogeneous. *Angew. Chem., Int. Ed.* **2014**, *54*, 687−690.
(335) Schröder, U.; Wadhawan, J. D.; Compton, R. G.; Marken, F.; Suarez, P. A. Z.; Consorti, C. S.; de Souza, R. F.; Dupont, J. Water-Induced Accelerated Ion Diffusion: Voltammetric Studies in 1-Methyl-3-[2,6-(S)-dimethylocten-2-yl]imidazolium Tetrafluoroborate, 1-Butyl-3-methylimidazolium Tetrafluoroborate and Hexafluorophosphate Ionic Liquids. *New J. Chem.* **2000**, *24*, 1009−1015.
(336) Wang, Y.; Voth, G. A. Unique Spatial Heterogeneity in Ionic Liquids. *J. Am. Chem. Soc.* **2005**, *127*, 12192−12193.
(337) Wang, Y.; Voth, G. A. Tail Aggregation and Domain Diffusion in Ionic Liquids. *J. Phys. Chem. B* **2006**, *110*, 18601−18608.
(338) Cao, W.; Wang, Y.; Saielli, G. Metastable State During Melting and Solid-Solid Phase Transition of $[C_nMim][NO_3]$(n = 4−12) Ionic Liquids by Molecular Dynamics Simulation. *J. Phys. Chem. B* **2018**, *122*, 229−239.
(339) Saielli, G.; Wang, Y. Role of the Electrostatic Interactions in the Stabilization of Ionic Liquid Crystals: Insights From Coarse-Grained MD Simulations of an Imidazolium Model. *J. Phys. Chem. B* **2016**, *120*, 9152−9160.
(340) Shi, R.; Wang, Y. Ion-Cage Interpretation for the Structural and Dynamic Changes of Ionic Liquids Under an External Electric Field. *J. Phys. Chem. B* **2013**, *117*, 5102−5112.
(341) Saielli, G.; Voth, G. A.; Wang, Y. Diffusion Mechanisms in Smectic Ionic Liquid Crystals: Insights From Coarse-Grained MD Simulations. *Soft Matter* **2013**, *9*, 5716−5725.
(342) Urahata, S. M.; Ribeiro, M. C. C. Unraveling Dynamical Heterogeneity in the Ionic Liquid 1-Butyl-3-methylimidazolium Chloride. *J. Phys. Chem. Lett.* **2010**, *1*, 1738−1742.
(343) Canongia Lopes, J. N. A.; Pádua, A. A. H. Nanostructural Organization in Ionic Liquids. *J. Phys. Chem. B* **2006**, *110*, 3330−3335.
(344) Nemoto, F.; Kofu, M.; Yamamuro, O. Thermal and Structural Studies of Imidazolium-Based Ionic Liquids With and Without Liquid-Crystalline Phases: The Origin of Nanostructure. *J. Phys. Chem. B* **2015**, *119*, 5028−5034.
(345) Triolo, A.; Russina, O.; Fazio, B.; Triolo, R.; Di Cola, E. Morphology of 1-Alkyl-3-methylimidazolium Hexafluorophosphate Room Temperature Ionic Liquids. *Chem. Phys. Lett.* **2008**, *457*, 362−365.
(346) Russina, O.; Triolo, A.; Gontrani, L.; Caminiti, R.; Xiao, D.; Hines Jr, L. G; Bartsch, R. A; Quitevis, E. L; Pleckhova, N.; Seddon, K. R Morphology and Intermolecular Dynamics of 1-Alkyl-3-methylimidazolium Bis(trifluoromethane)sulfonylimide Ionic Liquids: Structural and Dynamic Evidence of Nanoscale Segregation. *J. Phys.: Condens. Matter* **2009**, *21*, 424121.
(347) Hardacre, C.; Holbrey, J. D.; Mullan, C. L.; Youngs, T. G. A.; Bowron, D. T. Small Angle Neutron Scattering From 1-Alkyl-3-methylimidazolium Hexafluorophosphate Ionic Liquids ($[C_nmim][PF_6]$, n= 4, 6, and 8). *J. Chem. Phys.* **2010**, *133*, 074510.
(348) Hardacre, C.; Holbrey, J. D.; Nieuwenhuyzen, M.; Youngs, T. G. A. Structure and Solvation in Ionic Liquids. *Acc. Chem. Res.* **2007**, *40*, 1146−1155.
(349) Shimizu, K.; Bernardes, C. E. S.; Canongia Lopes, J. N. Structure and Aggregation in the 1-Alkyl-3-methylimidazolium Bis(trifluoromethylsulfonyl)imide Ionic Liquid Homologous Series. *J. Phys. Chem. B* **2014**, *118*, 567−576.
(350) Shimizu, K.; Bernardes, C. E. S.; Triolo, A.; Canongia Lopes, J. N. Nano-Segregation in Ionic Liquids: Scorpions and Vanishing Chains. *Phys. Chem. Chem. Phys.* **2013**, *15*, 16256−16262.
(351) Lo Celso, F.; Appetecchi, G. B.; Jafta, C. J.; Gontrani, L.; Canongia Lopes, J. N.; Triolo, A.; Russina, O. Nanoscale Organization in the Fluorinated Room Temperature Ionic Liquid: TetraethylAmmonium (Trifluoromethanesulfonyl)(Nonafluorobutylsulfonyl)imide. *J. Chem. Phys.* **2018**, *148*, 193816.
(352) Bulut, S.; Ab Rani, M. A.; Welton, T.; Lickiss, P. D.; Krossing, I. Preparation of $[Al(hfip)_4]$-Based Ionic Liquids with Siloxane-Functionalized Cations and Their Physical Properties in Comparison with Their $[Tf_2N]$ Analogues. *ChemPhysChem* **2012**, *13*, 1802−1805.
(353) Yamada, S. A.; Bailey, H. E.; Tamimi, A.; Li, C.; Fayer, M. D. Dynamics in a Room-Temperature Ionic Liquid From the Cation Perspective: 2D IR Vibrational Echo Spectroscopy. *J. Am. Chem. Soc.* **2017**, *139*, 2408−2420.
(354) Xue, L.; Tamas, G.; Matthews, R. P.; Stone, A. J.; Hunt, P. A.; Quitevis, E. L.; Lynden-Bell, R. M. An OHD-RIKES and Simulation Study Comparing a Benzylmethylimidazolium Ionic Liquid with an Equimolar Mixture of Dimethylimidazolium and Benzene. *Phys. Chem. Chem. Phys.* **2015**, *17*, 9973−9983.
(355) Tao, R.; Gurung, E.; Cetin, M. M.; Mayer, M. F.; Quitevis, E. L.; Simon, S. L. Fragility of Ionic Liquids Measured by Flash Differential Scanning Calorimetry. *Thermochim. Acta* **2017**, *654*, 121−129.
(356) Shirota, H.; Matsuzaki, H.; Ramati, S.; Wishart, J. F. Effects of Aromaticity in Cations and Their Functional Groups on the Low-Frequency Spectra and Physical Properties of Ionic Liquids. *J. Phys. Chem. B* **2015**, *119*, 9173−9187.
(357) Wu, B.; Shirota, H.; Lall-Ramnarine, S.; Castner, E. W., Jr Structure of Ionic Liquids with Cationic Silicon-Substitutions. *J. Chem. Phys.* **2016**, *145*, 114501.
(358) Zheng, W.; Mohammed, A.; Hines, L. G., Jr; Xiao, D.; Martinez, O. J.; Bartsch, R. A.; Simon, S. L.; Russina, O.; Triolo, A.; Quitevis, E. L. Effect of Cation Symmetry on the Morphology and Physicochemical Properties of Imidazolium Ionic Liquids. *J. Phys. Chem. B* **2011**, *115*, 6572−6584.
(359) Li, S.; Bañuelos, J. L.; Zhang, P.; Feng, G.; Dai, S.; Rother, G.; Cummings, P. T. Toward Understanding the Structural Heterogeneity and Ion Pair Stability in Dicationic Ionic Liquids. *Soft Matter* **2014**, *10*, 9193−9200.
(360) Menges, F. S.; Zeng, H. J.; Kelleher, P. J.; Gorlova, O.; Johnson, M. A.; Niemann, T.; Strate, A.; Ludwig, R. Structural Motifs in Cold Ternary Ion Complexes of Hydroxyl-Functionalized Ionic Liquids: Isolating the Role of Cation-Cation Interactions. *J. Phys. Chem. Lett.* **2018**, *9*, 2979−2984.

https://dx.doi.org/10.1021/acs.chemrev.9b00693
Chem. Rev. 2020, 120, 5798−5877

(361) Strate, A.; Niemann, T.; Michalik, D.; Ludwig, R. When Like Charged Ions Attract in Ionic Liquids: Controlling the Formation of Cationic Clusters by the Interaction Strength of the Counterions. *Angew. Chem., Int. Ed.* **2017**, *56*, 496−500.
(362) Dhungana, K. B.; Margulis, C. J. Comparison of the Structural Response to Pressure of Ionic Liquids with Ether and Alkyl Functionalities. *J. Phys. Chem. B* **2017**, *121*, 6890−6897.
(363) Smith, J. A.; Webber, G. B.; Warr, G. G.; Atkin, R. Rheology of Protic Ionic Liquids and Their Mixtures. *J. Phys. Chem. B* **2013**, *117*, 13930−13935.
(364) Wakeham, D.; Niga, P.; Ridings, C.; Andersson, G.; Nelson, A.; Warr, G. G.; Baldelli, S.; Rutland, M. W.; Atkin, R. Surface Structure of a "Non-Amphiphilic" Protic Ionic Liquid. *Phys. Chem. Chem. Phys.* **2012**, *14*, 5106−5114.
(365) Wu, B.; Kuroda, K.; Takahashi, K.; Castner, E. W., Jr Structural Analysis of Zwitterionic Liquids vs. Homologous Ionic Liquids. *J. Chem. Phys.* **2018**, *148*, 193807.
(366) Fakhraee, M.; Gholami, M. R. Effect of Anion and Alkyl Side Chain on Structural and Dynamic Features of Ester Functionalized Ionic Liquids: Confirming Nanoscale Organization. *J. Phys. Chem. B* **2016**, *120*, 11539−11555.
(367) Shirota, H.; Castner, E. W., Jr. Why Are Viscosities Lower for Ionic Liquids with $-CH_2Si(CH_3)_3$ vs $-CH_2C(CH_3)_3$ Substitutions on the Imidazolium Cations? *J. Phys. Chem. B* **2005**, *109*, 21576−21585.
(368) Shirota, H.; Wishart, J. F.; Castner, E. W., Jr. Intermolecular Interactions and Dynamics of Room Temperature Ionic Liquids that Have Silyl- and Siloxy-Substituted Imidazolium Cations. *J. Phys. Chem. B* **2007**, *111*, 4819−4829.
(369) Niedermeyer, H.; Ab Rani, M. A.; Lickiss, P. D.; Hallett, J. P.; Welton, T.; White, A. J. P.; Hunt, P. A. Understanding Siloxane Functionalised Ionic Liquids. *Phys. Chem. Chem. Phys.* **2010**, *12*, 2018−2029.
(370) Endo, T.; Nemugaki, S.; Matsushita, Y.; Sakai, Y.; Ozaki, H.; Hiejima, Y.; Kimura, Y.; Takahashi, K. Fast Solute Diffusivity in Ionic Liquids with Silyl or Siloxane Groups Studied by the Transient Grating Method. *Chem. Phys.* **2016**, *472*, 128−134.
(371) Serra, P. B. P.; Ribeiro, F. M. S.; Rocha, M. A. A.; Fulem, M.; Růžička, K.; Santos, L. M. N. B. F. Phase Behavior and Heat Capacities of the 1-Benzyl-3-methylimidazolium Ionic Liquids. *J. Chem. Thermodyn.* **2016**, *100*, 124−130.
(372) Shirota, H.; Kakinuma, S.; Itoyama, Y.; Umecky, T.; Takamuku, T. Effects of Tetrafluoroborate and Bis(trifluoromethylsulfonyl)amide Anions on the Microscopic Structures of 1-Methyl-3-octylimidazolium-Based Ionic Liquids and Benzene Mixtures: A Multiple Approach by ATR-IR, NMR, and Femtosecond Raman-Induced Kerr Effect Spectroscopy. *J. Phys. Chem. B* **2016**, *120*, 513−526.
(373) Xue, L.; Tamas, G.; Quitevis, E. L. Comparative OHD-RIKES Study of the Low-Frequency (0−250 cm^{-1}) Vibrational Dynamics of Dibenzyl- and Monobenzyl-Substituted Imidazolium Ionic Liquids and Benzene/Dimethylimidazolium Mixtures. *ACS Sustainable Chem. Eng.* **2016**, *4*, 514−524.
(374) Łachwa, J.; Bento, I.; Duarte, M. T.; Lopes, J. N. C.; Rebelo, L. P. N. Condensed Phase Behaviour of Ionic Liquid-Benzene Mixtures: Congruent Melting of a $[EMIM][NTf_2]$-C_6H_6 Inclusion Crystal. *Chem. Commun.* **2006**, 2445−2447.
(375) Rocha, M. A.; Neves, C. M.; Freire, M. G.; Russina, O.; Triolo, A.; Coutinho, J.; Santos, L. M. N. B. F. Alkylimidazolium Based Ionic Liquids: Impact of Cation Symmetry on Their Nanoscale Structural Organization. *J. Phys. Chem. B* **2013**, *117*, 10889−10897.
(376) Xiao, D.; Hines, L. G., Jr; Li, S.; Bartsch, R. A.; Quitevis, E. L.; Russina, O.; Triolo, A. Effect of Cation Symmetry and Alkyl Chain Length on the Structure and Intermolecular Dynamics of 1,3-Dialkylimidazolium Bis(trifluoromethanesulfonyl)amide Ionic Liquids. *J. Phys. Chem. B* **2009**, *113*, 6426−6433.
(377) Bernardes, C. E. S.; Shimizu, K.; Lobo Ferreira, A. I. M. C.; Santos, L. M. N. B. F.; Canongia Lopes, J. N. Structure and Aggregation in the 1,3-Dialkyl-imidazolium Bis(trifluoromethylsulfonyl)imide Ionic Liquid Family: 2. From Single to Double Long Alkyl Side Chains. *J. Phys. Chem. B* **2014**, *118*, 6885−6895.
(378) Saielli, G.; Margola, T.; Satoh, K. Tuning Coulombic Interactions to Stabilize Nematic and Smectic Ionic Liquid Crystal Phases in Mixtures of Charged Soft Ellipsoids and Spheres. *Soft Matter* **2017**, *13*, 5204−5213.
(379) Pitawala, J.; Matic, A.; Martinelli, A.; Jacobsson, P.; Koch, V.; Croce, F. Thermal Properties and Ionic Conductivity of Imidazolium Bis(trifluoromethanesulfonyl)imide Dicationic Ionic Liquids. *J. Phys. Chem. B* **2009**, *113*, 10607−10610.
(380) Lynden-Bell, R. M.; Quitevis, E. L. A Simulation Study of CS_2 Solutions in Two Related Ionic Liquids with Dications and Monocations. *J. Chem. Phys.* **2018**, *148*, 193844.
(381) Rocha, M. A. A.; Coutinho, J. A. P.; Santos, L. M. N. B. F. Vapor Pressures of 1,3-Dialkylimidazolium Bis(trifluoromethylsulfonyl)imide Ionic Liquids with Long Alkyl Chains. *J. Chem. Phys.* **2014**, *141*, 134502.
(382) Rocha, M. A. A.; Coutinho, J. A. P.; Santos, L. M. N. B. F. Cation Symmetry Effect on the Volatility of Ionic Liquids. *J. Phys. Chem. B* **2012**, *116*, 10922−10927.
(383) Ishida, T.; Shirota, H. Dicationic versus Monocationic Ionic Liquids: Distinctive Ionic Dynamics and Dynamical Heterogeneity. *J. Phys. Chem. B* **2013**, *117*, 1136−1150.
(384) Bodo, E.; Chiricotto, M.; Caminiti, R. Structure of Geminal Imidazolium Bis(trifluoromethylsulfonyl)imide Dicationic Ionic Liquids: A Theoretical Study of the Liquid Phase. *J. Phys. Chem. B* **2011**, *115*, 14341−14347.
(385) Yeganegi, S.; Soltanabadi, A.; Farmanzadeh, D. Molecular Dynamic Simulation of Dicationic Ionic Liquids: Effects of Anions and Alkyl Chain Length on Liquid Structure and Diffusion. *J. Phys. Chem. B* **2012**, *116*, 11517−11526.
(386) Sahu, P. K.; Das, S. K.; Sarkar, M. Toward Understanding Solute-Solvent Interaction in Room-Temperature Mono- and Dicationic Ionic Liquids: A Combined Fluorescence Spectroscopy and Mass Spectrometry Analysis. *J. Phys. Chem. B* **2014**, *118*, 1907−1915.
(387) Majhi, D.; Seth, S.; Sarkar, M. Differences in the Behavior of Dicationic and Monocationic Ionic Liquids as Revealed by Time Resolved-Fluorescence, NMR and Fluorescence Correlation Spectroscopy. *Phys. Chem. Chem. Phys.* **2018**, *20*, 7844−7856.
(388) Li, S.; Feng, G.; Bañuelos, J. L.; Rother, G.; Fulvio, P. F.; Dai, S.; Cummings, P. T. Distinctive Nanoscale Organization of Dicationic Versus Monocationic Ionic Liquids. *J. Phys. Chem. C* **2013**, *117*, 18251−18257.
(389) Moosavi, M.; Khashei, F.; Sedghamiz, E. Molecular Dynamics Simulation of Geminal Dicationic Ionic Liquids $[C_n(mim)_2][NTf_2]_2$-Structural and Dynamical Properties. *Phys. Chem. Chem. Phys.* **2018**, *20*, 435−448.
(390) Alavi, S. M.; Yeganegi, S. DFT Study of Structures and Hydrogen Bonds of Imidazolium Based Halogen-Free Boron Containing Dicationic Ionic Liquids. *J. Mol. Liq.* **2018**, *256*, 330−343.
(391) Moosavi, M.; Khashei, F.; Sharifi, A.; Mirzaei, M. Transport Properties of Short Alkyl Chain Length Dicationic Ionic Liquids. The Effects of Alkyl Chain Length and Temperature. *Ind. Eng. Chem. Res.* **2016**, *55*, 9087−9099.
(392) Donati, C.; Glotzer, S. C.; Poole, P. H.; Kob, W.; Plimpton, S. J. Spatial Correlations of Mobility and Immobility in a Glass-Forming Lennard-Jones Liquid. *Phys. Rev. E: Stat. Phys., Plasmas, Fluids, Relat. Interdiscip. Top.* **1999**, *60*, 3107−3119.
(393) Wang, B.; Kuo, J.; Bae, S. C.; Granick, S. When Brownian Diffusion is Not Gaussian. *Nat. Mater.* **2012**, *11*, 481−485.
(394) Giammanco, C. H.; Yamada, S. A.; Kramer, P. L.; Tamimi, A.; Fayer, M. D. Structural and Rotational Dynamics of Carbon Dioxide in 1-Alkyl-3-methylimidazolium Bis(trifluoromethylsulfonyl)imide Ionic Liquids: The Effect of Chain Length. *J. Phys. Chem. B* **2016**, *120*, 6698−6711.
(395) Shin, J. Y.; Yamada, S. A.; Fayer, M. D. Carbon Dioxide in A Supported Ionic Liquid Membrane: Structural and Rotational

https://dx.doi.org/10.1021/acs.chemrev.9b00693
Chem. Rev. 2020, 120, 5798−5877

Dynamics Measured With 2D IR and Pump−Probe Experiments. *J. Am. Chem. Soc.* **2017**, *139*, 11222−11232.
(396) Shin, J. Y.; Yamada, S. A.; Fayer, M. D. Dynamics of a Room Temperature Ionic Liquid in Supported Ionic Liquid Membranes vs the Bulk Liquid: 2D IR and Polarized IR Pump−Probe Experiments. *J. Am. Chem. Soc.* **2017**, *139*, 311−323.
(397) Kramer, P. L.; Giammanco, C. H.; Fayer, M. D. Dynamics of Water, Methanol, and Ethanol in a Room Temperature Ionic Liquid. *J. Chem. Phys.* **2015**, *142*, 212408.
(398) Driver, G.; Huang, Y.; Laaksonen, A.; Sparrman, T.; Wang, Y.-L.; Westlund, P.-O. Correlated/Non-Correlated Ion Dynamics of Charge-Neutral Ion Couples: The Origin of Ionicity in Ionic Liquids. *Phys. Chem. Chem. Phys.* **2017**, *19*, 4975−4988.
(399) Ivanov, M. Y.; Prikhod'ko, S. A.; Adonin, N. Y.; Kirilyuk, I. A.; Adichtchev, S. V.; Surovtsev, N. V.; Dzuba, S. A.; Fedin, M. V. Structural Anomalies in Ionic Liquids Near the Glass Transition Revealed by Pulse EPR. *J. Phys. Chem. Lett.* **2018**, *9*, 4607−4612.
(400) Lo Celso, F.; Triolo, A.; Gontrani, L.; Russina, O. Anion-Specific Response of Mesoscopic Organization in Ionic Liquids Upon Pressurization. *J. Chem. Phys.* **2018**, *148*, 211102.
(401) Russina, O.; Celso, F. L.; Triolo, A. Pressure-Responsive Mesoscopic Structures in Room Temperature Ionic Liquids. *Phys. Chem. Chem. Phys.* **2015**, *17*, 29496−29500.
(402) Chen, F.; You, T.; Yuan, Y.; Pei, C.; Ren, X.; Huang, Y.; Yu, Z.; Li, X.; Zheng, H.; Pan, Y.; Yang, K.; Wang, L. Pressure-Induced Structural Transitions of a Room Temperature Ionic Liquid—1-Ethyl-3-methylimidazolium Chloride. *J. Chem. Phys.* **2017**, *146*, 094502.
(403) Yoshimura, Y.; Shigemi, M.; Takaku, M.; Yamamura, M.; Takekiyo, T.; Abe, H.; Hamaya, N.; Wakabayashi, D.; Nishida, K.; Funamori, N.; Sato, T.; Kikegawa, T. Stability of the Liquid State of Imidazolium-Based Ionic Liquids Under High Pressure at Room Temperature. *J. Phys. Chem. B* **2015**, *119*, 8146−8153.
(404) Russina, O.; Fazio, B.; Schmidt, C.; Triolo, A. Structural Organization and Phase Behaviour of 1-Butyl-3-methylimidazolium Hexafluorophosphate: An High Pressure Raman Spectroscopy Study. *Phys. Chem. Chem. Phys.* **2011**, *13*, 12067−12074.
(405) Yoshimura, Y.; Takekiyo, T.; Koyama, Y.; Takaku, M.; Yamamura, M.; Kikuchi, N.; Wakabayashi, D.; Funamori, N.; Matsuishi, K.; Abe, H.; Hamaya, N. High-Pressure Glass Formation of a Series of 1-Alkyl-3-methylimidazolium Bis-(trifluoromethanesulfonyl)imide Homologues. *Phys. Chem. Chem. Phys.* **2018**, *20*, 199−205.
(406) Yamaguchi, T. Coupling Between the Mesoscopic Dynamics and Shear Stress of a Room-Temperature Ionic Liquid. *Phys. Chem. Chem. Phys.* **2018**, *20*, 17809−17817.
(407) Wang, Y. Disordering and Reordering of Ionic Liquids Under an External Electric Field. *J. Phys. Chem. B* **2009**, *113*, 11058−11060.
(408) Zhao, Y.; Dong, K.; Liu, X.; Zhang, S.; Zhu, J.; Wang, J. Structure of Ionic Liquids Under External Electric Field: A Molecular Dynamics Simulation. *Mol. Simul.* **2012**, *38*, 172−178.
(409) Chen, F.; Fang, G.; Yan, Z.; Pan, Y.; Liu, J.; Wang, L. Cation Conformational Changes of 1-Butyl-3-methylimidazolium Halides at High Pressures. *J. Phys. Chem. C* **2018**, *122*, 9320−9331.
(410) Abe, H.; Hamaya, N.; Koyama, Y.; Kishimura, H.; Takekiyo, T.; Yoshimura, Y.; Wakabayashi, D.; Funamori, N.; Matsuishi, K. Long Periodic Structure of a Room-Temperature Ionic Liquid by High-Pressure Small-Angle X-ray Scattering and Wide-Angle X-ray Scattering: 1-Decyl-3-methylimidazolium Chloride. *ChemPhysChem* **2018**, *19*, 1441−1447.
(411) Takekiyo, T.; Koyama, Y.; Shigemi, M.; Matsuishi, K.; Abe, H.; Hamaya, N.; Yoshimura, Y. Conformational Adjustment for High-Pressure Glass Formation of 1-Alkyl-3-methylimidazolium Tetrafluoroborate. *Phys. Chem. Chem. Phys.* **2017**, *19*, 863−870.
(412) Endo, T.; Kato, T.; Tozaki, K.-i.; Nishikawa, K. Phase Behaviors of Room Temperature Ionic Liquid Linked with Cation Conformational Changes: 1-Butyl-3-methylimidazolium Hexafluorophosphate. *J. Phys. Chem. B* **2010**, *114*, 407−411.
(413) Jiang, H. J.; Imberti, S.; Atkin, R.; Warr, G. G. Dichotomous Well-Defined Nanostructure with Weakly Arranged Ion Packing Explains the Solvency of Pyrrolidinium Acetate. *J. Phys. Chem. B* **2017**, *121*, 6610−6617.
(414) Das, L.; Kumar, R.; Maity, D. K.; Adhikari, S.; Dhiman, S. B.; Wishart, J. F. Pulse Radiolysis and Computational Studies on a Pyrrolidinium Dicyanamide Ionic Liquid: Detection of the Dimer Radical Anion. *J. Phys. Chem. A* **2018**, *122*, 3148−3155.
(415) Araque, J. C.; Hettige, J. J.; Margulis, C. J. Ionic Liquids—Conventional Solvent Mixtures, Structurally Different but Dynamically Similar. *J. Chem. Phys.* **2015**, *143*, 134505.
(416) Santos, C. S.; Murthy, N. S.; Baker, G. A.; Castner, E. W., Jr X-ray Scattering From Ionic Liquids with Pyrrolidinium Cations. *J. Chem. Phys.* **2011**, *134*, 121101.
(417) Li, S.; Bañuelos, J. L.; Guo, J.; Anovitz, L.; Rother, G.; Shaw, R. W.; Hillesheim, P. C.; Dai, S.; Baker, G. A.; Cummings, P. T. Alkyl Chain Length and Temperature Effects on Structural Properties of Pyrrolidinium-Based Ionic Liquids: A Combined Atomistic Simulation and Small-Angle X-ray Scattering Study. *J. Phys. Chem. Lett.* **2012**, *3*, 125−130.
(418) Kashyap, H. K.; Hettige, J. J.; Annapureddy, H. V. R.; Margulis, C. J. SAXS Anti-Peaks Reveal the Length-Scales of Dual Positive-Negative and Polar-Apolar Ordering in Room-Temperature Ionic Liquids. *Chem. Commun.* **2012**, *48*, 5103−5105.
(419) Borodin, O.; Smith, G. D. Structure and Dynamics of N-methyl-N-propylpyrrolidinium Bis(trifluoromethanesulfonyl)imide Ionic Liquid from Molecular Dynamics Simulations. *J. Phys. Chem. B* **2006**, *110*, 11481−11490.
(420) Kashyap, H. K.; Santos, C. S.; Daly, R. P.; Hettige, J. J.; Murthy, N. S.; Shirota, H.; Castner, E. W., Jr; Margulis, C. J. How Does the Ionic Liquid Organizational Landscape Change When Nonpolar Cationic Alkyl Groups Are Replaced by Polar Isoelectronic Diethers? *J. Phys. Chem. B* **2013**, *117*, 1130−1135.
(421) Smith, A. M.; Lovelock, K. R. J.; Gosvami, N. N.; Licence, P.; Dolan, A.; Welton, T.; Perkin, S. Monolayer to Bilayer Structural Transition in Confined Pyrrolidinium-Based Ionic Liquids. *J. Phys. Chem. Lett.* **2013**, *4*, 378−382.
(422) Sharma, S.; Gupta, A.; Kashyap, H. K. How the Structure of Pyrrolidinium Ionic Liquids is Susceptible to High Pressure. *J. Phys. Chem. B* **2016**, *120*, 3206−3214.
(423) Kashyap, H. K.; Santos, C. S.; Murthy, N. S.; Hettige, J. J.; Kerr, K.; Ramati, S.; Gwon, J.; Gohdo, M.; Lall-Ramnarine, S. I.; Wishart, J. F.; Margulis, C. J.; Castner, E. W. Structure of 1-Alkyl-1-methylpyrrolidinium Bis(trifluoromethylsulfonyl)amide Ionic Liquids with Linear, Branched, and Cyclic Alkyl Groups. *J. Phys. Chem. B* **2013**, *117*, 15328−15337.
(424) Lima, T. A.; Faria, L. F.; Paschoal, V. H.; Ribeiro, M. C. Glass Transition and Melting Lines of an Ionic Liquid. *J. Chem. Phys.* **2018**, *148*, 171101.
(425) Montanino, M.; Carewska, M.; Alessandrini, F.; Passerini, S.; Appetecchi, G. B. The Role of the Cation Aliphatic Side Chain Length in Piperidinium Bis(trifluoromethansulfonyl)imide Ionic Liquids. *Electrochim. Acta* **2011**, *57*, 153−159.
(426) Kakinuma, S.; Shirota, H. Femtosecond Raman-Induced Kerr Effect Study of Temperature-Dependent Intermolecular Dynamics in Molten Bis(trifluoromethylsulfonyl)amide Salts: Effects of Cation Species. *J. Phys. Chem. B* **2018**, *122*, 6033−6047.
(427) Wu, C.; De Visscher, A.; Gates, I. D. Comparison of Electronic and Physicochemical Properties Between Imidazolium-Based and Pyridinium-Based Ionic Liquids. *J. Phys. Chem. B* **2018**, *122*, 6771−6780.
(428) Araque, J. C.; Yadav, S. K.; Shadeck, M.; Maroncelli, M.; Margulis, C. J. How is Diffusion of Neutral and Charged Tracers Related to the Structure and Dynamics of a Room-Temperature Ionic Liquid? Large Deviations from Stokes-Einstein Behavior Explained. *J. Phys. Chem. B* **2015**, *119*, 7015−7029.
(429) Wu, E. C.; Kim, H. J.; Peteanu, L. A. Spectroscopic and MD Study of Dynamic and Structural Heterogeneities in Ionic Liquids. *J. Phys. Chem. B* **2017**, *121*, 1100−1107.

https://dx.doi.org/10.1021/acs.chemrev.9b00693
Chem. Rev. 2020, 120, 5798−5877

(430) Costa, R.; Pereira, C. M.; Silva, F. Electric Double Layer Studies at the Interface of Mercury-Binary Ionic Liquid Mixtures with a Common Anion. *RSC Adv.* **2013**, *3*, 11697−11706.
(431) Lawler, C.; Fayer, M. D. The Influence of Lithium Cations on Dynamics and Structure of Room Temperature Ionic Liquids. *J. Phys. Chem. B* **2013**, *117*, 9768−9774.
(432) Liu, H.; Maginn, E. Effect of Ion Structure on Conductivity in Lithium-Doped Ionic Liquid Electrolytes: A Molecular Dynamics Study. *J. Chem. Phys.* **2013**, *139*, 114508.
(433) Nasrabadi, A. T.; Gelb, L. D. Structural and Transport Properties of Tertiary Ammonium Triflate Ionic Liquids: A Molecular Dynamics Study. *J. Phys. Chem. B* **2017**, *121*, 1908−1921.
(434) Tsuzuki, S.; Shinoda, W.; Miran, M. S.; Kinoshita, H.; Yasuda, T.; Watanabe, M. Interactions in Ion Pairs of Protic Ionic Liquids: Comparison with Aprotic Ionic Liquids. *J. Chem. Phys.* **2013**, *139*, 174504.
(435) Pott, T.; Méléard, P. New Insight into the Nanostructure of Ionic Liquids: A Small Angle X-ray Scattering (SAXS) Study on Liquid Trialkylmethylammonium Bis(trifluoromethanesulfonyl)-amides and Their Mixtures. *Phys. Chem. Chem. Phys.* **2009**, *11*, 5469−5475.
(436) Santos, C. S.; Annapureddy, H. V.; Murthy, N. S.; Kashyap, H. K.; Castner, E. W., Jr; Margulis, C. J. Temperature-Dependent Structure of Methyltributylammonium Bis(trifluoromethylsulfonyl)-amide: X-ray Scattering and Simulations. *J. Chem. Phys.* **2011**, *134*, 064501.
(437) Shimizu, K.; Pádua, A. l. A.; Canongia Lopes, J. N. Nanostructure of Trialkylmethylammonium Bistriflamide Ionic Liquids Studied by Molecular Dynamics. *J. Phys. Chem. B* **2010**, *114*, 15635−15641.
(438) Iimori, T.; Iwahashi, T.; Ishii, H.; Seki, K.; Ouchi, Y.; Ozawa, R.; Hamaguchi, H.-O.; Kim, D. Orientational Ordering of Alkyl Chain at the Air/Liquid Interface of Ionic Liquids Studied by Sum Frequency Vibrational Spectroscopy. *Chem. Phys. Lett.* **2004**, *389*, 321−326.
(439) Yasui, Y.; Kitazumi, Y.; Ishimatsu, R.; Nishi, N.; Kakiuchi, T. Ultraslow Response of Interfacial Tension to the Change in the Phase-Boundary Potential at the Interface Between Water and a Room-Temperature Ionic Liquid, Trioctylmethylammonium Bis-(nonafluorobutanesulfonyl)amide. *J. Phys. Chem. B* **2009**, *113*, 3273−3276.
(440) Hanke, K.; Kaufmann, M.; Schwaab, G.; Havenith, M.; Wolke, C. T.; Gorlova, O.; Johnson, M. A.; Kar, B. P.; Sander, W.; Sanchez-Garcia, E. Understanding the Ionic Liquid $[N_{4111}][NTf_2]$ From Individual Building Blocks: An IR-Spectroscopic Study. *Phys. Chem. Chem. Phys.* **2015**, *17*, 8518−8529.
(441) Mendil-Jakani, H.; Baroni, P.; Noirez, L.; Chancelier, L.; Gebel, G. Highlighting a Solid-Like Behavior in RTILs: Trioctylmethylammonium Bis(trifluoromethanesulfonyl)imide TOMA-TFSI. *J. Phys. Chem. Lett.* **2013**, *4*, 3775−3778.
(442) Yamaguchi, T.; Nakahara, E.; Sueda, K.; Koda, S. Interpretation of the Variation of the Walden Product of Ionic Liquids with Different Alkyl Chain Lengths in Terms of Relaxation Spectra. *J. Phys. Chem. B* **2013**, *117*, 4121−4126.
(443) Ke, Y.; Jin, W.; Yang, Q.; Suo, X.; Yang, Y.; Ren, Q.; Xing, H. Nanostructured Branched-Chain Carboxylate Ionic Liquids: Synthesis, Characterization and Extraordinary Solubility for Bioactive Molecules. *ACS Sustainable Chem. Eng.* **2018**, *6*, 8983−8991.
(444) del Olmo, L.; Lage-Estebanez, I.; López, R.; Garcia de la Vega, J. M. Understanding the Structure and Properties of Cholinium Amino Acid Based Ionic Liquids. *J. Phys. Chem. B* **2016**, *120*, 10327−10335.
(445) Campetella, M.; Le Donne, A.; Daniele, M.; Gontrani, L.; Lupi, S.; Bodo, E.; Leonelli, F. Hydrogen Bonding Features in Cholinium-Based Protic Ionic Liquids From Molecular Dynamics Simulations. *J. Phys. Chem. B* **2018**, *122*, 2635−2645.
(446) Campetella, M.; Bodo, E.; Montagna, M.; De Santis, S.; Gontrani, L. Theoretical Study of Ionic Liquids Based on the Cholinium Cation. Ab Initio Simulations of Their Condensed Phases. *J. Chem. Phys.* **2016**, *144*, 104504.
(447) Aparicio, S.; Atilhan, M.; Pala, N. Insights on Cholinium- and Piperazinium-Based Ionic Liquids Under External Electric Fields: A Molecular Dynamics Study. *J. Chem. Phys.* **2013**, *139*, 224502.
(448) Triolo, A.; Russina, O.; Caminiti, R.; Shirota, H.; Lee, H. Y.; Santos, C. S.; Murthy, N. S.; Castner, E. W., Jr. Comparing Intermediate Range Order for Alkyl- vs. Ether-Substituted Cations in Ionic Liquids. *Chem. Commun.* **2012**, *48*, 4959−4961.
(449) Siqueira, L. J.; Ribeiro, M. C. Charge Ordering and Intermediate Range Order in Ammonium Ionic Liquids. *J. Chem. Phys.* **2011**, *135*, 204506.
(450) Siqueira, L. J.; Ribeiro, M. C. Molecular Dynamics Simulation of the Ionic Liquid N-ethyl-N,N-dimethyl-N-(2-methoxyethyl)-ammonium Bis(trifluoromethanesulfonyl)imide. *J. Phys. Chem. B* **2007**, *111*, 11776−11785.
(451) Lee, H. Y.; Shirota, H.; Castner, E. W., Jr Differences in Ion Interactions for Isoelectronic Ionic Liquid Homologs. *J. Phys. Chem. Lett.* **2013**, *4*, 1477−1483.
(452) Shirota, H.; Fukazawa, H.; Fujisawa, T.; Wishart, J. F. Heavy Atom Substitution Effects in non-Aromatic Ionic Liquids: Ultrafast Dynamics and Physical Properties. *J. Phys. Chem. B* **2010**, *114*, 9400−9412.
(453) Scarbath-Evers, L. K.; Hunt, P. A.; Kirchner, B.; MacFarlane, D. R.; Zahn, S. Molecular Features Contributing to the Lower Viscosity of Phosphonium Ionic Liquids Compared to Their Ammonium Analogues. *Phys. Chem. Chem. Phys.* **2015**, *17*, 20205−20216.
(454) Philippi, F.; Rauber, D.; Zapp, J.; Hempelmann, R. Transport Properties and Ionicity of Phosphonium Ionic Liquids. *Phys. Chem. Chem. Phys.* **2017**, *19*, 23015−23023.
(455) Carvalho, P. J.; Ventura, S. P.; Batista, M. L.; Schröder, B.; Gonçalves, F.; Esperança, J.; Mutelet, F.; Coutinho, J. A. Understanding the Impact of the Central Atom on the Ionic Liquid Behavior: Phosphonium vs Ammonium Cations. *J. Chem. Phys.* **2014**, *140*, 064505.
(456) Marták, J.; Schlosser, Š. New Mechanism and Model of Butyric Acid Extraction by Phosphonium Ionic Liquid. *J. Chem. Eng. Data* **2016**, *61*, 2979−2996.
(457) Chen, F.; Jin, L.; De Leeuw, S.; Pringle, J.; Forsyth, M. Atomistic Simulation of Structure and Dynamics of the Plastic Crystal Diethyl(methyl)(isobutyl)phosphonium Hexafluorophosphate. *J. Chem. Phys.* **2013**, *138*, 244503.
(458) Carignano, M. A. Structure and Dynamics of $[PF_6][P_{1,2,2,4}]$ from Molecular Dynamics Simulations. *J. Phys. Chem. B* **2013**, *117*, 15176−15183.
(459) Gupta, A.; Sharma, S.; Kashyap, H. K. Composition Dependent Structural Organization in Trihexyl(tetradecyl)-phosphonium Chloride Ionic Liquid-Methanol Mixtures. *J. Chem. Phys.* **2015**, *142*, 134503.
(460) Sharma, S.; Gupta, A.; Dhabal, D.; Kashyap, H. K. Pressure-Dependent Morphology of Trihexyl(tetradecyl)phosphonium Ionic Liquids: A Molecular Dynamics Study. *J. Chem. Phys.* **2016**, *145*, 134506.
(461) Yamaguchi, T.; Koda, S. Dielectric and Shear Relaxations of Ionic Liquid Composed of Symmetric Ions. *J. Chem. Phys.* **2014**, *141*, 144503.
(462) Hettige, J. J.; Araque, J. C.; Kashyap, H. K.; Margulis, C. J. Nanoscale Structure of Tetradecyltrihexylphosphonium Based Ionic Liquids. *J. Chem. Phys.* **2016**, *144*, 121102.
(463) Tanner, E. E. L.; Barnes, E. O.; Tickell, C. B.; Goodrich, P.; Hardacre, C.; Compton, R. G. Application of Asymmetric Marcus-Hush Theory to Voltammetry in Room-Temperature Ionic Liquids. *J. Phys. Chem. C* **2015**, *119*, 7360−7370.
(464) Liu, H.; Paddison, S. J. Direct Calculation of the X-ray Structure Factor of Ionic Liquids. *Phys. Chem. Chem. Phys.* **2016**, *18*, 11000−11007.

https://dx.doi.org/10.1021/acs.chemrev.9b00693
Chem. Rev. 2020, 120, 5798−5877

(465) Hettige, J. J.; Kashyap, H. K.; Margulis, C. J. Anomalous Temperature Dependence of the Intermediate Range Order in Phosphonium Ionic Liquids. *J. Chem. Phys.* **2014**, *140*, 111102.
(466) An, R.; Zhou, G.; Zhu, Y.; Zhu, W.; Huang, L.; Shah, F. U. Friction of Ionic Liquid−Glycol Ether Mixtures at Titanium Interfaces: Negative Load Dependence. *Adv. Mater. Interfaces* **2018**, *5*, 1800263.
(467) Sarman, S.; Wang, Y.-L.; Rohlmann, P.; Glavatskih, S.; Laaksonen, A. Rheology of Phosphonium Ionic Liquids: A Molecular Dynamics and Experimental Study. *Phys. Chem. Chem. Phys.* **2018**, *20*, 10193−10203.
(468) Pei, H.-W.; Li, B.; Laaksonen, A.; Wang, Y.-L. How Molecular Chiralities of Bis(mandelato)borate Anions Affect Their Binding Structures with Alkali Metal Ions and Microstructural Properties in Tetraalkylphosphonium Ionic Liquids. *Front. Chem.* **2020**, *8*, 65.
(469) Hanke, C. G.; Lynden-Bell, R. M. A Simulation Study of Water-Dialkylimidazolium Ionic Liquid Mixtures. *J. Phys. Chem. B* **2003**, *107*, 10873−10878.
(470) Klähn, M.; Stüber, C.; Seduraman, A.; Wu, P. What Determines the Miscibility of Ionic Liquids with Water? Identification of the Underlying Factors to Enable a Straightforward Prediction. *J. Phys. Chem. B* **2010**, *114*, 2856−2868.
(471) Anthony, J. L.; Maginn, E. J.; Brennecke, J. F. Solution Thermodynamics of Imidazolium-Based Ionic Liquids and Water. *J. Phys. Chem. B* **2001**, *105*, 10942−10949.
(472) Lynden-Bell, R.; Atamas, N.; Vasilyuk, A.; Hanke, C. Chemical Potentials of Water and Organic Solutes in Imidazolium Ionic Liquids: A Simulation Study. *Mol. Phys.* **2002**, *100*, 3225−3229.
(473) Wang, Y.-L.; Sarman, S.; Kloo, L.; Antzutkin, O. N.; Glavatskih, S.; Laaksonen, A. Solvation Structures of Water in Trihexyltetradecylphosphonium-Orthoborate Ionic Liquids. *J. Chem. Phys.* **2016**, *145*, 064507.
(474) Seddon, K. R.; Stark, A.; Torres, M.-J. Influence of Chloride, Water, and Organic Solvents on the Physical Properties of Ionic Liquids. *Pure Appl. Chem.* **2000**, *72*, 2275−2287.
(475) Freire, M. G.; Carvalho, P. J.; Gardas, R. L.; Marrucho, I. M.; Santos, L. M.; Coutinho, J. A. Mutual Solubilities of Water and the $[C_n mim][Tf_2N]$ Hydrophobic Ionic Liquids. *J. Phys. Chem. B* **2008**, *112*, 1604−1610.
(476) Alfassi, Z.; Huie, R. E.; Milman, B.; Neta, P. Electrospray Ionization Mass Spectrometry of Ionic Liquids and Determination of Their Solubility in Water. *Anal. Bioanal. Chem.* **2003**, *377*, 159−164.
(477) Maiti, A.; Kumar, A.; Rogers, R. D. Water-Clustering in Hygroscopic Ionic Liquids—An Implicit Solvent Analysis. *Phys. Chem. Chem. Phys.* **2012**, *14*, 5139−5146.
(478) Aki, S. N.; Brennecke, J. F.; Samanta, A. How Polar Are Room-Temperature Ionic Liquids? *Chem. Commun.* **2001**, 413−414.
(479) Freire, M. G.; Neves, C. M.; Carvalho, P. J.; Gardas, R. L.; Fernandes, A. M.; Marrucho, I. M.; Santos, L. M.; Coutinho, J. A. Mutual Solubilities of Water and Hydrophobic Ionic Liquids. *J. Phys. Chem. B* **2007**, *111*, 13082−13089.
(480) Kaneko, K.; Saihara, K.; Masuda, Y.; Yoshimura, Y.; Shimizu, A. Dynamic Properties of Water Molecules in Ionic Liquid/Water Mixture with Various Alkyl Chain Length. *J. Mol. Liq.* **2018**, *264*, 337−342.
(481) Saihara, K.; Yoshimura, Y.; Ohta, S.; Shimizu, A. Properties of Water Confined in Ionic Liquids. *Sci. Rep.* **2015**, *5*, 10619.
(482) Fadeeva, T. A.; Husson, P.; DeVine, J. A.; Costa Gomes, M. F.; Greenbaum, S. G.; Castner, E. W., Jr Interactions Between Water and 1-Butyl-1-methylpyrrolidinium Ionic Liquids. *J. Chem. Phys.* **2015**, *143*, 064503.
(483) Cha, S.; Ao, M.; Sung, W.; Moon, B.; Ahlström, B.; Johansson, P.; Ouchi, Y.; Kim, D. Structures of Ionic Liquid-Water Mixtures Investigated by IR and NMR Spectroscopy. *Phys. Chem. Chem. Phys.* **2014**, *16*, 9591−9601.
(484) Jeon, Y.; Sung, J.; Kim, D.; Seo, C.; Cheong, H.; Ouchi, Y.; Ozawa, R.; Hamaguchi, H.-O. Structural Change of 1-Butyl-3-methylimidazolium Tetrafluoroborate+Water Mixtures Studied by Infrared Vibrational Spectroscopy. *J. Phys. Chem. B* **2008**, *112*, 923−928.
(485) Sun, B.; Jin, Q.; Tan, L.; Wu, P.; Yan, F. Trace of the Interesting "V"-Shaped Dynamic Mechanism of Interactions Between Water and Ionic Liquids. *J. Phys. Chem. B* **2008**, *112*, 14251−14259.
(486) Cammarata, L.; Kazarian, S.; Salter, P.; Welton, T. Molecular States of Water in Room Temperature Ionic Liquids. *Phys. Chem. Chem. Phys.* **2001**, *3*, 5192−5200.
(487) Takamuku, T.; Kyoshoin, Y.; Shimomura, T.; Kittaka, S.; Yamaguchi, T. Effect of Water on Structure of Hydrophilic Imidazolium-Based Ionic Liquid. *J. Phys. Chem. B* **2009**, *113*, 10817−10824.
(488) van der Post, S. T.; Scheidelaar, S.; Bakker, H. J. Water Dynamics in Aqueous Solutions of Tetra-n-alkylammonium Salts: Hydrophobic and Coulomb Interactions Disentangled. *J. Phys. Chem. B* **2013**, *117*, 15101−15110.
(489) D'Angelo, P.; Zitolo, A.; Migliorati, V.; Bodo, E.; Aquilanti, G.; Hazemann, J. L.; Testemale, D.; Mancini, G.; Caminiti, R. X-Ray Absorption Spectroscopy Investigation of 1-Alkyl-3-methylimidazolium Bromide Salts. *J. Chem. Phys.* **2011**, *135*, 074505.
(490) Danten, Y.; Cabaco, M.; Besnard, M. Interaction of Water Highly Diluted in 1-Alkyl-3-methylimidazolium Ionic Liquids with the PF_6 and BF_4 Anions. *J. Phys. Chem. A* **2009**, *113*, 2873−2889.
(491) Wang, Y.-L.; Sarman, S.; Glavatskih, S.; Antzutkin, O. N.; Rutland, M. W.; Laaksonen, A. Atomistic Insight into Tetraalkylphosphonium-Bis(oxalato)borate Ionic Liquid/Water Mixtures. I. Local Microscopic Structure. *J. Phys. Chem. B* **2015**, *119*, 5251−5264.
(492) Jiang, W.; Wang, Y.; Voth, G. A. Molecular Dynamics Simulation of Nanostructural Organization in Ionic Liquid/Water Mixtures. *J. Phys. Chem. B* **2007**, *111*, 4812−4818.
(493) Serva, A.; Migliorati, V.; Lapi, A.; Aquilanti, G.; Arcovito, A.; D'Angelo, P. Structural Properties of Geminal Dicationic Ionic Liquid/Water Mixtures: A Theoretical and Experimental Insight. *Phys. Chem. Chem. Phys.* **2016**, *18*, 16544−16554.
(494) Abe, H.; Imai, Y.; Takekiyo, T.; Yoshimura, Y. Deuterated Water Effect in a Room Temperature Ionic Liquid: N, N-diethyl-N-methyl-N-2-methoxyethyl Ammonium Tetrafluoroborate. *J. Phys. Chem. B* **2010**, *114*, 2834−2839.
(495) López-Pastor, M.; Ayora-Cañada, M. J.; Valcárcel, M.; Lendl, B. Association of Methanol and Water in Ionic Liquids Elucidated by Infrared Spectroscopy Using Two-Dimensional Correlation and Multivariate Curve Resolution. *J. Phys. Chem. B* **2006**, *110*, 10896−10902.
(496) Abe, H.; Takekiyo, T.; Yoshimura, Y.; Saihara, K.; Shimizu, A. Anomalous Freezing of Nano-Confined Water in Room-Temperature Ionic Liquid 1-Butyl-3-methylimidazolium Nitrate. *ChemPhysChem* **2016**, *17*, 1136−1142.
(497) Usula, M.; Mocci, F.; Marincola, F. C.; Porcedda, S.; Gontrani, L.; Caminiti, R. The Structural Organization of N-methyl-2-pyrrolidone+Water Mixtures: A Densitometry, X-ray Diffraction, and Molecular Dynamics Study. *J. Chem. Phys.* **2014**, *140*, 124503.
(498) Bailey, H. E.; Wang, Y.-L.; Lynch, S. R.; Fayer, M. D. Dynamics and Microstructures of Nicotine/Water Binary Mixtures Near the Lower Critical Solution Temperature. *J. Phys. Chem. B* **2018**, *122*, 9538−9548.
(499) Kraack, J. P.; Hamm, P. Surface-Sensitive and Surface-Specific Ultrafast Two-Dimensional Vibrational Spectroscopy. *Chem. Rev.* **2017**, *117*, 10623−10664.
(500) Huang, Y.; Wan, Z.; Yang, Z.; Ji, Y.; Li, L.; Yang, D.; Zhu, M.; Chen, X. Concentration-Dependent Hydrogen Bond Behavior of Ethylammonium Nitrate Protic Ionic Liquid-Water Mixtures Explored by Molecular Dynamics Simulations. *J. Chem. Eng. Data* **2017**, *62*, 2340−2349.
(501) Migliorati, V.; Ballirano, P.; Gontrani, L.; Materazzi, S.; Ceccacci, F.; Caminiti, R. A Combined Theoretical and Experimental Study of Solid Octyl and Decylammonium Chlorides and of Their Aqueous Solutions. *J. Phys. Chem. B* **2013**, *117*, 7806−7818.
(502) Salma, U.; Usula, M.; Caminiti, R.; Gontrani, L.; Plechkova, N. V.; Seddon, K. R. X-ray and Molecular Dynamics Studies of

https://dx.doi.org/10.1021/acs.chemrev.9b00693
Chem. Rev. 2020, 120, 5798−5877

Butylammonium Butanoate-Water Binary Mixtures. *Phys. Chem. Chem. Phys.* **2017**, *19*, 1975−1981.
(503) Hayes, R.; Imberti, S.; Warr, G. G.; Atkin, R. How Water Dissolves in Protic Ionic Liquids. *Angew. Chem., Int. Ed.* **2012**, *51*, 7468−7471.
(504) Greaves, T. L.; Kennedy, D. F.; Weerawardena, A.; Tse, N. M. K.; Kirby, N.; Drummond, C. J. Nanostructured Protic Ionic Liquids Retain Nanoscale Features in Aqueous Solution While Precursor Brønsted Acids and Bases Exhibit Different Behavior. *J. Phys. Chem. B* **2011**, *115*, 2055−2066.
(505) Reichardt, C. Polarity of Ionic Liquids Determined Empirically by Means of Solvatochromic Pyridinium N-phenolate Betaine Dyes. *Green Chem.* **2005**, *7*, 339−351.
(506) Hadded, M.; Mayaffre, A.; Letellier, P. Surface-Tension of Ideal Solutions-Application to Binary-Mixtures of Methanol and Molten Ethylammonium Nitrate at 298 K. *J. Chim. Phys. Phys.-Chim. Biol.* **1989**, *86*, 525−537.
(507) Heimburg, T.; Mirzaev, S.; Kaatze, U. Heat Capacity Behavior in the Critical Region of the Ionic Binary Mixture Ethylammonium Nitrate-n-Octanol. *Phys. Rev. E: Stat. Phys., Plasmas, Fluids, Relat. Interdiscip. Top.* **2000**, *62*, 4963−4967.
(508) Russina, O.; Sferrazza, A.; Caminiti, R.; Triolo, A. Amphiphile Meets Amphiphile: Beyond the Polar-Apolar Dualism in Ionic Liquid/Alcohol Mixtures. *J. Phys. Chem. Lett.* **2014**, *5*, 1738−1742.
(509) Varela, L.; Méndez-Morales, T.; Carrete, J.; Gómez-González, V.; Docampo-Álvarez, B.; Gallego, L.; Cabeza, O.; Russina, O. Solvation of Molecular Cosolvents and Inorganic Salts in Ionic Liquids: A Review of Molecular Dynamics Simulations. *J. Mol. Liq.* **2015**, *210*, 178−188.
(510) Kundu, N.; Roy, A.; Dutta, R.; Sarkar, N. Translational and Rotational Diffusion of Two Differently Charged Solutes in Ethylammonium Nitrate-Methanol Mixture: Does the Nanostructure of the Amphiphiles Influence the Motion of the Solute? *J. Phys. Chem. B* **2016**, *120*, 5481−5490.
(511) Murphy, T.; Hayes, R.; Imberti, S.; Warr, G. G.; Atkin, R. Ionic Liquid Nanostructure Enables Alcohol Self Assembly. *Phys. Chem. Chem. Phys.* **2016**, *18*, 12797−12809.
(512) Shrivastav, G.; Gupta, A.; Rastogi, A.; Dhabal, D.; Kashyap, H. K. Molecular Dynamics Study of Nanoscale Organization and Hydrogen Bonding in Binary Mixtures of Butylammonium Nitrate Ionic Liquid and Primary Alcohols. *J. Chem. Phys.* **2017**, *146*, 064503.
(513) Montes-Campos, H.; Otero-Mato, J. M.; Méndez-Morales, T.; López-Lago, E.; Russina, O.; Cabeza, O.; Gallego, L. J.; Varela, L. M. Nanostructured Solvation in Mixtures of Protic Ionic Liquids and Long-Chained Alcohols. *J. Chem. Phys.* **2017**, *146*, 124503.
(514) Chakraborty, T.; Ghosh, S.; Moulik, S. P. Micellization and Related Behavior of Binary and Ternary Surfactant Mixtures in Aqueous Medium: Cetyl Pyridinium Chloride (CPC), Cetyl Trimethyl Ammonium Bromide (CTAB), and Polyoxyethylene (10) Cetyl Ether (Brij-56) Derived System. *J. Phys. Chem. B* **2005**, *109*, 14813−14823.
(515) Schroer, W.; Triolo, A.; Russina, O. Nature of Mesoscopic Organization in Protic Ionic Liquid-Alcohol Mixtures. *J. Phys. Chem. B* **2016**, *120*, 2638−2643.
(516) Domańska, U.; Marciniak, A. Solubility of Ionic Liquid [Emim][PF_6] in Alcohols. *J. Phys. Chem. B* **2004**, *108*, 2376−2382.
(517) Domanska, U.; Rekawek, A.; Marciniak, A. Solubility of 1-Alkyl-3-ethylimidazolium-Based Ionic Liquids in Water and 1-Octanol. *J. Chem. Eng. Data* **2008**, *53*, 1126−1132.
(518) Vale, V. R.; Rathke, B.; Will, S.; Schröer, W. Liquid-Liquid Phase Behavior of Solutions of 1-Octyl- and 1-Decyl-3-methylimidazolium Bis(trifluoromethylsulfonyl)imide ($C_{8,10}$mimNTf_2) in n-Alkyl Alcohols. *J. Chem. Eng. Data* **2010**, *55*, 2030−2038.
(519) Vaz, I. C.; Bhattacharjee, A.; Rocha, M. A.; Coutinho, J. A.; Bastos, M.; Santos, L. M. Alcohols as Molecular Probes in Ionic Liquids: Evidence for Nanostructuration. *Phys. Chem. Chem. Phys.* **2016**, *18*, 19267−19275.
(520) Heintz, A.; Lehmann, J. K.; Wertz, C. Thermodynamic Properties of Mixtures Containing Ionic Liquids. 3. Liquid−Liquid Equilibria of Binary Mixtures of 1-Ethyl-3-methylimidazolium Bis-(trifluoromethylsulfonyl)imide with Propan-1-ol, Butan-1-ol, and Pentan-1-ol. *J. Chem. Eng. Data* **2003**, *48*, 472−474.
(521) Heintz, A.; Klasen, D.; Lehmann, J. K.; Wertz, C. Excess Molar Volumes and Liquid-Liquid Equilibria of the Ionic Liquid 1-Methyl-3-octyl-imidazolium Tetrafluoroborate Mixed with Butan-1-ol and Pentan-1-ol. *J. Solution Chem.* **2005**, *34*, 1135−1144.
(522) Crosthwaite, J. M.; Aki, S. N.; Maginn, E. J.; Brennecke, J. F. Liquid Phase Behavior of Imidazolium-Based Ionic Liquids with Alcohols: Effect of Hydrogen Bonding and non-Polar Interactions. *Fluid Phase Equilib.* **2005**, *228*, 303−309.
(523) Łachwa, J.; Morgado, P.; Esperanca, J. M.; Guedes, H. J.; Canongia Lopes, J. N.; Rebelo, L. P. N. Fluid-Phase Behavior of {1-Hexyl-3-methylimidazolium Bis(trifluoromethylsulfonyl)imide, [C_6mim][NTf_2], + C_2−C_8 n-Alcohol} Mixtures: Liquid-Liquid Equilibrium and Excess Volumes. *J. Chem. Eng. Data* **2006**, *51*, 2215−2221.
(524) Vale, V. R.; Will, S.; Schröer, W.; Rathke, B. The General Phase Behavior of Mixtures of 1-Alkyl-3-methylimidazolium Bis-[(trifluoromethyl)sulfonyl]amide Ionic Liquids with n-Alkyl Alcohols. *ChemPhysChem* **2012**, *13*, 1860−1867.
(525) Pereiro, A.; Rodriguez, A. Study on the Phase Behaviour and Thermodynamic Properties of Ionic Liquids Containing Imidazolium Cation with Ethanol at Several Temperatures. *J. Chem. Thermodyn.* **2007**, *39*, 978−989.
(526) Abe, H.; Fukushima, R.; Onji, M.; Hirayama, K.; Kishimura, H.; Yoshimura, Y.; Ozawa, S. Two-Length Scale Description of Hydrophobic Room-Temperature Ionic Liquid-Alcohol Systems. *J. Mol. Liq.* **2016**, *215*, 417−422.
(527) Rodrigues, A. S.; Rocha, M. A.; Almeida, H. F.; Neves, C. M.; Lopes-da-Silva, J. A.; Freire, M. G.; Coutinho, J. o. A.; Santos, L. M. Effect of the Methylation and N-H Acidic Group on the Physicochemical Properties of Imidazolium-Based Ionic Liquids. *J. Phys. Chem. B* **2015**, *119*, 8781−8792.
(528) Crosthwaite, J. M.; Aki, S. N.; Maginn, E. J.; Brennecke, J. F. Liquid Phase Behavior of Imidazolium-Based Ionic Liquids with Alcohols. *J. Phys. Chem. B* **2004**, *108*, 5113−5119.
(529) Paduszyński, K.; Królikowski, M.; Domańska, U. Excess Enthalpies of Mixing of Piperidinium Ionic Liquids with Short-Chain Alcohols: Measurements and PC-SAFT Modeling. *J. Phys. Chem. B* **2013**, *117*, 3884−3891.
(530) Cláudio, A. F. M.; Swift, L.; Hallett, J. P.; Welton, T.; Coutinho, J. A.; Freire, M. G. Extended Scale for the Hydrogen-Bond Basicity of Ionic Liquids. *Phys. Chem. Chem. Phys.* **2014**, *16*, 6593−6601.
(531) Bernardes, C. E S; Shimizu, K.; Canongia Lopes, J. N Solvent Effects on the Polar Network of Ionic Liquid Solutions. *J. Phys.: Condens. Matter* **2015**, *27*, 194116.
(532) Jahangiri, S.; Taghikhani, M.; Behnejad, H.; Ahmadi, S. Theoretical Investigation of Imidazolium Based Ionic Liquid/Alcohol Mixture: A Molecular Dynamic Simulation. *Mol. Phys.* **2008**, *106*, 1015−1023.
(533) Mendez-Morales, T.; Carrete, J.; Cabeza, O.; Gallego, L.; Varela, L. Molecular Dynamics Simulations of the Structural and Thermodynamic Properties of Imidazolium-Based Ionic Liquid Mixtures. *J. Phys. Chem. B* **2011**, *115*, 11170−11182.
(534) Agrawal, S.; Kashyap, H. K. Structures of Binary Mixtures of Ionic Liquid 1-Butyl-3-methylimidazolium Bis-(trifluoromethylsulfonyl)imide with Primary Alcohols: The Role of Hydrogen-Bonding. *J. Mol. Liq.* **2018**, *261*, 337−349.
(535) Chen, M.; Pendrill, R.; Widmalm, G. r.; Brady, J. W.; Wohlert, J. Molecular Dynamics Simulations of the Ionic Liquid 1-n-Butyl-3-methylimidazolium Chloride and Its Binary Mixtures with Ethanol. *J. Chem. Theory Comput.* **2014**, *10*, 4465−4479.
(536) Sharma, A.; Ghorai, P. K. Effect of Alcohols on the Structure and Dynamics of [BMIM][PF_6] Ionic Liquid: A Combined Molecular Dynamics Simulation and Voronoi Tessellation Investigation. *J. Chem. Phys.* **2018**, *148*, 204514.

https://dx.doi.org/10.1021/acs.chemrev.9b00693
Chem. Rev. 2020, 120, 5798−5877

(537) Méndez-Morales, T.; Carrete, J.; García, M.; Cabeza, O.; Gallego, L. J.; Varela, L. M. Dynamical Properties of Alcohol+1-Hexyl-3-methylimidazolium Ionic Liquid Mixtures: A Computer Simulation Study. *J. Phys. Chem. B* **2011**, *115*, 15313−15322.
(538) Vaz, I. C. M.; Bastos, M.; Bernardes, C. E. S.; Canongia Lopes, J. N.; Santos, L. M. N. B. F. Solvation of Alcohols in Ionic Liquids-Understanding the Effect of the Anion and Cation. *Phys. Chem. Chem. Phys.* **2018**, *20*, 2536−2548.
(539) Kurnia, K. A.; Lima, F.; Cláudio, A. F. M.; Coutinho, J. A.; Freire, M. G. Hydrogen-Bond Acidity of Ionic Liquids: An Extended Scale. *Phys. Chem. Chem. Phys.* **2015**, *17*, 18980−18990.
(540) Vahid, A.; Maginn, E. J. Monte Carlo Simulation and SAFT Modeling Study of the Solvation Thermodynamics of Dimethylformamide, Dimethylsulfoxide, Ethanol and 1-Propanol in the Ionic Liquid Trimethylbutylammonium Bis(trifluoromethylsulfonyl)imide. *Phys. Chem. Chem. Phys.* **2015**, *17*, 7449−7462.
(541) Barra, K. M.; Sabatini, R. P.; McAtee, Z. P.; Heitz, M. P. Solvation and Rotation Dynamics in the Trihexyl(tetradecyl)-phosphonium Chloride Ionic Liquid/Methanol Cosolvent System. *J. Phys. Chem. B* **2014**, *118*, 12979−12992.
(542) Forse, A. C.; Griffin, J. M.; Merlet, C.; Bayley, P. M.; Wang, H.; Simon, P.; Grey, C. P. NMR Study of Ion Dynamics and Charge Storage in Ionic Liquid Supercapacitors. *J. Am. Chem. Soc.* **2015**, *137*, 7231−7242.
(543) Zhang, S.; Zhang, Y.; Ma, X.; Lu, L.; He, Y.; Deng, Y. Benzonitrile as a Probe of Local Environment in Ionic Liquids. *J. Phys. Chem. B* **2013**, *117*, 2764−2772.
(544) Mariani, A.; Caminiti, R.; Ramondo, F.; Salvitti, G.; Mocci, F.; Gontrani, L. Inhomogeneity in Ethylammonium Nitrate-Acetonitrile Binary Mixtures: The Highest "Low q Excess" Reported to Date. *J. Phys. Chem. Lett.* **2017**, *8*, 3512−3522.
(545) Mancini, P.; Fortunato, G.; Vottero, L. Molecular Solvent/Ionic Liquid Binary Mixtures: Designing Solvents Based on the Determination of Their Microscopic Properties. *Phys. Chem. Liq.* **2004**, *42*, 625−632.
(546) Mariani, A.; Bonomo, M.; Wu, B.; Centrella, B.; Dini, D.; Castner, E. W., Jr.; Gontrani, L. Intriguing Transport Dynamics of Ethylammonium Nitrate−Acetonitrile Binary Mixtures Arising from Nano-Inhomogeneity. *Phys. Chem. Chem. Phys.* **2017**, *19*, 27212−27220.
(547) Sonnleitner, T.; Nikitina, V.; Nazet, A.; Buchner, R. Do H-bonds Explain Strong Ion Aggregation in Ethylammonium Nitrate + Acetonitrile Mixtures? *Phys. Chem. Chem. Phys.* **2013**, *15*, 18445−18452.
(548) Xu, J.; Deng, G.; Zhou, Y.; Ashraf, H.; Yu, Z.-W. Hydroxyl Group as IR Probe to Detect the Structure of Ionic Liquid-Acetonitrile Mixtures. *J. Mol. Struct.* **2018**, *1161*, 424−432.
(549) Bešter-Rogač, M.; Stoppa, A.; Buchner, R. Ion Association of Imidazolium Ionic Liquids in Acetonitrile. *J. Phys. Chem. B* **2014**, *118*, 1426−1435.
(550) Asaki, M.; Redondo, A.; Zawodzinski, T.; Taylor, A. Dielectric Relaxation and Underlying Dynamics of Acetonitrile and 1-Ethyl-3-methylimidazolium Triflate Mixtures Using THz Transmission Spectroscopy. *J. Chem. Phys.* **2002**, *116*, 10377−10385.
(551) Feng, G.; Huang, J.; Sumpter, B. G.; Meunier, V.; Qiao, R. A "Counter-Charge Layer in Generalized Solvents" Framework for Electrical Double Layers in Neat and Hybrid Ionic Liquid Electrolytes. *Phys. Chem. Chem. Phys.* **2011**, *13*, 14723−14734.
(552) Conway, B.; Uitvlugt, C.; Maroncelli, M. Simulations of 1-Butyl-3-methylimidazolium Tetrafluoroborate + Acetonitrile Mixtures: Force-Field Validation and Frictional Characteristics. *J. Phys. Chem. B* **2018**, *122*, 7385−7393.
(553) Koverga, V.; Kalugin, O. N.; Miannay, F.-A.; Smortsova, Y.; Goloviznina, K.; Marekha, B.; Jedlovszky, P.; Idrissi, A. The Local Structure in $BmimPF_6$/Acetonitrile Mixture: The Charge Distribution Effect. *Phys. Chem. Chem. Phys.* **2018**, *20*, 21890−21902.
(554) Canongia Lopes, J. N.; Costa Gomes, M. F.; Husson, P.; Pádua, A. A. H.; Rebelo, L. P. N.; Sarraute, S.; Tariq, M. Polarity, Viscosity, and Ionic Conductivity of Liquid Mixtures Containing $[C_4C_1im][Ntf_2]$ and a Molecular Component. *J. Phys. Chem. B* **2011**, *115*, 6088−6099.
(555) Palumbo, O.; Trequattrini, F.; Navarra, M.; Brubach, J.-B.; Roy, P.; Paolone, A. Tailoring the Physical Properties of the Mixtures of Ionic Liquids: A Microscopic Point of View. *Phys. Chem. Chem. Phys.* **2017**, *19*, 8322−8329.
(556) Chatel, G.; Pereira, J. F.; Debbeti, V.; Wang, H.; Rogers, R. D. Mixing Ionic Liquids−"Simple Mixtures" or "Double Salts"? *Green Chem.* **2014**, *16*, 2051−2083.
(557) Clough, M. T.; Crick, C. R.; Gräsvik, J.; Hunt, P. A.; Niedermeyer, H.; Welton, T.; Whitaker, O. P. A Physicochemical Investigation of Ionic Liquid Mixtures. *Chem. Sci.* **2015**, *6*, 1101−1114.
(558) Brooks, N. J.; Castiglione, F.; Doherty, C. M.; Dolan, A.; Hill, A. J.; Hunt, P. A.; Matthews, R. P.; Mauri, M.; Mele, A.; Simonutti, R.; Villar-Garcia, I. J.; Weber, C. C.; Welton, T. Linking the Structures, Free Volumes, and Properties of Ionic Liquid Mixtures. *Chem. Sci.* **2017**, *8*, 6359−6374.
(559) Kapoor, U.; Shah, J. K. Preferential Ionic Interactions and Microscopic Structural Changes Drive Nonideality in Binary Ionic Liquid Mixtures as Revealed From Molecular Simulations. *Ind. Eng. Chem. Res.* **2016**, *55*, 13132−13146.
(560) Bayley, P. M.; Best, A. S.; MacFarlane, D. R.; Forsyth, M. Transport Properties and Phase Behaviour in Binary and Ternary Ionic Liquid Electrolyte Systems of Interest in Lithium Batteries. *ChemPhysChem* **2011**, *12*, 823−827.
(561) Xiao, D.; Rajian, J. R.; Hines, L. G., Jr; Li, S.; Bartsch, R. A.; Quitevis, E. L. Nanostructural Organization and Anion Effects in the Optical Kerr Effect Spectra of Binary Ionic Liquid Mixtures. *J. Phys. Chem. B* **2008**, *112*, 13316−13325.
(562) Jarosik, A.; Krajewski, S. R.; Lewandowski, A.; Radzimski, P. Conductivity of Ionic Liquids in Mixtures. *J. Mol. Liq.* **2006**, *123*, 43−50.
(563) Voroshylova, I. V.; Ferreira, E. S.; Malček, M.; Costa, R.; Pereira, C. M.; Cordeiro, M. N. D. Influence of the Anion on the Properties of Ionic Liquid Mixtures: A Molecular Dynamics Study. *Phys. Chem. Chem. Phys.* **2018**, *20*, 14899−14918.
(564) Payal, R. S.; Balasubramanian, S. Homogenous Mixing of Ionic Liquids: Molecular Dynamics Simulations. *Phys. Chem. Chem. Phys.* **2013**, *15*, 21077−21083.
(565) Avula, N. V.; Mondal, A.; Balasubramanian, S. Charge Environment and Hydrogen Bond Dynamics in Binary Ionic Liquid Mixtures: A Computational Study. *J. Phys. Chem. Lett.* **2018**, *9*, 3511−3516.
(566) Andanson, J.-M.; Beier, M. J.; Baiker, A. Binary Ionic Liquids with a Common Cation: Insight into Nanoscopic Mixing by Infrared Spectroscopy. *J. Phys. Chem. Lett.* **2011**, *2*, 2959−2964.
(567) Matthews, R. P.; Villar-Garcia, I. J.; Weber, C. C.; Griffith, J.; Cameron, F.; Hallett, J. P.; Hunt, P. A.; Welton, T. A Structural Investigation of Ionic Liquid Mixtures. *Phys. Chem. Chem. Phys.* **2016**, *18*, 8608−8624.
(568) Aparicio, S.; Atilhan, M. Mixed Ionic Liquids: The Case of Pyridinium-Based Fluids. *J. Phys. Chem. B* **2012**, *116*, 2526−2537.
(569) Castiglione, F.; Raos, G.; Battista Appetecchi, G.; Montanino, M.; Passerini, S.; Moreno, M.; Famulari, A.; Mele, A. Blending Ionic Liquids: How Physico-Chemical Properties Change. *Phys. Chem. Chem. Phys.* **2010**, *12*, 1784−1792.
(570) Annat, G.; Forsyth, M.; MacFarlane, D. R. Ionic Liquid Mixtures: Variations in Physical Properties and Their Origins in Molecular Structure. *J. Phys. Chem. B* **2012**, *116*, 8251−8258.
(571) Cha, S.; Kim, D. Change of Hydrogen Bonding Structure in Ionic Liquid Mixtures by Anion Type. *J. Chem. Phys.* **2018**, *148*, 193827.
(572) Shimizu, K.; Tariq, M.; Rebelo, L. P.; Lopes, J. N. C. Binary Mixtures of Ionic Liquids with a Common Ion Revisited: A Molecular Dynamics Simulation Study. *J. Mol. Liq.* **2010**, *153*, 52−56.
(573) Bruce, D. W.; Cabry, C. P.; Canongia Lopes, J. N.; Costen, M. L.; D'Andrea, L.; Grillo, I.; Marshall, B. C.; McKendrick, K. G.; Minton, T. K.; Purcell, S. M.; Rogers, S.; Slattery, J. M.; Shimizu, K.;

https://dx.doi.org/10.1021/acs.chemrev.9b00693
Chem. Rev. 2020, 120, 5798−5877

Smoll, E.; Tesa-Serrate, M. A. Nanosegregation and Structuring in the Bulk and at the Surface of Ionic-Liquid Mixtures. *J. Phys. Chem. B* **2017**, *121*, 6002−6020.
(574) Canongia Lopes, J. N.; Cordeiro, T. C.; Esperança, J. M.; Guedes, H. J.; Huq, S.; Rebelo, L. P.; Seddon, K. R. Deviations from Ideality in Mixtures of Two Ionic Liquids Containing a Common Ion. *J. Phys. Chem. B* **2005**, *109*, 3519−3525.
(575) Stoppa, A.; Buchner, R.; Hefter, G. How Ideal are Binary Mixtures of Room-Temperature Ionic Liquids? *J. Mol. Liq.* **2010**, *153*, 46−51.
(576) Docampo-Alvarez, B.; Gómez-González, V.; Méndez-Morales, T.; Rodríguez, J. R.; Cabeza, O.; Turmine, M.; Gallego, L. J.; Varela, L. M. The Effect of Alkyl Chain Length on the Structure and Thermodynamics of Protic-Aprotic Ionic Liquid Mixtures: A Molecular Dynamics Study. *Phys. Chem. Chem. Phys.* **2018**, *20*, 9938−9949.
(577) Lepre, L. F.; Costa Gomes, M.; Pádua, A. l. A.; Ando, R. M. A.; Ribeiro, M. C. On the Regular Behavior of a Binary Mixture of Ionic Liquids. *J. Phys. Chem. B* **2019**, *123*, 6579−6587.
(578) Docampo-Álvarez, B.; Gómez-González, V.; Méndez-Morales, T.; Rodríguez, J. R.; López-Lago, E.; Cabeza, O.; Gallego, L. J.; Varela, L. M. Molecular Dynamics Simulations of Mixtures of Protic and Aprotic Ionic Liquids. *Phys. Chem. Chem. Phys.* **2016**, *18*, 23932−23943.
(579) Hollóczki, O.; Malberg, F.; Welton, T.; Kirchner, B. On the Origin of Ionicity in Ionic Liquids. Ion Pairing versus Charge Transfer. *Phys. Chem. Chem. Phys.* **2014**, *16*, 16880−16890.
(580) Stark, A.; Brehm, M.; Brüssel, M.; Lehmann, S. B.; Pensado, A. S.; Schöppke, M.; Kirchner, B. A Theoretical and Experimental Chemist's Joint View on Hydrogen Bonding in Ionic Liquids and Their Binary Mixtures. *Top. Curr. Chem.* **2013**, *351*, 149−187.
(581) Arce, A.; Earle, M. J.; Katdare, S. P.; Rodríguez, H.; Seddon, K. R. Mutually Immiscible Ionic Liquids. *Chem. Commun.* **2006**, 2548−2550.
(582) Omar, S.; Lemus, J.; Ruiz, E.; Ferro, V. R.; Ortega, J.; Palomar, J. Ionic Liquid Mixtures - An Analysis of Their Mutual Miscibility. *J. Phys. Chem. B* **2014**, *118*, 2442−2450.
(583) Arce, A.; Earle, M. J.; Katdare, S. P.; Rodríguez, H.; Seddon, K. R. Phase Equilibria of Mixtures of Mutually Immiscible Ionic Liquids. *Fluid Phase Equilib.* **2007**, *261*, 427−433.
(584) Hori, Y.; Chikai, T.; Ida, T.; Mizuno, M. Local Structure and Hydrogen Bond Characteristics of Imidazole Molecules for Proton Conduction in Acid and Base Proton-Conducting Composite Materials. *Phys. Chem. Chem. Phys.* **2018**, *20*, 10311−10318.
(585) Turner, A. H.; Imberti, S.; Swadźba-Kwaśny, M.; Holbrey, J. D. Applying Neutron Diffraction with Isotopic Substitution to the Structure and Proton-Transport Pathways in Protic Imidazolium Bis{(trifluoromethyl)sulfonyl}imide Ionic Liquids. *Faraday Discuss.* **2018**, *206*, 247−263.
(586) Shin, J. Y.; Wang, Y.-L.; Yamada, S. A.; Hung, S. T.; Fayer, M. D. Imidazole and 1-Methylimidazole Hydrogen Bonding and Nonhydrogen Bonding Liquid Dynamics: Ultrafast IR Experiments. *J. Phys. Chem. B* **2019**, *123*, 2094−2105.
(587) Leclère, M.; Bernard, L.; Livi, S.; Bardet, M.; Guillermo, A.; Picard, L.; Duchet-Rumeau, J. Gelled Electrolyte Containing Phosphonium Ionic Liquids for Lithium-Ion Batteries. *Nanomaterials* **2018**, *8*, 435.
(588) Miyamoto, H.; Yokota, Y.; Imanishi, A.; Inagaki, K.; Morikawa, Y.; Fukui, K.-I. Potential Dependent Changes in the Structural and Dynamical Properties of 1-Butyl-3-methylimidazolium Bis(trifluoromethanesulfonyl)imide on Graphite Electrodes Revealed by Molecular Dynamics Simulations. *Phys. Chem. Chem. Phys.* **2018**, *20*, 19408−19415.
(589) Lahiri, A.; Schubert, T. J.; Iliev, B.; Endres, F. LiTFSI in 1-Butyl-1-methylpyrrolidinium Bis(fluorosulfonyl)amide: A Possible Electrolyte for Ionic Liquid Based Lithium Ion Batteries. *Phys. Chem. Chem. Phys.* **2015**, *17*, 11161−11164.
(590) Vardar, G.; Sleightholme, A. E.; Naruse, J.; Hiramatsu, H.; Siegel, D. J.; Monroe, C. W. Electrochemistry of Magnesium Electrolytes in Ionic Liquids for Secondary Batteries. *ACS Appl. Mater. Interfaces* **2014**, *6*, 18033−18039.
(591) Russina, O.; Caminiti, R.; Méndez-Morales, T.; Carrete, J.; Cabeza, O.; Gallego, L.; Varela, L.; Triolo, A. How Does Lithium Nitrate Dissolve in a Protic Ionic Liquid? *J. Mol. Liq.* **2015**, *205*, 16−21.
(592) Prabhu, S. R.; Dutt, G. Does Addition of an Electrolyte Influence the Rotational Diffusion of Nondipolar Solutes in a Protic Ionic Liquid? *J. Phys. Chem. B* **2015**, *119*, 6311−6316.
(593) Méndez-Morales, T.; Carrete, J. S.; Cabeza, O. S.; Russina, O.; Triolo, A.; Gallego, L. J.; Varela, L. M. Solvation of Lithium Salts in Protic Ionic Liquids: A Molecular Dynamics Study. *J. Phys. Chem. B* **2014**, *118*, 761−770.
(594) Lo Nostro, P.; Ninham, B. W. Hofmeister Phenomena: An Update on Ion Specificity in Biology. *Chem. Rev.* **2012**, *112*, 2286−2322.
(595) Hjalmarsson, N.; Atkin, R.; Rutland, M. W. Effect of Lithium Ions on Rheology and Interfacial Forces in Ethylammonium Nitrate and Ethanolammonium Nitrate. *J. Phys. Chem. C* **2016**, *120*, 26960−26967.
(596) Hayes, R.; Bernard, S. A.; Imberti, S.; Warr, G. G.; Atkin, R. Solvation of Inorganic Nitrate Salts in Protic Ionic Liquids. *J. Phys. Chem. C* **2014**, *118*, 21215−21225.
(597) Méndez-Morales, T.; Carrete, J.; Rodríguez, J. R.; Cabeza, Ó.; Gallego, L. J.; Russina, O.; Varela, L. M. Nanostructure of Mixtures of Protic Ionic Liquids and Lithium Salts: Effect of Alkyl Chain Length. *Phys. Chem. Chem. Phys.* **2015**, *17*, 5298−5307.
(598) Umecky, T.; Saito, Y.; Okumura, Y.; Maeda, S.; Sakai, T. Ionization Condition of Lithium Ionic Liquid Electrolytes Under the Solvation Effect of Liquid and Solid Solvents. *J. Phys. Chem. B* **2008**, *112*, 3357−3364.
(599) Haskins, J. B.; Bennett, W. R.; Wu, J. J.; Hernández, D. M.; Borodin, O.; Monk, J. D.; Bauschlicher, C. W., Jr; Lawson, J. W. Computational and Experimental Investigation of Li-Doped Ionic Liquid Electrolytes:[Pyr_{14}][TFSI], [Pyr_{13}][FSI], and [EMIM][BF_4]. *J. Phys. Chem. B* **2014**, *118*, 11295−11309.
(600) Kadyan, A.; Pandey, S. Florescence Quenching within Lithium Salt-Added Ionic Liquid. *J. Phys. Chem. B* **2018**, *122*, 5106−5113.
(601) Niu, S.; Cao, Z.; Li, S.; Yan, T. Structure and Transport Properties of the $LiPF_6$ Doped 1-Ethyl-2,3-dimethyl-imidazolium Hexafluorophosphate Ionic Liquids: A Molecular Dynamics Study. *J. Phys. Chem. B* **2010**, *114*, 877−881.
(602) Lassègues, J.-C.; Grondin, J.; Aupetit, C.; Johansson, P. Spectroscopic Identification of the Lithium Ion Transporting Species in LiTFSI-Doped Ionic Liquids. *J. Phys. Chem. A* **2009**, *113*, 305−314.
(603) Dubnikova, F.; Zeiri, Y. Structure, Energies, and Vibrational Frequencies of Solvated Li^+ in Ionic Liquids: Role of Cation Type. *J. Phys. Chem. A* **2016**, *120*, 3079−3087.
(604) Li, Z.; Smith, G. D.; Bedrov, D. Li^+ Solvation and Transport Properties in Ionic Liquid/Lithium Salt Mixtures: A Molecular Dynamics Simulation Study. *J. Phys. Chem. B* **2012**, *116*, 12801−12809.
(605) Brinkkötter, M.; Giffin, G. A.; Moretti, A.; Jeong, S.; Passerini, S.; Schönhoff, M. Relevance of Ion Clusters for Li Transport at Elevated Salt Concentrations in [$Pyr_{12}O_1$][FTFSI] Ionic Liquid-Based Electrolytes. *Chem. Commun.* **2018**, *54*, 4278−4281.
(606) Kerner, M.; Plylahan, N.; Scheers, J.; Johansson, P. Ionic Liquid Based Lithium Battery Electrolytes: Fundamental Benefits of Utilising Both TFSI and FSI Anions? *Phys. Chem. Chem. Phys.* **2015**, *17*, 19569−19581.
(607) Costa, R.; Pereira, C. M.; Silva, A. F. Charge Storage on Ionic Liquid Electric Double Layer: The Role of the Electrode Material. *Electrochim. Acta* **2015**, *167*, 421−428.
(608) Flachard, D.; Rolland, J.; Obadia, M.; Serghei, A.; Bouchet, R.; Drockenmuller, E. A 1,2,3-Triazolate Lithium Salt with Ionic Liquid Properties at Room Temperature. *Chem. Commun.* **2018**, *54*, 9035−9038.
(609) Menne, S.; Vogl, T.; Balducci, A. Lithium Coordination in Protic Ionic Liquids. *Phys. Chem. Chem. Phys.* **2014**, *16*, 5485−5489.

https://dx.doi.org/10.1021/acs.chemrev.9b00693
Chem. Rev. 2020, 120, 5798−5877

(610) Menne, S.; Pires, J.; Anouti, M.; Balducci, A. Protic Ionic Liquids as Electrolytes for Lithium-Ion Batteries. *Electrochem. Commun.* **2013**, *31*, 39−41.
(611) Kunze, M.; Jeong, S.; Paillard, E.; Schönhoff, M.; Winter, M.; Passerini, S. New Insights to Self-Aggregation in Ionic Liquid Electrolytes for High-Energy Electrochemical Devices. *Adv. Energy Mater.* **2011**, *1*, 274−281.
(612) Eftekhari, A.; Liu, Y.; Chen, P. Different Roles of Ionic Liquids in Lithium Batteries. *J. Power Sources* **2016**, *334*, 221−239.
(613) Gómez-González, V.; Docampo-Álvarez, B.; Cabeza, O.; Fedorov, M.; Lynden-Bell, R. M.; Gallego, L. J.; Varela, L. M. Molecular Dynamics Simulations of the Structure and Single-Particle Dynamics of Mixtures of Divalent Salts and Ionic Liquids. *J. Chem. Phys.* **2015**, *143*, 124507.
(614) Giffin, G. A.; Moretti, A.; Jeong, S.; Passerini, S. Complex Nature of Ionic Coordination in Magnesium Ionic Liquid-Based Electrolytes: Solvates with Mobile Mg^{2+} Cations. *J. Phys. Chem. C* **2014**, *118*, 9966−9973.
(615) Chaumont, A.; Klimchuk, O.; Gaillard, C.; Billard, I.; Ouadi, A.; Hennig, C.; Wipff, G. Perrhenate Complexation by Uranyl in Traditional Solvents and in Ionic Liquids: A Joint Molecular Dynamics/Spectroscopic Study. *J. Phys. Chem. B* **2012**, *116*, 3205−3219.
(616) Pringle, J. M. Recent Progress in the Development and Use of Organic Ionic Plastic Crystal Electrolytes. *Phys. Chem. Chem. Phys.* **2013**, *15*, 1339−1351.
(617) Makhlooghiazad, F.; Howlett, P. C.; Wang, X.; Hilder, M.; MacFarlane, D. R.; Armand, M.; Forsyth, M. Phosphonium Plastic Crystal Salt Alloyed with a Sodium Salt as a Solid-State Electrolyte for Sodium Devices: Phase Behaviour and Electrochemical Performance. *J. Mater. Chem. A* **2017**, *5*, 5770−5780.
(618) Palumbo, O.; Trequattrini, F.; Vitucci, F.; Paolone, A. Relaxation Dynamics and Phase Transitions in Ionic Liquids: Viscoelastic Properties From the Liquid to the Solid State. *J. Phys. Chem. B* **2015**, *119*, 12905−12911.
(619) Ray, P.; Vogl, T.; Balducci, A.; Kirchner, B. Structural Investigations on Lithium-Doped Protic and Aprotic Ionic Liquids. *J. Phys. Chem. B* **2017**, *121*, 5279−5292.
(620) Pilar, K.; Balédent, V.; Zeghal, M.; Judeinstein, P.; Jeong, S.; Passerini, S.; Greenbaum, S. Investigation of Ion Aggregation in Ionic Liquids and Their Solutions with Lithium Salt Under High Pressure. *J. Chem. Phys.* **2018**, *148*, 031102.
(621) Yamaguchi, T.; Mikawa, K.-I.; Koda, S.; Serizawa, N.; Seki, S.; Fujii, K.; Umebayashi, Y. Effects of Lithium Salts on Shear Relaxation Spectra of Pyrrolidinium-Based Ionic Liquids. *J. Phys. Chem. B* **2012**, *116*, 7322−7327.
(622) Aguilera, L.; Völkner, J.; Labrador, A.; Matic, A. The Effect of Lithium Salt Doping on the Nanostructure of Ionic Liquids. *Phys. Chem. Chem. Phys.* **2015**, *17*, 27082−27087.
(623) Lesch, V.; Li, Z.; Bedrov, D.; Borodin, O.; Heuer, A. The Influence of Cations on Lithium Ion Coordination and Transport in Ionic Liquid Electrolytes: A MD Simulation Study. *Phys. Chem. Chem. Phys.* **2016**, *18*, 382−392.
(624) Al-Masri, D.; Yunis, R.; Hollenkamp, A. F.; Pringle, J. M. A Symmetrical Ionic Liquid/Li Salt System for Rapid Ion Transport and Stable Lithium Electrochemistry. *Chem. Commun.* **2018**, *54*, 3660−3663.
(625) Castiglione, F.; Ragg, E.; Mele, A.; Appetecchi, G. B.; Montanino, M.; Passerini, S. Molecular Environment and Enhanced Diffusivity of Li^+ ions in Lithium-Salt-Doped Ionic Liquid Electrolytes. *J. Phys. Chem. Lett.* **2011**, *2*, 153−157.
(626) Maier, F.; Niedermaier, I.; Steinrück, H.-P. Perspective: Chemical Reactions in Ionic Liquids Monitored Through the Gas (Vacuum)/Liquid Interface. *J. Chem. Phys.* **2017**, *146*, 170901.
(627) Law, G.; Watson, P. R. Surface Orientation in Ionic Liquids. *Chem. Phys. Lett.* **2001**, *345*, 1−4.
(628) Nishi, N.; Yasui, Y.; Uruga, T.; Tanida, H.; Yamada, T.; Nakayama, S.-I.; Matsuoka, H.; Kakiuchi, T. Ionic Multilayers at Free Surface of an Ionic Liquid, Trioctylmethylammonium Bis(nonafluorobutanesulfonyl)amide, Probed by X-ray Reflectivity Measurements. *J. Chem. Phys.* **2010**, *132*, 164705.
(629) Wakeham, D.; Nelson, A.; Warr, G. G.; Atkin, R. Probing the Protic Ionic Liquid Surface Using X-ray Reflectivity. *Phys. Chem. Chem. Phys.* **2011**, *13*, 20828−20835.
(630) Sloutskin, E.; Ocko, B. M.; Tamam, L.; Kuzmenko, I.; Gog, T.; Deutsch, M. Surface Layering in Ionic Liquids: An X-ray Reflectivity Study. *J. Am. Chem. Soc.* **2005**, *127*, 7796−7804.
(631) Lynden-Bell, R.; Del Popolo, M. Simulation of the Surface Structure of Butylmethylimidazolium Ionic Liquids. *Phys. Chem. Chem. Phys.* **2006**, *8*, 949−954.
(632) Bhargava, B.; Balasubramanian, S. Layering at an Ionic Liquid-Vapor Interface: A Molecular Dynamics Simulation Study of [Bmim][Pf_6]. *J. Am. Chem. Soc.* **2006**, *128*, 10073−10078.
(633) Sarangi, S. S.; Raju, S. G.; Balasubramanian, S. Molecular Dynamics Simulations of Ionic Liquid-Vapour Interfaces: Effect of Cation Symmetry on Structure at Interface. *Phys. Chem. Chem. Phys.* **2011**, *13*, 2714−2722.
(634) Rivera-Rubero, S.; Baldelli, S. Influence of Water on the Surface of Hydrophilic and Hydrophobic Room-Temperature Ionic Liquids. *J. Am. Chem. Soc.* **2004**, *126*, 11788−11789.
(635) Iwahashi, T.; Miyamae, T.; Kanai, K.; Seki, K.; Kim, D.; Ouchi, Y. Anion Configuration at Air/Liquid Interface of Ionic Liquid [Bmim]OTf studied by Sum-Frequency Generation Spectroscopy. *J. Phys. Chem. B* **2008**, *112*, 11936−11941.
(636) Bowers, J.; Vergara-Gutierrez, M. C.; Webster, J. R. Surface Ordering of Amphiphilic Ionic Liquids. *Langmuir* **2004**, *20*, 309−312.
(637) Shi, R.; Wang, Y. Surface Structure of Ionic Liquids Under an External Electric Field. *Mol. Simul.* **2017**, *43*, 1295−1299.
(638) Anaredy, R. S.; Shaw, S. K. Long-Range Ordering of Ionic Liquid Fluid Films. *Langmuir* **2016**, *32*, 5147−5154.
(639) Jurado, L. A.; Kim, H.; Arcifa, A.; Rossi, A.; Leal, C.; Spencer, N. D.; Espinosa-Marzal, R. M. Irreversible Structural Change of a Dry Ionic Liquid Under Nanoconfinement. *Phys. Chem. Chem. Phys.* **2015**, *17*, 13613−13624.
(640) Nagata, Y.; Ohto, T.; Backus, E. H. G.; Bonn, M. Molecular Modeling of Water Interfaces: From Molecular Spectroscopy to Thermodynamics. *J. Phys. Chem. B* **2016**, *120*, 3785−3796.
(641) Sloutskin, E.; Lynden-Bell, R.; Balasubramanian, S.; Deutsch, M. The Surface Structure of Ionic Liquids: Comparing Simulations with X-ray Measurements. *J. Chem. Phys.* **2006**, *125*, 174715.
(642) Lynden-Bell, R. Gas-Liquid Interfaces of Room Temperature Ionic Liquids. *Mol. Phys.* **2003**, *101*, 2625−2633.
(643) Shimizu, K.; Heller, B. S.; Maier, F.; Steinrück, H.-P.; Canongia Lopes, J. N. Probing the Surface Tension of Ionic Liquids Using the Langmuir Principle. *Langmuir* **2018**, *34*, 4408−4416.
(644) Hettige, J. J.; Amith, W. D.; Castner, E. W., Jr; Margulis, C. J. Ionic Liquids with Symmetric Diether Tails: Bulk and Vacuum-Liquid Interfacial Structures. *J. Phys. Chem. B* **2017**, *121*, 174−179.
(645) Wang, Y.-L.; Laaksonen, A.; Lu, Z.-Y. Influence of Ionic Liquid Film Thickness on Ion Pair Distributions and Orientations at Graphene and Vacuum Interfaces. *Phys. Chem. Chem. Phys.* **2013**, *15*, 13559−13569.
(646) Hantal, G.; Voroshylova, I.; Cordeiro, M. N. D.; Jorge, M. A Systematic Molecular Simulation Study of Ionic Liquid Surfaces Using Intrinsic Analysis Methods. *Phys. Chem. Chem. Phys.* **2012**, *14*, 5200−5213.
(647) Haddad, J.; Pontoni, D.; Murphy, B. M.; Festersen, S.; Runge, B.; Magnussen, O. M.; Steinrück, H.-G.; Reichert, H.; Ocko, B. M.; Deutsch, M. Surface Structure Evolution in a Homologous Series of Ionic Liquids. *Proc. Natl. Acad. Sci. U. S. A.* **2018**, *115*, E1100−E1107.
(648) Wang, Y.-L.; Lu, Z.-Y.; Laaksonen, A. Heterogeneous Dynamics of Ionic Liquids in Confined Films with Varied Film Thickness. *Phys. Chem. Chem. Phys.* **2014**, *16*, 20731−20740.
(649) Lísal, M.; Posel, Z.; Izák, P. Air−Liquid Interfaces of Imidazolium-Based [TF_2N^-] Ionic Liquids: Insight From Molecular Dynamics Simulations. *Phys. Chem. Chem. Phys.* **2012**, *14*, 5164−5177.

https://dx.doi.org/10.1021/acs.chemrev.9b00693
Chem. Rev. 2020, 120, 5798−5877

(650) Mezger, M.; Ocko, B. M.; Reichert, H.; Deutsch, M. Surface Layering and Melting in an Ionic Liquid Studied by Resonant Soft X-ray Reflectivity. *Proc. Natl. Acad. Sci. U. S. A.* **2013**, *110*, 3733−3737.
(651) Martinelli, A.; Maréchal, M.; Östlund, Å.; Cambedouzou, J. Insights into the Interplay Between Molecular Structure and Diffusional Motion in 1-Alkyl-3-methylimidazolium Ionic Liquids: A Combined PFG NMR and X-ray Scattering Study. *Phys. Chem. Chem. Phys.* **2013**, *15*, 5510−5517.
(652) Aliaga, C.; Baker, G. A.; Baldelli, S. Sum Frequency Generation Studies of Ammonium and Pyrrolidinium Ionic Liquids Based on the Bistrifluoromethanesulfonimide Anion. *J. Phys. Chem. B* **2008**, *112*, 1676−1684.
(653) Men, S.; Hurisso, B. B.; Lovelock, K. R. J.; Licence, P. Does the Influence of Substituents Impact upon the Surface Composition of Pyrrolidinium-Based Ionic Liquids? An Angle Resolved XPS Study. *Phys. Chem. Chem. Phys.* **2012**, *14*, 5229−5238.
(654) Paredes, X.; Fernández, J.; Pádua, A. A. H.; Malfreyt, P.; Malberg, F.; Kirchner, B.; Pensado, A. S. Bulk and Liquid-Vapor Interface of Pyrrolidinium-Based Ionic Liquids: A Molecular Simulation Study. *J. Phys. Chem. B* **2014**, *118*, 731−742.
(655) García, G.; Atilhan, M.; Aparicio, S. Theoretical Study on the Solvation of C_{60} Fullerene by Ionic Liquids. *J. Phys. Chem. B* **2014**, *118*, 11330−11340.
(656) Huang, J.; Sumpter, B. G.; Meunier, V.; Yushin, G.; Portet, C.; Gogotsi, Y. Curvature Effects in Carbon Nanomaterials: Exohedral versus Endohedral Supercapacitors. *J. Mater. Res.* **2010**, *25*, 1525−1531.
(657) Li, S.; Van Aken, K. L.; McDonough, J. K.; Feng, G.; Gogotsi, Y.; Cummings, P. T. The Electrical Double Layer of Dicationic Ionic Liquids at Onion-like Carbon Surface. *J. Phys. Chem. C* **2014**, *118*, 3901−3909.
(658) Dong, K.; Zhou, G.; Liu, X.; Yao, X.; Zhang, S.; Lyubartsev, A. Structural Evidence for the Ordered Crystallites of Ionic Liquid in Confined Carbon Nanotubes. *J. Phys. Chem. C* **2009**, *113*, 10013−10020.
(659) Yu, Z.; He, Y.; Wang, Y.; Madsen, L. A.; Qiao, R. Molecular Structure and Dynamics of Ionic Liquids in a Rigid-Rod Polyanion-Based Ion Gel. *Langmuir* **2017**, *33*, 322−331.
(660) Zhou, G.; Li, Y.; Yang, Z.; Fu, F.; Huang, Y.; Wan, Z.; Li, L.; Chen, X.; Hu, N.; Huang, L. Structural Properties and Vibrational Spectra of Ethylammonium Nitrate Ionic Liquid Confined in Single-Walled Carbon Nanotubes. *J. Phys. Chem. C* **2016**, *120*, 5033−5041.
(661) Han, T.; Park, M.-S.; Kim, J.; Kim, J. H.; Kim, K. The Smallest Quaternary Ammonium Salts with Ether Groups for High-Performance Electrochemical Double Layer Capacitors. *Chem. Sci.* **2016**, *7*, 1791−1796.
(662) Fedorov, M. V.; Lynden-Bell, R. M. Probing the Neutral Graphene-Ionic Liquid Interface: Insights from Molecular Dynamics Simulations. *Phys. Chem. Chem. Phys.* **2012**, *14*, 2552−2556.
(663) Ebeling, D.; Bradler, S.; Roling, B.; Schirmeisen, A. 3-Dimensional Structure of a Prototypical Ionic Liquid-Solid Interface: Ionic Crystal-like Behavior Induced by Molecule-Substrate Interactions. *J. Phys. Chem. C* **2016**, *120*, 11947−11955.
(664) Monk, J.; Singh, R.; Hung, F. R. Effects of Pore Size and Pore Loading on the Properties of Ionic Liquids Confined Inside Nanoporous CMK-3 Carbon Materials. *J. Phys. Chem. C* **2011**, *115*, 3034−3042.
(665) Lei, Z.; Liu, Z.; Wang, H.; Sun, X.; Lu, L.; Zhao, X. S. A High-Energy-Density Supercapacitor with Graphene-CMK-5 as the Electrode and Ionic Liquid as the Electrolyte. *J. Mater. Chem. A* **2013**, *1*, 2313−2321.
(666) He, X.; Monk, J.; Singh, R.; Hung, F. R. Molecular Modelling of Ionic Liquids in the Ordered Mesoporous Carbon CMK-5. *Mol. Simul.* **2016**, *42*, 753−763.
(667) Fukushima, T.; Kosaka, A.; Ishimura, Y.; Yamamoto, T.; Takigawa, T.; Ishii, N.; Aida, T. Molecular Ordering of Organic Molten Salts Triggered by Single-Walled Carbon Nanotubes. *Science* **2003**, *300*, 2072−2074.
(668) Chaban, V. V.; Fileti, E. E. Free Energy of Solvation of Carbon Nanotubes in Pyridinium-Based Ionic Liquids. *Phys. Chem. Chem. Phys.* **2016**, *18*, 20357−20362.
(669) Largeot, C.; Portet, C.; Chmiola, J.; Taberna, P.-L.; Gogotsi, Y.; Simon, P. Relation Between the Ion Size and Pore Size for an Electric Double-Layer Capacitor. *J. Am. Chem. Soc.* **2008**, *130*, 2730−2731.
(670) Chmiola, J.; Largeot, C.; Taberna, P. L.; Simon, P.; Gogotsi, Y. Desolvation of Ions in Subnanometer Pores and its Effect on Capacitance and Double-Layer Theory. *Angew. Chem., Int. Ed.* **2008**, *47*, 3392−3395.
(671) Zhang, L. L.; Zhou, R.; Zhao, X. Graphene-Based Materials as Supercapacitor Electrodes. *J. Mater. Chem.* **2010**, *20*, 5983−5992.
(672) Pech, D.; Brunet, M.; Durou, H.; Huang, P.; Mochalin, V.; Gogotsi, Y.; Taberna, P.-L.; Simon, P. Ultrahigh-Power Micrometre-Sized Supercapacitors Based on Onion-Like Carbon. *Nat. Nanotechnol.* **2010**, *5*, 651−654.
(673) Li, S.; Feng, G.; Fulvio, P. F.; Hillesheim, P. C.; Liao, C.; Dai, S.; Cummings, P. T. Molecular Dynamics Simulation Study of the Capacitive Performance of a Binary Mixture of Ionic Liquids near an Onion-Like Carbon Electrode. *J. Phys. Chem. Lett.* **2012**, *3*, 2465−2469.
(674) Li, S.; Zhang, P.; Fulvio Pasquale, F; Hillesheim Patrick, C; Feng, G.; Dai, S.; Cummings Peter, T Enhanced Performance of Dicationic Ionic Liquid Electrolytes by Organic Solvents. *J. Phys.: Condens. Matter* **2014**, *26*, 284105.
(675) Shi, W.; Sorescu, D. C. Molecular Simulations of CO_2 and H_2 Sorption into Ionic Liquid 1-n-Hexyl-3-methylimidazolium Bis-(trifluoromethylsulfonyl)amide ([Hmim][Tf_2N]) Confined in Carbon Nanotubes. *J. Phys. Chem. B* **2010**, *114*, 15029−15041.
(676) Chaban, V. V.; Prezhdo, O. V. Nanoscale Carbon Greatly Enhances Mobility of a Highly Viscous Ionic Liquid. *ACS Nano* **2014**, *8*, 8190−8197.
(677) Shim, Y.; Kim, H. J. Solvation of Carbon Nanotubes in a Room-Temperature Ionic Liquid. *ACS Nano* **2009**, *3*, 1693−1702.
(678) Chen, S.; Kobayashi, K.; Miyata, Y.; Imazu, N.; Saito, T.; Kitaura, R.; Shinohara, H. Morphology and Melting Behavior of Ionic Liquids Inside Single-Walled Carbon Nanotubes. *J. Am. Chem. Soc.* **2009**, *131*, 14850−14856.
(679) Li, L.-J.; Khlobystov, A.; Wiltshire, J.; Briggs, G.; Nicholas, R. Diameter-Selective Encapsulation of Metallocenes in Single-Walled Carbon Nanotubes. *Nat. Mater.* **2005**, *4*, 481−485.
(680) Ohba, T.; Chaban, V. V. A Highly Viscous Imidazolium Ionic Liquid Inside Carbon Nanotubes. *J. Phys. Chem. B* **2014**, *118*, 6234−6240.
(681) Pamies, R.; Espejo, C.; Carrión, F.; Morina, A.; Neville, A.; Bermúdez, M. Rheological Behavior of Multiwalled Carbon Nanotube-Imidazolium Tosylate Ionic Liquid Dispersions. *J. Rheol.* **2017**, *61*, 279−289.
(682) Weingarth, D.; Drumm, R.; Foelske-Schmitz, A.; Kötz, R.; Presser, V. An Electrochemical in situ Study of Freezing and Thawing of Ionic Liquids in Carbon Nanopores. *Phys. Chem. Chem. Phys.* **2014**, *16*, 21219−21224.
(683) Chen, S.; Wu, G.; Sha, M.; Huang, S. Transition of Ionic Liquid [Bmim][PF_6] from Liquid to High-Melting-Point Crystal when Confined in Multiwalled Carbon Nanotubes. *J. Am. Chem. Soc.* **2007**, *129*, 2416−2417.
(684) Ehre, D.; Lavert, E.; Lahav, M.; Lubomirsky, I. Water Freezes Differently on Positively and Negatively Charged Surfaces of Pyroelectric Materials. *Science* **2010**, *327*, 672−675.
(685) Christenson, H. K. Confinement Effects on Freezing and Melting. *J. Phys.: Condens. Matter* **2001**, *13*, R95−R133.
(686) Dou, Q.; Sha, M.; Fu, H.; Wu, G. Melting Transition of Ionic Liquid [Bmim][PF_6] Crystal Confined in Nanopores: A Molecular Dynamics Simulation. *J. Phys. Chem. C* **2011**, *115*, 18946−18951.
(687) Taherkhani, F.; Minofar, B. Effect of Nitrogen Doping on Glass Transition and Electrical Conductivity of [EMIM][PF_6] Ionic Liquid Encapsulated in a Zigzag Carbon Nanotube. *J. Phys. Chem. C* **2017**, *121*, 15493−15508.

https://dx.doi.org/10.1021/acs.chemrev.9b00693
Chem. Rev. 2020, 120, 5798−5877

(688) Akbarzadeh, H.; Abbaspour, M.; Salemi, S.; Abdollahzadeh, S. Investigation of the Melting of Ionic Liquid [EMIM][PF_6] Confined Inside Carbon Nanotubes Using Molecular Dynamics Simulations. *RSC Adv.* **2015**, *5*, 3868−3874.
(689) Singh, R.; Monk, J.; Hung, F. R. A Computational Study of the Behavior of the Ionic Liquid [BMIM][PF_6] Confined Inside Multiwalled Carbon Nanotubes. *J. Phys. Chem. C* **2010**, *114*, 15478−15485.
(690) Shim, Y.; Kim, H. J. Nanoporous Carbon Supercapacitors in an Ionic Liquid: A Computer Simulation Study. *ACS Nano* **2010**, *4*, 2345−2355.
(691) Ma, K.; Wang, X.; Forsman, J.; Woodward, C. E. Molecular Dynamic Simulations of Ionic Liquid's Structural Variations from Three to One Layers Inside a Series of Slit and Cylindrical Nanopores. *J. Phys. Chem. C* **2017**, *121*, 13539−13548.
(692) Frolov, A. I.; Kirchner, K.; Kirchner, T.; Fedorov, M. V. Molecular-Scale Insights into the Mechanisms of Ionic Liquids Interactions with Carbon Nanotubes. *Faraday Discuss.* **2012**, *154*, 235−247.
(693) Ohba, T.; Hata, K.; Chaban, V. V. Nanocrystallization of Imidazolium Ionic Liquid in Carbon Nanotubes. *J. Phys. Chem. C* **2015**, *119*, 28424−28429.
(694) Li, S.; Han, K. S.; Feng, G.; Hagaman, E. W.; Vlcek, L.; Cummings, P. T. Dynamic and Structural Properties of Room-Temperature Ionic Liquids Near Silica and Carbon Surfaces. *Langmuir* **2013**, *29*, 9744−9749.
(695) Sha, M.; Wu, G.; Liu, Y.; Tang, Z.; Fang, H. Drastic Phase Transition in Ionic Liquid [Dmim][Cl] Confined Between Graphite Walls: New Phase Formation. *J. Phys. Chem. C* **2009**, *113*, 4618−4622.
(696) Ghoufi, A.; Szymczyk, A.; Malfreyt, P. Ultrafast Diffusion of Ionic Liquids Confined in Carbon Nanotubes. *Sci. Rep.* **2016**, *6*, 28518.
(697) Berrod, Q.; Ferdeghini, F.; Judeinstein, P.; Genevaz, N.; Ramos, R.; Fournier, A.; Dijon, J.; Ollivier, J.; Rols, S.; Yu, D.; Mole, R. A.; Zanotti, J.-M. Enhanced Ionic Liquid Mobility Induced by Confinement in 1D CNT Membranes. *Nanoscale* **2016**, *8*, 7845−7848.
(698) Kanakubo, M.; Hiejima, Y.; Minami, K.; Aizawa, T.; Nanjo, H. Melting Point Depression of Ionic Liquids Confined in Nanospaces. *Chem. Commun.* **2006**, 1828−1830.
(699) Zhou, G.; Yang, Z.; Fu, F.; Huang, Y.; Chen, X.; Lu, Z.; Hu, N. Molecular-Level Understanding of Solvation Structures and Vibrational Spectra of an Ethylammonium Nitrate Ionic Liquid Around Single-Walled Carbon Nanotubes. *Ind. Eng. Chem. Res.* **2015**, *54*, 8166−8174.
(700) Yin, J.; Li, X.; Yu, J.; Zhang, Z.; Zhou, J.; Guo, W. Generating Electricity by Moving a Droplet of Ionic Liquid Along Graphene. *Nat. Nanotechnol.* **2014**, *9*, 378−383.
(701) Kim, H.-Y.; dos Santos, M. C.; Cole, M. W. Wetting Transitions of Water on Graphite and Graphene. *J. Phys. Chem. A* **2014**, *118*, 8237−8241.
(702) Rafiee, J.; Mi, X.; Gullapalli, H.; Thomas, A. V.; Yavari, F.; Shi, Y.; Ajayan, P. M.; Koratkar, N. A. Wetting Transparency of Graphene. *Nat. Mater.* **2012**, *11*, 217−222.
(703) Herrera, C.; García, G.; Atilhan, M.; Aparicio, S. Nanowetting of Graphene by Ionic Liquid Droplets. *J. Phys. Chem. C* **2015**, *119*, 24529−24537.
(704) Baldelli, S.; Bao, J.; Wu, W.; Pei, S.-S. Sum Frequency Generation Study on the Orientation of Room-Temperature Ionic Liquid at the Graphene-Ionic Liquid Interface. *Chem. Phys. Lett.* **2011**, *516*, 171−173.
(705) Xu, S.; Xing, S.; Pei, S.-S.; Ivaništšev, V.; Lynden-Bell, R.; Baldelli, S. Molecular Response of 1-Butyl-3-Methylimidazolium Dicyanamide Ionic Liquid at Graphene Electrode Interface Investigated by Sum Frequency Generation Spectroscopy and Molecular Dynamics Simulations. *J. Phys. Chem. C* **2015**, *119*, 26009−26019.
(706) Maruyama, S.; Takeyama, Y.; Taniguchi, H.; Fukumoto, H.; Itoh, M.; Kumigashira, H.; Oshima, M.; Yamamoto, T.; Matsumoto, Y. Molecular Beam Deposition of Nanoscale Ionic Liquids in Ultrahigh Vacuum. *ACS Nano* **2010**, *4*, 5946−5952.
(707) Buchner, F.; Forster-Tonigold, K.; Bozorgchenani, M.; Gross, A.; Behm, R. J. Interaction of a Self-Assembled Ionic Liquid Layer with Graphite(0001): A Combined Experimental and Theoretical Study. *J. Phys. Chem. Lett.* **2016**, *7*, 226−233.
(708) Page, A. J.; Elbourne, A.; Stefanovic, R.; Addicoat, M. A.; Warr, G. G.; Voïtchovsky, K.; Atkin, R. 3-Dimensional Atomic Scale Structure of the Ionic Liquid-Graphite Interface Elucidated by AM-AFM and Quantum Chemical Simulations. *Nanoscale* **2014**, *6*, 8100−8106.
(709) Carstens, T.; Gustus, R.; Höfft, O.; Borisenko, N.; Endres, F.; Li, H.; Wood, R. J.; Page, A. J.; Atkin, R. Combined STM, AFM, and DFT Study of the Highly Ordered Pyrolytic Graphite/1-Octyl-3-methyl-imidazolium Bis(trifluoromethylsulfonyl)imide Interface. *J. Phys. Chem. C* **2014**, *118*, 10833−10843.
(710) Dou, Q.; Sha, M.; Fu, H.; Wu, G. Molecular Dynamics Simulation of the Interfacial Structure of [$C_n$mim][PF_6] Adsorbed on a Graphite Surface: Effects of Temperature and Alkyl Chain Length. *J. Phys.: Condens. Matter* **2011**, *23*, 175001.
(711) Bordes, E.; Douce, L.; Quitevis, E. L.; Pádua, A. A.; Costa Gomes, M. Ionic Liquids at the Surface of Graphite: Wettability and Structure. *J. Chem. Phys.* **2018**, *148*, 193840.
(712) Herrera, C.; Alcalde, R.; Atilhan, M.; Aparicio, S. Theoretical Study on Amino Acid-Based Ionic Pairs and Their Interaction with Carbon Nanostructures. *J. Phys. Chem. C* **2014**, *118*, 9741−9757.
(713) Gómez-González, V.; García-Fuente, A.; Vega, A.; Carrete, J.; Cabeza, O.; Gallego, L. J.; Varela, L. M. Density Functional Study of Charge Transfer at the Graphene/Ionic Liquid Interface. *J. Phys. Chem. C* **2018**, *122*, 15070−15077.
(714) Shakourian-Fard, M.; Jamshidi, Z.; Bayat, A.; Kamath, G. Meta-Hybrid Density Functional Theory Study of Adsorption of Imidazolium- and Ammonium-Based Ionic Liquids on Graphene sheet. *J. Phys. Chem. C* **2015**, *119*, 7095−7108.
(715) Ruzanov, A.; Lembinen, M.; Ers, H.; García de la Vega, J. M.; Lage-Estebanez, I.; Lust, E.; Ivaništšev, V. B. Density Functional Theory Study of Ionic Liquid Adsorption on Circumcoronene Shaped Graphene. *J. Phys. Chem. C* **2018**, *122*, 2624−2631.
(716) Burt, R.; Birkett, G.; Salanne, M.; Zhao, X. S. Molecular Dynamics Simulations of the Influence of Drop Size and Surface Potential on the Contact Angle of Ionic-Liquid Droplets. *J. Phys. Chem. C* **2016**, *120*, 15244−15250.
(717) Dong, D.; Vatamanu, J. P.; Wei, X.; Bedrov, D. The 1-Ethyl-3-methylimidazolium Bis(trifluoromethylsulfonyl)imide Ionic Liquid Nanodroplets on Solid Surfaces and in Electric Field: A Molecular Dynamics Simulation Study. *J. Chem. Phys.* **2018**, *148*, 193833.
(718) Taherian, F.; Leroy, F.; Heim, L.-O.; Bonaccurso, E.; van der Vegt, N. F. A. Mechanism for Asymmetric Nanoscale Electrowetting of an Ionic Liquid on Graphene. *Langmuir* **2016**, *32*, 140−150.
(719) Wang, S.; Zhang, Y.; Abidi, N.; Cabrales, L. Wettability and Surface Free Energy of Graphene Films. *Langmuir* **2009**, *25*, 11078−11081.
(720) Salemi, S.; Akbarzadeh, H.; Abdollahzadeh, S. Nano-Confined Ionic Liquid [Emim][PF_6] Between Graphite Sheets: A Molecular Dynamics Study. *J. Mol. Liq.* **2016**, *215*, 512−519.
(721) Alibalazadeh, M.; Foroutan, M. Specific Distributions of Anions and Cations of an Ionic Liquid Through Confinement Between Graphene Sheets. *J. Mol. Model.* **2015**, *21*, 168.
(722) Rajput, N. N.; Monk, J.; Hung, F. R. Structure and Dynamics of an Ionic Liquid Confined Inside a Charged Slit Graphitic Nanopore. *J. Phys. Chem. C* **2012**, *116*, 14504−14513.
(723) Singh, R.; Monk, J.; Hung, F. R. Heterogeneity in the Dynamics of the Ionic Liquid [BMIM][PF_6] Confined in a Slit Nanopore. *J. Phys. Chem. C* **2011**, *115*, 16544−16554.
(724) Shen, Y.; He, X.; Hung, F. R. Structural and Dynamical Properties of a Deep Eutectic Solvent Confined inside a Slit Pore. *J. Phys. Chem. C* **2015**, *119*, 24489−24500.
(725) Rajput, N. N.; Monk, J.; Singh, R.; Hung, F. R. On the Influence of Pore Size and Pore Loading on Structural and Dynamical

https://dx.doi.org/10.1021/acs.chemrev.9b00693
Chem. Rev. 2020, 120, 5798−5877

Heterogeneities of an Ionic Liquid Confined in a Slit Nanopore. *J. Phys. Chem. C* **2012**, *116*, 5169−5181.
(726) Yokota, Y.; Miyamoto, H.; Imanishi, A.; Inagaki, K.; Morikawa, Y.; Fukui, K.-I. Structural and Dynamic Properties of 1-Butyl-3-methylimidazolium Bis(trifluoromethanesulfonyl)imide/Mica and Graphite Interfaces Revealed by Molecular Dynamics Simulation. *Phys. Chem. Chem. Phys.* **2018**, *20*, 6668−6676.
(727) Rajput, N. N.; Monk, J.; Hung, F. R. Ionic Liquids Confined in a Realistic Activated Carbon Model: A Molecular Simulation Study. *J. Phys. Chem. C* **2014**, *118*, 1540−1553.
(728) He, Y.; Qiao, R.; Vatamanu, J.; Borodin, O.; Bedrov, D.; Huang, J.; Sumpter, B. G. Importance of Ion Packing on the Dynamics of Ionic Liquids During Micropore Charging. *J. Phys. Chem. Lett.* **2016**, *7*, 36−42.
(729) Merlet, C.; Salanne, M.; Rotenberg, B.; Madden, P. A. Imidazolium Ionic Liquid Interfaces with Vapor and Graphite: Interfacial Tension and Capacitance from Coarse-Grained Molecular Simulations. *J. Phys. Chem. C* **2011**, *115*, 16613−16618.
(730) Méndez-Morales, T.; Burbano, M.; Haefele, M.; Rotenberg, B.; Salanne, M. Ion-Ion Correlations Across and Between Electrified Graphene Layers. *J. Chem. Phys.* **2018**, *148*, 193812.
(731) Le Ma, J.; Meng, Q.; Fan, J. Charge Driven Lateral Structural Evolution of Ions in Electric Double Layer Capacitors Strongly Correlates with Differential Capacitance. *Phys. Chem. Chem. Phys.* **2018**, *20*, 8054−8063.
(732) Limmer, D. T. Interfacial Ordering and Accompanying Divergent Capacitance at Ionic Liquid-Metal Interfaces. *Phys. Rev. Lett.* **2015**, *115*, 256102.
(733) Feng, G.; Li, S.; Presser, V.; Cummings, P. T. Molecular Insights into Carbon Supercapacitors Based on Room-Temperature Ionic Liquids. *J. Phys. Chem. Lett.* **2013**, *4*, 3367−3376.
(734) Salanne, M.; Rotenberg, B.; Naoi, K.; Kaneko, K.; Taberna, P.-L.; Grey, C. P.; Dunn, B.; Simon, P. Efficient Storage Mechanisms for Building Better Supercapacitors. *Nat. Energy* **2016**, *1*, 16070.
(735) Hu, G.; Pandey, G. P.; Liu, Q.; Anaredy, R. S.; Ma, C.; Liu, M.; Li, J.; Shaw, S. K.; Wu, J. Self-Organization of Ions at the Interface Between Graphene and Ionic Liquid DEME-TFSI. *ACS Appl. Mater. Interfaces* **2017**, *9*, 35437−35443.
(736) Capozza, R.; Benassi, A.; Vanossi, A.; Tosatti, E. Electrical Charging Effects on the Sliding Friction of a Model Nano-Confined Ionic Liquid. *J. Chem. Phys.* **2015**, *143*, 144703.
(737) Li, H.; Wood, R. J.; Rutland, M. W.; Atkin, R. An Ionic Liquid Lubricant Enables Superlubricity to be "Switched On" in situ Using an Electrical Potential. *Chem. Commun.* **2014**, *50*, 4368−4370.
(738) Pivnic, K.; Fajardo, O. Y.; Bresme, F.; Kornyshev, A. A.; Urbakh, M. Mechanisms of Electrotunable Friction in Friction Force Microscopy Experiments with Ionic Liquids. *J. Phys. Chem. C* **2018**, *122*, 5004−5012.
(739) Liu, X.; Wang, Y.; Li, S.; Yan, T. Effects of Anion on the Electric Double Layer of Imidazolium-Based Ionic Liquids on Graphite Electrode by Molecular Dynamics Simulation. *Electrochim. Acta* **2015**, *184*, 164−170.
(740) Jin, W.; Liu, X.; Han, Y.; Li, S.; Yan, T. Effects of Repulsive Interaction on the Electric Double Layer of an Imidazolium-Based Ionic Liquid by Molecular Dynamics Simulation. *Phys. Chem. Chem. Phys.* **2015**, *17*, 2628−2633.
(741) Liu, X.; Han, Y.; Yan, T. Temperature Effects on the Capacitance of an Imidazolium-Based Ionic Liquid on a Graphite Electrode: A Molecular Dynamics Simulation. *ChemPhysChem* **2014**, *15*, 2503−2509.
(742) Si, X.; Li, S.; Wang, Y.; Ye, S.; Yan, T. Effects of Specific Adsorption on the Differential Capacitance of Imidazolium-Based Ionic Liquid Electrolytes. *ChemPhysChem* **2012**, *13*, 1671−1676.
(743) Zhang, Q.; Han, Y.; Wang, Y.; Ye, S.; Yan, T. Comparing the Differential Capacitance of Two Ionic Liquid Electrolytes: Effects of Specific Adsorption. *Electrochem. Commun.* **2014**, *38*, 44−46.
(744) Vatamanu, J.; Borodin, O.; Smith, G. D. Molecular Insights into the Potential and Temperature Dependences of the Differential Capacitance of a Room-Temperature Ionic Liquid at Graphite Electrodes. *J. Am. Chem. Soc.* **2010**, *132*, 14825−14833.
(745) Vatamanu, J.; Vatamanu, M.; Bedrov, D. Non-Faradaic Energy Storage by Room Temperature Ionic Liquids in Nanoporous Electrodes. *ACS Nano* **2015**, *9*, 5999−6017.
(746) Vatamanu, J.; Borodin, O.; Smith, G. D. Molecular Simulations of the Electric Double Layer Structure, Differential Capacitance, and Charging Kinetics for N-methyl-N-propylpyrrolidinium Bis(fluorosulfonyl)imide at Graphite Electrodes. *J. Phys. Chem. B* **2011**, *115*, 3073−3084.
(747) Vatamanu, J.; Cao, L.; Borodin, O.; Bedrov, D.; Smith, G. D. On the Influence of Surface Topography on the Electric Double Layer Structure and Differential Capacitance of Graphite/Ionic Liquid Interfaces. *J. Phys. Chem. Lett.* **2011**, *2*, 2267−2272.
(748) Hu, Z.; Vatamanu, J.; Borodin, O.; Bedrov, D. A Molecular Dynamics Simulation Study of the Electric Double Layer and Capacitance of [BMIM][PF_6] and [BMIM][BF_4] Room Temperature Ionic Liquids Near Charged Surfaces. *Phys. Chem. Chem. Phys.* **2013**, *15*, 14234−14247.
(749) Vatamanu, J.; Xing, L.; Li, W.; Bedrov, D. Influence of Temperature on the Capacitance of Ionic Liquid Electrolytes on Charged Surfaces. *Phys. Chem. Chem. Phys.* **2014**, *16*, 5174−5182.
(750) Feng, G.; Huang, J.; Sumpter, B. G.; Meunier, V.; Qiao, R. Structure and Dynamics of Electrical Double Layers in Organic Electrolytes. *Phys. Chem. Chem. Phys.* **2010**, *12*, 5468−5479.
(751) Vatamanu, J.; Vatamanu, M.; Borodin, O.; Bedrov, D. A Comparative Study of Room Temperature Ionic Liquids and Their Organic Solvent Mixtures Near Charged Electrodes. *J. Phys.: Condens. Matter* **2016**, *28*, 464002.
(752) Gómez-González, V.; Docampo-Álvarez, B.; Méndez-Morales, T.; Cabeza, O.; Ivaništšev, V. B.; Fedorov, M. V.; Gallego, L. J.; Varela, L. M. Molecular Dynamics Simulation of Structure and Interfacial Free Energy Barriers of Mixtures of Ionic Liquids and Divalent Salts Near a Graphene Wall. *Phys. Chem. Chem. Phys.* **2017**, *19*, 846−853.
(753) Ivaništšev, V.; Méndez-Morales, T.; Lynden-Bell, R. M.; Cabeza, O.; Gallego, L. J.; Varela, L. M.; Fedorov, M. V. Molecular Origin of High Free Energy Barriers for Alkali Metal Ion Transfer Through Ionic Liquid-Graphene Electrode Interfaces. *Phys. Chem. Chem. Phys.* **2016**, *18*, 1302−1310.
(754) Vatamanu, J.; Borodin, O. Ramifications of Water-in-Salt Interfacial Structure at Charged Electrodes for Electrolyte Electrochemical Stability. *J. Phys. Chem. Lett.* **2017**, *8*, 4362−4367.
(755) Gómez-González, V.; Docampo-Álvarez, B.; Montes-Campos, H.; Otero, J. C.; Lago, E. L.; Cabeza, O.; Gallego, L. J.; Varela, L. M. Solvation of Al^{3+} Cations in Bulk and Confined Protic Ionic Liquids: A Computational Study. *Phys. Chem. Chem. Phys.* **2018**, *20*, 19071−19081.
(756) Osti, N. C.; Dyatkin, B.; Thompson, M. W.; Tiet, F.; Zhang, P.; Dai, S.; Tyagi, M.; Cummings, P. T.; Gogotsi, Y.; Wesolowski, D. J.; Mamontov, E. Influence of Humidity on Performance and Microscopic Dynamics of an Ionic Liquid in Supercapacitor. *Phys. Rev. Mater.* **2017**, *1*, 035402.
(757) Montes-Campos, H.; Otero-Mato, J. M.; Méndez-Morales, T.; Cabeza, O.; Gallego, L. J.; Ciach, A.; Varela, L. M. Two-Dimensional Pattern Formation in Ionic Liquids Confined Between Graphene Walls. *Phys. Chem. Chem. Phys.* **2017**, *19*, 24505−24512.
(758) Paek, E.; Pak, A. J.; Hwang, G. S. Large Capacitance Enhancement Induced by Metal-Doping in Graphene-Based Supercapacitors: A *First-Principles*-Based Assessment. *ACS Appl. Mater. Interfaces* **2014**, *6*, 12168−12176.
(759) Kondrat, S.; Wu, P.; Qiao, R.; Kornyshev, A. A. Accelerating Charging Dynamics in Subnanometre Pores. *Nat. Mater.* **2014**, *13*, 387−393.
(760) Xing, L.; Vatamanu, J.; Borodin, O.; Bedrov, D. On the Atomistic Nature of Capacitance Enhancement Generated by Ionic Liquid Electrolyte Confined in Subnanometer Pores. *J. Phys. Chem. Lett.* **2013**, *4*, 132−140.

https://dx.doi.org/10.1021/acs.chemrev.9b00693
Chem. Rev. 2020, 120, 5798−5877

(761) Wu, P.; Huang, J.; Meunier, V.; Sumpter, B. G.; Qiao, R. Complex Capacitance Scaling in Ionic Liquids-Filled Nanopores. *ACS Nano* **2011**, *5*, 9044−9051.
(762) Guan, Y.; Shao, Q.; Chen, W.; Zhang, J.; Zhang, X.; Deng, Y. Flow-Induced Voltage Generation by Driving Imidazolium-Based Ionic Liquids Over a Graphene Nano-Channel. *J. Mater. Chem. A* **2018**, *6*, 11941−11950.
(763) Futamura, R.; Iiyama, T.; Takasaki, Y.; Gogotsi, Y.; Biggs, M. J.; Salanne, M.; Ségalini, J.; Simon, P.; Kaneko, K. Partial Breaking of the Coulombic Ordering of Ionic Liquids Confined in Carbon Nanopores. *Nat. Mater.* **2017**, *16*, 1225−1232.
(764) Breitsprecher, K.; Abele, M.; Kondrat, S.; Holm, C. The Effect of Finite Pore Length on Ion Structure and Charging. *J. Chem. Phys.* **2017**, *147*, 104708.
(765) Merlet, C.; Rotenberg, B.; Madden, P. A.; Taberna, P.-L.; Simon, P.; Gogotsi, Y.; Salanne, M. On the Molecular Origin of Supercapacitance in Nanoporous Carbon Electrodes. *Nat. Mater.* **2012**, *11*, 306−310.
(766) Merlet, C.; Péan, C.; Rotenberg, B.; Madden, P. A.; Daffos, B.; Taberna, P.-L.; Simon, P.; Salanne, M. Highly Confined Ions Store Charge More Efficiently in Supercapacitors. *Nat. Commun.* **2013**, *4*, 2701.
(767) Wu, P.; Huang, J.; Meunier, V.; Sumpter, B. G.; Qiao, R. Voltage Dependent Charge Storage Modes and Capacity in Subnanometer Pores. *J. Phys. Chem. Lett.* **2012**, *3*, 1732−1737.
(768) Black, J. M.; Feng, G.; Fulvio, P. F.; Hillesheim, P. C.; Dai, S.; Gogotsi, Y.; Cummings, P. T.; Kalinin, S. V.; Balke, N. Strain-Based in situ Study of Anion and Cation Insertion into Porous Carbon Electrodes with Different Pore Sizes. *Adv. Energy Mater.* **2014**, *4*, 1300683.
(769) Feng, G.; Cummings, P. T. Supercapacitor Capacitance Exhibits Oscillatory Behavior as a Function of Nanopore Size. *J. Phys. Chem. Lett.* **2011**, *2*, 2859−2864.
(770) Lucio, A. J.; Shaw, S. K.; Zhang, J.; Bond, A. M. Double-Layer Capacitance at Ionic Liquid-Boron-Doped Diamond Electrode Interfaces Studied by Fourier Transformed Alternating Current Voltammetry. *J. Phys. Chem. C* **2018**, *122*, 11777−11788.
(771) Vatamanu, J.; Hu, Z.; Bedrov, D.; Perez, C.; Gogotsi, Y. Increasing Energy Storage in Electrochemical Capacitors with Ionic Liquid Electrolytes and Nanostructured Carbon Electrodes. *J. Phys. Chem. Lett.* **2013**, *4*, 2829−2837.
(772) Yokota, Y.; Miyamoto, H.; Imanishi, A.; Takeya, J.; Inagaki, K.; Morikawa, Y.; Fukui, K.-I. Microscopic Properties of Ionic Liquid/Organic Semiconductor Interfaces Revealed by Molecular Dynamics Simulations. *Phys. Chem. Chem. Phys.* **2018**, *20*, 13075−13083.
(773) Park, S.-W.; DeYoung, A. D.; Dhumal, N. R.; Shim, Y.; Kim, H. J.; Jung, Y. Computer Simulation Study of Graphene Oxide Supercapacitors: Charge Screening Mechanism. *J. Phys. Chem. Lett.* **2016**, *7*, 1180.
(774) Kondrat, S.; Kornyshev, A. Charging Dynamics and Optimization of Nanoporous Supercapacitors. *J. Phys. Chem. C* **2013**, *117*, 12399−12406.
(775) Pean, C.; Daffos, B.; Rotenberg, B.; Levitz, P.; Haefele, M.; Taberna, P.-L.; Simon, P.; Salanne, M. Confinement, Desolvation, and Electrosorption Effects on the Diffusion of Ions in Nanoporous Carbon Electrodes. *J. Am. Chem. Soc.* **2015**, *137*, 12627−12632.
(776) Péan, C.; Merlet, C.; Rotenberg, B.; Madden, P. A.; Taberna, P.-L.; Daffos, B.; Salanne, M.; Simon, P. On the Dynamics of Charging in Nanoporous Carbon-Based Supercapacitors. *ACS Nano* **2014**, *8*, 1576−1583.
(777) Schütter, C.; Husch, T.; Korth, M.; Balducci, A. Toward New Solvents for EDLCs: From Computational Screening to Electrochemical Validation. *J. Phys. Chem. C* **2015**, *119*, 13413−13424.
(778) Burt, R.; Breitsprecher, K.; Daffos, B.; Taberna, P.-L.; Simon, P.; Birkett, G.; Zhao, X. S.; Holm, C.; Salanne, M. Capacitance of Nanoporous Carbon-Based Supercapacitors is a Trade-off Between Concentration and Separability of Ions. *J. Phys. Chem. Lett.* **2016**, *7*, 4015−4021.
(779) Ocko, B.; Kraack, H.; Pershan, P. S.; Sloutskin, E.; Tamam, L.; Deutsch, M. Crystalline Phases of Alkyl-Thiol Monolayers on Liquid Mercury. *Phys. Rev. Lett.* **2005**, *94*, 017802.
(780) Elfassy, E.; Mastai, Y.; Pontoni, D.; Deutsch, M. Liquid-Mercury-Supported Langmuir Films of Ionic Liquids: Isotherms, Structure, and Time Evolution. *Langmuir* **2016**, *32*, 3164−3173.
(781) Buchner, F.; Forster-Tonigold, K.; Uhl, B.; Alwast, D.; Wagner, N.; Farkhondeh, H.; Groß, A.; Behm, R. J. Toward the Microscopic Identification of Anions and Cations at the Ionic Liquid-Ag(111) Interface: A Combined Experimental and Theoretical Investigation. *ACS Nano* **2013**, *7*, 7773−7784.
(782) Costa, R.; Pereira, C. M.; Silva, F. Double Layer in Room Temperature Ionic Liquids: Influence of Temperature and Ionic Size on the Differential Capacitance and Electrocapillary Curves. *Phys. Chem. Chem. Phys.* **2010**, *12*, 11125−11132.
(783) Nishi, N.; Hashimoto, A.; Minami, E.; Sakka, T. Electrocapillarity and Zero-Frequency Differential Capacitance at the Interface Between Mercury and Ionic Liquids Measured Using the Pendant Drop Method. *Phys. Chem. Chem. Phys.* **2015**, *17*, 5219−5226.
(784) Alam, M. T.; Islam, M. M.; Okajima, T.; Ohsaka, T. Measurements of Differential Capacitance at Mercury/Room-Temperature Ionic Liquids Interfaces. *J. Phys. Chem. C* **2007**, *111*, 18326−18333.
(785) Kornyshev, A. A. Double-Layer in Ionic Liquids: Paradigm Change? *J. Phys. Chem. B* **2007**, *111*, 5545−5557.
(786) Fedorov, M. V.; Kornyshev, A. A. Ionic Liquid Near a Charged Wall: Structure and Capacitance of Electrical Double Layer. *J. Phys. Chem. B* **2008**, *112*, 11868−11872.
(787) Pilkington, G. A.; Harris, K.; Bergendal, E.; Reddy, A. B.; Palsson, G. K.; Vorobiev, A.; Antzutkin, O. N.; Glavatskih, S.; Rutland, M. W. Electro-Responsivity of Ionic Liquid Boundary Layers in a Polar Solvent Revealed by Neutron Reflectance. *J. Chem. Phys.* **2018**, *148*, 193806.
(788) Rotenberg, B.; Salanne, M. Structural Transitions at Ionic Liquid Interfaces. *J. Phys. Chem. Lett.* **2015**, *6*, 4978−4985.
(789) Rietzler, F.; Piermaier, M.; Deyko, A.; Steinrück, H.-P.; Maier, F. Electrospray Ionization Deposition of Ultrathin Ionic Liquid Films: $[C_8C_1Im]Cl$ and $[C_8C_1Im][Tf_2N]$ on Au(111). *Langmuir* **2014**, *30*, 1063−1071.
(790) Foulston, R.; Gangopadhyay, S.; Chiutu, C.; Moriarty, P.; Jones, R. G. Mono- and Multi-Layer Adsorption of an Ionic Liquid on Au(110). *Phys. Chem. Chem. Phys.* **2012**, *14*, 6054−6066.
(791) Zein El Abedin, S.; Saad, A.Y.; Farag, H.K.; Borisenko, N.; Liu, Q.X.; Endres, F. Electrodeposition of Selenium, Indium and Copper in an Air- and Water-Stable Ionic Liquid at Variable Temperatures. *Electrochim. Acta* **2007**, *52*, 2746−2754.
(792) Gnahm, M.; Pajkossy, T.; Kolb, D. The Interface Between Au (111) and an Ionic Liquid. *Electrochim. Acta* **2010**, *55*, 6212−6217.
(793) Uhl, B.; Huang, H.; Alwast, D.; Buchner, F.; Behm, R. J. Interaction of Ionic Liquids with Noble Metal Surfaces: Structure Formation and Stability of [OMIM][TFSA] and [EMIM][TFSA] on Au (111) and Ag (111). *Phys. Chem. Chem. Phys.* **2015**, *17*, 23816−23832.
(794) Pajkossy, T.; Müller, C.; Jacob, T. The Metal-Ionic Liquid Interface as Characterized by Impedance Spectroscopy and in situ Scanning Tunneling Microscopy. *Phys. Chem. Chem. Phys.* **2018**, *20*, 21241−21250.
(795) Uhl, B.; Cremer, T.; Roos, M.; Maier, F.; Steinrück, H.-P.; Behm, R. J. At the Ionic Liquid|Metal Interface: Structure Formation and Temperature Dependent Behavior of an Ionic Liquid Adlayer on Au(111). *Phys. Chem. Chem. Phys.* **2013**, *15*, 17295−17302.
(796) Waldmann, T.; Huang, H. H.; Hoster, H. E.; Höfft, O.; Endres, F.; Behm, R. J. Imaging an Ionic Liquid Adlayer by Scanning Tunneling Microscopy at the Solid-Vacuum Interface. *ChemPhysChem* **2011**, *12*, 2565−2567.
(797) Su, Y.; Yan, J.; Li, M.; Zhang, M.; Mao, B. Electric Double Layer of Au(100)/Imidazolium-Based Ionic Liquids Interface: Effect of Cation Size. *J. Phys. Chem. C* **2013**, *117*, 205−212.

https://dx.doi.org/10.1021/acs.chemrev.9b00693
Chem. Rev. 2020, 120, 5798−5877

(798) Borisenko, N.; Zein El Abedin, S.; Endres, F. An in situ STM and DTS Study of the Extremely Pure [EMIM]FAP/Au(111) Interface. *ChemPhysChem* **2012**, *13*, 1736−1742.
(799) Biedron, A. B.; Garfunkel, E. L.; Castner, E. W., Jr; Rangan, S. Ionic Liquid Ultrathin Films at the Surface of Cu(100) and Au(111). *J. Chem. Phys.* **2017**, *146*, 054704.
(800) Wang, F.-X.; Pan, G.-B.; Liu, Y.-D.; Xiao, Y. Pb Deposition onto Au(111) From Acidic Chloroaluminate Ionic Liquid. *Chem. Phys. Lett.* **2010**, *488*, 112−115.
(801) Zhong, Y.-X.; Yan, J.-W.; Li, M.-G.; Zhang, X.; He, D.-W.; Mao, B.-W. Resolving Fine Structures of the Electric Double Layer of Electrochemical Interfaces in Ionic Liquids with an AFM Tip Modification Strategy. *J. Am. Chem. Soc.* **2014**, *136*, 14682−14685.
(802) Hayes, R.; Borisenko, N.; Tam, M. K.; Howlett, P. C.; Endres, F.; Atkin, R. Double Layer Structure of Ionic Liquids at the Au(111) Electrode Interface: An Atomic Force Microscopy Investigation. *J. Phys. Chem. C* **2011**, *115*, 6855−6863.
(803) Li, H.; Endres, F.; Atkin, R. Effect of Alkyl Chain Length and Anion Species on Interfacial Nanostructure of Ionic Liquids at Au(111)-Ionic Liquid Interface as a Function of Potential. *Phys. Chem. Chem. Phys.* **2013**, *15*, 14624−14633.
(804) Hjalmarsson, N.; Wallinder, D.; Glavatskih, S.; Atkin, R.; Aastrup, T.; Rutland, M. W. Weighing the Surface Charge of an Ionic Liquid. *Nanoscale* **2015**, *7*, 16039−16045.
(805) Sweeney, J.; Hausen, F.; Hayes, R.; Webber, G. B.; Endres, F.; Rutland, M. W.; Bennewitz, R.; Atkin, R. Control of Nanoscale Friction on Gold in an Ionic Liquid by a Potential-Dependent Ionic Lubricant Layer. *Phys. Rev. Lett.* **2012**, *109*, 155502.
(806) Li, H.; Rutland, M. W.; Atkin, R. Ionic Liquid Lubrication: Influence of Ion Structure, Surface Potential and Sliding Velocity. *Phys. Chem. Chem. Phys.* **2013**, *15*, 14616−14623.
(807) Krämer, G.; Hausen, F.; Bennewitz, R. Dynamic Shear Force Microscopy of Confined Liquids at a Gold Electrode. *Faraday Discuss.* **2017**, *199*, 299−309.
(808) Kornyshev, A. A.; Qiao, R. Three-Dimensional Double Layers. *J. Phys. Chem. C* **2014**, *118*, 18285−18290.
(809) Atkin, R.; El Abedin, S. Z.; Hayes, R.; Gasparotto, L. H. S.; Borisenko, N.; Endres, F. AFM and STM Studies on the Surface Interaction of [BMP]TFSA and [EMIm]TFSA Ionic Liquids with Au(111). *J. Phys. Chem. C* **2009**, *113*, 13266−13272.
(810) Endres, F.; Borisenko, N.; El Abedin, S. Z.; Hayes, R.; Atkin, R. The Interface Ionic Liquid(s)/Electrode(s): In situ STM and AFM Measurements. *Faraday Discuss.* **2012**, *154*, 221−233.
(811) Carstens, T.; Hayes, R.; Abedin, S. Z. E.; Corr, B.; Webber, G. B.; Borisenko, N.; Atkin, R.; Endres, F. In situ STM, AFM and DTS Study of Interface 1-Hexyl-3-methylimidazolium Tris-(pentafluoroethyl)-trifluorophosphate/Au (111). *Electrochim. Acta* **2012**, *82*, 48−59.
(812) Atkin, R.; Borisenko, N.; Drüschler, M.; El Abedin, S. Z.; Endres, F.; Hayes, R.; Huber, B.; Roling, B. An in situ STM/AFM and Impedance Spectroscopy Study of the Extremely Pure 1-Butyl-1-methylpyrrolidinium Tris(pentafluoroethyl)trifluorophosphate/Au(111) Interface: Potential Dependent Solvation Layers and the Herringbone Reconstruction. *Phys. Chem. Chem. Phys.* **2011**, *13*, 6849−6857.
(813) Borisenko, N.; Lahiri, A.; Pulletikurthi, G.; Cui, T.; Carstens, T.; Zahlbach, J.; Atkin, R.; Endres, F. The Au(111)/IL Interfacial Nanostructure in the Presence of Precursors and Its Influence on the Electrodeposition Process. *Faraday Discuss.* **2018**, *206*, 459−473.
(814) Hoffmann, V.; Pulletikurthi, G.; Carstens, T.; Lahiri, A.; Borodin, A.; Schammer, M.; Horstmann, B.; Latz, A.; Endres, F. Influence of a Silver Salt on the Nanostructure of a Au(111)/Ionic Liquid Interface: An Atomic Force Microscopy Study and Theoretical Concepts. *Phys. Chem. Chem. Phys.* **2018**, *20*, 4760−4771.
(815) McLean, B.; Li, H.; Stefanovic, R.; Wood, R. J.; Webber, G. B.; Ueno, K.; Watanabe, M.; Warr, G. G.; Page, A.; Atkin, R. Nanostructure of $[Li(G_4)]TFSI$ and $[Li(G_4)]NO_3$ Solvate Ionic Liquids at HOPG and Au(111) Electrode Interfaces as a Function of Potential. *Phys. Chem. Chem. Phys.* **2015**, *17*, 325−333.
(816) Carstens, T.; Lahiri, A.; Borisenko, N.; Endres, F. $[Py_{1,4}]FSI$-NaFSI-Based Ionic Liquid Electrolyte for Sodium Batteries: Na^+ Solvation and Interfacial Nanostructure on Au(111). *J. Phys. Chem. C* **2016**, *120*, 14736−14741.
(817) Lahiri, A.; Carstens, T.; Atkin, R.; Borisenko, N.; Endres, F. In situ Atomic Force Microscopic Studies of the Interfacial Multilayer Nanostructure of LiTFSI-$[Py_{1,4}]TFSI$ on Au(111): Influence of Li^+ Ion Concentration on the Au(111)/IL Interface. *J. Phys. Chem. C* **2015**, *119*, 16734−16742.
(818) Hayes, R.; Borisenko, N.; Corr, B.; Webber, G. B.; Endres, F.; Atkin, R. Effect of Dissolved LiCl on the Ionic Liquid-Au(111) Electrical Double Layer Structure. *Chem. Commun.* **2012**, *48*, 10246−10248.
(819) Cui, T.; Lahiri, A.; Carstens, T.; Borisenko, N.; Pulletikurthi, G.; Kuhl, C.; Endres, F. Influence of Water on the Electrified Ionic Liquid/Solid Interface: A Direct Observation of the Transition From a Multilayered Structure to a Double-Layer Structure. *J. Phys. Chem. C* **2016**, *120*, 9341−9349.
(820) Zhong, Y.; Yan, J.; Li, M.; Chen, L.; Mao, B. The Electric Double Layer in an Ionic Liquid Incorporated with Water Molecules: Atomic Force Microscopy Force Curve Study. *ChemElectroChem* **2016**, *3*, 2221−2226.
(821) Friedl, J.; Markovits, I. I.; Herpich, M.; Feng, G.; Kornyshev, A. A.; Stimming, U. Interface Between an Au(111) Surface and an Ionic Liquid: The Influence of Water on Double-Layer Capacitance. *ChemElectroChem* **2017**, *4*, 216−220.
(822) Motobayashi, K.; Minami, K.; Nishi, N.; Sakka, T.; Osawa, M. Hysteresis of Potential-Dependent Changes in Ion Density and Structure of an Ionic Liquid on a Gold Electrode: In situ Observation by Surface-Enhanced Infrared Absorption Spectroscopy. *J. Phys. Chem. Lett.* **2013**, *4*, 3110−3114.
(823) Motobayashi, K.; Nishi, N.; Inoue, Y.; Minami, K.; Sakka, T.; Osawa, M. Potential-Induced Restructuring Dynamics of Ionic Liquids on a Gold Electrode: Steric Effect of Constituent Ions Studied by Surface-Enhanced Infrared Absorption Spectroscopy. *J. Electroanal. Chem.* **2017**, *800*, 126−133.
(824) Wen, R.; Rahn, B.; Magnussen, O. M. In situ Video-STM Study of Adlayer Structure and Surface Dynamics at the Ionic Liquid/Au (111) Interface. *J. Phys. Chem. C* **2016**, *120*, 15765−15771.
(825) Nishi, N.; Hirano, Y.; Motokawa, T.; Kakiuchi, T. Ultraslow Relaxation of the Structure at Ionic Liquid Gold Electrode Interface to a Potential Step Probed by Electrochemical Surface Plasmon Resonance Measurements: Asymmetry of Relaxation Time to the Potential-Step Direction. *Phys. Chem. Chem. Phys.* **2013**, *15*, 11615−11619.
(826) Liu, Z.; Cui, T.; Li, G.; Endres, F. Interfacial Nanostructure and Asymmetric Electrowetting of Ionic Liquids. *Langmuir* **2017**, *33*, 9539−9547.
(827) Labuda, A.; Grütter, P. Atomic Force Microscopy in Viscous Ionic Liquids. *Langmuir* **2012**, *28*, 5319−5322.
(828) Schmidt, E.; Shi, S.; Ruden, P. P.; Frisbie, C. D. Characterization of the Electric Double Layer Formation Dynamics of a Metal/Ionic Liquid/Metal Structure. *ACS Appl. Mater. Interfaces* **2016**, *8*, 14879−14884.
(829) Delcheva, I.; Beattie, D. A.; Ralston, J.; Krasowska, M. Dynamic Wetting of Imidazolium-Based Ionic Liquids on Gold and Glass. *Phys. Chem. Chem. Phys.* **2018**, *20*, 2084−2093.
(830) Jha, K. C.; Liu, H.; Bockstaller, M. R.; Heinz, H. Facet Recognition and Molecular Ordering of Ionic Liquids on Metal Surfaces. *J. Phys. Chem. C* **2013**, *117*, 25969−25981.
(831) Ferreira, E. S. C.; Pereira, C. M.; Cordeiro, M. N. D. S.; dos Santos, D. J. V. A. Molecular Dynamics Study of the Gold/Ionic Liquids Interface. *J. Phys. Chem. B* **2015**, *119*, 9883−9892.
(832) Nikitina, V. A.; Kislenko, S. A.; Nazmutdinov, R. R.; Bronshtein, M. D.; Tsirlina, G. A. Ferrocene/Ferrocenium Redox Couple at Au(111)/Ionic Liquid and Au(111)/Acetonitrile Interfaces: A Molecular-Level View at the Elementary Act. *J. Phys. Chem. C* **2014**, *118*, 6151−6164.

https://dx.doi.org/10.1021/acs.chemrev.9b00693
Chem. Rev. 2020, 120, 5798−5877

(833) Ruzanov, A.; Lembinen, M.; Jakovits, P.; Srirama, S. N.; Voroshylova, I. V.; Cordeiro, M. N. D. S.; Pereira, C. M.; Rossmeisl, J.; Ivaništšev, V. B. On the Thickness of the Double Layer in Ionic Liquids. *Phys. Chem. Chem. Phys.* **2018**, *20*, 10275−10285.
(834) Sha, M.; Dou, Q.; Luo, F.; Zhu, G.; Wu, G. Molecular Insights into the Electric Double Layers of Ionic Liquids on Au(100) Electrodes. *ACS Appl. Mater. Interfaces* **2014**, *6*, 12556−12565.
(835) Matsumoto, M.; Shimizu, S.; Sotoike, R.; Watanabe, M.; Iwasa, Y.; Itoh, Y.; Aida, T. Exceptionally High Electric Double Layer Capacitances of Oligomeric Ionic Liquids. *J. Am. Chem. Soc.* **2017**, *139*, 16072−16075.
(836) Xu, B.; Siler, C. G.; Madix, R. J.; Friend, C. M. Ag/Au Mixed Sites Promote Oxidative Coupling of Methanol on the Alloy Surface. *Chem. - Eur. J.* **2014**, *20*, 4646−4652.
(837) Lexow, M.; Talwar, T.; Heller, B. S.; May, B.; Bhuin, R. G.; Maier, F.; Steinrück, H.-P. Time-Dependent Changes in the Growth of Ultrathin Ionic Liquid Films on Ag(111). *Phys. Chem. Chem. Phys.* **2018**, *20*, 12929−12938.
(838) Cremer, T.; Stark, M.; Deyko, A.; Steinrück, H.-P.; Maier, F. Liquid/Solid Interface of Ultrathin Ionic Liquid Films:$[C_1C_1Im]$-$[Tf_2N]$ and $[C_8C_1Im][Tf_2N]$ on Au(111). *Langmuir* **2011**, *27*, 3662−3671.
(839) Cremer, T.; Wibmer, L.; Calderón, S. K.; Deyko, A.; Maier, F.; Steinrück, H.-P. Interfaces of Ionic Liquids and Transition Metal Surfaces—Adsorption, Growth, and Thermal Reactions of Ultrathin $[C_1C_1Im][Tf_2N]$ Films on Metallic and Oxidised Ni(111) Surfaces. *Phys. Chem. Chem. Phys.* **2012**, *14*, 5153−5163.
(840) Rietzler, F.; Nagengast, J.; Steinrück, H.-P.; Maier, F. Interface of Ionic Liquids and Carbon: Ultrathin $[C_1C_1Im][Tf_2N]$ Films on Graphite and Graphene. *J. Phys. Chem. C* **2015**, *119*, 28068−28076.
(841) Lexow, M.; Heller, B. S.; Maier, F.; Steinrück, H. P. Anion Exchange at the Liquid/Solid Interface of Ultrathin Ionic Liquid Films on Ag(111). *ChemPhysChem* **2018**, *19*, 2978−2984.
(842) Muller, E. A.; Strader, M. L.; Johns, J. E.; Yang, A.; Caplins, B. W.; Shearer, A. J.; Suich, D. E.; Harris, C. B. Femtosecond Electron Solvation at Ionic Liquid/Metal Electrode Interface. *J. Am. Chem. Soc.* **2013**, *135*, 10646−10653.
(843) Yildirim, H.; Haskins, J. B.; Bauschlicher, C. W.; Lawson, J. W. Decomposition of Ionic Liquids at Lithium Interfaces. 1. Ab Initio Molecular Dynamics Simulations. *J. Phys. Chem. C* **2017**, *121*, 28214−28234.
(844) Buchner, F.; Bozorgchenani, M.; Uhl, B.; Farkhondeh, H.; Bansmann, J.; Behm, R. J. Reactive Interaction of (Sub-)Monolayers and Multilayers of the Ionic Liquid 1-Butyl-1-methylpyrrolidinium Bis(trifluoro-methylsulfonyl)imide with Coadsorbed Lithium on Cu(111). *J. Phys. Chem. C* **2015**, *119*, 16649−16659.
(845) Syres, K. L.; Jones, R. G. Adsorption, Desorption, and Reaction of 1-Octyl-3-methylimidazolium Tetrafluoroborate, $[C_8C_1Im][BF_4]$, Ionic Liquid Multilayers on Cu(111). *Langmuir* **2015**, *31*, 9799−9808.
(846) Gindri, I. M.; Siddiqui, D. A.; Frizzo, C. P.; Martins, M. A. P.; Rodrigues, D. C. Ionic Liquid Coatings for Titanium Surfaces: Effect of IL Structure on Coating Profile. *ACS Appl. Mater. Interfaces* **2015**, *7*, 27421−27431.
(847) Lebedeva, O.; Kudryavtsev, I.; Kultin, D.; Dzhungurova, G.; Kalmykov, K.; Kustov, L. Self-Organized Hexagonal Nanostructures on Nickel and Steel Formed by Anodization in 1-Butyl-3-methylimidazolium Bis(triflate)imide Ionic Liquid. *J. Phys. Chem. C* **2014**, *118*, 21293−21298.
(848) Dold, C.; Amann, T.; Kailer, A. Influence of Electric Potentials on Friction of Sliding Contacts Lubricated by an Ionic Liquid. *Phys. Chem. Chem. Phys.* **2015**, *17*, 10339−10342.
(849) Pensado, A. S.; Pádua, A. A. Solvation and Stabilization of Metallic Nanoparticles in Ionic Liquids. *Angew. Chem., Int. Ed.* **2011**, *50*, 8683−8687.
(850) Schernich, S.; Wagner, V.; Taccardi, N.; Wasserscheid, P.; Laurin, M.; Libuda, J. Interface Controls Spontaneous Crystallization in Thin Films of the Ionic Liquid $[C_2C_1Im][OTf]$ on Atomically Clean Pd(111). *Langmuir* **2014**, *30*, 6846−6851.
(851) Pikma, P.; Siinor, L.; Selberg, S.; Lust, E. In situ STM Studies of Electrochemically Polished Cd (0001) Electrode in 1-Ethyl-3-methylimidazolium Tetrafluoroborate. *ECS Trans.* **2015**, *66*, 41−47.
(852) Liu, Y.-C.; Chen, Y.-C.; Hsieh, Y.-T.; Sun, I. W. Anomalous Voltammetric Behavior Observed for Electrodeposition of Indium in the 1-Butyl-1-methylpyrrolidinium Dicyanamide Ionic Liquid. A Result of the Ionic Liquid Cation Adsorption. *J. Phys. Chem. C* **2017**, *121*, 8907−8913.
(853) Drüschler, M.; Huber, B.; Passerini, S.; Roling, B. Hysteresis Effects in Potential-Dependent Double Layer Capacitance of Room Temperature Ionic Liquids at a Polycrystalline Platinum Interface. *J. Phys. Chem. C* **2010**, *114*, 3614−3617.
(854) Jitvisate, M.; Seddon, J. R. T. Direct Measurement of the Differential Capacitance of Solvent-Free and Dilute Ionic Liquids. *J. Phys. Chem. Lett.* **2018**, *9*, 126−131.
(855) Anderson, E.; Grozovski, V.; Siinor, L.; Siimenson, C.; Ivaništšev, V.; Lust, K.; Kallip, S.; Lust, E. Influence of Electrode Potential and in situ STM Scanning Conditions on the Phase Boundary Structure of the Single Crystal Bi(111)|1-Butyl-4-methylpyridinium Tetrafluoroborate Interface. *J. Electroanal. Chem.* **2013**, *709*, 46−56.
(856) Grosberg, A. Y.; Nguyen, T.; Shklovskii, B. Colloquium: The Physics of Charge Inversion in Chemical and Biological Systems. *Rev. Mod. Phys.* **2002**, *74*, 329−345.
(857) Chen, Y.-G.; Weeks, J. D. Local Molecular Field Theory for Effective Attractions Between Like Charged Objects in Systems with Strong Coulomb Interactions. *Proc. Natl. Acad. Sci. U. S. A.* **2006**, *103*, 7560−7565.
(858) Mezger, M.; Schramm, S.; Schröder, H.; Reichert, H.; Deutsch, M.; De Souza, E. J.; Okasinski, J. S.; Ocko, B. M.; Honkimäki, V.; Dosch, H. Layering of [BMIM]-Based Ionic Liquids at a Charged Sapphire Interface. *J. Chem. Phys.* **2009**, *131*, 094701.
(859) Köhler, R.; Restolho, J.; Krastev, R.; Shimizu, K.; Canongia Lopes, J. N.; Saramago, B. Liquid- or Solid-Like Behavior of $[Omim][BF_4]$ at a Solid Interface? *J. Phys. Chem. Lett.* **2011**, *2*, 1551−1555.
(860) Restolho, J.; Mata, J. L.; Shimizu, K.; Canongia Lopes, J. N.; Saramago, B. Wetting Films of Two Ionic Liquids: $[C_8mim][BF_4]$ and $[C_2OHmim][BF_4]$. *J. Phys. Chem. C* **2011**, *115*, 16116−16123.
(861) Sobota, M.; Nikiforidis, I.; Hieringer, W.; Paape, N.; Happel, M.; Steinrück, H.-P.; Görling, A.; Wasserscheid, P.; Laurin, M.; Libuda, J. Toward Ionic-Liquid-Based Model Catalysis: Growth, Orientation, Conformation, and Interaction Mechanism of the $[Tf_2N]$ Anion in $[BMIM][Tf_2N]$ Thin Films on a Well-Ordered Alumina Surface. *Langmuir* **2010**, *26*, 7199−7207.
(862) Schernich, S.; Kostyshyn, D.; Wagner, V.; Taccardi, N.; Laurin, M.; Wasserscheid, P.; Libuda, J. Interactions Between the Room-Temperature Ionic Liquid $[C_2C_1Im][OTf]$ and Pd (111), Well-Ordered Al_2O_3, and Supported Pd Model Catalysts From IR Spectroscopy. *J. Phys. Chem. C* **2014**, *118*, 3188−3193.
(863) Chen, S.; Liu, Y.; Fu, H.; He, Y.; Li, C.; Huang, W.; Jiang, Z.; Wu, G. Unravelling the Role of the Compressed Gas on Melting Point of Liquid Confined in Nanospace. *J. Phys. Chem. Lett.* **2012**, *3*, 1052−1055.
(864) Singh, M. P.; Singh, R. K.; Chandra, S. Studies on Imidazolium-Based Ionic Liquids Having a Large Anion Confined in a Nanoporous Silica Gel Matrix. *J. Phys. Chem. B* **2011**, *115*, 7505−7514.
(865) Zhang, J.; Zhang, Q.; Li, X.; Liu, S.; Ma, Y.; Shi, F.; Deng, Y. Nanocomposites of Ionic Liquids Confined in Mesoporous Silica Gels: Preparation, Characterization and Performance. *Phys. Chem. Chem. Phys.* **2010**, *12*, 1971−1981.
(866) Tripathi, A. K.; Verma, Y. L.; Singh, R. K. Thermal, Electrical and Structural Studies on Ionic Liquid Confined in Ordered Mesoporous MCM-41. *J. Mater. Chem. A* **2015**, *3*, 23809−23820.
(867) Verma, Y. L.; Singh, R. K. Conformational States of Ionic Liquid 1-Ethyl-3-methylimidazolium Bis(trifluoromethylsulfonyl)-imide in Bulk and Confined Silica Nanopores Probed by

https://dx.doi.org/10.1021/acs.chemrev.9b00693
Chem. Rev. 2020, 120, 5798−5877

Crystallization Kinetics Study. *J. Phys. Chem. C* **2015**, *119*, 24381−24392.
(868) Göbel, R.; Hesemann, P.; Weber, J.; Möller, E.; Friedrich, A.; Beuermann, S.; Taubert, A. Surprisingly High, Bulk Liquid-like Mobility of Silica-Confined Ionic Liquids. *Phys. Chem. Chem. Phys.* **2009**, *11*, 3653−3662.
(869) Singh, M. P.; Verma, Y. L.; Gupta, A. K.; Singh, R. K.; Chandra, S. Changes in Dynamical Behavior of Ionic Liquid in Silica Nano-Pores. *Ionics* **2014**, *20*, 507−516.
(870) Li, C.; Guo, X.; He, Y.; Jiang, Z.; Wang, Y.; Chen, S.; Fu, H.; Zou, Y.; Dai, S.; Wu, G.; Xu, H. Compression of Ionic Liquid When Confined in Porous Silica Nanoparticles. *RSC Adv.* **2013**, *3*, 9618−9621.
(871) Sieffert, N.; Wipff, G. Ordering of Imidazolium-Based Ionic Liquids at the α-Quartz(001) Surface: A Molecular Dynamics Study. *J. Phys. Chem. C* **2008**, *112*, 19590−19603.
(872) Ballone, P.; Del Pópolo, M. G.; Bovio, S.; Podestà, A.; Milani, P.; Manini, N. Nano-Indentation of a Room-Temperature Ionic Liquid Film on Silica: A Computational Experiment. *Phys. Chem. Chem. Phys.* **2012**, *14*, 2475−2482.
(873) Shah, F. U.; Holmgren, A.; Rutland, M. W.; Glavatskih, S.; Antzutkin, O. N. Interfacial Behavior of Orthoborate Ionic Liquids at Inorganic Oxide Surfaces Probed by NMR, IR, and Raman Spectroscopy. *J. Phys. Chem. C* **2018**, *122*, 19687−19698.
(874) Gupta, A. K.; Verma, Y. L.; Singh, R. K.; Chandra, S. Studies on an Ionic Liquid Confined in Silica Nanopores: Change in T_g and Evidence of Organic-Inorganic Linkage at Pore Wall Surface. *J. Phys. Chem. C* **2014**, *118*, 1530−1539.
(875) Pal, T.; Beck, C.; Lessnich, D.; Vogel, M. Effects of Silica Surfaces on the Structure and Dynamics of Room-Temperature Ionic Liquids: A Molecular Dynamics Simulation Study. *J. Phys. Chem. C* **2018**, *122*, 624−634.
(876) Kruk, D.; Wojciechowski, M.; Brym, S.; Singh, R. K. Dynamics of Ionic Liquids in Bulk and in Confinement by Means of ^{1}H NMR Relaxometry − $BMIMOcSO_4$ in an SiO_2 Matrix as an Example. *Phys. Chem. Chem. Phys.* **2016**, *18*, 23184−23194.
(877) Coasne, B.; Viau, L.; Vioux, A. Loading-Controlled Stiffening in Nanoconfined Ionic Liquids. *J. Phys. Chem. Lett.* **2011**, *2*, 1150−1154.
(878) Federici Canova, F.; Mizukami, M.; Imamura, T.; Kurihara, K.; Shluger, A. L. Structural Stability and Polarisation of Ionic Liquid Films on Silica Surfaces. *Phys. Chem. Chem. Phys.* **2015**, *17*, 17661−17669.
(879) Castillo, M. R.; Fraile, J. M.; Mayoral, J. A. Structure and Dynamics of 1-Butyl-3-methylimidazolium Hexafluorophosphate Phases on Silica and Laponite Clay: From Liquid to Solid Behavior. *Langmuir* **2012**, *28*, 11364−11375.
(880) Ori, G.; Villemot, F.; Viau, L.; Vioux, A.; Coasne, B. Ionic Liquid Confined in Silica Nanopores: Molecular Dynamics in the Isobaric-Isothermal Ensemble. *Mol. Phys.* **2014**, *112*, 1350−1361.
(881) Martinelli, A.; Nordstierna, L. An Investigation of the Sol-Gel Process in Ionic Liquid-Silica Gels by Time Resolved Raman and ^{1}H NMR Spectroscopy. *Phys. Chem. Chem. Phys.* **2012**, *14*, 13216−13223.
(882) Shi, W.; Luebke, D. R. Enhanced Gas Absorption in the Ionic Liquid 1-n-Hexyl-3-methylimidazolium Bis(trifluoromethylsulfonyl)-amide ([Hmim][Tf_2N]) Confined in Silica Slit Pores: A Molecular Simulation Study. *Langmuir* **2013**, *29*, 5563−5572.
(883) Garaga, M. N.; Persson, M.; Yaghini, N.; Martinelli, A. Local Coordination and Dynamics of a Protic Ammonium Based Ionic Liquid Immobilized in Nano-Porous Silica Micro-Particles Probed by Raman and NMR Spectroscopy. *Soft Matter* **2016**, *12*, 2583−2592.
(884) Ueno, K.; Kasuya, M.; Watanabe, M.; Mizukami, M.; Kurihara, K. Resonance Shear Measurement of Nanoconfined Ionic Liquids. *Phys. Chem. Chem. Phys.* **2010**, *12*, 4066−4071.
(885) Federici Canova, F.; Matsubara, H.; Mizukami, M.; Kurihara, K.; Shluger, A. L. Shear Dynamics of Nanoconfined Ionic Liquids. *Phys. Chem. Chem. Phys.* **2014**, *16*, 8247−8256.
(886) Kritikos, G.; Vergadou, N.; Economou, I. G. Molecular Dynamics Simulation of Highly Confined Glassy Ionic Liquids. *J. Phys. Chem. C* **2016**, *120*, 1013−1024.
(887) Wu, C.-M.; Lin, S.-Y. Close Packing Existence of Short-Chain Ionic Liquid Confined in the Nanopore of Silica Ionogel. *J. Phys. Chem. C* **2015**, *119*, 12335−12344.
(888) Yan, Z.; Meng, D.; Wu, X.; Zhang, X.; Liu, W.; He, K. Two-Dimensional Ordering of Ionic Liquids Confined by Layered Silicate Lates via Molecular Dynamics Simulation. *J. Phys. Chem. C* **2015**, *119*, 19244−19252.
(889) Iacob, C.; Sangoro, J. R.; Kipnusu, W. K.; Valiullin, R.; Kärger, J.; Kremer, F. Enhanced Charge Transport in Nano-Confined Ionic Liquids. *Soft Matter* **2012**, *8*, 289−293.
(890) Kruk, D.; Wojciechowski, M.; Verma, Y. L.; Chaurasia, S. K.; Singh, R. K. Dynamical Properties of EMIM-SCN Confined in a SiO_2 Matrix by Means of ^{1}H NMR Relaxometry. *Phys. Chem. Chem. Phys.* **2017**, *19*, 32605−32616.
(891) Cerclier, C. V.; Zanotti, J.-M.; Bideau, J. L. Ionogel Based on Biopolymer−Silica Interpenetrated Networks: Dynamics of Confined Ionic Liquid with Lithium Salt. *Phys. Chem. Chem. Phys.* **2015**, *17*, 29707−29713.
(892) Castejón, H. J.; Wynn, T. J.; Marcin, Z. M. Wetting and Tribological Properties of Ionic Liquids. *J. Phys. Chem. B* **2014**, *118*, 3661−3668.
(893) Garaga, M. N.; Aguilera, L.; Yaghini, N.; Matic, A.; Persson, M.; Martinelli, A. Achieving Enhanced Ionic Mobility in Nanoporous Silica by Controlled Surface Interactions. *Phys. Chem. Chem. Phys.* **2017**, *19*, 5727−5736.
(894) Chu, M.; Miller, M.; Douglas, T.; Dutta, P. Ultraslow Dynamics at a Charged Silicon-Ionic Liquid Interface Revealed by X-ray Reflectivity. *J. Phys. Chem. C* **2017**, *121*, 3841−3845.
(895) Iacob, C.; Sangoro, J. R.; Papadopoulos, P.; Schubert, T.; Naumov, S.; Valiullin, R.; Kärger, J.; Kremer, F. Charge Transport and Diffusion of Ionic Liquids in Nanoporous Silica Membranes. *Phys. Chem. Chem. Phys.* **2010**, *12*, 13798−13803.
(896) Nishida, J.; Yan, C.; Fayer, M. D. Orientational Dynamics of a Functionalized Alkyl Planar Monolayer Probed by Polarization-Selective Angle-Resolved Infrared Pump-Probe Spectroscopy. *J. Am. Chem. Soc.* **2016**, *138*, 14057−14065.
(897) Wang, H. B.; Yao, N.; Wang, L.; Hu, Y. L. Brønsted-Lewis Dual Acidic Ionic Liquid Immobilized on Mesoporous Silica Materials as an Efficient Cooperative Catalyst for Mannich Reactions. *New J. Chem.* **2017**, *41*, 10528−10531.
(898) Vangeli, O. C.; Romanos, G. E.; Beltsios, K. G.; Fokas, D.; Kouvelos, E. P.; Stefanopoulos, K. L.; Kanellopoulos, N. K. Grafting of Imidazolium Based Ionic Liquid on the Pore Surface of Nanoporous Materials—Study of Physicochemical and Thermodynamic Properties. *J. Phys. Chem. B* **2010**, *114*, 6480−6491.
(899) Garaga, M. N.; Dracopoulos, V.; Werner-Zwanziger, U.; Zwanziger, J. W.; Maréchal, M.; Persson, M.; Nordstierna, L.; Martinelli, A. A Long-Chain Protic Ionic Liquid Inside Silica Nanopores: Enhanced Proton Mobility due to Efficient Self-Assembly and Decoupled Proton Transport. *Nanoscale* **2018**, *10*, 12337−12348.
(900) Arcifa, A.; Rossi, A.; Espinosa-Marzal, R. M.; Spencer, N. D. Influence of Environmental Humidity on the Wear and Friction of a Silica/Silicon Tribopair Lubricated with a Hydrophilic Ionic Liquid. *ACS Appl. Mater. Interfaces* **2016**, *8*, 2961−2973.
(901) Arcifa, A.; Rossi, A.; Ramakrishna, S. N.; Espinosa-Marzal, R.; Sheehan, A.; Spencer, N. D. Lubrication of Si-Based Tribopairs with a Hydrophobic Ionic Liquid: The Multiscale Influence of Water. *J. Phys. Chem. C* **2018**, *122*, 7331−7343.
(902) Arcifa, A.; Rossi, A.; Espinosa-Marzal, R. M.; Spencer, N. D. Environmental Influence on the Surface Chemistry of Ionic-Liquid-Mediated Lubrication in a Silica/Silicon Tribopair. *J. Phys. Chem. C* **2014**, *118*, 29389−29400.
(903) Kamijo, T.; Arafune, H.; Morinaga, T.; Honma, S.; Sato, T.; Hino, M.; Mizukami, M.; Kurihara, K. Lubrication Properties of Ammonium-Based Ionic Liquids Confined Between Silica Surfaces

https://dx.doi.org/10.1021/acs.chemrev.9b00693
Chem. Rev. 2020, 120, 5798−5877

Using Resonance Shear Measurements. *Langmuir* **2015**, *31*, 13265−13270.
(904) Sakai, K.; Okada, K.; Uka, A.; Misono, T.; Endo, T.; Sasaki, S.; Abe, M.; Sakai, H. Effects of Water on Solvation Layers of Imidazolium-Type Room Temperature Ionic Liquids on Silica and Mica. *Langmuir* **2015**, *31*, 6085−6091.
(905) Lertola, A. C.; Wang, B.; Li, L. Understanding the Friction of Nanometer-Thick Fluorinated Ionic Liquids. *Ind. Eng. Chem. Res.* **2018**, *57*, 11681−11685.
(906) Arcifa, A.; Rossi, A.; Spencer, N. D. Adsorption and Tribochemical Factors Affecting the Lubrication of Silicon-Based Materials by (Fluorinated) Ionic Liquids. *J. Phys. Chem. C* **2017**, *121*, 7259−7275.
(907) Horn, R.; Evans, D.; Ninham, B. Double-Layer and Solvation Forces Measured in a Molten Salt and Its Mixtures with Water. *J. Phys. Chem.* **1988**, *92*, 3531−3537.
(908) Wakeham, D.; Hayes, R.; Warr, G. G.; Atkin, R. Influence of Temperature and Molecular Structure on Ionic Liquid Solvation Layers. *J. Phys. Chem. B* **2009**, *113*, 5961−5966.
(909) Segura, J. J.; Elbourne, A.; Wanless, E. J.; Warr, G. G.; Voïtchovsky, K.; Atkin, R. Adsorbed and Near Surface Structure of Ionic Liquids at a Solid Interface. *Phys. Chem. Chem. Phys.* **2013**, *15*, 3320−3328.
(910) Hjalmarsson, N.; Atkin, R.; Rutland, M. W. Is the Boundary Layer of an Ionic Liquid Equally Lubricating at Higher Temperature? *Phys. Chem. Chem. Phys.* **2016**, *18*, 9232−9239.
(911) Sweeney, J.; Webber, G. B.; Rutland, M. W.; Atkin, R. Effect of Ion Structure on Nanoscale Friction in Protic Ionic Liquids. *Phys. Chem. Chem. Phys.* **2014**, *16*, 16651−16658.
(912) Elbourne, A.; Voïtchovsky, K.; Warr, G. G.; Atkin, R. Ion Structure Controls Ionic Liquid Near-Surface and Interfacial Nanostructure. *Chem. Sci.* **2015**, *6*, 527−536.
(913) Elbourne, A.; Cronshaw, S.; Voïtchovsky, K.; Warr, G. G.; Atkin, R. Near Surface Properties of Mixtures of Propylammonium Nitrate with n-Alkanols 1. Nanostructure. *Phys. Chem. Chem. Phys.* **2015**, *17*, 26621−26628.
(914) McDonald, S.; Elbourne, A.; Warr, G. G.; Atkin, R. Metal Ion Adsorption at the Ionic Liquid-Mica Interface. *Nanoscale* **2016**, *8*, 906−914.
(915) Wang, Z.; Li, H.; Atkin, R.; Priest, C. Influence of Water on the Interfacial Nanostructure and Wetting of [Rmim][NTf_2] Ionic Liquids at Mica Surfaces. *Langmuir* **2016**, *32*, 8818−8825.
(916) Black, J. M.; Zhu, M.; Zhang, P.; Unocic, R. R.; Guo, D.; Okatan, M. B.; Dai, S.; Cummings, P. T.; Kalinin, S. V.; Feng, G.; Balke, N. Fundamental Aspects of Electric Double Layer Force-Distance Measurements at Liquid-Solid Interfaces Using Atomic Force Microscopy. *Sci. Rep.* **2016**, *6*, 32389.
(917) Jitvisate, M.; Seddon, J. R. Near-Wall Molecular Ordering of Dilute Ionic Liquids. *J. Phys. Chem. C* **2017**, *121*, 18593−18597.
(918) Zhang, F.; Fang, C.; Qiao, R. Effects of Water on Mica-Ionic Liquid Interfaces. *J. Phys. Chem. C* **2018**, *122*, 9035−9045.
(919) Payal, R. S.; Balasubramanian, S. Effect of Cation Symmetry on the Organization of Ionic Liquids near a Charged Mica Surface. *J. Phys.: Condens. Matter* **2014**, *26*, 284101.
(920) Smith, A. M.; Lovelock, K. R.; Perkin, S. Monolayer and Bilayer Structures in Ionic Liquids and Their Mixtures Confined to Nano-Films. *Faraday Discuss.* **2014**, *167*, 279−292.
(921) Jurado, L. A.; Kim, H.; Rossi, A.; Arcifa, A.; Schuh, J. K.; Spencer, N. D.; Leal, C.; Ewoldt, R. H.; Espinosa-Marzal, R. M. Effect of the Environmental Humidity on the Bulk, Interfacial and Nanoconfined Properties of an Ionic Liquid. *Phys. Chem. Chem. Phys.* **2016**, *18*, 22719−22730.
(922) Wang, Z.; Priest, C. Impact of Nanoscale Surface Heterogeneity on Precursor Film Growth and Macroscopic Spreading of [Rmim][NTf_2] Ionic Liquids on Mica. *Langmuir* **2013**, *29*, 11344−11353.
(923) Gong, X.; Kozbial, A.; Li, L. What Causes Extended Layering of Ionic Liquids on the Mica Surface? *Chem. Sci.* **2015**, *6*, 3478−3482.
(924) Deyko, A.; Cremer, T.; Rietzler, F.; Perkin, S.; Crowhurst, L.; Welton, T.; Steinrück, H.-P.; Maier, F. Interfacial Behavior of Thin Ionic Liquid Films on Mica. *J. Phys. Chem. C* **2013**, *117*, 5101−5111.
(925) Hayes, R.; Warr, G. G.; Atkin, R. At the Interface: Solvation and Designing Ionic Liquids. *Phys. Chem. Chem. Phys.* **2010**, *12*, 1709−1723.
(926) Smith, A. M.; Parkes, M. A.; Perkin, S. Molecular Friction Mechanisms Across Nanofilms of a Bilayer-Forming Ionic Liquid. *J. Phys. Chem. Lett.* **2014**, *5*, 4032−4037.
(927) Fajardo, O. Y.; Bresme, F.; Kornyshev, A. A.; Urbakh, M. Electrotunable Friction with Ionic Liquid Lubricants: How Important is the Molecular Structure of the Ions? *J. Phys. Chem. Lett.* **2015**, *6*, 3998−4004.
(928) Lian, C.; Liu, K.; Liu, H.; Wu, J. Impurity Effects on Charging Mechanism and Energy Storage of Nanoporous Supercapacitors. *J. Phys. Chem. C* **2017**, *121*, 14066−14072.
(929) Freitas, A. A. D.; Shimizu, K.; Smith, A. M.; Perkin, S.; Canongia Lopes, J. N. Structure and Dynamics of Mica-Confined Films of [$C_{10}C_1$pyrr][ntf_2] Ionic Liquid. *J. Chem. Phys.* **2018**, *148*, 193808.
(930) Smith, A. M.; Lovelock, K. R.; Gosvami, N. N.; Welton, T.; Perkin, S. Quantized Friction Across Ionic Liquid Thin Films. *Phys. Chem. Chem. Phys.* **2013**, *15*, 15317−15320.
(931) Smith, A. M.; Lee, A. A.; Perkin, S. Switching the Structural Force in Ionic Liquid-Solvent Mixtures by Varying Composition. *Phys. Rev. Lett.* **2017**, *118*, 096002.
(932) Singh Payal, R.; Balasubramanian, S. Orientational Ordering of Ionic Liquids near a Charged Mica Surface. *ChemPhysChem* **2012**, *13*, 1764−1771.
(933) Seddon, J. R. T. Conservative and Dissipative Interactions of Ionic Liquids in Nanoconfinement. *J. Phys. Chem. C* **2014**, *118*, 22197−22201.
(934) Bou-Malham, I.; Bureau, L. Nanoconfined Ionic Liquids: Effect of Surface Charges on Flow and Molecular Layering. *Soft Matter* **2010**, *6*, 4062−4065.
(935) Hayes, R.; El Abedin, S. Z.; Atkin, R. Pronounced Structure in Confined Aprotic Room-Temperature Ionic Liquids. *J. Phys. Chem. B* **2009**, *113*, 7049−7052.
(936) Gorlov, M.; Kloo, L. Ionic Liquid Electrolytes for Dye-Sensitized Solar Cells. *Dalton Trans* **2008**, 2655−2666.
(937) Agosta, L.; Brandt, E. G.; Lyubartsev, A. P. Diffusion and Reaction Pathways of Water near Fully Hydrated TiO2 Surfaces from ab Initio Molecular Dynamics. *J. Chem. Phys.* **2017**, *147*, 024704.
(938) Wagstaffe, M.; Jackman, M. J.; Syres, K. L.; Generalov, A.; Thomas, A. G. Ionic Liquid Ordering at an Oxide Surface. *ChemPhysChem* **2016**, *17*, 3430−3434.
(939) Henderson, Z.; Walton, A.; Thomas, A. G.; Syres, K. L. Water-Induced Reordering in Ultrathin Ionic Liquid Films. *J. Phys.: Condens. Matter* **2018**, *30*, 334003.
(940) Uhl, B.; Hekmatfar, M.; Buchner, F.; Behm, R. J. Interaction of the Ionic Liquid [BMP][TFSA] with Rutile TiO_2 (110) and Coadsorbed Lithium. *Phys. Chem. Chem. Phys.* **2016**, *18*, 6618−6636.
(941) Singh, R.; Rajput, N. N.; He, X.; Monk, J.; Hung, F. R. Molecular Dynamics Simulations of the Ionic Liquid [EMIM]-[TFMSI] Confined Inside Rutile (110) Slit Nanopores. *Phys. Chem. Chem. Phys.* **2013**, *15*, 16090−16103.
(942) Weber, H.; Kirchner, B. Ionic Liquid Induced Band Shift of Titanium Dioxide. *ChemSusChem* **2016**, *9*, 2505−2514.
(943) Weber, H.; Bredow, T.; Kirchner, B. Adsorption Behavior of the 1,3-Dimethylimidazolium Thiocyanate and Tetracyanoborate Ionic Liquids at Anatase (101) Surface. *J. Phys. Chem. C* **2015**, *119*, 15137−15149.
(944) Weber, H.; Salanne, M.; Kirchner, B. Toward an Accurate Modeling of Ionic Liquid-TiO_2 Interfaces. *J. Phys. Chem. C* **2015**, *119*, 25260−25267.
(945) Pinilla, C.; Del Pópolo, M.; Kohanoff, J.; Lynden-Bell, R. Polarization Relaxation in an Ionic Liquid Confined Between Electrified Walls. *J. Phys. Chem. B* **2007**, *111*, 4877−4884.

https://dx.doi.org/10.1021/acs.chemrev.9b00693
Chem. Rev. 2020, 120, 5798−5877

(946) Babucci, M.; Balci, V.; Akçay, A.; Uzun, A. Interactions of [BMIM][BF_4] with Metal Oxides and Their Consequences on Stability Limits. *J. Phys. Chem. C* **2016**, *120*, 20089−20102.
(947) Schernich, S.; Laurin, M.; Lykhach, Y.; Steinruck, H.-P.; Tsud, N.; Skala, T.; Prince, K. C.; Taccardi, N.; Matolin, V.; Wasserscheid, P.; Libuda, J. Functionalization of Oxide Surfaces Through Reaction with 1,3-Dialkylimidazolium Ionic Liquids. *J. Phys. Chem. Lett.* **2013**, *4*, 30−35.
(948) Yuan, H.; Shimotani, H.; Ye, J.; Yoon, S.; Aliah, H.; Tsukazaki, A.; Kawasaki, M.; Iwasa, Y. Electrostatic and Electrochemical Nature of Liquid-Gated Electric-Double-Layer Transistors Based on Oxide Semiconductors. *J. Am. Chem. Soc.* **2010**, *132*, 18402−18407.
(949) Black, J. M.; Come, J.; Bi, S.; Zhu, M.; Zhao, W.; Wong, A. T.; Noh, J. H.; Pudasaini, P. R.; Zhang, P.; Okatan, M. B.; Dai, S.; Kalinin, S. V.; Rack, P. D.; Ward, T. Z.; Feng, G.; Balke, N. Role of Electrical Double Layer Structure in Ionic Liquid Gated Devices. *ACS Appl. Mater. Interfaces* **2017**, *9*, 40949−40958.
(950) Jeong, J.; Aetukuri, N.; Graf, T.; Schladt, T. D.; Samant, M. G.; Parkin, S. S. Suppression of Metal-Insulator Transition in VO_2 by Electric Field-Induced Oxygen Vacancy Formation. *Science* **2013**, *339*, 1402−1405.
(951) Nakano, M.; Shibuya, K.; Okuyama, D.; Hatano, T.; Ono, S.; Kawasaki, M.; Iwasa, Y.; Tokura, Y. Collective Bulk Carrier Delocalization Driven by Electrostatic Surface Charge Accumulation. *Nature* **2012**, *487*, 459−462.
(952) Li, M.; Han, W.; Jiang, X.; Jeong, J.; Samant, M. G.; Parkin, S. S. Suppression of Ionic Liquid Gate-Induced Metallization of $SrTiO_3$(001) by Oxygen. *Nano Lett.* **2013**, *13*, 4675−4678.
(953) Petach, T. A.; Mehta, A.; Marks, R.; Johnson, B.; Toney, M. F.; Goldhaber-Gordon, D. Voltage-Controlled Interfacial Layering in an Ionic Liquid on $SrTiO_3$. *ACS Nano* **2016**, *10*, 4565−4569.
(954) Xu, T.; Waehler, T.; Vecchietti, J.; Bonivardi, A.; Bauer, T.; Schwegler, J.; Schulz, P. S.; Wasserscheid, P.; Libuda, J. Interaction of Ester-Functionalized Ionic Liquids with Atomically-Defined Cobalt Oxides Surfaces: Adsorption, Reaction and Thermal Stability. *ChemPhysChem* **2017**, *18*, 3443−3453.
(955) Voeltzel, N.; Giuliani, A.; Fillot, N.; Vergne, P.; Joly, L. Nanolubrication by Ionic Liquids: Molecular Dynamics Simulations Reveal an Anomalous Effective Rheology. *Phys. Chem. Chem. Phys.* **2015**, *17*, 23226−23235.
(956) Cooper, P. K.; Wear, C. J.; Li, H.; Atkin, R. Ionic Liquid Lubrication of Stainless Steel: Friction is Inversely Correlated with Interfacial Liquid Nanostructure. *ACS Sustainable Chem. Eng.* **2017**, *5*, 11737−11743.
(957) Sandhu, P.; Gindri, I.; Siddiqui, D.; Rodrigues, D. Dicationic Imidazolium-Based Ionic Liquid Coatings on Zirconia Surfaces: Physico-Chemical and Biological Characterization. *J. Funct. Biomater.* **2017**, *8*, 50.
(958) Ori, G.; Massobrio, C.; Pradel, A.; Ribes, M.; Coasne, B. Structure and Dynamics of Ionic Liquids Confined in Amorphous Porous Chalcogenides. *Langmuir* **2015**, *31*, 6742−6751.
(959) Perera, M. M.; Lin, M.-W.; Chuang, H.-J.; Chamlagain, B. P.; Wang, C.; Tan, X.; Cheng, M. M.-C.; Tománek, D.; Zhou, Z. Improved Carrier Mobility in Few-Layer MoS_2 Field-Effect Transistors with Ionic-Liquid Gating. *ACS Nano* **2013**, *7*, 4449−4458.
(960) Chen, D.; Ying, W.; Guo, Y.; Ying, Y.; Peng, X. Enhanced Gas Separation Through Nanoconfined Ionic Liquid in Laminated MoS_2 Membrane. *ACS Appl. Mater. Interfaces* **2017**, *9*, 44251−44257.

https://dx.doi.org/10.1021/acs.chemrev.9b00693
Chem. Rev. 2020, 120, 5798−5877